UCSF
UC San Francisco Electronic Theses and Dissertations

Title
Epithelial organization of the adult neural stem cell niche

Permalink
https://escholarship.org/uc/item/8qz0602t

Author
Mirzadeh, Zaman

Publication Date
2008-05-08

Supplemental Material
https://escholarship.org/uc/item/8qz0602t#supplemental

Peer reviewed|Thesis/dissertation

eScholarship.org Powered by the California Digital Library
University of California

Epithelial Organization of the Adult Neural Stem Cell Niche

by

Zaman Mirzadeh

DISSERTATION

Submitted in partial satisfaction of the requirements for the degree of

DOCTOR OF PHILOSOPHY

in

Biomedical Sciences

in the

GRADUATE DIVISION

of the

UNIVERSITY OF CALIFORNIA, SAN FRANCISCO

Copyright 2008

by

Zaman Mirzadeh

For my parents,

Mariam and Sohrab

Acknowledgements

The work presented here is the culmination of 5 years of scientific endeavor that would not have been possible without the help of many. First and foremost, I must thank forever my wife, Melissa Sandoval, who supported me through graduate school. Her encouragement and love were unwavering. Similarly, I would like to thank my parents, Mariam and Sohrab, and my sisters, Ladan and Nastaran, who provided an escape from the rigors of experimentation.

Many, many thanks to Young-Goo Han for his help with both oral presentations and manuscripts, for our discussions and passionate arguments about the biology of cilia, and for his great friendship. In addition, this work would not have been possible without the gifted hands of Florian Merkle, my friend and co-graduate student, who helped with mouse surgeries and was always ready with a keen intellect to review experimental design. Cynthia Yaschine was essential to the daily operation of the lab and went out of her way to ensure that I had all the resources and protocols necessary for my experiments. Ricardo Romero was always willing to offer his technical expertise with perfusions, mouse surgeries, and EM sample preparation. Minoree Kohwi and Rui Galvao were fellow graduate students who taught me basic lab techniques. Dan Lim was extremely helpful with the construction of the adeno-GFAPp::Cre virus used in Chapter 3 and for mentorship regarding MD/PhD training. Oscar Gonzales was a great friend who first turned my attention to wholemounts. Hirohide Takebayashi was ready to review cloning strategies and listen to crazy

experimental ideas when we were both burning the midnight oil. Rebecca Ihrie was incredibly helpful with oral presentations and figures.

I am grateful to the collaborative environment provided by the UCSF stem cell community. Thanks to Ashkan Javaherian and William Walantus of the Kriegstein lab who helped with *in utero* injections. Thanks to Kevin Corbit and Veena Singla for discussions about cilia and basal bodies and for providing useful reagents. I would like to thank Kenneth Probst for his beautiful illustration on page 96. Many thanks to Kurt Thorn and the Nikon imaging center for help with confocal microscopy.

I also thank my thesis committee members John Rubenstein, Sam Pleasure, and Jeremy Reiter for their support. Thanks to John for discussion of promoter elements that may be active in type C cells, Sam for providing in situ probes for the Wnt pathways, and Jeremy for encouraging my then nascent interest in cilia and planar polarity. I received tremendous mentorship from Jose Manuel García-Verdugo, our close collaborator in Valencia, Spain, who showed me the beauty and power of careful anatomical observation.

Finally, I am forever indebted to my advisor, Arturo Alvarez-Buylla. His approach to science is infectious and has instilled in me not only an enthusiasm for the subject, but also a maturity about how it should be conducted. In addition to discussing experiments, Arturo was always willing to hear my gripes about the nature of humanity. For his sensitivity on this subject in particular, he inspires my journey as a physician-scientist.

Abstract

Epithelial Organization of the Adult Neural Stem Cell Niche

by

Zaman Mirzadeh

The adult mammalian brain, for all of its complexity, develops from a single cell layered epithelium of neural stem cells. These stem cells are retained in the epithelium lining the embryonic brain ventricles throughout development. Postnatally however, this germinal epithelium is replaced by postmitotic multiciliated ependymal cells. Neural stem cells are retained in the adult brain, but they are displaced from the ventricular epithelium and it is generally thought that they do not maintain epithelial properties. In this dissertation, I challenge this notion. Using a wholemount imaging technique that allows en-face examination of the ventricular walls, I show that the adult brain lateral ventricle is lined by a mixed neuroepithelium of multiciliated ependymal cells and adult neural stem cells (type B cells). Type B cells have very small ventricle-contacting apical surfaces observed only in neurogenic niches of the adult ventricular system. At their apical surface, B cells extend a primary cilium into the ventricle and are surrounded by ependymal cells, forming pinwheel structures that appear as repeating units across the neuroepithelium. Type B cells also contain a previously unidentified long basal process ending on blood vessels. These adult neural stem cells therefore display apical-basal polarity. En-face analysis of the

ventricular walls also reveals a third cell type in the ventricular epithelium, which I call E2 cells. These cells are bi-ciliated with a novel basal body structure containing elaborate lateral extensions. Finally, in addition to apical-basal polarity, the adult ventricular epithelium has planar polarity evident in the polarized beating of ependymal cilia, which propels cerebrospinal fluid through the ventricular system and is essential to normal brain function. I describe two reliable anatomical correlates to ependymal planar polarity: the rotational orientation of basal bodies and their translational position on the apical surface of ependymal cells. I show that this planar polarity does not require ependymal cilia. Altogether, this work reveals the epithelial organization of the adult neural stem cell niche, characterized by the apical surfaces of stem cells surrounded by ependymal cells in unique pinwheel structures.

Table of Contents

Title i
Copyright ii
Dedication iii
Acknowledgements iv
Abstract vi
Table of Contents viii
List of Tables xi
List of Figures and Illustrations xii
List of Abbreviations xv
Chapter 1. Introduction 1
Epithelia, neuroepithelial cells, and radial glia 1
Historical perspective on adult neurogenesis 7
Identification of the adult mammalian neural stem cell 9
The ependymal epithelium 13
Cilia and basal bodies 15
SVZ type B cells are derived from radial glia 19
Evidence for apical-basal polarity of type B cells 21
Chapter 2. Materials and Methods 32
Section 1: Animals and Stereotactic Viral Injections 32
Animals 32
Construction of Ad-GFAPp::Cre virus 33
Stereotactic Viral Injections of Adult and Neonatal Mice 34
Section 2: Tissue processing and cell culture 35
Wholemount dissection 35
Ependymal flow movies 36
Sectioning, X-gal staining, and Hematoxylin staining 37
In situ Hybridization 39
Immunostaining and confocal microscopy 41
Electron microscopy 43
Adherent neural stem cell cultures 43

Section 3: Data analysis 45
Reconstruction of surface maps 45
Quantification of the ventricle-contacting cell types 45
Quantification of basal body patch angle and apical surface orientation of ependymal cells 46
Chapter 3. A new perspective on the adult neural stem cell niche: a neurogenic ventricular zone persists in the adult brain 49
Introduction 50
Results 53
Three cell types contact the lateral ventricle 53
B1 and E1/E2 cells have complementary expression patterns of molecular markers at their apical surfaces 56
B1 cells confer unique pinwheel architecture to the ventricular surface in neurogenic regions of the adult brain 56
Apical intercellular junctional complexes at B1-B1 and B1-ependymal junctions 58
Surface maps of the lateral ventricle walls reveal “hot spots” of B1 cells 60
B1 cells have a long basal process similar to their radial glial progenitors 62
Ventricle-contacting B1 cells undergo mitosis and are neurogenic 66
Discussion 70
B1 cells retain a long basal process 70
B1 cells maintain a modified ventricular zone in the adult brain 73
Chapter 4. A unique biciliated cell in the walls of the brain ventricles 109
Introduction 109
Results 112
Apical structures of E2 cells by confocal microscopy 112
Ultrastructure of E2 cells 115
Distribution of E2 cells throughout the adult ventricular system 116
Discussion 119
E2 cells vs. tanycytes 119
Possible functions of E2 cells 121

Chapter 5. Ependymal planar polarity does not require motile cilia **140**
Introduction 141
Results 144
Functional assays for ependymal planar polarity 144
Anatomical correlates to ependymal planar polarity 146
Basal body patch angle, but not apical surface orientation, correlates with ependymal planar polarity throughout the adult ventricular system 151
Planar polarity of basal body patches does not require motile (9+2) cilia .. 152
Timing of cilia loss in *hGFAP::Cre;Kif3a*$^{fl/fl}$ mutants 154
Discussion 157
Apical surface orientation vs. the position of the basal body patch 158
Motile (9+2) vs. Primary (9+0) cilia in basal body planar polarity 160
Chapter 6. Concluding Remarks and Future Directions **179**
Type B cells 179
Multiciliated Ependymal (Type E1) cells 185
Chapter 7. References **195**
UCSF library release 218

List of Tables

Table 1. Mouse strains and relevant information 32

Table 2. Primary antibodies 42

List of Figures and Illustrations

Chapter 1

Figure 1. Different types of epithelium 26
Figure 2. Neural tube formation in chick embryos 27
Figure 3. Convergent extension of NE cells is essential for neural tube closure 28
Figure 4. Cell types and cytoarchitecture of the adult SVZ 29
Figure 5. Axonemal structure of cilia and basal bodies 30
Figure 6. Three dimensional drawing of the basal body illustrating the relationship with the cilium 31

Chapter 3

Figure 1. Three cell types contact the lateral ventricle 78
Figure 2. Complementary expression patterns of molecular markers at the apical surface of B1 and E1/E2 cells 80
Figure 3. Pinwheel architecture of the ventricular surface in neurogenic regions of the adult ventricular system 82
Figure 4. Apical intercellular junctional complexes differ at B1-B1, B1-E1, and E1-E2 junctions 84
Figure 5. Apical intercellular membranes at B1-B1 and B1-ependymal junctions localize gap junction protein Cx43 and several adherens junction proteins 86
Figure 6. Surface maps of the walls of the lateral ventricle revealed “hot spots” of B1 apical surfaces 88
Figure 7. B1 cells with an apical surface contacting the ventricle have a long basal process 90
Figure 8. B1 cells in mitosis maintain contact with the ventricle 92
Figure 9. B1 cells with a ventricle-contacting apical surface are neurogenic *in vivo* and exhibit multilineage differentiation *in vitro* 94
Figure 10. 3-dimensional model of the adult VZ neurogenic niche 96
Figure S1. Wholemount dissection of the lateral wall of the lateral ventricle 97
Figure S2. The orientation of long GFAP+ fibers varies depending on the

region in the lateral wall of the lateral ventricle 98
Figure S3. Long GFAP+ fibers were observed in 100 um coronal and horizontal SVZ sections 100
Figure S4. Chains of migrating neuroblasts in the SVZ are oriented parallel to long GFAP+ fibers 102
Figure S5. Morphology of ventricle-contacting B1 cells in wholemounts and sections 104
Figure S6. Morphological differences between ventricle-contacting B1 cells and typical parenchymal astrocytes 106
Figure S7. The basal process of B1 cells made specialized contacts with blood vessels 107
Figure S8. Diagram of the lateral wall illustrating how it was divided into four regions quantified for the density of B1, E1, and E2 cells 108
Chapter 4
Figure 1. Basal body structure of E2 cells by confocal microscopy 124
Figure 2. Cilia of E2 cells by confocal microscopy 126
Figure 3. Ultrastructure of E2 cells in transverse sections 128
Figure 4. Ultrastructure of E2 cells in en-face sections 129
Figure 5. Distribution of E2 cells in the lateral and medial walls of the lateral ventricle 130
Figure 6. Distribution of E2 cells in the walls of the 3rd ventricle 132
Figure 7. E2 cilia on the floor of the 3rd ventricle 134
Figure 8. Distribution of E2 cells in the floor of the 4th ventricle 136
Figure 9. E2 cilia on the midline floor of the 4th ventricle 138
Chapter 5
Figure 1. Functional and anatomical planar polarity of the ependymal epithelium 165
Figure 2. Basal body patch position and apical surface orientation are anatomical correlates to ependyma planar polarity in regions AD and AV of the lateral wall 167
Figure 3. Basal body patch angle, but not apical surface orientation, correlates

with ependymal planar polarity throughout the adult ventricular system 169
Figure 4. Planar polarity of basal body patches does not require motile cilia 171
Figure 5. Timing of cilia loss in *hGFAP::Cre;Kif3a*$^{fl/fl}$ mutants 173
Figure S1. Regions AD, AV, and PM of the lateral wall of the lateral ventricle were defined by 4 lines 175
Figure S2. Orientation of fluid flow on the anterior medial wall of the lateral ventricle 176
Figure S3. Hematoxylin-stained coronal sections from control and *hGFAP::Cre;Kif3a*$^{fl/fl}$ mutants demonstrate hydrocephalus in mutants ... 177
Figure S4. CD24 immunostaining on wholemounts reveals gradients of ependymal cell differentiation on the lateral and medial walls of the lateral ventricle in the early postnatal period 178

Chapter 6

Figure 1. Hypothetical model demonstrating how the elaborate morphology and topological relationships of type B cells may allow them to integrate spatially segregated regulatory signals 191
Figure 2. Heterogeneity of radial glial apical surface size on the lateral wall of the lateral ventricle at P0 192
Figure 3. Preliminary evidence that basal bodies of radial glia undergoing ependymal transformation have a polarized position on the apical surface 193
Figure 4. Core PCP genes are expressed in the lateral ventricle walls of neonatal mice 194

List of Symbols, Abbreviations and Nomenclature

Symbol	Definition
Ad:Cre	Adenovirus expressing Cre
Ad:GFAP-Cre	Adenovirus expressing Cre under the murine GFAP promoter
AP	Anterior-Posterior
AraC	Cytosine Arabinoside
BABB	Benzyl Alcohol Benzyl Benzoate clearing solution
bFGF/FGF_2	basic Fibroblast Growth Factor
BMP	Bone Morphogenetic Protein
BPE	Bovine Pituitary Extract
CNS	Central Nervous System
Cre	Cre recombinase protein from bacteriophage P1
CSF	Cerebrospinal Fluid
D	Dorsal
DAB	Diaminobenzidine
DAPI	4’,6-diamidino-2-phenylindole
Dcx	Doublecortin
DG	Dentate Gyrus
DIV	Days In Vitro
DMEM	Dulbecco's Modified Eagle's Medium
DMEM/F12	Dulbecco's Modified Eagle's Medium/Ham’s F12 50:50 mix
E	Embryonic day
EGF	Epidermal Growth Factor

eGFP	enhanced Green Fluorescent Protein
EM	Electron Microscopy
FBS	Fetal Bovine Serum
FCS	Fetal Calf Serum
FGF	Fibroblast Growth Factor
FoxJ1	Forkhead box J1 transcription factor
GFAP	Glial Fibrillary Acidic Protein
GFP	Green Fluorescent Protein
HRP	Horseradish Peroxidase
ICC	Immunocytochemistry
IHC	Immunohistochemistry
L15	Leibovitz's L-15 Medium
LoxP	Locus of crossing over in phage P1
LacZ	Beta-galactosidase encoding gene from *Escherichia coli*
LV	Lateral Ventricle
M	Medial
NE	Neuroepithelium
NEC	Neuroepithelial Cell
Notch1	Notch gene homolog 1
NSC	Neural Stem Cell
Numb	Numb gene homolog
OB	Olfactory Bulb

Olig2	Oligodendrocyte transcription factor 2
P	Postnatal day
PB	Phosphate Buffer
PBS	Phosphate Buffered Saline
PBST	Phosphate Buffered Saline + Triton X-100
PCR	Polymerase Chain Reaction
PDGF	Platelet-Derived Growth Factor
PFA	Paraformaldehyde
RC2	Radial Cell 2 antigen
RMS	Rostral Migratory Stream
RT	Room Temperature
S phase	Synthesis phase
SCZ	Subcallosal Zone
SD	Standard Deviation
SEM	Standard Error of the Mean
SGZ	Subgranular Zone
Shh	Sonic hedgehog
SVZ	Subventricular Zone
Tuj1	Beta III tubulin
TX	Triton X-100 detergent
UA	Uranyl Acetate
V	Ventral
VZ	Ventricular Zone
Wnt	Wingless

Chapter 1

Introduction

The adult mammalian brain is perhaps the most complex biological system under scientific study. It is comprised of billions of neurons and glial cells, interwoven into intricate circuits that control thought, emotion, perception and movement. Yet for all of its complexity, the brain develops from an epithelium. Throughout development, embryonic neural stem cells remain part of this neuroepithelium lining the brain ventricles. However, it is thought that neural stem cells in the adult brain, which are displaced to the subventricular zone of the lateral ventricle and the subgranular zone of the hippocampus, are not retained within this epithelium. This thesis explores the apical structures of cells lining the ventricles in the adult rodent brain and reveals that a mixed neuroepithelium persists in the adult that contains ependymal cells, including a novel type of ependymal cell, as well as adult neural stem cells.

Epithelia, Neuroepithelial Cells, and Radial Glia

Epithelia are sheets of tissue that line the cavities and surfaces of organs throughout the body. They are found in the lining of the gut (intestinal epithelial cells), the skin (epidermis), blood vessels (endothelial cells), and the brain (ependymal cells). Epithelial sheets are cell-rich and have only a thin layer of extracellular matrix, called the basal lamina, deposited beneath the epithelial sheet. Within the sheet, epithelial cells have distinct apical and basal

membranes specialized for diverse functions (Alberts et al., 1994). The apical membrane faces the cavity or lumen of an organ (or the outside world in the case of the skin), while the basal membrane faces the basal lamina and other cell types within the organ. Characteristic protein and lipid composition distinguish the apical and basal membranes, which are delimited by intercellular junctional complexes (Martin-Belmonte and Mostov, 2008). These complexes consist of adherens and tight junctions that recruit molecules involved in regulating apical-basal polarity of the epithelium. Although less well understood, epithelial cells also have planar polarity, which is the orientation of the cell with respect to the epithelial plane (orthogonal to the apical-basal axis) (Wang and Nathans, 2007; Zallen, 2007). Planar polarity accounts for the relatively uniform direction in which hairs exit the hair follicle across a patch of skin epithelium. Another property of epithelia is high tensile strength, derived from cytoskeletal filaments (i.e. actin and intermediate filaments) expressed by cells within the sheet that interconnect across the epithelium at junctional complexes (Alberts et al., 1994). The expression of cytoskeletal filaments and intercellular junctional complexes, and apical-basal and planar polarity are common properties of epithelial cells, even though these cells can have different shapes (squamous, cuboidal, and columnar) and be organized into single or multiple cell layers (simple, pseudostratified, and stratified) (**Fig. 1**).

The brain develops from a pseudostratified columnar epithelium. Early in development, this flat neuroepithelium (the neural plate) bends at the midline of the embryo and the lateral ridges fold over and fuse, forming an epithelial tube

called the neural tube (Colas and Schoenwolf, 2001; Schoenwolf and Smith, 2000) (**Fig. 2**). A single layer of neuroepithelial (NE) cells forms the walls of the neural tube, each cell spanning from the lumen of the tube (prospective brain ventricle) at its apical membrane to the basal lamina of the tube (prospective brain pia) at its basal membrane. The stratified appearance ('pseudostratified') of NE cells is a result of cell-cycle dependent to-and-fro movements of their nuclei, called interkinetic nuclear migration, along the apical-basal axis (Misson et al., 1988; Noctor et al., 2001; Sauer, 1935). The nucleus migrates to the basal membrane to replicate its DNA, and then migrates back to the apical luminal surface to undergo mitosis. NE cells also have other indicators of apical-basal polarity, such as the organization of their apical and basal membranes (Gotz and Huttner, 2005; Wodarz and Huttner, 2003). The apical membrane is enriched in prominin-1 (CD133) (Weigmann et al., 1997), while the basal membrane localizes integrin α_6 (Wodarz and Huttner, 2003), a transmembrane receptor that binds to the basal lamina. In addition, NE cells have adherens and tight junctions at the apical end of their lateral membranes (Aaku-Saraste et al., 1996; Chenn et al., 1998). Knocking out AF-6 (also called afadin), a multi-domain scaffold protein that is a component of these junctional complexes, has been shown to disrupt the polarization of neuroepithelial cells (Ikeda et al., 1999; Ooshio et al., 2007; Zhadanov et al., 1999). Interestingly, although the apical-basal polarity of NE cells is maintained during formation of the neural tube (Colas and Schoenwolf, 2001; Schoenwolf and Smith, 2000), the composition of NE cell junctional complexes is dynamic. NE cell adherens junctions lose E-cadherin

expression and increase N-cadherin expression during neural tube closure (Hatta et al., 1987; Takeichi, 1995). Occludin, a component of tight junctions, is also lost during this time, as are functional tight junctions (Aaku-Saraste et al., 1996). It has been suggested that these changes reflect a remodeling of the neuroepithelium that is necessary for neurogenesis to occur.

Neurogenesis in the mouse forebrain begins at E10-E11 (Caviness et al., 1995), resulting in the production of basally migrating neuroblasts that thicken the neural tube wall and transform it into multilayered structure (Huttner and Kosodo, 2005). In the course of this transformation, NE cells are replaced by a distinct, but related, progenitor cell type called the radial glial cell (Gotz and Huttner, 2005; Malatesta et al., 2003). These cells are the principal neuronal progenitors of the embryonic forebrain (Anthony et al., 2004; Malatesta et al., 2000; Miyata et al., 2001; Noctor et al., 2001; Tamamaki et al., 2001). Radial glia keep their cell body at the luminal side of the thickening neural tube in a pseudostratified layer called the ventricular zone (VZ) (Committee, 1970). The stratified appearance of the VZ is due to interkinetic nuclear migration of radial glial cells (Misson et al., 1988; Noctor et al., 2001), a behavior very similar to that of NE cells. From their cell body in the VZ, radial glia extend a long, radially-oriented basal process that contacts the pial basal lamina (Halfter et al., 2002; Haubst et al., 2006), and a short apical process that contacts the neural tube lumen. The radial process forms additional en-passant contacts with blood vessel basal lamina as it courses through the neuronal layers towards the pia (Alvarez-Buylla et al., 1987; Misson et al., 1988; Noctor et al., 2001). Radial glia, therefore, maintain the topology of

NE cells. It is thought that signals arising from both apical and basal poles of these cells are essential for proper neurogenesis (e.g. apical: (Bittman et al., 1997; Kosodo et al., 2004; Nadarajah et al., 1997; Weissman et al., 2004), e.g. basal: (Halfter et al., 2002; Haubst et al., 2006)). In addition to maintained apical and basal contacts, radial glia share other epithelial characteristics with NE cells such as apical membrane specializations: extension of a primary cilium from the apical surface, which is associated to a basal body and centriole directly beneath the apical surface (discussed below) (Chenn et al., 1998; Tramontin et al., 2003), apical expression of prominin-1 (CD133) (Weigmann et al., 1997), and apical membrane concentration of ASIP/Par3, Par-6, and aPKC (Manabe et al., 2002), cytoplasmic proteins that are known regulators of apical-basal polarity (Martin-Belmonte and Mostov, 2008; Munro, 2006). The apical and basolateral membranes of radial glia are delimited by junctional complexes including adherens junctions (Chenn et al., 1998; Kosodo et al., 2004). Surprisingly, the integrity of radial glial adherens junctions was recently shown to require numb, a molecule well studied for its roles in neuronal cell fate determination (Kuo et al., 2006; Rasin et al., 2007). Loss of Numb and Numb-like in radial glia disrupts proper basolateral insertion of cadherins, and results in abnormal adherens junctions and polarity (Rasin et al., 2007). Other epithelial characteristics shared by NE cells and radial glia include expression of the intermediate filament protein nestin (Frederiksen and McKay, 1988; Hockfield and McKay, 1985) and the intermediate filament associated protein RC2 (Misson et al., 1988).

Planar polarity is an epithelial property that has been studied in NE cells early in neural tube development. Before the neural tube closes, NE cells undergo mediolateral intercalation within the plane of the neural plate (Schoenwolf and Alvarez, 1989). Net cell movement is towards the midline. This polarized rearrangement of cells, called convergent extension, simultaneously narrows and elongates the neural plate, and brings together the elevating lateral folds that will fuse to form the neural tube (**Fig. 3**) (Copp et al., 2003; Wallingford, 2006). Failure of this planar polarized movement of NE cells results in open neural tube defects (Greene et al., 1998; Murdoch et al., 2003; Wallingford and Harland, 2002; Wallingford et al., 2000). In contrast, planar polarized behavior of radial glial cells has not been demonstrated. However, recent evidence shows that the large majority of radial glial mitoses in the cortical VZ occur with a vertical cleavage plane (perpendicular to the ventricular surface) (Noctor et al., 2008), suggesting that the mitotic spindle is oriented within the epithelial plane of the VZ. Although it has been previously suggested that such cleavage planes produce symmetric divisions, it is now understood that vertical cleavages are capable of producing asymmetric divisions (Huttner and Brand, 1997; Huttner and Kosodo, 2005). This may occur through asymmetric inheritance of the apical membrane (Kosodo et al., 2004) or a fate determining molecule, such as the EGF receptor (Sun et al., 2005). The prevalence of vertical cleavage planes indicates that asymmetric distribution of these factors would occur with an orientation orthogonal to the apical-basal axis. It will be interesting to determine

whether radial glia in the VZ have planar polarity that is predictive of this asymmetric distribution.

Despite the shared epithelial characteristics, radial glia are distinct from NE cells. Specifically, radial glia acquire several astroglial properties: glycogen granules (Gadisseux and Evrard, 1985), and the expression of the intermediate filament protein vimentin (Pixley and De Vellis, 1984), the astrocyte-specific glutamate transporter GLAST (Shibata et al., 1997), brain lipid binding protein (BLBP) (Feng and Heintz, 1995), tenascin-C (Peretto et al., 2005), and in primates (Levitt and Rakic, 1980) and some murine radial glia (Rickmann et al., 1987), the intermediate filament protein and astrocyte marker GFAP (Glial Fibrillary Acidic Protein). It has been suggested that these molecular changes are related to the function of radial glia as guides for neuronal migration (Hatten, 1999; Malatesta et al., 2003; Rakic, 1972). Radial glia and NE cells are therefore distinct cell types, but these embryonic neural stem cells are both epithelial cells that remain part of an epithelium lining the brain ventricles throughout development.

Historical Perspective on Adult Neurogenesis

Shortly after birth in mammals, radial glia transform into parenchymal astrocytes (Schmechel and Rakic, 1979; Voigt, 1989) and ependymal cells (discussed below) (Spassky et al., 2005) and little remains of their unique morphology and behavior. The VZ is replaced by a simple ependymal epithelium. This stark transformation of the embryonic germinal epithelium in

part fueled the notion that neurogenesis was a prenatal or early postnatal phenomenon. In addition, primate studies, where adult neurogenesis is in fact poorly represented (Rakic, 1985), supported the feeling that the adult brain was too complex for the useful integration of new neurons. However, studies in the 1960s started to challenge this notion. A series of papers by Joseph Altman and colleagues suggested that specific regions in the adult rodent brain did generate new neurons, which could be labeled by [^{3}H]-thymidine (Altman, 1962, 1963, 1967, 1969; Altman and Das, 1965). A decade later, electron microscopy studies of [^{3}H]-thymidine labeled neurons added more support to the controversial claim of adult neurogenesis (Kaplan and Hinds, 1977). Finally, experiments in songbirds would provide definitive evidence that neurons generated in the adult did functionally integrate into existing circuits. Paton and Nottebohm showed that new neurons, labeled with [^{3}H]-thymidine, could be impaled with microelectrodes and (1) exhibited action potentials, (2) responded to auditory stimuli, and (3) could be filled with peroxidase to reveal typical dendritic and axonal morphology (Nottebohm, 2004; Paton and Nottebohm, 1984). Later studies revisited and confirmed the original findings of Altman that the adult rodent brain contains two major proliferative regions, the lateral wall of the lateral ventricle (LV) and the dentate gyrus of the hippocampus (Alvarez-Buylla and Garcia-Verdugo, 2002; Kaplan and Bell, 1983; Lois and Alvarez-Buylla, 1993; Reynolds and Weiss, 1992; van Praag et al., 2002; Zhao et al., 2008). With adult neurogenesis becoming a more widely accepted phenomenon, the search was on for the adult neural stem cells *in vivo*, the primary progenitors from which new neurons in the

adult brain are derived. To date, it has been shown that in adult songbirds (Alvarez-Buylla et al., 1990), lizards (Garcia-Verdugo et al., 2002), turtles (Russo et al., 2004), and fish (Zupanc, 2006), neurogenic radial glia are retained as the adult neural stem cells. However, in mammals, the adult neural stem cells appear to have an astroglial phenotype (discussed below) (Doetsch et al., 1999a; Seri et al., 2001).

Identification of the Adult Mammalian Neural Stem Cell

In contrast to neural stem cells (neuroepithelial cells and radial glia) of the embryonic mammalian brain, neural stem cells in the adult are not considered to be part of an epithelium. Adult neural stem cells are displaced from the ventricular lining to either the subventricular zone (SVZ) of the LV (Alvarez-Buylla and Garcia-Verdugo, 2002) or the subgranular zone (SGZ) of the hippocampal dentate gyrus (Zhao et al., 2008). Here we will review the epithelial properties, such as apical-basal polarity, of adult neural stem cells in the SVZ. A similar analysis has not been conducted for the progenitors in the adult hippocampal SGZ, although these cells have been studied extensively (Altman and Bayer, 1990; Alvarez-Buylla et al., 2002; Eves et al., 1992; Palmer et al., 2000; Pleasure et al., 2000; Seaberg and van der Kooy, 2002; Seri and Alvarez-Buylla, 2002; Seri et al., 2004; Zhao et al., 2008).

The first evidence that the walls of the adult lateral ventricle retained neural stem cells came from *in vitro* studies in which dissociated cells were cultured in the presence of EGF and FGF (Morshead et al., 1994; Reynolds and

Weiss, 1992). Under these conditions, some cells proliferated to form free-floating balls of cells called neurospheres. Neurospheres could be passaged and differentiated into neurons, astrocytes, and oligodendrocytes, thereby exhibiting self-renewal and multipotency. These criteria, which are used to define stem cells in other systems, have been used to define the adult NSC *in vitro* (Capela and Temple, 2002; Geschwind et al., 2001; Tropepe et al., 1999). However, the walls of the LV, the lateral wall in particular, contain at least four different cell types identified by morphology, ultrastructure, and molecular markers (**Fig. 4**) (Doetsch et al., 1997). For this reason, and the concern that culturing cells may alter their potential (Doetsch et al., 2002; Gabay et al., 2003), determining the identity of the adult neural stem cell required *in vivo* analysis.

The walls of the adult LV are lined by a simple epithelium of multiciliated ependymal (Type E) cells. Although these cells have been suggested to be the stem cells (Johansson et al., 1999), further analysis has shown that they do not divide in the adult brain and do not act as progenitors *in vitro* (Capela and Temple, 2002; Chiasson et al., 1999; Doetsch et al., 1999a; Laywell et al., 2000; Spassky et al., 2005). Beneath the ependymal lining lies the subependymal or subventricular zone, occupied by three additional cell types (Types A, B, and C cells), described by immunohistochemistry and electron microscopy (Doetsch et al., 1997). Type A cells are neuroblasts that have a migratory morphology and express the markers typical of young neurons: Tuj1, Dcx, and PSA-NCAM. These cells migrate in chains, found throughout the lateral wall of the LV (Doetsch and Alvarez-Buylla, 1996), that coalesce in the anterior SVZ to form the

rostral migratory stream (RMS) to the olfactory bulb (OB) (Lois and Alvarez-Buylla, 1994; Luskin, 1993). Once they have reached their final destination in the OB, the neuroblasts mature into multiple different subtypes of OB interneurons (Carleton et al., 2003; Hack et al., 2005; Kelsch et al., 2007; Kohwi et al., 2005; Kohwi et al., 2007; Merkle et al., 2007; Petreanu and Alvarez-Buylla, 2002). Chains of migrating A cells are ensheathed by glial tubes formed by astrocytic processes (Jankovski and Sotelo, 1996; Lois et al., 1996; Peretto et al., 1997), some of which belong to Type B cells. The astrocytic properties of B cells include GFAP expression, abundant intermediate filaments, specialized contact with blood vessels, and glycogen granules. B cells have processes that form a lamina separating E cells from A cells. Type C cells are similar in size to B cells but have a simpler morphology, contain deeply invaginated nuclei, no intermediate filaments, and express the markers Mash1 (Parras et al., 2004) and Dlx2 (Doetsch et al., 2002). A subpopulation of C cells also expresses Olig2 (Menn et al., 2006). Of these three cell types, B and C cells can act as stem cells *in vitro* and give rise to large colonies of A cells (Doetsch et al., 2002; Lim and Alvarez-Buylla, 1999), whereas A cells themselves have limited self-renewal (Lim and Alvarez-Buylla, 1999).

The adult neural stem cell was identified *in vivo* by its ability to generate the other SVZ cell types. First, intracranial infusion of cytosine arabinoside (Ara-C), a nucleoside analog chemotherapeutic drug, was used to deplete the SVZ of rapidly dividing cells. This ablated C and A cells but not ependymal cells or the more slowly-dividing B cells. Surprisingly, Type B cells (SVZ astrocytes) then

regenerated the SVZ by dividing and generating C cells, which in turn divided and generated A cells (Doetsch et al., 1999a). In addition, specific labeling of SVZ astrocytes by an avian retrovirus resulted in the generation of labeled neurons that migrated to and integrated in the OB, again through a C cell intermediate. Much like intermediate progenitors of the embryonic SVZ (Haubensak et al., 2004; Noctor et al., 2004; Noctor et al., 2007), it appears that C cells are a transit-amplifying cell type that expands the progenitor pool which ultimately produces neuroblasts. More recent work in transgenic mice, either tracing the fate of (Garcia et al., 2004), or ablating (Imura et al., 2003), GFAP+ SVZ astrocytes, has confirmed the finding that Type B cells are the primary progenitors for adult neurogenesis from the SVZ. Type B cells were also recently shown to produce oligodendrocyte progenitors that migrate to, and generate oligodendrocytes in, the corpus callosum (Menn et al., 2006). While the adult SVZ neurogenic niche was initially described as residing along the anterior lateral wall of the LV (Luskin, 1993), recent studies have shown that the neurogenic niche is far more extensive, including the RMS (Bonfanti et al., 1997; Gritti et al., 2002; Hack et al., 2005; Liu and Martin, 2003; Merkle et al., 2007; Pencea et al., 2001) and more posterior regions of the lateral wall (Merkle et al., 2007), and also the dorsal or pallial wall of the LV (Kohwi et al., 2007; Merkle et al., 2007; Ventura and Goldman, 2007), the anterior medial wall of the LV (Doetsch et al., 1999a; Merkle et al., 2007; Morshead et al., 1994), and the subcallosal zone (Seri et al., 2006). Unlike in the embryo, neural stem cells in these regions

occupy a subventricular or subependymal position, displaced from the ventricle by postnatal development of ependymal cells.

The Ependymal Epithelium

A bona fide epithelium, with both apical-basal and planar polarity, does remain lining the ventricles in the adult brain. This epithelium consists of a single layer of ependymal cells, which are postmitotic (Spassky et al., 2005). The ependyma plays an important role as a protective barrier at the brain-cerebrospinal fluid (CSF) interface (Del Bigio, 1995). Ependymal cells have been conceived as a filtration system, transporting ions, small molecules, and fluid between the brain and CSF (Bruni, 1998; Kuchler et al., 1994). In addition, they have the enzymatic and structural characteristics necessary for scavenging and detoxifying various substances in the CSF (Del Bigio, 1995). Monoamine oxidase enzymes, which metabolize biogenic amines, are expressed in ependymal cells and suggest that the ependyma functions as an amine-barrier system (Saura et al., 1994; Williams et al., 1979). Structurally, ependymal cells are specialized for the propulsion of CSF, which helps redistribute and dilute local concentrations of toxins and metabolites (Del Bigio, 1995). Ependymal cells extend multiple motile (9+2) cilia from their apical surface into the ventricles (Bruni, 1998). Through coordinated, planar-polarized beating of these cilia across the epithelium, ependymal cells generate directed cerebrospinal fluid (CSF) flow in the ventricles (Ibanez-Tallon et al., 2004; Sawamoto et al., 2006; Worthington and Cathcart, 1963) and help maintain CSF homeostasis (Cathcart and Worthington, 1964).

Although there are functional assays for the planar polarity of ependymal cells, which measure the orientation of fluid flow across the epithelium (Ibanez-Tallon et al., 2004; Sawamoto et al., 2006), to date there are no anatomical correlates within these cells indicative of their planar polarity. In other multiciliated epithelia, such as the lining of the quail oviduct (Boisvieux-Ulrich et al., 1985), the mammalian respiratory tract (Satir and Dirksen, 1985), or the *Xenopus* larval skin (Mitchell et al., 2007), the basal foot, an accessory structure of the basal body (discussed below), points in the direction of the ciliary beat. It remains to be determined whether this basal body accessory is also an indicator of the planar polarity of ependymal cells.

Recent studies have shown that both ependymal cells (Spassky et al., 2005) and SVZ Type B cells (Merkle et al., 2004) are derived from radial glia (discussed below), providing evidence of continuity between the embryonic and adult germinal niches. The epithelial organization of ependymal cells, including their apical-basal polarity and perhaps their planar polarity, is likely inherited from their radial glial progenitors. In radial glia undergoing differentiation into ependymal cells, ultrastructural analyses reveal the presence of deuterosomes, electron-dense spheres of material in the supranuclear or apical compartment of the cell, used to build multiple basal bodies (Dawe et al., 2007; Spassky et al., 2005). The nascent basal bodies then migrate to the apical surface of the formerly uni-ciliated (9+0) radial glial cell, where they nucleate multiple (9+2) cilia (Jose Manuel García-Verdugo, personal communication). While it has not been tested whether ependymal cells also acquire planar polarity information from their

radial glial progenitors, evidence from other multiciliated epithelia, such as the Xenopus larval skin (Tung and Y-F., 1940; Twitty, 1928) or the quail oviduct (Boisvieux-Ulrich and Sandoz, 1991), suggests that the establishment of planar polarity precedes multiciliated cell differentiation. Interestingly, a recent study of hair cells in the mammalian cochlea suggests that the primary cilium may relay planar polarity signals from the cell membrane to the cytoskeleton (Jones et al., 2008). Determining whether radial glia are planar polarized, and if and how they transmit planar polarity information, perhaps via the primary cilium, to their ependymal progeny are provocative and unresolved questions.

Cilia and Basal Bodies

Cilia are hair-like cell surface projections that are bounded by membrane and composed of a microtubule cytoskeleton. However, the cilium and its membrane are not simply extensions of the cytoplasm and the plasma membrane. Cilia are specialized organelles that have diverse functions and have recently been recognized as the basis of various human diseases including primary ciliary dyskinesia, polycystic kidney disease, Bardet-Biedl syndrome, retinal degeneration and neural tube defects (Bisgrove and Yost, 2006; Marshall, 2008). Cilia are generally divided into two different types, (9+2) and (9+0), based on the structure of their microtubule cytoskeleton, called the ciliary axoneme (Satir and Christensen, 2007). (9+2) axonemes consist of a ring of 9 doublet microtubules surrounding a central pair of singlet microtubules, whereas (9+0) axonemes lack the central pair (**Fig. 5a**). These two types of cilia are found in different tissue types and have different basic functions. (9+2) cilia are found, up

to 200-300 per cell, on multiciliated epithelial cells lining the respiratory airway, the oviduct, and the ependymal lining of the brain ventricles, where they beat to propel mucus or fluid along the epithelium. A single (9+2) cilium propels the sperm cell. In addition to their microtubule cytoskeleton, the axonemes of (9+2) cilia have associated molecular motors, the axonemal dyneins (Gibbons and Rowe, 1965). These motors form the inner and outer dynein arms (**Fig. 5a**), which extend from one doublet to the next around the ring, acting to slide one doublet with respect to the other (Satir, 1965; Satir and Christensen, 2007; Summers and Gibbons, 1971). This is called doublet sliding and it is the basic motion underlying ciliary motility (Lindemann, 2004). (9+0) cilia, also called primary cilia, are found one per cell on almost all vertebrate cell types (Singla and Reiter, 2006). These cilia, with the exception of nodal (9+0) cilia found in the embryonic node (Nonaka et al., 1998), do not have the associated molecular motors required for doublet sliding and are immotile (Satir and Christensen, 2007).

The ciliary axoneme is constructed from a template provided by the basal body, which has a ring of 9 triplet microtubules (**Fig. 5b**) (Anderson, 1972; Bettencourt-Dias and Glover, 2007; Dawe et al., 2007). The basal body is nearly identical to the centriole, an important component of the mitotic spindle apparatus (Bornens, 2002; Rieder et al., 2001) (**Fig. 5c**). During interphase, the centriole acquires several accessory structures and docks at the plasma membrane, where it nucleates the axoneme (Dawe et al., 2007). Accessory structures of the basal body include the striated rootlet, which emanates from the proximal end of

the basal body and extends longitudinally into the cytoplasm, and the basal foot, a single laterally projecting cone-shaped structure (**Fig. 6**) (Anderson, 1972). The basal foot bestows rotational asymmetry to the basal body. As discussed above, in several multiciliated epithelia, the basal foot points in the direction of the ciliary beat (Boisvieux-Ulrich et al., 1985; Mitchell et al., 2007; Satir and Dirksen, 1985) and is a structural basis of the planar polarity in these epithelial cells. Structural specializations are also found at the distal end of the basal body where it meets the ciliary axoneme. These include the terminal plate and transition fibers (Anderson, 1972; Bettencourt-Dias and Glover, 2007). It has been suggested that these structures form a molecular sieve that restricts the entry of proteins into the cilium. In addition, no protein synthesis occurs within the cilium.

Construction of the axoneme therefore requires a specialized intracellular trafficking system called intraflagellar transport (IFT) (Rosenbaum and Witman, 2002). IFT shuttles ciliary components between the cell body and the tip of the cilium in large complexes, called IFT particles, carried by microtubule-based motors. This transport occurs in both the anterograde and retrograde directions (Marshall and Rosenbaum, 2001; Qin et al., 2004). Anterograde transport, driven by the heterotrimeric motor kinesin-2 (Kozminski et al., 1995), moves axonemal components from the cell body to the distal tip of the cilium, where the axoneme is assembled. Retrograde transport, driven by an isoform of cytoplasmic dynein called dynein 2 (or dynein 1b) (Pazour et al., 1998), returns turnover products to the cell body. An understanding of IFT and its role in

ciliogenesis has been instrumental to recent functional studies of primary (9+0) cilia. Mouse mutants for IFT motors (*Kif3a*, a subunit of kinesin-2) and IFT particle subunits (*Ift88, Ift172*) have revealed that primary (9+0) cilia are essential for mammalian development (Huangfu et al., 2003; Marszalek et al., 1999; Takeda et al., 1999).

The primary cilium is now understood to play a central role in several developmental signaling pathways, including Hedgehog and Wnt signaling (Singla and Reiter, 2006). Hedgehog signaling requires the primary cilium for both activation and repression of the pathway (Haycraft et al., 2005; Huangfu and Anderson, 2005; Huangfu et al., 2003; Liu et al., 2005; May et al., 2005). Several essential components of the pathway, including patched (Rohatgi et al., 2007), smoothened (Corbit et al., 2005), and the gli transcription factors (Haycraft et al., 2005), are concentrated in the cilium. In addition, a recent study showed that Hedgehog signaling through the primary cilium was required for the establishment of adult neural stem cells in the dentate gyrus of the hippocampus (Han et al., 2008). Wnt signaling, which diverges into at least two pathways, the canonical (β-catenin dependent) pathway and the non-canonical (planar cell polarity or PCP) pathway (Logan and Nusse, 2004; Veeman et al., 2003), also appears to be regulated by the primary cilium. These two pathways diverge at the level of the Wnt pathway protein Dishevelled (Dsh); cytoplasmic Dsh functions in the canonical pathway while membrane-bound Dsh functions in the non-canonical PCP pathway (Axelrod et al., 1998). A recent study showed that inversin, which localizes to primary cilia, acts as a switch from the canonical to

the non-canonical pathway by targeting cytoplasmic Dsh for degradation (Simons et al., 2005). Several additional studies, in the kidney (Lin et al., 2003), the pancreas (Cano et al., 2004), and in mouse embryos and embryonic stem cells (Corbit et al., 2008), have supported the conclusion that the primary cilium normally suppresses canonical Wnt signaling. Disrupting ciliogenesis in these systems results in hyper-activity of the canonical Wnt pathway. In addition, disrupting the primary cilium leads to PCP defects, such as misalignment of cochlear stereociliary bundles and an open neural tube due to failed convergent extension (Jones et al., 2008; Ross et al., 2005). Interestingly, disrupting the PCP pathway in Xenopus results not only in planar polarity defects, but also defects in ciliogenesis and consequently, Hedgehog signaling (Park et al., 2006). The primary cilium has therefore been likened to an antenna, where several intercellular signaling pathways intersect (Eggenschwiler and Anderson, 2007; Singla and Reiter, 2006).

SVZ Type B cells are derived from Radial Glia

Radial glia, the embryonic neural stem cells, transform into astrocytes (Schmechel and Rakic, 1979; Voigt, 1989) and ependymal cells (Spassky et al., 2005) shortly after birth. In the lateral wall of the LV, these cells (striatal radial glia) persist for approximately one week postnatally. They can be identified by their radial morphology, ultrastructure, and their expression of RC2 (Merkle et al., 2004). In addition, these neonatal radial glia exhibit the typical properties of interkinetic nuclear migration (Tramontin et al., 2003). In contrast, there are no SVZ astrocytes observed in the lateral wall of the LV at birth. Over the course of

the first week, RC2 expression and radial glial morphology gradually disappears and is replaced by the expression of GFAP and S100B, markers of SVZ astrocytes and ependymal cells, respectively (Merkle et al., 2004; Spassky et al., 2005). Although the transformation of radial glia into parenchymal astrocytes had been shown (Schmechel and Rakic, 1979; Voigt, 1989), definitive evidence was lacking that radial glia also generate SVZ astrocytes, the Type B cells that function as adult neural stem cells. To provide this evidence, Merkle et al. (Merkle et al., 2004) traced the lineage of neonatal striatal radial glia in Z/EG mice, a Cre reporter transgenic line. Z/EG mice carry a constitutively-expressed transgene encoding lacZ and a STOP cassette, flanked by loxP sites, followed by enhanced GFP (eGFP). Cre-mediated excision replaces the expression of lacZ with eGFP, providing a permanent labeling of cells and their progeny. To specifically label only radial glial cell bodies in the striatal VZ, adenovirus expressing Cre was injected into the ventrolateral striatum of neonatal Z/EG mice. This resulted in infection of local striatal neurons and radial glial processes that passed through the injection site. Because adenovirus is efficiently retrogradely transported in the radial process to the radial glial cell body, this resulted in permanent labeling of radial glia in the lateral wall of the lateral ventricle. Importantly, radial glia were the only cell types in the lateral wall labeled by this method, confirmed by electron microscopy at 2 days after injection. At longer survivals, labeled radial glia had produced labeled SVZ Type B cells, which were shown to behave like neural stem cells in vitro and generate C cells, A cells and olfactory bulb interneurons in vivo. Control experiments

demonstrated that viral diffusion was limited to a small area around the injection site and that infective viral activity disappeared in less than an hour after infection, confirming that Type B cells were not labeled directly. In addition, transplantation experiments confirmed that labeled radial glia, not labeled striatal cells at the injection site, were the progenitors of the Type B cells. These experiments provided a unified view on the lineage of neural stem cells as belonging to a radial-astroglial lineage.

Evidence for Apical-Basal Polarity of Type B cells

The finding of a continuous lineage of radial-astroglial neural stem cells for the embryonic and adult brain suggests that SVZ Type B cells, like ependymal cells, may inherit apical-basal polarity and epithelial organization from their radial glial progenitors. There are several additional clues that SVZ Type B cells may be organized into a specialized epithelium. One clue comes from early experiments aimed at identifying the neural stem cells in the adult SVZ. Following Ara-C treatment, it was observed that a few Type B cells made apical contact with the ventricle (Doetsch et al., 1999b). This contact occurred through an apical extension interposed between ependymal cells. Often, a primary cilium was observed extending from the apical surface into the ventricular lumen. Type B cells in contact with the ventricle were rarely observed in untreated animals. It was inferred from these experiments that ventricular contact may be an indication of an “activated” Type B cell, stimulated to regenerate the SVZ. In addition to Ara-C treatment, other methods of SVZ stimulation, including intraventricular infusions of epidermal growth factor (EGF) (Doetsch et al., 2002) or activation of

Ephrin B signaling (Conover et al., 2000), also result in increased numbers of Type B cells making apical contact with the ventricle. This apical contact, including the extension of a primary cilium into the ventricle, is reminiscent of the apical ventricular contact of NE and radial glial cells in the embryo and suggests that at least some Type B cells have the potential to form apical specializations. However, it was not known whether this was an induced, transient organization or a stable property of Type B cells. In addition, since all these studies relied on EM to identify the apical structures, it was difficult to quantify or provide a comprehensive view on the relationship of Type B cells touching the ventricle to other cells within this region.

In the embryonic brain, the apical membrane domain of NE and radial glial cells is segregated from the basolateral membrane by adherens and tight junctions located just beneath the apical ventricular surface (Aaku-Saraste et al., 1996; Chenn et al., 1998; Kosodo et al., 2004). The basal compartment of these cells is readily identified by the radial fiber and its basal contacts with both cortical blood vessels and pial basal lamina (Alvarez-Buylla et al., 1987; Halfter et al., 2002; Haubst et al., 2006; Misson et al., 1988; Noctor et al., 2001). It has been shown that soluble factors secreted by endothelial cells promote stem cell self-renewal and enhance neuronal production of both embryonic VZ and adult SVZ neural stem cells in vitro (Shen et al., 2004). Type B cells of the SVZ may therefore be regulated by factors in and around blood vessels similar to their radial glial progenitors (Jackson et al., 2006; Jiang et al., 1998; Kerever et al., 2007; Shingo et al., 2003). Recent evidence shows that an extensive network of

blood vessel basal lamina infiltrates the adult SVZ neurogenic niche and makes contact with various SVZ cell types and astrocytic processes (Alvarez-Buylla and Lim, 2004; Mercier et al., 2002). This suggests that Type B cells may also have basal membrane domains in contact with basal lamina. It is intriguing that vascular development in the embryonic brain begins at the pial surface and progresses inward towards the ventricles. Could this outside-in pattern mean that adult Type B cells and embryonic radial glia have a topologically equivalent interaction with blood vessel basal lamina? Interestingly, SVZ astrocytes in the ventral part of the adult LV have a long GFAP+ basal process that extends deep into the parenchyma (Sundholm-Peters et al., 2004). This is likely a remnant of the radial glial fiber. Radial glial morphology can also be re-induced in some adult SVZ astrocytes of the pallial wall of the LV by re-expression of ErbB2, one of the EGF receptors (Ghashghaei et al., 2007). These data suggest that Type B cells retain apical-basal polarity information, derived from their radial glial progenitors, and that they may also have an underlying epithelial organization.

In the chapters that follow, I will describe the work I have done that demonstrates that Type B cells in the adult neurogenic germinal niche do maintain apical-basal polarity and an epithelial organization. In particular, my work focuses on the apical structures of cells lining the walls of the adult ventricular system, including type B cells, multi-ciliated ependymal (Type E1) cells, and a novel type of ependymal cell identified as Type E2 cells. In contrast to the previous notion that Type B cells occupy a position in the sub-ventricular or sub-ependymal zone, I have shown that most, if not all, of these cells (also

referred to as Type B1 cells) have a small apical surface in contact with the lateral ventricle that is difficult to discern in thin sections but is readily observed in wholemounts of the lateral wall. This apical surface is much smaller than that of E1 and E2 cells and is also distinguished from ependymal cells by the presence of a single basal body associated to a primary cilium. Apical surfaces of Type B cells are encircled by apical surfaces of ependymal cells forming “pinwheels,” a previously unappreciated organization of the ventricular surface that incorporates not only ependymal cells, but also the adult neural stem cells into a single epithelium. In addition to apical contact with the ventricle, I have found that Type B cells have a long GFAP+ basal process that terminates in an endfoot on blood vessels. These ventricle-contacting Type B cells are derived from radial glia and in fact, appear to be modified radial glia; the long basal process may be a remnant of the radial fiber, suggesting that the basal contact with blood vessels is topologically equivalent to the pial contact of the radial fiber. Finally, I have characterized an anatomical correlate to the planar polarization of Type E1 cells, which was previously only assayed functionally by measuring the flow of fluid across the ventricular surface. Specifically, the basal bodies of Type E1 cells are polarized to one side of the cell’s apical surface across the epithelium, corresponding to the “downstream” side of the cell with respect to CSF flow and the ciliary active stroke. I found that the planar polarization of the basal bodies does not require the presence of motile (9+2) cilia of E1 cells. Altogether, this work advances our previous understanding of the largest germinal niche in the

adult brain by demonstrating that it is, like the embryonic germinal niche, organized into an epithelium.

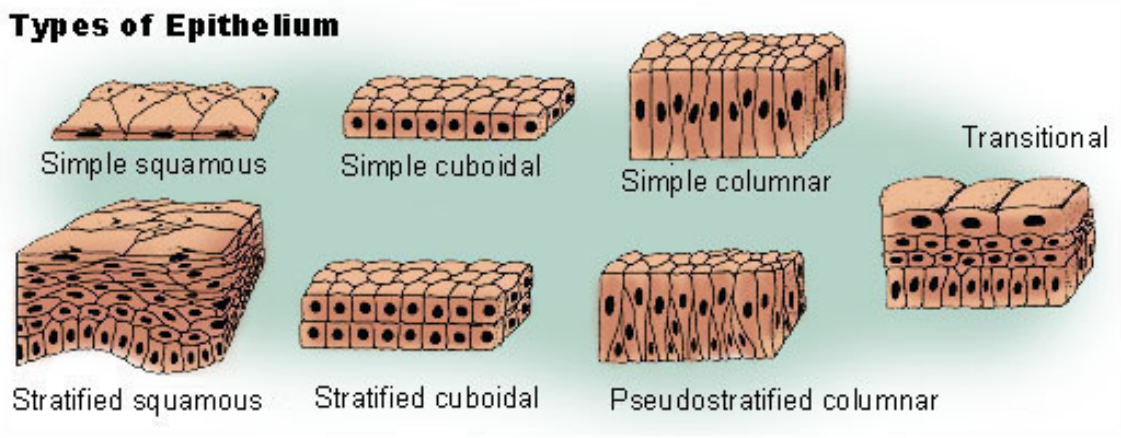


Fig. 1. Different types of epithelium. Epithelia may consist of a single layer of cells (simple), multiple layers of cells (stratified), or a single layer of cells that appears stratified due to apical-basal differences in nuclear position (pseudostratified). Different epithelia consist of cells of different shapes, including squamous (or flat), cuboidal, and columnar.

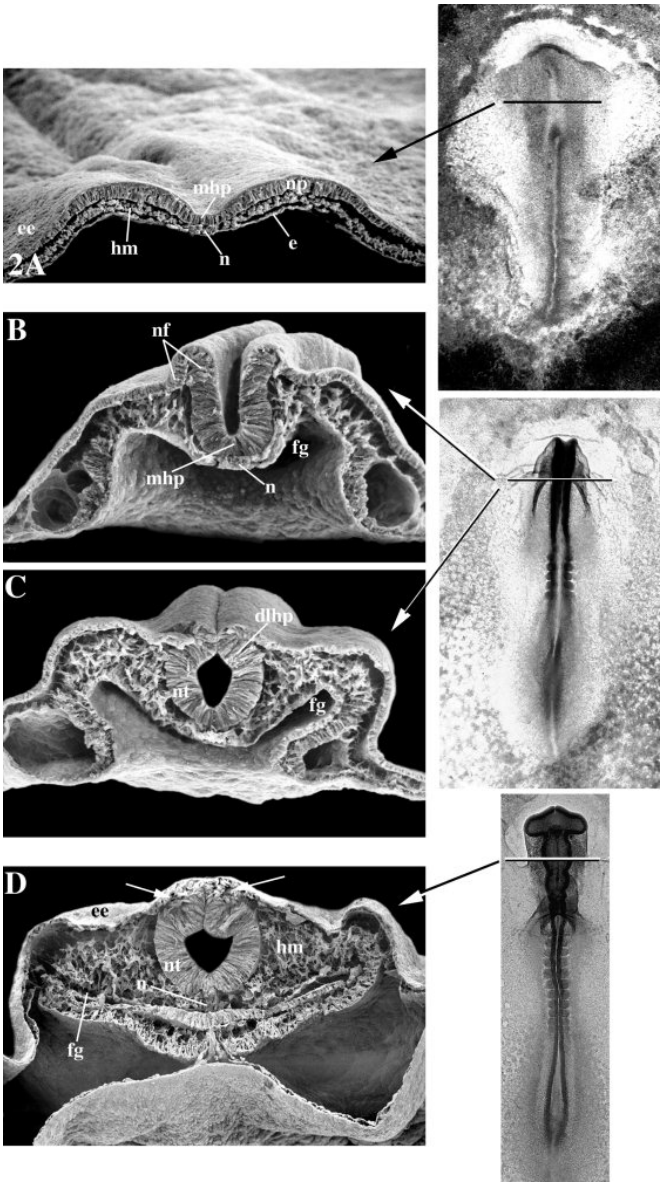


Fig. 2. Neural tube formation in chick embryos. Wholemounts at right indicate level of transverse sections at left, viewed with scanning electron microscopy.

A. Flat neural plate stage. Early bending is seen at the midline, where the median hinge point (mhp) is located. Note the laterally located epidermal ectoderm (ee) is continuous with the neural plate (np).

B. Neural groove stage. Bending of the neural plate, as well as convergent extension movements (see Fig. 3) of NE cells, have brought together elevating lateral folds (neural folds) of the neuroepithelium.

C. Incipient neural tube stage. The neural folds are in contact with one another but have not yet fused.

D. Definitive neural tube stage. The neural folds have largely fused and formed the roof of the neural tube. The epidermal ectoderm, overlying the neural tube, has also come together and fused at the dorsal midline of the embryo. Adapted from Colas & Schoenwolf (2001).

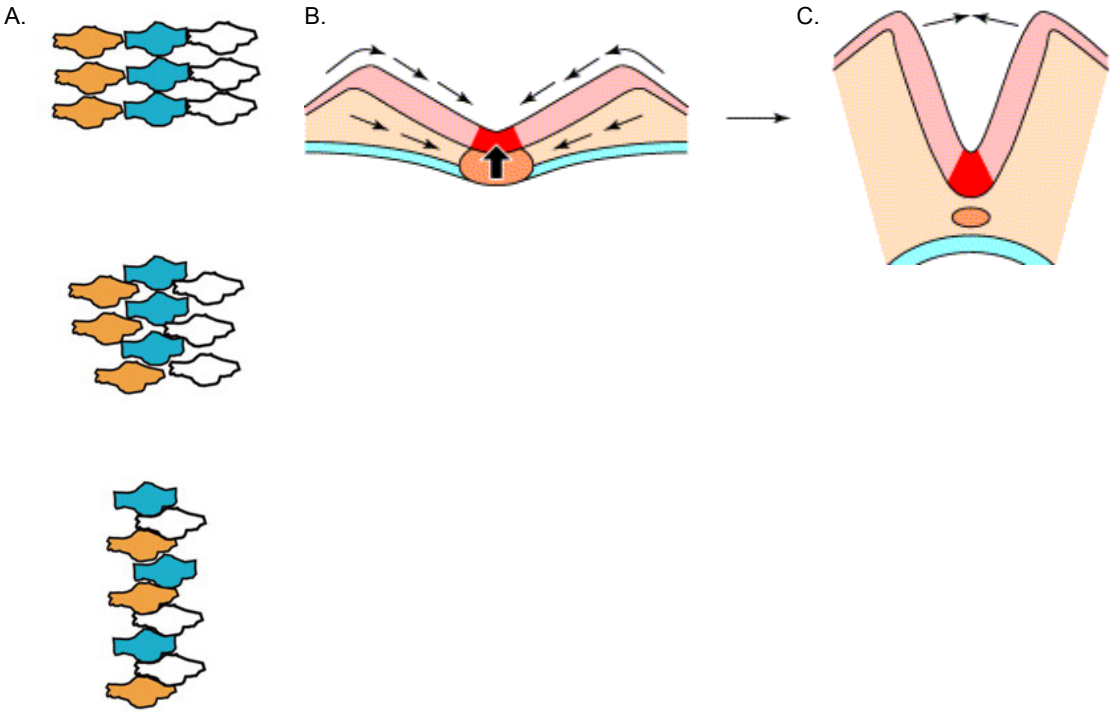


Fig. 3. Convergent extension of NE cells is essential for neural tube closure.

A. Diagram of NE cells intercalating in the neural plate. This intercalation is called convergent extension, a polarized cell movement within the plane that simultaneously narrows and elongates the epithelium.

B. Diagram of a transverse section of the embryo showing the neural plate (pink and red). Thin arrows show convergent extension with net cell movement of NE cells towards the midline (red).

C. Convergent extension at the midline helps to bring the elevating neural folds together. Adapted from Wallingford J.B. (2006) and Copp et al. (2003).

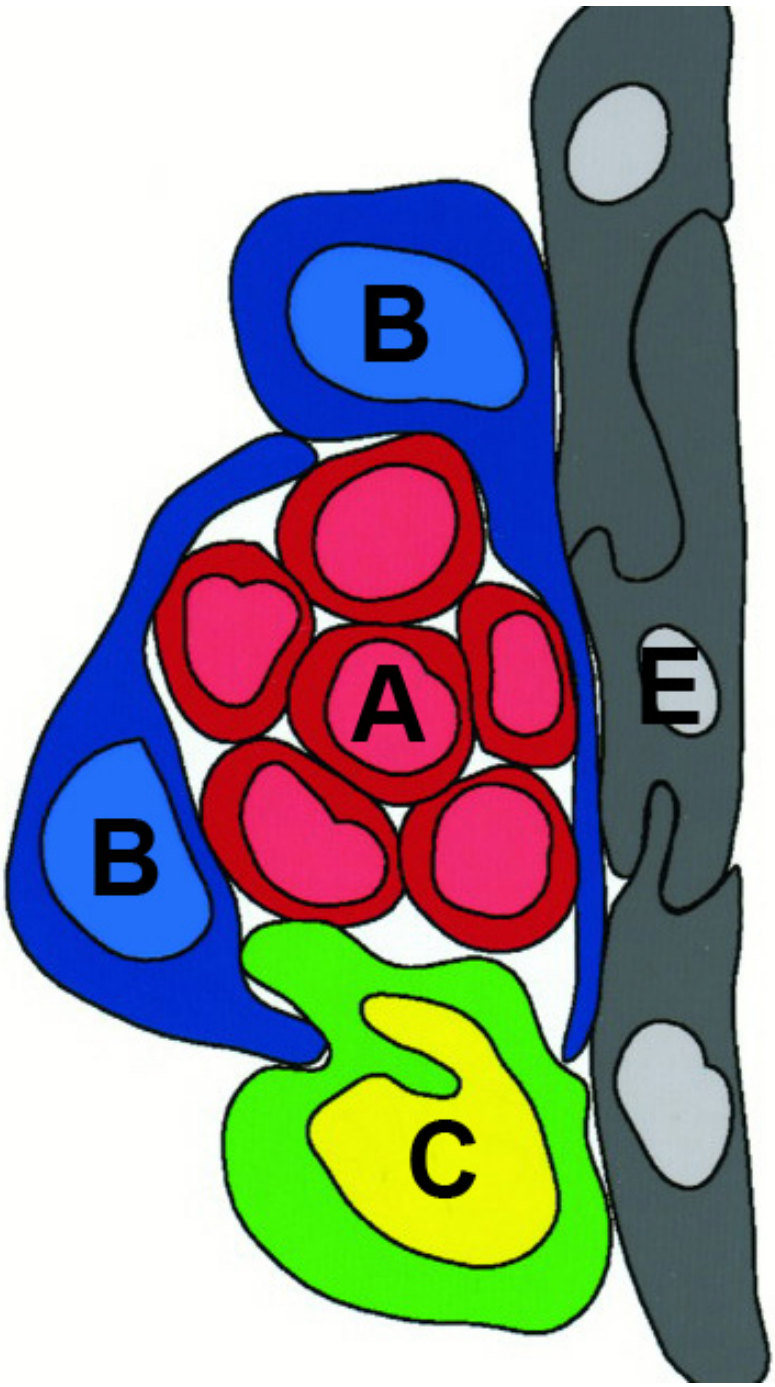


Fig. 4. Cell types and cytoarchitecture of the adult SVZ.

Ependymal (E) cells (gray) line the lateral ventricle. Beneath the monolayer of E cells, three additional cell types (B, C, A) are located in the SVZ. Type B cells (blue) are adult neural stem cells that generate migratory neuroblasts (A cells, red) through an intermediate progenitor (C cell, green). Type B cells form glial tubes that ensheath chains of migrating A cells destined for the olfactory bulb. Adapted from Doetsch et al. (1997).

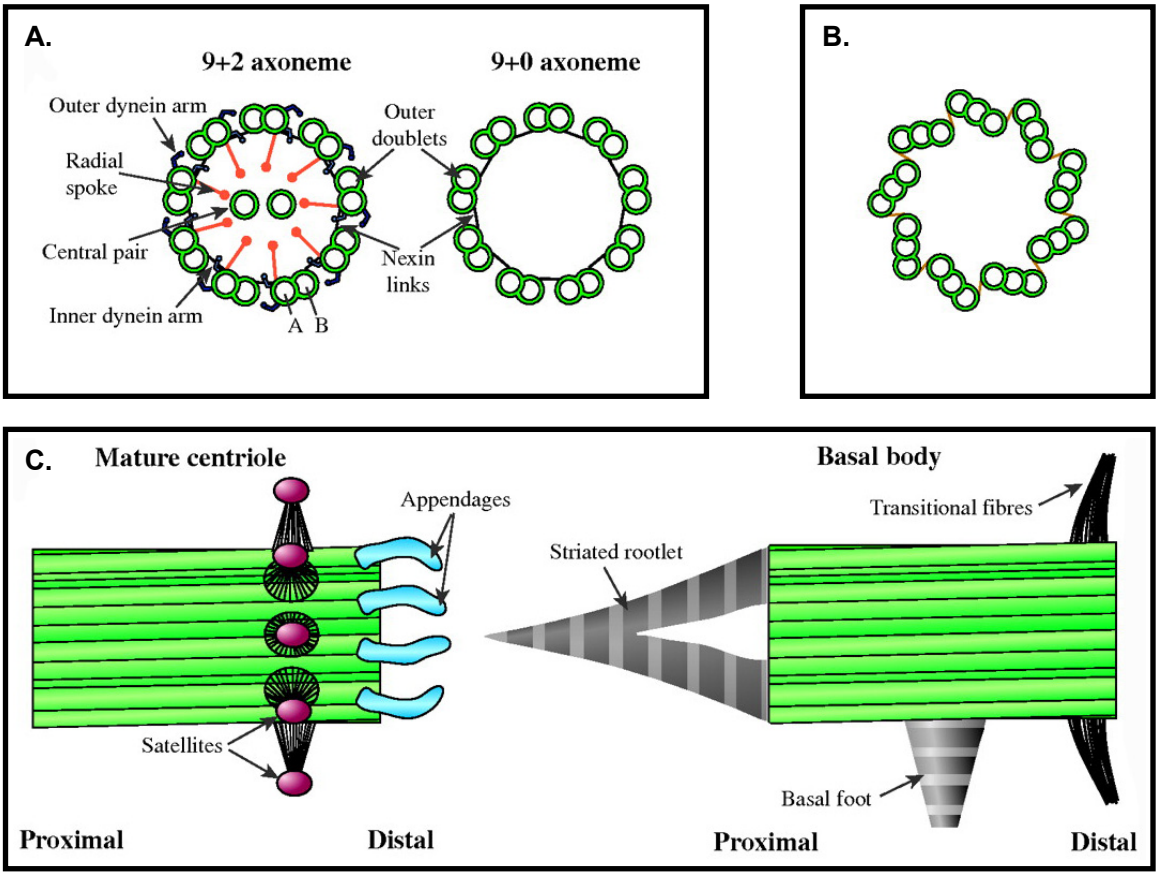


Fig. 5. Axonemal structure of cilia and basal bodies.

A. Cross-section of (9+2) and (9+0) axonemes. (9+2) axonemes have a ring of 9 doublet microtubules (A and B tubules) surrounding 2 central singlet microtubules. (9+0) axonemes lack the central pair of microtubules. (9+2) axonemes also have associated molecular motors, the inner and outer dynein arms, which are required for ciliary motility and radial spokes, which regulate ciliary bending.

B. Cross-section of a basal body, showing a ring of 9 triplet microtubules.

C. Longitudinal views comparing a mature centriole and a basal body. Note the accessory structures of the basal body, including a single basal foot, the striated rootlet which extends away from the proximal end of the basal body, and transition fibers at the distal end. Adapted from Dawe et al. (2007).

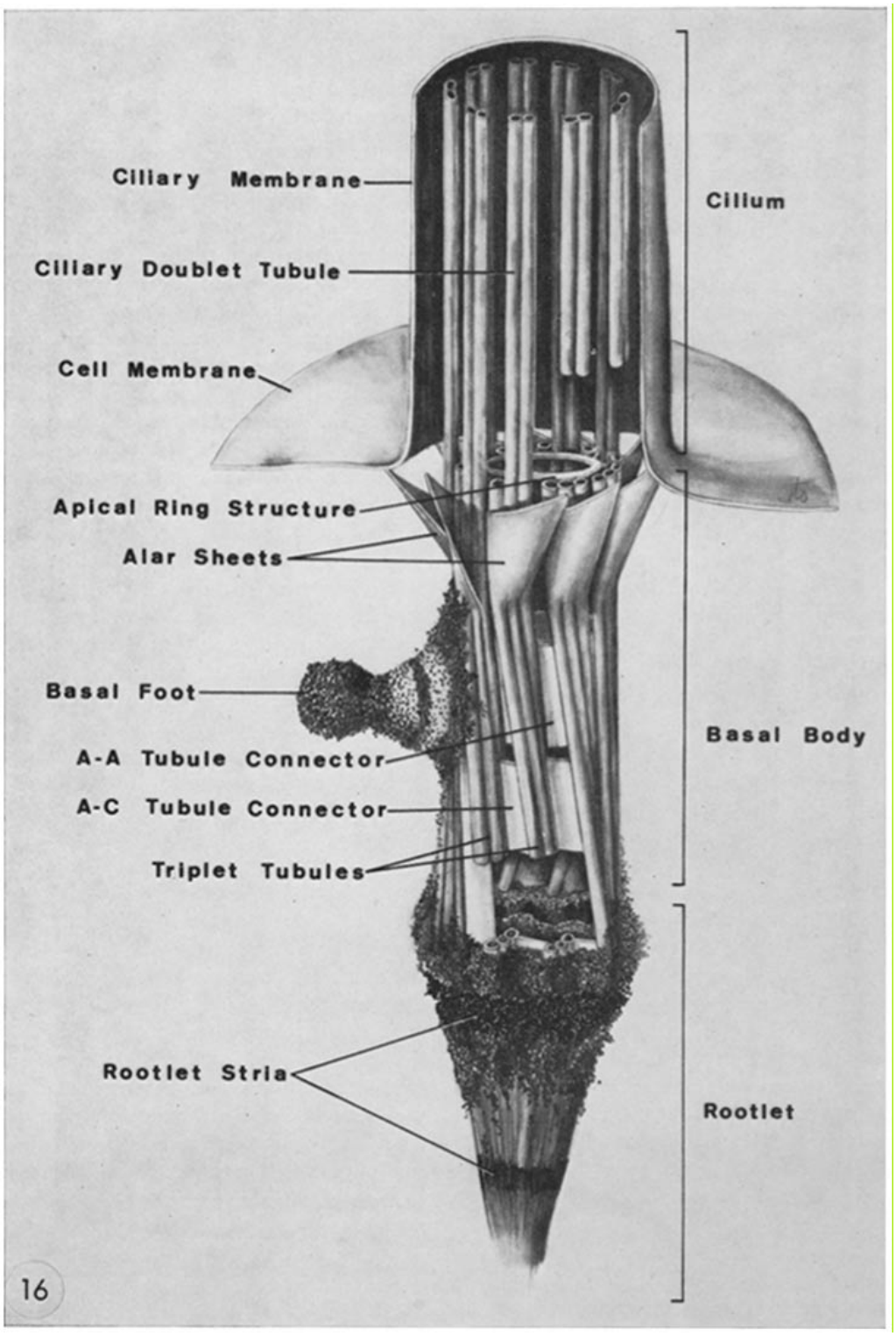


Fig. 6. Three-dimensional drawing of the basal body illustrating the relationship with the cilium. Accessory structures of the basal bodyinclude the striated rootlet (”Rootlet Stria”), emanating from the proximal end of the basal body and tapering into the cytoplasm, the basalfoot, which bestows rotational asymmetry to the basal body, and the transition fibers, referred to as “Alar Sheets” in this drawing. Drawing from Anderson R.G. (1972).

Chapter 2

Materials and Methods

Section 1: Animals and Stereotactic Viral Injections

Animals

All experiments were performed on mice according to the guidelines put forth by the University of California, San Francisco Laboratory Animal Care and Use Committee. Mouse strains are described in Table 1.

Table 1. Mouse strains and relevant information.

Strain	Ref.	Description	Use in this study
CD1	N/A	Outbred wild-type from Charles River	Descriptive analyses of cell types touching the ventricles and of ependymal planar polarity
Z/EG	(Novak et al., 2000)	carry a transgene encoding lacZ and a STOP cassette, flanked by loxP sites, followed by enhanced GFP (eGFP), all under control of the CMV enhancer/ chicken βactin promoter; Cre excision replaces lacZ with eGFP expression	adult lateral ventricle injections of Ad-GFAPp::Cre to label Type B1 cells; neonatal striatal injections of Ad:Cre to label radial glia; crossed to *hGFAP::Cre* mice to determine Cre activity
R26R	(Soriano, 1999)	Knock-in of a floxed STOP cassette followed by lacZ into the *Rosa26* locus; Cre excision results in constitutive lacZ expression	crossed to *hGFAP::Cre* mice to determine Cre activity

hGFAP ::Cre	(Zhuo et al., 2001)	Transgenic mice expressing Cre under the human GFAP promoter	Crossed with *Kif3a*$^{fl/fl}$ mice to ablate cilia in ependymal cells
Kif3a$^{fl/fl}$	(Marszalek et al., 2000)	Knock-in of loxP sites flanking exon 2 of *Kif3a*, a subunit of kinesin-2 motor essential for ciliogenesis	See above
FoxJ1:: Cre	(Zhang et al., 2007)	Transgenic mice expressing Cre under the FoxJ1 promoter; drives expression in multiciliated cells	Crossed with Z/EG mice to label ependymal cells

Construction of Ad-GFAPp::Cre virus (relevant to Chapter 3 only)

To specifically and permanently label GFAP+ cells and their progeny in conditional (Cre) reporter mice, we made an adenovirus in which Cre was placed under the control of the mouse GFAP promoter (GFAPp) (Merkle et al., 2007), which has been previously confirmed to be specifically active in GFAP+ cells (Doetsch et al., 1999). The NLSCre fragment was removed from βactin::Cre plasmid (Lewandoski et al., 1997) with SalI and EcoRI and ligated into SalI and EcoRI digested pCI vector (Promega). NLSCre was then released from pCI vector with SalI and XhoI and ligated into XhoI digested adenoviral transfer plasmid pAd5-GFAPp (Doetsch et al., 1999), which contains the 2.5 kb mouse GFAP promoter region. The resulting plasmid was cut with NotI, then filled in and partially digested with EcoRV to release the GFAPp::NLSCre construct, which was then ligated into XmnI digested pENTR11 plasmid (Invitrogen) 5' of a previously inserted BGH polyA sequence. The resulting GFAPp::NLSCre-pA fragment was then transferred from pENTR11 into pAd/PL-DEST using LR clonase (Invitrogen). This created pAd/PL-GFAPp::NLSCre-pA, which contains

the wild-type Ad5 genome deleted for E1 and E3. This vector was then transfected into HEK293 cells to produce replication-incompetent adenovirus (pAd5-GFAPp::NLSCre or Ad:GFAPp::Cre), which was purified twice by cesium chloride banding. The final titer was 1 x 10^{12} particles/ml.

Stereotactic Viral Injections of Adult and Neonatal Mice (relevant to Chapter 3 only)

For adult injections, Z/EG mice (P60-P120) were anesthetized with 250 mg/kg tribromoethanol (Avertin) until pedal reflex was abolished, and placed in ear bars on a stereotactic injection rig. After making a small incision in the scalp, a small hole was drilled into the skull at the injection coordinate to expose the brain surface. A pulled glass micropipette (30° bevel, taper point to tip distance ~10 mm) loaded with virus was then lowered to the desired depth within the brain where virus was injected. Stereotactic injection coordinates (x, y, z) were zeroed with x (anterior-posterior) and y (medial-lateral) relative to bregma and z (depth) relative to the brain surface. Lateral ventricle injections of 100 nl (*in vivo* experiments) or 500 nl (*in vitro* experiments) of Ad-GFAPp::Cre (Merkle et al., 2007) were performed at stereotactic coordinates (0 AP, 0.9 L, 1.9 D).

Striatal targeting of radial glia at P0 was performed as described in (Merkle et al., 2004). Briefly, neonatal Z/EG mice were anesthetized by hypothermia (60 seconds on ice) and then placed on the platform of a stereotactic injection rig with their head secured in a customized head mold. Injections were made using a pulled glass micropipette (30° Bevel, taper point to

tip distance ~5 mm) at an angle of 45° from above the head. The glass micropipettes pulled for neonatal injections are made differently (shorter and stronger) than those for adult injections because these are inserted directly through the scalp and skull of the neonate. Injection coordinates (x, y, z) were zeroed in the following way: x (anterior-posterior) centered on the eyeball, y (medial-lateral) centered on the midline, and z (depth) centered on the skin surface. To infect radial glial fibers in the ventrolateral striatum, adenovirus expressing Cre was injected at coordinates (1.6, 2.8, -1.6).

Section 2: Tissue processing and cell culture

Wholemount dissection

Sequential stereomicroscopic images taken during dissection of a wholemount of the lateral wall of the lateral ventricle are shown in Chapter 3:Supplementary Figure S1. After cervical dislocation, the brain was extracted fresh and placed on a dissection dish in L-15 Leibovitz media warmed to 37°C. The olfactory bulbs were dissected away from the brain and immersion-fixed in 4% paraformaldehyde (PFA) with 0.1% Triton-X100 overnight at 4°C. After separating the hemispheres, a coronal cut was made at the posterior-most aspect of the interhemispheric fissure, allowing the caudal hippocampus to be visualized in cross-section. The hippocampus was then released from the cortex both dorsally and ventrally with small cuts using a 22.5° microsurgical stab knife (Sharpoint ref. 72-2201). Next the hippocampus was pulled towards midline, which opened the caudal part of the lateral ventricle and allowed the lateral wall

and choroid plexus to be visualized. The hippocampus and more rostrally located septum, which comprise the bulk of tissue underlying the medial wall of the lateral ventricle were then pulled forward and spread apart from the lateral wall and underlying striatum. To further separate the medial and lateral walls anteriorly, small cuts were made dorsally and ventrally where the two walls are joined and again the medial wall was pulled forward. These steps were reiterated until the most anterior part of the lateral ventricle was visualized where the lateral and medial walls come together. Dissecting at this anterior tip of the ventricle released the medial wall from the lateral wall. To further expose the surface of the lateral wall, the thalamus and overlying dorsal cortex were removed. The dissected lateral and medial walls were immersion-fixed in 4% PFA with 0.1% Triton-X100 in a 24-well plate overnight at 4°C, being careful to keep the ventricular surface facing up, away from the walls of the well.

For confocal microscopy of immunostained wholemounts, the lateral and medial walls were further dissected from underlying striatum and septum, respectively, as slivers of tissue 200-300 um in thickness. For the lateral wall, the tissue was placed in a dissection dish in PBS and the overlying cortex was completely removed allowing visualization of the interface between the striatum and SVZ from above. Following the contours of the ventricular surface, the lateral wall was then dissected away from the striatum from anterior to posterior. The sliver of tissue was then mounted on a slide with mounting media and a coverslip.

<u>Ependymal flow movies (relevant to Chapter 4 only)</u>

To determine the orientation of fluid flow across the ependymal epithelium lining the walls of the lateral ventricle, we examined the movement of fluorescent microbeads (2 um) deposited on the surface of acutely dissected wholemounts. First, we freshly dissected wholemounts of the lateral wall (or medial wall) of the lateral ventricle and placed them in 37°C Leibovitz media under a fluorescent stereomicroscope. Then, a glass micropipette filled with the fluorescent microbeads and attached to a micromanipulator was lowered onto the wholemount, where microbeads were ejected onto the surface. We recorded the flow of microbeads using a Retiga 2000R high speed digital camera plugged into OpenLab imaging software (Improvision), with an acquisition rate of 10 frames per second.

Sectioning, X-gal staining, and Hematoxylin staining (relevant to Chapter 4 only)

After transcardial perfusion of normal saline followed by 4% PFA, the brain was extracted from the skull and post-fixed in 4% PFA for 1 hour at 4°C. Although for immunostaining, brains can be left in postfix overnight at 4°C, for X-gal staining this should not be done because β-galactosidase enzyme activity is sensitive to PFA. After post-fixation, the brain was washed in PBS 3 times, 5 minutes each, and then cryoprotected in 30% sucrose overnight at 4°C. The following day, sunken brains (embedded with sucrose) were removed from the sucrose solution and placed in Tissue-Tek optimal cutting temperature solution (OCT) in 1 inch square plastic molds for 1 hour at 4°C. The brains were then transferred to a new mold with fresh OCT and frozen on a block of dry ice. The 1 hour pre-incubation in OCT is important to remove excess sucrose from the brain

surface, which otherwise would not allow the OCT to freeze intimately against and hold the brain during sectioning. Sections were cut at 12 um onto SuperFrost plus slides (Fisher) using a cryostat and stored at -80°C for months. However, for best results, X-gal staining should be performed as soon as possible because there is a slow decay in β-galactosidase activity. For X-gal staining, sections were first post-fixed on slides in 4% PFA for 5 minutes at room temperature (RT), and then washed 3 x 5 minutes in PBS, before immersion into X-gal. X-gal buffer contained 120 ul X-gal solution, 20 ul MgCl solution, 0.5 ml K3 solution, 0.5 ml K4 solution, brought to 10 ml with 0.1 M PB. X-gal solution was made by dissolving 200 mg X-gal in 5 ml dimethylformamide and is stored in dark at -20°C. MgCl solution was made by dissolving 0.95 g MgCl in 10 ml ddH2O. K3 and K4 solutions were made by dissolving 1.646 g K^+ ferricyanide or 2.112 g K^+ ferrocyanide in 50 ml 0.1 M PB, respectively. MgCl, K3, and K4 solutions are stored in the dark at RT. All solutions (X-gal, MgCl, K3, and K4) were filter sterilized for long term storage. Sections were immersed in X-gal buffer at 37°C and monitored for development of blue precipitate (30 minutes to overnight). X-gal reaction was stopped by washing 3 x 5 minutes in PBS. Slides were then cover-slipped with Aqua Poly/ Mount.

For Hematoxylin staining, sections were postfixed on slides as above and then immersed in filtered Hematoxylin solution (Harris formula, Surgipath) for 45 seconds to 2 minutes. Slides were transferred to tap water for 2 minutes, rinsed in ddH2O for 30 seconds, de-stained by 3 dips in acid alcohol (1ml 10N HCl in 400 ml 70% ethanol), tap water for 1 minute, ddH2O for 30 seconds, bluing

solution (6.16 g lithium bicarbonate in 400 ml ddH2O) for 1 minute, tap water for 1 minute, ddH2O for 30 seconds, and then dehydrated through an alcohol series (2 minutes each in 50%, 70%, 95%, 100% x2), cleared in benzyl alcohol-benzyl benzoate (1 part benzyl alcohol to 2 parts benzyl benzoate) for 5 minutes, and mounted with DPX neutral mounting medium (Sigma).

In situ Hybridization (relevant to Chapter 6 only)

To make RNA probes, plasmid DNA containing the gene of interest was first linearized with appropriate restriction endonuclease and then purified using a Qiagen PCR purification kit and eluted in water. The following transcription reaction was set up:

1 ug linearized DNA

4 ul 5X transcription buffer (Promega)

2 ul 0.1M DTT (Promega)

2 ul 10X Digoxigenin mix (Roche)

2 ul polymerase (Promega)

0.5 ul RNasin

Add water to final volume 20 ul → 37°C 2 hrs

Nucleic acids were then precipitated with EtOH and resuspended in TE/formamide:

1. add 0.3 M NaOAc and two volumes 100% EtOH
2. mix gently and put 30 min at -20°C (longer freezing decreases RNA yield)
3. Centrifuge 15000rpm 15 min
4. remove EtOH and add 180 ul 70% EtOH
5. centrifuge 15000rpm 5 min
6. remove EtOH and dry 2 min (no longer!)

7. dissolve pellet in 21 ul TE and run 1 ul on 1% TAE gel (clean gel box first) to determine concentration of transcribed probe. Compare with 3 ul RNA ladder (Invitrogen 15620-016).

8. Add 20 ul formamide and store at -80°C.

In situ hybridization protocol for staining sectioned tissue on slides:

DAY 1

1. Warm slides to RT and let dry 15 min (for best results, do ISH on tissues as soon as they have been perfused, frozen and sectioned)

2. Fix with 4% PFA in PBS, 20 min, RT.

3. Wash with DEPC-PBS, 2 x 5 min, RT.

4. Digest with 2 ug/ml Proteinase K in PK buffer, 8 min, RT (optimal Prot K concentration may vary depending on tissue type and probe)

5. Wash with previous DEPC-PBS, 5 min, RT.

6. Fix with previous 4% PFA, 15 min, RT.

7. Rinse in DEPC-water

>>>Make 200 ml 0.1 M RNAse-free triethanolamine-HCl pH 8.0

8. Put slides, RNAse-free stir bar, and 0.5 ml acetic anhydride into triethanolamine solution. Stir until in solution

9. Leave 10 min more with stirring.

10. Wash in DEPC-PBS 5 min, RT

11. Prehybridize 2 hrs, 65°C.

Hybridization Buffer:	(for 1 ml) (usually make 50 ml and store at -20°C)
50% Formamide	500 ul
5X SSC	250
0.2 mg/ml yeast tRNA	20
100 ug/ml heparin	2
1X Denhardt's soln	20
0.1% Tween 20	10

0.1% CHAPS	10
5 mM EDTA	10
dH2O	178

>>>to prepare probe for hybridization, first heat 1 ml hyb. Buffer to 80°C for 5 min, then add appropriate amount of probe (300 ng/ml – 1 ug/ml), incubate at 80°C 5 min more, then transfer tube to ice

12. Hybridize in hybridization solution 12-16 hrs, 65°C. Coverslip with parafilm to prevent drying

DAY 2

1. Wash in 0.2X SSC 20-30 min x3 at 65°C (pre-warm solution)

2. Wash in PBT (PBS/0.1%TX) 10 min x3 at RT.

3. Block with 20% Heat Inactivated Sheep Serum (HISS) in PBT 30 min RT

4. Incubate in blocking buffer with anti-Dig-AP (1:2000) overnight at 4°C.

DAY 3

1. Rinse with PBT 10 min x3 at RT

2. Rinse with AP buffer 15 min x 3 at RT

AP buffer:

100 mM Tris 9.5	10 ml	1M
50 mM MgCl2	5 ml	1M
100 mM NaCl	2 ml	5M
0.1% Tween20	1 ml	10%
Water	82 ml	

3. Incubate with NBT/BCIP in AP buffer (100 ul NBT/BCIP for 10 ml AP buffer) wrapped in aluminum foil at RT

4. Change solution next day

<u>Immunostaining and confocal microscopy</u>

For immunostaining of structures on the ventricular surface, primary and secondary antibodies were incubated in PBS with 0.5% Triton-X100 and 10%

normal goat or donkey serum for 24 hours at 4°C. For immunostaining of structures deeper within the SVZ, primary and secondary antibodies were incubated in PBS with 2% Triton-X100 and 10% normal goat or donkey serum for 48 hours at 4°C. Primary antibodies are listed in Table 2.

Table 2. Primary antibodies.

Antigen	Host	Dilution	Source
Acetylated-tubulin	Mouse IgG2b	1:1000	Sigma T6793
γ-tubulin	Rabbit	1:1000	Sigma T5192
γ-tubulin	Mouse IgG1	1:500	Abcam ab11316
γ-tubulin	Goat	1:200	Santa Cruz sc-7396
β-catenin	Mouse IgG1	1:500	BD Transduction Labs 610153
β-catenin	Rabbit	1:1000	Sigma C2206
ZO1	Rabbit	1:100	Zymed 40-2200
Ncaderin	Rabbit	1:200	Abcam ab12221
Vinculin	Mouse hVin1	1:200	Sigma V9131
Vinculin	Mouse 7F9	1:100	Chemicon 90227
Connexin43	Rabbit	1:50	Zymed 71-0700
GFAP	Mouse IgG1	1:500	Chemicon MAB3402
Vimentin	Mouse IgM	1:1000	Sigma V-2258
S100β	Rabbit	1:500	DAKO A5110
CD24	Rat IgG2b	1:500	BD Pharmingen 557436
CD133	Rat IgG1	1:100	eBioscience 14-1331
Olig2	Rabbit	1:3000	D. Rowitch

GFP	Chicken	1:500	Aves Labs GFP-1020
phosphorylated histone H3	Rabbit	1:500	Upstate 06-570
Ki67	Rabbit	1:500	Vector VP-K451

Secondary antibodies used to visualize primary antibodies were conjugated either (1) to Alexa Fluor 488, 546, 568, 594, or 647 (goat or donkey polyclonal, 1:400, Molecular Probes) or (2) to biotin (goat polyclonal, 1:250, Jackson ImmunoResearch) followed by streptavidin-HRP and diaminobenzidine. Confocal images were taken on a Nikon C1si at the Nikon Imaging Center at UCSF or on a Leica SP5.

Electron microscopy

For transmission electron microscopy (TEM) analysis, 200 um coronal sections were cut from perfused adult mice as described in (Doetsch et al., 1997). The sections were post-fixed in 2% osmium for 2 hr, rinsed, dehydrated, and embedded in Araldite (Durcupan, Fluka BioChemika). Semithin (1.5 um) sections of the SVZ cut in the coronal plane or en-face to the ventricular surface were stained with toluidine blue and used to identify ventricle-contacting B1 cells. For reconstruction of type B1, E2, and E1 cells we cut 500-600 serial ultrathin (0.05 um) sections that were placed on Formvar-coated single-slot grids, stained with lead citrate, and examined under a Jeol 100CX electron microscope.

Adherent neural stem cell cultures (relevant to Chapter 3 only)

Adult Z/EG mice were injected with 500 nl of Ad-GFAPp::Cre unilaterally into the lateral ventricle at (0 AP, 0.9 L, 1.9 D) (see "Stereotactic Injections of Adult and Neonatal Mice" above). Two days later, the walls of the contralateral and ipsilateral lateral ventricles were dissected separately, dissociated, and used to establish adherent neural stem cell cultures as previously described in (Scheffler et al., 2005). Briefly, dissected tissue was incubated in 0.25 ml 0.25% Trypsin-EDTA for 30 minutes at 37°C, and then 0.75 ml Dulbecco's modified eagle medium (DMEM) containing 10% fetal bovine serum (FBS) was added to quench trypsin activity. The trypsin-digested tissue was then triturated to single cell suspension and pelleted by centrifugation. Cells were resuspended in 2 ml N5 medium and plated into one well of a 12 well tissue culture plate. N5 medium contained 2.5 ml FBS, 0.5 ml 100x antibiotic/antimycotic, 0.5 ml N2 supplement (Gibco), 87.5 ul bovine pituitary extract, bFGF (20 ng/ml final concentration) and EGF (20 ng/ml final concentration) in DMEM/F12+Glutamax (Gibco) to a final volume of 50 ml. Cells were transferred to an incubator overnight at 37°C, 5% CO_2. One day after plating, weakly adherent cells were washed off the plate using the medium in the well and transferred to a new well of the plate. This procedure had been previously described to remove strongly adherent non-stem cell astrocytes and microglia from the culture, thereby enriching for stem cell astrocytes (Scheffler et al., 2005). Cells were then allowed to grow to confluence, with N5 medium being replaced every 3 days. At confluence, cells were passaged into 3 new wells to expand the population. To passage cells, medium was removed from the well, cells were rinsed with 2 ml of PBS (Ca^{2+} and

Mg^{2+} free), and then incubated for 2-3 minutes in 0.25 ml 0.05% Trypsin. 0.75 ml fresh N5 medium was then added to the well, the medium was washed over the cells to mechanically detach them from the plate, the cells were collected in a 15 ml Falcon tube and pelleted by centrifugation. Cells were resuspended in 6 ml N5 medium and transferred into 3 new wells. After two passages, neural stem cell monolayers were allowed to reach confluence and N5 medium was replaced with N6 medium to differentiate the cells. N6 medium contained 49 ml DMEM/F12+Glutamax (Gibco), 0.5 ml antibiotic/antimycotic, 0.5 ml N2 supplement (Gibco), and 87.5 ul bovine pituitary extract. Neural stem cell monolayers were allowed to differentiate in N6 medium for 7 days and then fixed and immunostained as described above.

Section 3: Data Analysis

Reconstruction of surface maps (relevant to Chapter 3 only)

The reconstructions of the entire lateral wall and the anterior medial wall (Chapter 3:Figure 6A) of the lateral ventricle were made from 222 (lateral wall) and 106 (medial wall) tiled, high-power confocal fields (212 x 212 um^2). Each high-power field was comprised of 1-3 individual confocal images taken at different depths to reconstruct only the surface of each field. This was necessary because the wholemounts, even with the secondary dissection to partially flatten the surface, maintain some degree of curvature.

Quantification of the ventricle-contacting cell types (relevant to Chapter 3 only)

To quantify the number of B1, E1, and E2 cells contacting the lateral ventricle in different regions of the lateral wall, we immunostained wholemounts from 3 animals for γ-tubulin and β-catenin. We imaged 4 non-overlapping high power fields (127 x 127 um^2) from each of 4 regions, as shown in (Chapter 3:Figure S8), and counted the number of each cell type in these regions. The number of each cell type was divided by the surface area examined to determine the density of each cell type in each region. To determine the average density of each cell type across the entire wholemount, we combined the data for all 4 regions. The data for the histogram of apical surface area (Chapter 3:Figure 1I) was obtained from 771 B1 cells, 1716 E1 cells, and 201 E2 cells in random high power fields (89.1 x 89.1 um^2) taken from the lateral wall of 4 animals stained for γ-tubulin and β-catenin. The data for the histogram of cilia length (Chapter 3:Figure 1J) was obtained from 361 B1 primary cilia, 55 ependymal cilia, and 106 E2 cilia in random high power fields (89.1 x 89.1 um^2) taken from the lateral wall of 3 animals stained for γ-tubulin and acetylated-tubulin.

Quantification of basal body (BB) patch angle and apical surface orientation of ependymal cells (relevant to Chapter 4 only)

To quantify the position of the basal body patch relative to the apical surface of an ependymal cell, we wrote a program in Metamorph imaging software (Molecular Devices) to draw a vector connecting the center of two sequentially traced regions: the apical surface of the cell and the area covered by that cell's basal body patch. The angle of this vector was called the BB patch angle. To determine the similarity of BB patch angles within a given high power

field (127 x 127 um^2), we calculated the deviation of each cell's BB patch angle from the median within the field, and this data was plotted as a histogram. Note that only ependymal cells that had their entire apical surface within the high power field were analyzed. For each of Regions AD, AV, and PM of the lateral wall of the lateral ventricle, we combined data from high power fields in 4 mice. These regions were defined with respect to landmarks on the wholemount, as illustrated in (Chapter 4:supplemental Fig. S1). Note that Regions AD and AV defined in the analysis of ependymal planar polarity cover a more restricted area of the lateral ventricle wholemount than regions AD and AV defined in the quantification of ventricle contacting cell types (see above). For apical surface orientation, which was defined in our Metamorph program as the angle of the long axis of the traced cell surface, a similar analysis was conducted calculating the deviation of each cell's long axis angle from the median within the field.

BB patch angles of ependymal cells on the lateral wall in *hGFAP::Cre;Kif3a*$^{fl/fl}$ mutants (n=5) and control littermates (n=5) were analyzed in 6 non-overlapping high power fields (127 x 127 um^2). Three high power fields were taken posterior to the adhesion point, along the dorsal-ventral midline of the lateral wall (corresponding to Region PM), and three high power fields were taken anterior to the adhesion point along the dorsal-ventral midline. However, since *Kif3a* mutants lack an adhesion point, likely due to hydrocephalus and expanded ventricles, we could not use this landmark as a reference in mutants. Instead, the anterior-posterior position of high power fields taken in controls was recorded relative to the anterior boundary of the wholemount (0.2-0.7 mm for the

anterior region and 1.7 to 2.5 mm for the posterior region) and corresponding fields were imaged in mutant wholemounts. The data from all six high power fields in each of 5 mutants and 5 control littermates was combined and depicted as a histogram showing the control and mutant distribution of BB patch angles around the median.

Chapter 3

A new perspective on the adult neural stem cell niche: a neurogenic ventricular zone persists in the adult brain

During development, neural stem cells reside in the ventricular zone (VZ) lining the walls of the brain ventricles. The VZ is thought to disappear in early postnatal life. Neural stem cells (SVZ B cells) are retained in the adult mammalian brain, but these cells are displaced to the subventricular zone (SVZ) by the postnatal development of ependymal cells. Using adult mice we developed new methods to image the brain ventricular surfaces. In addition to multiciliated ependymal cells, we found that two other cell types touch the lateral ventricle: 1) a bi-ciliated cell characterized by a novel basal body with elaborate lateral extensions; and 2) B cells with a very small apical surface that contain a single primary cilium and a previously unidentified long basal process ending on blood vessels. Ventricle-contacting B cells undergo mitosis and generate neurons that migrate to the olfactory bulb. Ependymal cells encircle B cells' apical surfaces forming "pinwheels", structures we only found in neurogenic ventricular walls. These findings reveal a novel organization for adult neural stem cells demonstrating that a VZ persists in this adult neurogenic niche.

Introduction

New neurons and glial cells continue to be born in the postnatal and adult mammalian brain in restricted germinal regions (Alvarez-Buylla and Lim, 2004; Gage, 2000; Morshead and van der Kooy, 2004). The largest germinal region of the postnatal brain is found on the walls of the lateral ventricles. In this region, primary neural progenitors reside in the subventricular (SVZ) or subependymal zone, displaced from the ventricles by ependymal cells, epithelial cells that line the brain ventricles and contribute to CSF homeostasis (Bruni, 1998). In contrast, primary neural progenitors in the developing brain reside in the ventricular zone (VZ), a pseudostratified epithelium in direct contact with the embryonic brain ventricles. Contact with the ventricle through an apical process is critical for maintaining germinal activity of the primary progenitors in the developing brain (Bittman et al., 1997; Kosodo et al., 2004; Nadarajah et al., 1997; Weissman et al., 2004). It is therefore intriguing that the primary progenitors in the adult brain are displaced from the ventricle.

In the embryonic VZ, the primary neural progenitors are radial glia (Anthony et al., 2004; Malatesta et al., 2000; Miyata et al., 2001; Noctor et al., 2001; Tamamaki et al., 2001). These elongated stem cells maintain contact with both the ventricular surface and the pial surface. In the VZ, radial glial cell bodies undergo a series of precisely timed movements known as interkinetic nuclear migration, whereby these cells divide and generate neuroblasts (Gray and Sanes, 1992; Malatesta et al., 2000; Misson et al., 1988; Noctor et al., 2001; Sauer, 1935). Shortly after birth however, radial glia transform into parenchymal

astrocytes (Schmechel and Rakic, 1979; Voigt, 1989) and ependymal cells (Spassky et al., 2005) and little remains of their unique morphology and behavior. The VZ is replaced by a simple ependymal epithelium.

Recently, it was shown that some radial glia in a restricted region of the ventricular system, mostly along the lateral wall of the lateral ventricle, transform into astrocyte-like neural stem cells that are the primary neural progenitors of the SVZ (Merkle et al., 2004). These adult neural stem cells, or B cells, generate interneurons for the olfactory bulb (Doetsch et al., 1999a). Although rarely observed, some B cells have an apical membrane that contacts the ventricle similar to the apical contact of their radial glial progenitors (Doetsch et al., 1999b). For radial glia in the embryo, this apical membrane is a specialized structure enriched in prominin-1(Weigmann et al., 1997), par-3 (Manabe et al., 2002), and numb (Rasin et al., 2007). It is the site where the primary cilium, basal body and daughter centriole are located during interphase (Cohen et al., 1988), where the nucleus migrates for mitosis (Committee, 1970), and where the midbody is found at the end of cytokinesis (Dubreuil et al., 2007). Recent evidence suggests that the apical membrane may determine the symmetry of radial glial cell division (Kosodo et al., 2004): symmetric proliferative divisions result when the apical membrane is bisected by the cleavage furrow and it is inherited equally by daughter cells, while asymmetric neurogenic divisions result when the apical membrane is bypassed by the cleavage furrow and only one daughter, which appears to remain as the stem cell, inherits the apical membrane. The apical membrane of the ventricle-contacting B cells is therefore

a potentially important link between adult neurogenesis from the SVZ and developmental neurogenesis from the VZ and may yield many insights into adult neural stem cell function and niche organization. However, due to technical difficulties in identifying them, the ventricle-contacting B cells and their apical membranes have not been carefully studied since they were initially observed.

Initial observations of the ventricle-contacting B cells were made by transmission electron microscopy (TEM) after serial reconstructions of ultrathin sections (Doetsch et al., 1999b). Two types of B cells were identified in the SVZ, B1 and B2 (Doetsch et al., 1997). B1 cells had lighter cytoplasm and were located just beneath the ependymal layer while B2 cells had darker cytoplasm and were located at the striatal border with the SVZ. Based on the low incidence of B cell apical membranes at the ventricular surface, it was inferred that only a small subpopulation of B1 cells contacted the lateral ventricle. This contact occurred through an apical extension interposed between ependymal cells. Often, a primary cilium was observed extending from the apical surface into the ventricular lumen (Doetsch et al., 1999b). Ventricle-contacting B1 cells were rarely observed, however, and usually only in the context of SVZ stimulation following treatment with anti-mitotic drugs (Doetsch et al., 1999b) or growth factors (Doetsch et al., 2002). It was inferred that under normal conditions, very few, if any, B1 cells touched the ventricle.

Here we developed a new technique for staining and imaging wholemounts that simplifies the study of the apical and basal specializations and organization of different cell types that touch the ventricle in the adult brain. We

have used this method to find that B1 cells comprise a modified VZ in the adult brain with a unique pinwheel architecture. We have also characterized a novel cell type at the ventricular surface that has a previously undescribed basal body structure. This significantly reshapes our view of the niche architecture of the VZ and SVZ and their roles in adult neurogenesis.

Results

Three cell types contact the lateral ventricle

B1 cells contacting the lateral ventricle extend a primary cilium into the ventricular lumen (Doetsch et al., 1999b). Because it is nearly impossible to observe and quantify the short primary cilium or the thin ventricle-contacting apical process of B1 cells in sections, we turned our attention to wholemounts. Wholemounts provide an en-face view of the ventricular surface and can be dissected from any region of the ventricular system from embryonic ages to adulthood (**Figure S1**)(Doetsch and Alvarez-Buylla, 1996). For this study, all wholemounts were dissected from animals 60-120 days old. We used this method to identify cells that contact the ventricular surface.

We first tried to find ventricle-contacting B1 cells by looking for their primary cilia by scanning electron microscopy in wholemounts of the lateral wall of the lateral ventricle (data not shown). However it was difficult to find primary cilia, either because the ventricle-contacting B1 cells are very rare or because the primary cilia of these cells are difficult to find among the many long cilia of ependymal cells. Similarly, it was difficult to find primary cilia in wholemounts

that were immunostained for acetylated-tubulin, a marker for cilia (**Figure 1A**). To obtain an unobstructed view of the surface of the ventricular wall, we used γ-tubulin antibodies to label basal bodies and β-catenin antibodies to delineate the cell membrane (**Figures 1B and 1C**). This revealed three distinct cellular profiles in contact with the lateral ventricle: (1) cells with a large apical surface and multiple (32-73) basal bodies, with γ-tubulin distributed as small, individual points (diameter: 0.54 um) at each basal body, (2) cells with a small apical surface and a single basal body, with γ-tubulin distributed in a donut configuration (diameter: 0.94 um) presumably around the basal body in the pericentriolar material tube (Ou et al., 2004), and (3) cells with an intermediate-sized apical surface and 2 large, complex basal bodies, with more intense γ-tubulin expression distributed in small, individual points as in (1), but arranged in large donut or horseshoe formations (diameter: 1.35 um). Immunostaining for acetylated-tubulin in combination with γ-tubulin revealed that these three cell types could also be distinguished by their cilia (**Figure 1D**): (1) cells with multiple basal bodies had multiple long cilia, corresponding to ependymal cells, (2) cells with a single basal body had a single, short primary cilium, corresponding to B1 cells, and (3) cells with complex basal bodies were often biciliated, with long cilia comparable to those of ependymal cells. We will refer to these biciliated cells as E2 cells and to multiciliated ependymal cells as E1 cells. E2 cells will be described in detail in Chapter 5.

By correlative TEM, we confirmed the ultrastructural properties of cells we identified as E1 (**Figure 1F**): multiple basal bodies, short microvilli, an

interdigitating cell membrane, very light cytoplasm, and spherical nuclei with no invaginations and dispersed chromatin (Doetsch et al., 1997). We also confirmed the ultrastructural properties of cells we identified as B1 (**Figure 1E**): a single basal body and centriole, very long and thin microvilli, an irregular cell membrane contour, light cytoplasm containing intermediate filaments, irregular and frequently invaginated nuclei, and dispersed chromatin. These astrocytic properties are associated to B cells in the SVZ (Doetsch et al., 1997).

Surprisingly, we found B1 cells with a ventricle-contacting apical surface were not rare: we counted 6,225 on the lateral wall of one lateral ventricle in a single, untreated adult mouse (**Figures 6A and 6B**). These B1 apical surfaces were often found clustered with one another. When quantified, the number of B1 cells was nearly one-third (31.0%) of all cells touching the lateral ventricle wall (**Figure 1H**). This finding is in stark contrast to the conventional view that the walls of the adult ventricular system are lined by a monolayer of ependymal cells (Bruni, 1998). However, it was now clear why the B1 cells were previously difficult to find by TEM. While they were substantial in number, the average size of the apical surface of a B1 cell was 24.1 um^2, compared to 265.0 um^2 for an ependymal cell (**Figure 1I**). Additionally, the average size of the primary cilium of a B1 cell was 3.2 um compared to 11.5 um for ependymal cilia (**Figure 1J**), making B1 cells equally difficult to find with SEM on wholemounts. Our modified wholemount staining technique provided an efficient way to identify rare cell profiles on the ventricular surface.

B1 and E1/E2 cells have complementary expression patterns of molecular markers at their apical surfaces

The small apical surfaces of B1 cells could be distinguished from the apical surfaces of E1 and E2 cells by GFAP staining (**Figure 2A**). These small apical surfaces always contained a single basal body. In serial confocal optical sections, GFAP+ B1 apical terminations were associated to cell bodies in the SVZ that had additional basal processes (see below). The GFAP staining, ultrastructure, and cell body location within the SVZ further identified these cells as B1 cells. E1 cells were GFAP-, but were CD24+, a marker of ependymal cells (Calaora et al., 1996). Interestingly, E2 cells were also CD24+, another similarity between E1 and E2 cells (**Figure 2B**). Vimentin also marked the apical surface of both E1 and E2 cells, but not B1 cells (**Figure 2C**). Finally, S100β, although it was not strongly expressed at the apical surface, was found to be expressed in the cell body of both E1 and E2 cells, but not B1 cells (**Figure 2D**).

B1 cells confer unique pinwheel architecture to the ventricular surface in neurogenic regions of the adult brain

We used γ-tubulin and β-catenin staining of the ventricular surface to compare the cellular profiles on neurogenic vs. non-neurogenic adult ventricular walls. Adult neurogenesis occurs throughout most of the lateral wall of the lateral ventricle and part of the anterior medial wall overlying the septum, but not in the caudal medial wall or the third ventricle. While E1 and E2 cells were found in all regions examined, B1 apical surfaces were found only on the lateral wall and in

the anterior medial wall of the lateral ventricles, coinciding with the neurogenic niche in the adult brain (**Figure 3**).

In the neurogenic niche, the presence of B1 apical surfaces appeared to influence the geometry of E1 apical surfaces and conferred a striking architecture to the ventricular wall (**Figures 3A, 3B, 3E, and 3F**). The apical surface of one or more B1 cells was surrounded by E1 cells in a specific pattern. The pattern, which resembled a pinwheel (**Figure 3G**), appeared to maximize the packing of E1 cells around the B1 apical surface. The shape of each E1 apical surface approximated a triangle or diamond with vertices contacting the B1 apical surface. The resulting pinwheel pattern was only observed on the ventricular surface in neurogenic regions, where B1 cells were found (**Figures 3A, 3B, 3E, 3F, 3G, and 3H**), and not in non-neurogenic regions, where E1 apical surfaces were more regularly shaped (**Figures 3C and 3D**).

The triangular geometry of E1 apical surfaces within pinwheels was polarized with respect to the central position of B1 apical surfaces; one vertex of the triangle was close to the center of the pinwheel while the other 2 (or 3) vertices were opposite the center. This radial polarity is inherent in each pinwheel and is therefore repeated across the plane of the epithelium where pinwheels are found. However E1 cells also have a different and more widely recognized planar polarity (Sawamoto et al., 2006). Planar polarity underlies a principal function of E1 cells, which is to propel cerebrospinal fluid in a uniform direction through the ventricular system (Cathcart and Worthington, 1964; Worthington and Cathcart, 1963). This function relies on the coordinated beating

of motile cilia, which in turn relies on the planar polarity of E1 cells (Wang and Nathans, 2007). For the ependyma, planar polarity has been assayed functionally by observing the uniform flow of india ink deposited on the surface of a live wholemount (Sawamoto et al., 2006). Recently we have identified a structural indicator of this planar polarity based on the position of the basal body patch on the E1 apical surface (see Chapter 4). The basal body patch is found downstream with respect to the direction of ciliary beating (**Figure 3G**). Interestingly, the geometry and radial polarity of E1 apical surfaces found in pinwheels appeared to be independent of the planar polarity of their basal body patch. In **Figure 3G**, the patch of basal bodies is located on the right side of each E1 apical surface, which is close to the center of the pinwheel for the cells at the top-left but opposite the center for the cells in the bottom-right. This suggests that the mechanism governing the geometry of the E1 apical surface is distinct from that used for establishing or maintaining planar polarity of the apical surface.

Apical intercellular junctional complexes at B1-B1 and B1-ependymal junctions

The peripheral packing of E1 cells around central clusters of B1 cells suggested that these cells may have specialized intercellular junctions at their apical surfaces. EM analysis of the apical junctional complexes between the various combinations of cell types (B1-B1, B1-E1, E1-E1, and E1-E2) revealed

that B1-B1 and B1-E1 junctions were unique (**Figure 4**). For this analysis we used serial section reconstruction at the EM to confirm cell identity based on the number of cilia each cell had. B1-B1 junctions (white arrowheads in **Figures 4A and 4C**) had symmetric discontinuous adherens junctions with periodic electron-dense deposits at sites where membranes became tightly opposed or pinched. Interestingly, these junctions were very similar to those observed between radial glia in the neonatal VZ (**Figure 4D**). Short stretches of tight junctions were occasionally observed between B1 cells. E1-E2 junctions were symmetric; both tight (black arrowheads in **Figure 4E**) and adherens junctions (white arrows in **Figures 4E and 4F**) were observed and these junctions were indistinguishable from those observed between E1 cells. The adherens junctions were characterized by dense deposits of electron-dense material inside the membrane next to the junctional complex. Interestingly, B1-E1 junctions (**Figure 4B**) included both tight and adherens junctions, but the latter were asymmetric. More electron-dense material was accumulated inside the membrane on the E1 side than on the B1 side (black arrows in **Figure 4B**). This indicates that specialized junctional complexes characterized homotypic and heterotypic adhesions between the different cell types at their apical intercellular boundaries.

To determine specific components within these junctional complexes, we immunostained wholemounts for several proteins known to localize to gap junctions, adherens junctions, or tight junctions. Gap junctions are difficult to observe without doing freeze-fracture EM so we were unable to observe them in our ultrastructural analysis. However, immunostaining for Connexin 43 (Cx 43,

Figure 5A) revealed that gap junctions are localized to apical intercellular membranes at B1-B1 and B1-ependymal junctions. The expression at B1-B1 junctions is particularly intriguing because gap junctions in radial glial apical processes couple groups of radial glial cells and are critical to their maintained proliferative activity during embryonic neurogenesis (Bittman et al., 1997; Nadarajah et al., 1997; Weissman et al., 2004). We also stained for ZO-1, which is known to associate with both tight and adherens junctions. ZO-1 staining revealed sharp lines localized between apical intercellular membranes of all cell types (**Figure 5B**). Finally, in addition to β-catenin, we stained for two other components of adherens junctions: N-cadherin, an integral membrane protein that functions as a homotypic cell-cell adhesion molecule to bridge adherens junctions between cells, and vinculin, an intracellular component of adherens junctions that indirectly links the β-catenin/α-catenin complex to actin. N-cadherin was highly co-localized with β-catenin at adherens junctions between all cell types (**Figure 5C**). Vinculin was also observed at intercellular membranes between all cell types, but it appeared to be more highly expressed at junctions involving B1 cells (**Figure 5D**). The vinculin staining pattern may be indicative of differences in actin cytoskeletal regulation in B1 versus ependymal cells. Together with the ultrastructural data, this suggests that diverse junctional complexes may help shape the pinwheel architecture of the ventricular surface.

Surface maps of the lateral ventricle walls reveal "hot spots" of B1 cells

The above analysis showed that B1 cells were limited to neurogenic regions of the adult ventricular system, but did not show the distribution within the

neurogenic regions. To create a comprehensive map of the location of B1 cells on the walls of the lateral ventricle, we reconstructed the entire surface of one lateral wall and the anterior portion of one medial wall stained with γ-tubulin and β-catenin. These surface maps were reconstructed from a series of 222 (lateral wall) and 106 (medial wall) tiled, high-power confocal fields (212 x 212 um^2/field).

B1 cells with ventricle-contacting apical surfaces were found throughout the rostral-caudal and dorsal-ventral axes of the lateral wall (**Figure 6A**), in clusters of 1 cell up to 40 cells touching the ventricle. We quantified the number and position of B1 apical surfaces in the different regions of the lateral and anterior medial wall of the lateral ventricle. This data was color-coded to indicate clusters of 1, 2, 3, 4, 5, 6-10, or >10 B1 apical surfaces. These apical surfaces were relatively more concentrated in two "hot spots," in the anterior-ventral and posterior-dorsal regions, with respect to the lateral ventricle adhesion point, where the lateral and medial walls are fused within the ventricular lumen. Interestingly, many B1 apical surfaces were also found in the most anterior aspect of the medial wall of the lateral ventricle (**Figure 6A**). This region has recently been found to contain neurogenic precursors that generate specific subpopulations of olfactory bulb neurons in the postnatal rodent brain (Merkle et al., 2007). This is consistent with the idea that ventricle-contacting B1 cells function as progenitor cells and shows that the presence of B1 apical surfaces is an indicator of neurogenic ventricular walls in the adult.

Next, we quantified the number of B1 apical surfaces in 4 different lateral wall regions from 3 more animals (**Figure 6C**). We consistently found that the

anterior-ventral and posterior-dorsal regions had the highest number of B1 apical surfaces, with 2515 and 2206 per mm^2, respectively (**Figures 6G and 6H**). The anterior-dorsal region had fewer with 823 (**Figure 6F**), and the posterior-ventral region had the fewest with 442 B1 apical surfaces per mm^2. In contrast, the density of E1 cells was similar among the regions (3343-3584 per mm^2), except in the posterior-ventral region (2072 per mm^2) where E1 cells had a larger surface area. E2 cells were found in similar numbers throughout the different regions (185-211 per mm^2).

B1 cells have a long basal process similar to their radial glial progenitors

We next used the wholemount staining technique to look beneath the ventricular surface and the ependyma at the SVZ. One striking result was the presence of very long GFAP+ fibers throughout the lateral wall of the lateral ventricle. These fibers were oriented in different directions depending on their location. **Figure 7A** shows that most GFAP+ fibers found anterior to the adhesion were oriented tangentially to the surface and ran anteriorly, as did fibers found dorsal to the adhesion (**Figures S2A and S3C**). In contrast, **Figure 7B** shows that most fibers found immediately posterior to the adhesion were oriented tangentially to the surface but ran ventrally (also see **Figure S3A**). In the most dorsal region of the SVZ just beneath the corpus callosum, the fibers were oriented more obliquely to the surface of the ventricle and ran deeper into the parenchyma reaching into the striatum (**Figures S2B and S3B**). In fact, long GFAP+ fibers were observed extending into the striatum throughout most of the SVZ. In the most ventral regions of the SVZ the fibers also ran deeper into the

parenchyma, but were oriented ventrally (Sundholm-Peters et al., 2004) (**Figure S3D**). Previous ultrastructural reconstructions had missed this fundamental anatomical feature of the adult SVZ (Doetsch et al., 1997); the largely tangential orientation of these fibers made it difficult to observe them in thin sections.

It appeared that the long GFAP+ fibers were originating very close to the ventricular surface. To determine whether these fibers belonged to B1 cells with apical surfaces on the ventricle, we used high-power confocal stacks to image a block of lateral wall 50 um in depth in wholemounts stained for GFAP, γ-tubulin, and β-catenin. At the ventricular surface, we observed GFAP+ B1 apical endings as before (**Figure 7D**), but tracing the GFAP+ fibers deeper revealed that they extended for a long distance and were in fact the same long fibers we had observed at lower power (**Figure 7C, arrows indicate apical endings shown in Figure 7D**). The arrows in the rotated image in **Figure 7C'** indicate the apical processes extending towards the ventricular surface from the intense GFAP expression in the SVZ, with gaps between these apical processes corresponding to the position of ependymal cells. While it was difficult to quantify the percentage of long GFAP+ fibers that had an apical surface on the ventricle, it appeared to us that most of these fibers did have an apical surface and in every case where we traced individual fibers, we found the apical surface. While tracing individual fibers, we also observed that the thick bundle of GFAP+ intermediate filaments that comprised the long basal process frayed into many thinner bundles closer to the apical surface (**Figures 7E and 7F, blue arrow**). Based on nuclear counterstaining, it appeared that the cell body was located

near the position where the long basal process frayed at the apical termination. At the other end of this basal process, we observed many cases in which the basal fiber terminated in an endfoot on a blood vessel (**Figure 7E, yellow arrow**). GFAP+ B1 cells with an apical surface on the ventricle and a long basal process were observed in animals at all ages tested (up to 9 months old, data not shown). Chains of migrating neuroblasts in the SVZ are ensheathed by gliotubes that run parallel to the orientation of the chains (Lois et al., 1996; Peretto et al., 1997). Double-staining for GFAP to label B1 cells and doublecortin (or PSA-NCAM) to label chains of migrating cells showed that B1 basal processes contribute to the gliotubes. Basal processes of B1 cells wrapped around chains and then ran parallel to the orientation of these chains for some distance before terminating (**Figure S4**). In non-neurogenic regions such as the caudal medial wall or the third ventricle, GFAP+ astrocytes were observed beneath the ependymal layer, not in contact with the ventricle, and they had either a single long process or a stellate morphology, respectively (data not shown).

GFAP staining does not reveal the complete morphology of B1 cells. Consequently we injected an adenovirus expressing Cre under the GFAP promoter (Merkle et al., 2007) into the lateral ventricle of Z/EG mice (Novak et al., 2000), a Cre reporter line expressing GFP. This technique provided a way to label B1 cells, which have both a ventricle-contacting apical surface (allowing infection via the ventricle) and an active GFAP promoter (allowing Cre expression from the adenovirus). We then reconstructed high-power confocal stacks of labeled B1 cells filled with GFP (**Figures 7G-7I**). Most B1 cell bodies

were located immediately underneath ependymal cells, with a very short apical process extending between ependymal cells to make contact with the ventricle (**Figures 9E-9G and 9E'-9G'**). In some cases, rather than extending an apical process, it appeared that part of the B1 cell body was squeezed between ependymal cells to make direct contact with the ventricle (**Figures 7H and 7I**). A very long process emanated from the basal side of the cell body and extended obliquely away from the ventricular surface, often ending with an endfoot on a blood vessel (**Figure 7H, yellow arrow**). In addition, some B1 cells had lateral lamellar extensions of membrane from their cell body (like a fried egg) that spread across the basal side of adjacent ependymal cells. These lateral extensions have been described before as thin processes that separate ependymal cells from chains of neuroblasts in the SVZ (Doetsch et al., 1997). While in sections, these lateral extensions appeared as individual processes, the wholemount analysis revealed that many of these processes were part of a continuous thin sheet of membrane spanning in all directions away from the cell body.

The morphology of B1 cells was reminiscent of radial glia of the embryonic ventricular zone. Radial glia have a short, ventricle-contacting apical process and a very long, pial contacting basal process. This long basal process can be used to specifically label radial glia by injecting an adenovirus expressing Cre into the striatum of neonatal Z/EG mice (Merkle et al., 2004). In addition to labeling local striatal cells, the virus is retrogradely transported to the radial glial cell body in the ventricular zone where it labels these cells and their subsequent

progeny. Merkle et al. (Merkle et al., 2004) used this method to determine that B cells in the adult SVZ are derived from radial glia. To confirm that B1 cells are also derived from radial glia, we performed the same radial glial targeting in neonatal Z/EG mice, sacrificed the animals 2 months later and prepared wholemounts. We observed B1 cells as before. **Figure 7L** shows two of these B1 cells, each with a short apical process contacting the ventricle (**Figures 7J and 7K**) and a long basal process distally wrapped around a blood vessel. B1 cells derived from radial glia also exhibited the lateral lamellar extensions of membrane cupping the basal side of adjacent ependymal cells (**Figures S5A and S5B**). In addition, we traced, using a camera lucida, the fine details of eight B1 cells with apical contacts in 50 μm horizontal sections, where it was more common to see more of the basal process (**Figure S5C**). **Figure 7M** is a horizontal section of the SVZ, where B1 cells derived from radial glial targeting were seen extending their basal process into the striatum. In sharp contrast to the morphology of B1 cells, typical astrocytes elsewhere in the adult brain, including some found in the SVZ, were multipolar with bushy, highly branched processes (arrow in **Figure 7M**; also see **Figure S6**). This is consistent with previous work showing that dividing GFAP-expressing progenitors in the adult SVZ have a bipolar or unipolar morphology that differs from non-dividing multipolar stellate astrocytes (Garcia et al., 2004).

Ventricle-contacting B1 cells undergo mitosis and are neurogenic

The above observations indicated that B1 cells have an apical surface on the ventricle, that they are restricted to neurogenic regions of the adult ventricular

system, and that they are morphologically similar to their radial glial progenitors. These observations suggested that B1 cells may be the primary progenitors for adult neurogenesis in the olfactory bulb. To test this hypothesis further, we examined wholemounts for evidence of proliferation of B1 cells. Staining for γ-tubulin and β-catenin to identify B1 apical surfaces, and phospho-histone H3 (PH3) to identify cells in mitosis or Ki67 to identify cycling cells, revealed dividing B1 cells that had apical contacts with the ventricle. 91 dividing B1 cells contacting the ventricle were serially reconstructed with the confocal microscope. In all but one case, the mitotic soma from these ventricle-contacting B1 cells remained squeezed basally by neighboring ependymal cells. **Figure 8** shows several examples of dividing B1 cells (several in mitosis: **A-C**, **F**, **G**) with an apical surface contacting the ventricle. **Figure 8A** shows a B1 apical surface that is PH3+. Following the confocal stack deeper into the tissue revealed that this PH3+ cell was in anaphase, with one of the sister chromatids (yellow arrow) just beneath the apical membrane and the other (magenta arrow) deeper in the SVZ, beneath an ependymal cell. It appeared that this cell was undergoing an asymmetric division, where only one of the sister chromatids (yellow arrow) would retain the apical membrane. Another example of asymmetric division of a B1 cell with one of the sister chromatids retaining the apical membrane is shown in **Figure 8G**. We were also able to find mitotic B1 cells on the ventricular surface using Ki67 (**Figure 8B**). Interestingly, **Figure 8B** shows the Ki67+ apical surface of a B1 cell that deeper in the SVZ was flanked by a cluster of other Ki67+ cells, likely corresponding to SVZ transit-amplifying (Type C) cells.

Next we wanted to determine whether B1 cells maintain contact with the ventricle throughout the cell cycle. For this analysis, we used Ki67 because it is expressed from late G1 through mitosis but both its level of expression and its localization within the nucleus are cell cycle phase dependent (du Manoir et al., 1991; Scholzen and Gerdes, 2000). Briefly, the staining intensity of Ki67 increases from late G1 to S phase to G2 and reaches its highest levels during metaphase. The localization of Ki67 changes from being restricted to the nucleoli in late G1/S to a more diffuse nuclear distribution in G2, and finally to covering the condensed chromosomes during M phase. We found Ki67+ B1 apical surfaces with staining patterns corresponding to the late G1/S (**Figure 8D**), G2 (**Figure 8E**), and M phases (**Figures 8F and 8G**), suggesting that B1 cells maintain contact with the ventricle throughout the cell cycle. Intriguingly, of the 59 Ki67+ B1 apical surfaces we found from the anterior lateral wall of 3 animals, 41% were in M phase, 44% were in G2, and only 15% were in late G1/S phase. We elaborate on the potential implications of this bias in the discussion below.

To test whether B1 cells with a ventricular contact are neurogenic, we injected adeno-GFAPp:Cre into one lateral ventricle of Z/EG mice, and analyzed both ipsilateral and contralateral lateral wall wholemounts and olfactory bulbs one month later. Adeno-GFAPp:Cre injections into the lateral ventricle of Z/EG mice provide a way of permanently labeling B1 cells via their apical surface and tracing the fate of their progeny. To ensure that we were tracing the fate of only those B1 cells that were labeled via their ventricle-contacting surface, we focused

our analysis on the contralateral side. Labeling on the contralateral side could only occur through viral diffusion from the injected lateral ventricle through the third ventricle into the other lateral ventricle. In fact in most (5 of 6) contralateral wholemounts, the path of viral diffusion through the third ventricle was clear as the majority of labeled cells were close to the foramen of Monro (arrow in **Figure 9C**), which connects the third ventricle to the lateral ventricles. Labeled B1 cells in the contralateral wholemount had an apical surface on the ventricle (**Figures 9E'-9G'**) and a long basal process often ending on a blood vessel (**Figures 9E-9G**). Some of these labeled ventricle-contacting B1 cells were Ki67+ (**Figure 8C**). Furthermore, labeling only a few B1 cells contacting the lateral ventricle on the contralateral side resulted in the production of labeled neuroblasts in the contralateral SVZ (**Figure 9C, inset**) and in the contralateral olfactory bulb core (**Figure 9D**, arrowheads) and labeled neurons in the contralateral olfactory bulb (**Figure 9D**, arrow). Labeled neurons and neuroblasts were found in the contralateral olfactory bulb in 6/6 animals. This demonstrates that B1 cells labeled via their apical surface were capable of producing neurons and neuroblasts up to one month after labeling. To test whether labeled B1 cells on the contralateral side behaved like neural stem cells *in vitro*, we dissected the contralateral SVZ two days after unilateral injection and plated dissociated cells in an adherent neural stem cell culture system (Scheffler et al., 2005). GFP+ cells from the contralateral side could be passaged and differentiated into multiple lineages *in vitro* (**Figures 9H and 9I**). These data indicated that B1 cells labeled via their ventricle-contacting apical surface were neural stem cells

capable of generating olfactory bulb neurons *in vivo* and multiple lineages *in vitro*.

Discussion

By examining the walls of the lateral ventricles en-face, we uncovered a novel architecture for this germinal layer and identified three distinct cell types that contact the ventricle (**Figure 10**). In addition to ependymal (E1) cells, we found numerous type B1 cells that function as stem cells (Doetsch et al., 1999a) and previously unidentified cells with two cilia and complex basal bodies (E2 cells). The ventricular surface architecture, which resembled pinwheels, consisted of the apical surfaces of B1 cells surrounded by ependymal cells. This architecture was only observed in ventricular walls where neurogenesis occurs in adulthood. Within these neurogenic regions, we found hot spots where B1 cells with ventricle-contacting apical surfaces were more abundant. B1 cells not only had an apical surface, but also had a long basal process. We showed that these cells were derived from radial glia, exhibited self-renewal and multilineage differentiation in vitro, and generated olfactory bulb neurons in vivo. Some of these B1 cells were observed undergoing mitosis close to the ventricular surface. These observations suggest that B1 cells comprise a highly modified neurogenic ventricular zone niche in the adult brain.

B1 cells retain a long basal process

B1 cells on the walls of the lateral ventricle had a long basal process that penetrated the underlying brain parenchyma. Neural stem cells, in the embryo

(neuroepithelial cells and radial glia), in the adult hippocampus (radial astrocytes) or in adult song birds (radial cells), also have a long basal process. This cellular extension may allow neural stem cells to bridge information arising from basal and apical boundaries into the neurogenic niche. During earlier development, neuroepithelial cells and radial glia bridge between the ventricular and the subpial surfaces; signals arising at both poles are essential for proper germinal activity (e.g. ventricular: (Bittman et al., 1997; Kosodo et al., 2004; Nadarajah et al., 1997; Weissman et al., 2004), e.g. subpial: (Halfter et al., 2002; Haubst et al., 2006)). As development progresses and the brain thickens, many radial glia establish specialized endings with blood vessels (Alvarez-Buylla et al., 1987; Misson et al., 1988; Noctor et al., 2001). Interactions between the stem cell compartment and blood vessels are maintained in the heavily vascularized adult SVZ, where specialized extensions of extracellular matrix infiltrate within the adult germinal niche (Alvarez-Buylla and Lim, 2004; Mercier et al., 2002). In the subgranular zone of the adult hippocampal dentate gyrus, neural stem cells reside in close proximity to blood vessels (Palmer et al., 2000). Recently, it was shown that soluble factors secreted by endothelial cells promote stem cell self-renewal and enhance neuronal production of both embryonic VZ and adult SVZ neural stem cells in vitro (Shen et al., 2004). In the present study we found that the long basal process of most B1 cells terminated directly on blood vessels forming specialized endfeet. The basal process of some B1 cells also formed en-passant endings and contacted multiple blood vessels (**Figure S7**). Similar endings have been described in radial glial fibers in the developing neocortex

(Noctor et al., 2001) and radial cell fibers in song birds (Alvarez-Buylla et al., 1987). Interestingly, the basal processes of B1 cells did not necessarily terminate on nearby blood vessels within the SVZ. Instead, they terminated on blood vessels, often at a distance, located along the trajectory of the long basal process, suggesting that the basal processes are remnants of radial glial fibers. Therefore, in addition to contact with the apical surface, contact with blood vessels may be essential for neural stem cell function. For B1 cells, the function of the basal process and contact with the vasculature remains unknown, but these endfeet may allow B1 cells to respond to signals in the perivascular extracellular matrix (Kerever et al., 2007) or to hormones or growth factors present in the circulation, such as prolactin (Shingo et al., 2003), PDGF (Jackson et al., 2006), or IGFs (Jiang et al., 1998).

Radial glia of the developing neocortex (Noctor et al., 2001; Rakic, 1972), radial astrocytes in the hippocampus (Seri et al., 2004), and radial cells in song birds (Alvarez-Buylla and Nottebohm, 1988) use the long basal process to maintain contact with neuronal progeny during early stages of differentiation and migration. This contact may be important for guiding the migration and maturation of nascent progeny. Something similar may take place in the adult SVZ. We found in the present study that many of the basal processes of B1 cells were oriented in the same direction as neuroblast migration, especially in the dense dorsal corridor of the SVZ (Sawamoto et al., 2006) (**Figure S4**). In this region chains of migrating neuroblasts appeared to run along the basal process of B1 cells. B1 cells' basal processes may contribute to the directional migration.

Recent work suggests that chemorepellants in cerebrospinal fluid and its directional flow also contribute to directional migration (Sawamoto et al., 2006). We show here that B1 cells bridge these two compartments: they may detect chemorepellants through their apical ventricular ending and transfer this information to the SVZ along their basal processes that run parallel to chains of migrating neuroblasts. Therefore the organization of B1 cell's basal extensions could play important roles in both the regulation of stem cell proliferation by maintaining specialized contacts with blood vessels and the interaction of these stem cells with their progeny.

B1 cells maintain a modified ventricular zone in the adult brain

The embryonic ventricular zone is comprised of radial glia that have an apical surface in contact with the ventricle. We show that B1 cells in the adult brain also have an apical surface in contact with the ventricle, that they are morphologically similar to radial glia, that they are derived from radial glia, and that they are neurogenic. This suggests that B1 cells are modified radial glia that maintain an adult ventricular zone. However, unlike the embryonic ventricular zone that contains only radial glia, the adult ventricular zone was highly modified and contained ependymal cells in addition to B1 cells. Ependymal cells occupied most of the space in the adult VZ and squeezed the apical cytoplasm of neighboring B1 cells, pushing their cell bodies away from the lateral ventricle toward the subventricular zone. A ventricular zone comprised of a mixture of ependymal cells and B cells has also been described in the brains of adult canaries (Alvarez-Buylla et al., 1998) and adult reptiles (Garcia-Verdugo et al.,

2002). Both of these studies were done by serial section electron microscopy. The present study examined the adult ventricular zone niche en-face revealing a previously unappreciated center-surround organization, where B1 cells were surrounded by ependymal cells to form pinwheels. The pinwheels were abundant throughout the neurogenic niche, but absent from non-neurogenic ventricular walls, suggesting that they play a fundamental role for adult neurogenesis. Ependymal cells express high levels of noggin, which helps create a niche for B cells to function as neuronal progenitors (Lim et al., 2000). Ependymal cells also form specialized apical tight and adherens junctions with B1 cells. The pinwheels may provide the proper architecture for ependymal regulation of B1 cell behavior.

The pinwheel architecture of the adult ventricular zone may also hold clues about how it is derived from the embryonic ventricular zone. Ependymal cells and B1 cells are derived from radial glia (Spassky et al., 2005), and a subpopulation of radial glia becomes committed to the ependymal fate before birth (Spassky et al., 2005). In the embryonic ventricular zone, pinwheels or other planar organization may not be evident because the apical surfaces of radial glia that may be committed to different fates are similar in size (data not shown). However, as some radial glia begin to transform into ependymal cells, their apical surfaces expand and this expansion may push the apical surfaces of many neurogenic radial glia into central clusters held together by apical junctional complexes between these cells. The maintenance of apical junctional complexes between radial glia during the time of ependymal cell differentiation may

therefore explain the development of pinwheels in the adult ventricular zone. This scenario suggests that apical junctions between B1 cells are different than those between ependymal cells or between ependymal cells and B1 cells. This is precisely what we observed (**Figure 4**). Interestingly, a recent study showed that numb and numb-like are required for maintaining radial glial adherens junctions and that numb overexpression results, in a cadherin-dependent manner, in abnormal maintenance of radial glia postnatally (Rasin et al., 2007). The pinwheel pattern also suggests a possible role for lateral inhibition by Notch signaling. In the postnatal hippocampal dentate gyrus, Notch is actively required for GFAP+ stem cell maintenance vs. neurogenesis (Breunig et al., 2007). Similarly in the neonatal VZ, Notch-expressing B1 cells may signal to neighboring ependymal cells during their differentiation, resulting in the formation of pinwheels by lateral inhibition.

In the embryonic ventricular zone, radial glial cells undergo interkinetic nuclear migration (Misson et al., 1988; Sauer, 1935). In the adult ventricular zone of birds, B cells also exhibit this behavior (Alvarez-Buylla et al., 1998). In fact in the early postnatal mouse ventricular zone, where ependymal differentiation is underway, radial glia continue to undergo interkinetic nuclear migration (Tramontin et al., 2003). Now we observe that B1 cells in the adult ventricular zone may be attempting a similar behavior. A disproportionate number (41%) of Ki67+ B1 cells with an apical ending on the ventricular surface were found in mitosis. This bias was likely due to our method for identifying Ki67+ B1 apical surfaces. Our method relied on finding Ki67+ nuclei bounded by

β-catenin+ cell contours that could be traced through consecutive confocal slices back to the ventricular surface. It worked best for cells with nuclei close to the ventricular surface, not cells with nuclei deeper in the SVZ that contacted the ventricle through an apical process. The high percentage of cells we found in M phase therefore suggests that the nuclei of B1 cells migrate closer to the ventricular surface to undergo mitosis. It is likely that there were many S phase Ki67+ B1 cells that we were not able to identify because we were not able to follow the cell contour deep enough into the tissue. It is unlikely that this bias indicates that B1 cells contact the ventricular surface only when activated to proliferate because the majority of B1 apical surfaces were not Ki67+. Developing a method for time-lapse imaging on adult wholemounts would be invaluable to the investigation of the dynamic properties of B1 cells, such as possible interkinetic nuclear migration.

The persistence of an adult ventricular zone consisting of neurogenic B1 cells leads us to re-examine the roles of the ventricular and subventricular zones in adult neurogenesis. In the embryo, the ventricular and subventricular compartments are largely distinct: the ventricular zone for stem cells and the subventricular zone for transit-amplifying intermediate progenitors (Haubensak et al., 2004; Noctor et al., 2004; Noctor et al., 2007). Similarly, the adult neurogenic niche may be comprised of two compartments, a ventricular zone for B1 cells and a subventricular zone for transit-amplifying intermediate progenitors, or C cells, and neuroblasts, or A cells. In the adult, however, the distinction between these compartments may be less clear due to the apical expansion of ependymal

cells. Consistently, we show that the cell body of most B1 cells is pushed back towards the subventricular zone at the interface between ependymal cells and migratory neuroblasts. This model provides a unified hypothesis on the roles of the ventricular and subventricular zones in neurogenic niches of the brain, from embryo to adult. The study shows that contact with the ventricular cavity, being part of an epithelium, and having specialized apical structures are germinal niche properties retained by adult neural stem cells. It is likely that all of these are fundamental to their function. The en-face imaging methods developed here should facilitate understanding the function of apical structures in adult neural stem cells.

A
acetyl-tub
B
γtub
C
γtub
βcat
D
γtub
acetyl-tub
E
B1
F
E1
G
E2
H
B1 E2 E1
Number per mm²
3500
3000
2500
2000
1500
1000
500
0
I
B1 E2 E1
% cells
35
30
25
20
15
10
5
0
0 200 400 600
apical surface area, um²
J
B1 E2 E1
% cells
35
30
25
20
15
10
5
0
0 5 10 15 20
cilia length, um

Figure 1. Three cell types contact the lateral ventricle.
(A-D) Confocal optical sections taken at the surface of immunostained wholemounts of the lateral wall of the lateral ventricle.
(A) Staining wholemounts for acetylated-tubulin reveals many long cilia of ependymal cells. Scale bar = 10 um (A-D).
(B, C) γ-tubulin staining (B) labels the basal bodies of cilia and provides an unobstructed view of the ventricular surface. γ-tubulin and β-catenin staining (C) reveal three distinct cell types: cells (E1) with a large apical surface and multiple basal bodies, cells (B1) with a small apical surface and a single basal body (arrows), and cells (E2) with an intermediate-sized apical surface and two large, complex basal bodies (arrowheads).
(D) The three cell types are also distinguished by their cilia: cells (E1) with multiple basal bodies have multiple long cilia, cells (B1) with a single basal body have a single primary cilium (arrows), and cells (E2) with two complex basal bodies often have two long cilia (arrowheads).
(E) Electron micrograph showing the primary cilium, basal body and centriole of a B1 cell. The apical membrane at the base of the cilium of both B1 and E2 (G) cells was invaginated and engulfed the proximal part of the cilium into an extracellular pocket beneath the apical surface. Scale bar = 0.5 um (E-G).
(F) Electron micrograph of E1 cilia. E1 cilia are not invaginated.
(G) Electron micrograph of an E2 cilium shown for comparison. E2 cilia, like B1 primary cilia, were engulfed in an invagination of the apical membrane. Note the electron dense structure (arrowhead) that projected laterally from the basal body of E2 cells, in the shape of a raceme of grapes. E2 cells are described in detail in Chapter 5.
(H) Density of B1, E1, and E2 cells on the lateral wall of the lateral ventricle. Error bars show standard error.
(I) Histogram of the apical surface area of B1, E1, and E2 cells. B1 cells, while substantial in number, presented a rare profile on the ventricular surface due to their small apical area.
(J) Histogram of cilia length showed that the primary cilia of B1 cells was ¼ the size of the cilia of E1 and E2 cells, which had cilia of comparable length.

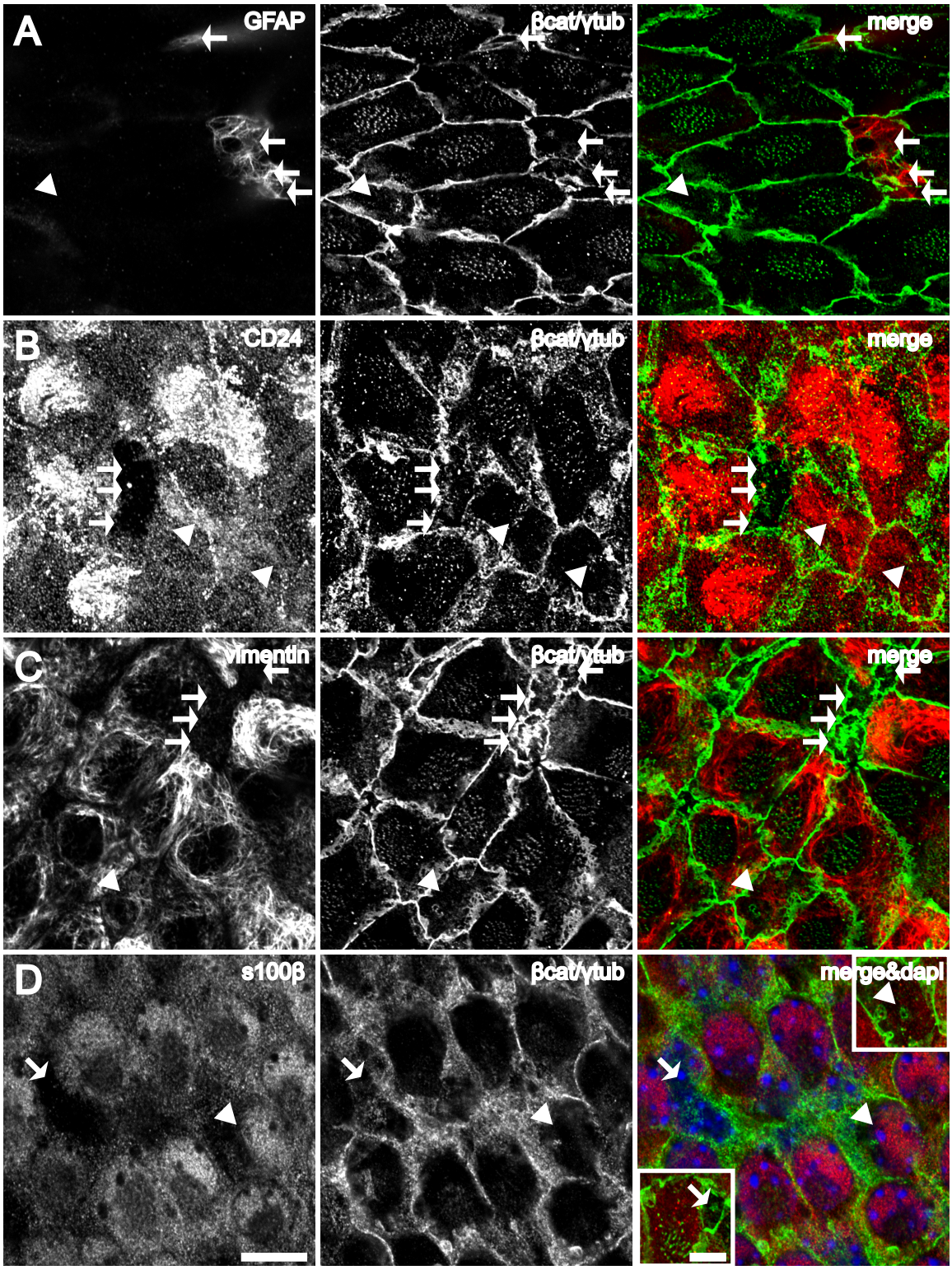

A
GFAP
βcat/γtub
merge
B
CD24
βcat/γtub
merge
C
vimentin
βcat/γtub
merge
D
s100β
βcat/γtub
merge&dapi

Figure 2. Complementary expression patterns of molecular markers at the apical surface of B1 and E1/E2 cells.

(A-C, D insets) are confocal optical sections taken at the surface of the wholemount and (D) was taken just below the surface. Arrows indicate B1 cells and arrowheads indicate E2 cells.

(A) GFAP staining is present in B1 apical surfaces, but not in E1 or E2 cells.

(B) CD24 is expressed highly in the cilia and also on the apical surface of E1 and E2 cells, but not B1 cells.

(C) Vimentin is expressed at the apical surface of E1 and E2 cells, but not B1 cells.

(D) Because S100β is not highly expressed at the apical surface, we examined expression at the level of the nucleus of cells contacting the ventricle. E1 and E2 cells express S100β but B1 cells do not. Insets show the apical surface of the indicated B1 and E2 cells. Scale bar = 10 um (A-D). Inset: Scale bar = 5 um.

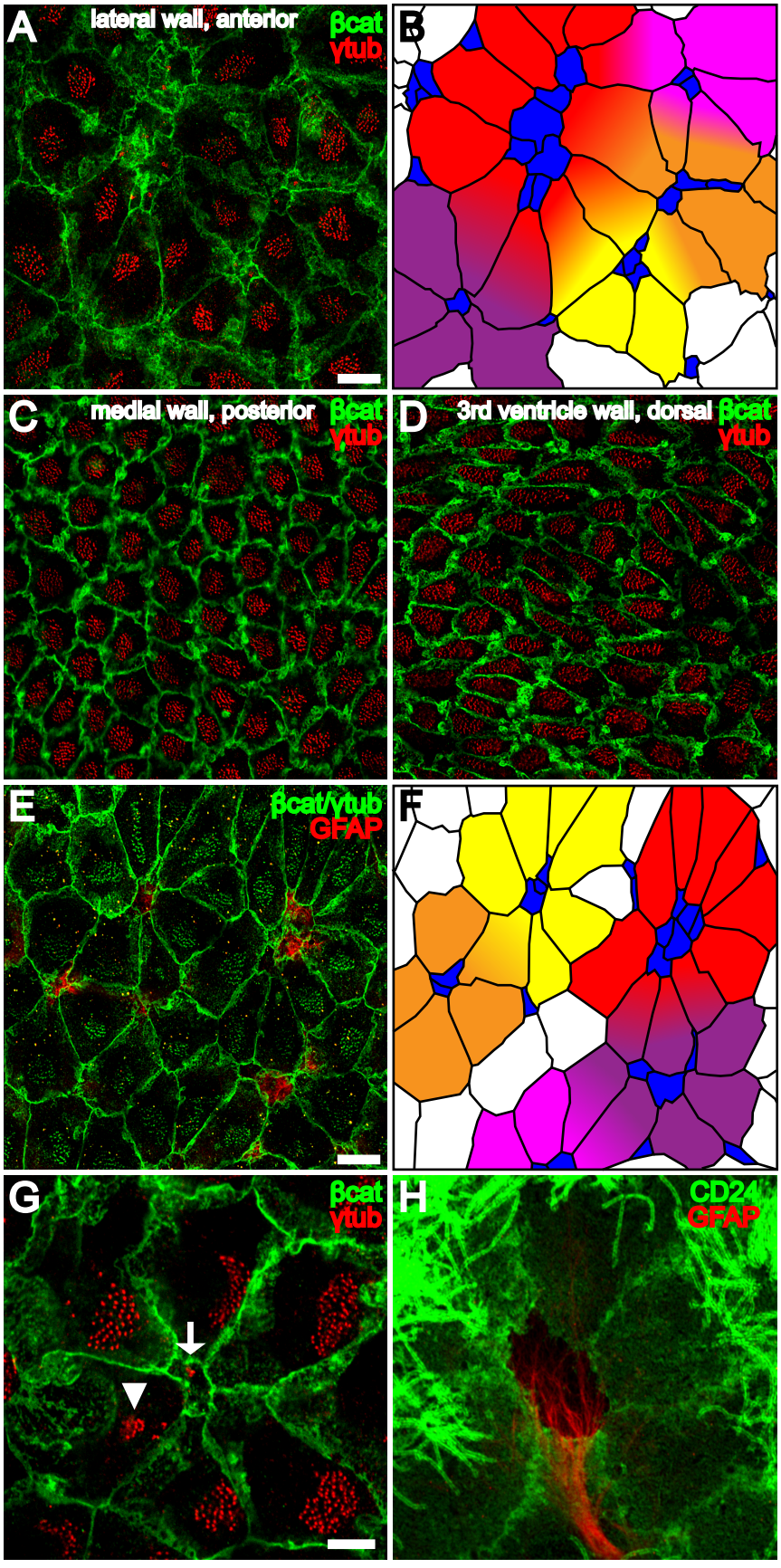

A
lateral wall, anterior
βcat
γtub
B
C
medial wall, posterior
βcat
γtub
D
3rd ventricle wall, dorsal
βcat
γtub
E
βcat/γtub
GFAP
F
G
βcat
γtub
H
CD24
GFAP

Figure 3. Pinwheel architecture of the ventricular surface in neurogenic regions of the adult ventricular system.

(A) Confocal image of the surface of the anterior lateral wall of the lateral ventricle stained for γ-tubulin (red) and β-catenin (green) reveals pinwheels with centrally located B1 apical surfaces surrounded by ependymal cells. Scale bar = 10 um (A-D).

(B) Tracing of the β-catenin+ membranes in (A) and color-coding of B1 cells (blue) and E1 cells (yellow, orange, red, purple, and magenta) to illustrate 5 pinwheels. Note that some E1 cells occupy positions in more than one pinwheel.

(C,D) Neither B1 apical surfaces nor pinwheels are observed in the posterior medial wall of the lateral ventricle or in the walls of the third ventricle.

(E) Confocal image of the surface of the anterior lateral wall of the lateral ventricle shows that pinwheels surround GFAP+ (red) B1 cells. β-catenin and γ-tubulin are in green. Scale bar = 10 um.

(F) Color-coded tracing (as in B) of the image in (E) to illustrate pinwheel organization.

(G) A higher magnification confocal image demonstrating the approximately triangular or diamond shape of E1 apical surfaces found in pinwheels. Note the polarized position of the basal body patch, found on the right side of each E1 surface in this image, is independent of the triangular geometry of the surface. A B1 apical surface is indicated in the center of the pinwheel (arrow) and an E2 apical surface (arrowhead) is indicated on the periphery. Scale bar = 5 um (G, H)

(H) The pinwheel architecture is also appreciated by immunostaining for GFAP and CD24, which label B1 cells and E1/E2 cells, respectively.

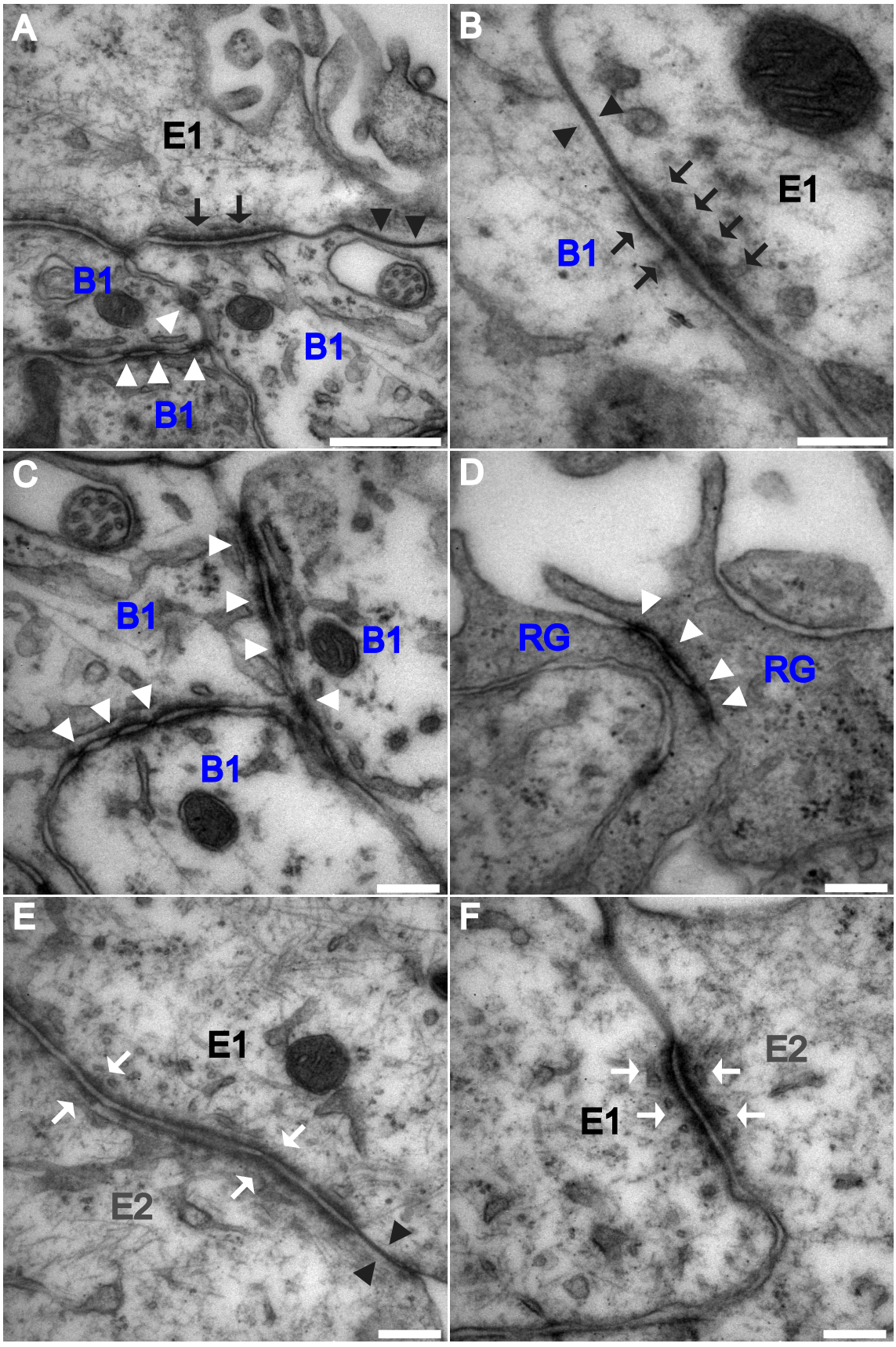

A
E1
B1
B1
B1
B
E1
B1
C
B1
B1
B1
D
RG
RG
E
E1
E2
F
E2
E1

Figure 4. Apical intercellular junctional complexes differ at B1-B1, B1-E1, and E1-E2 junctions.

Serial section reconstruction of these cells at the EM was used to confirm cell identity based on the number and ultrastructure of their cilia and basal bodies.

(A) In addition to tight junctions (black arrowheads), B1 and E1 cells form asymmetric adherens junctions (black arrows). Note that more electron-dense material is accumulated on the E1 side of the adherens junction than on the B1 side. B1 cells form symmetric but atypical adherens junctions with each other (white arrowheads), consisting of periodic pinching of the membrane with electron dense puncta in the intercellular gap. Scale bar = 500 nm.

(B) Higher magnification micrograph of an asymmetric adherens junction (black arrows) between B1 and E1 cells. Note there is more electron dense material on the E1 side. Black arrowheads indicate a tight junction. Scale bar = 200 nm.

(C) Higher magnification micrograph of atypical B1-B1 adherens junctions. Scale bar = 200 nm.

(D) Radial glia (RG) in the neonatal VZ have apically localized symmetric, atypical adherens junctions (white arrowheads) similar to those observed at B1-B1 junctions in the adult. Scale bar = 200 nm.

(E, F) In addition to forming tight junctions (black arrowheads in E), E1 and E2 cells form symmetric adherens junctions (white arrows) that are indistinguishable from those at E1-E1 junctions. Scale bar = 200 nm.

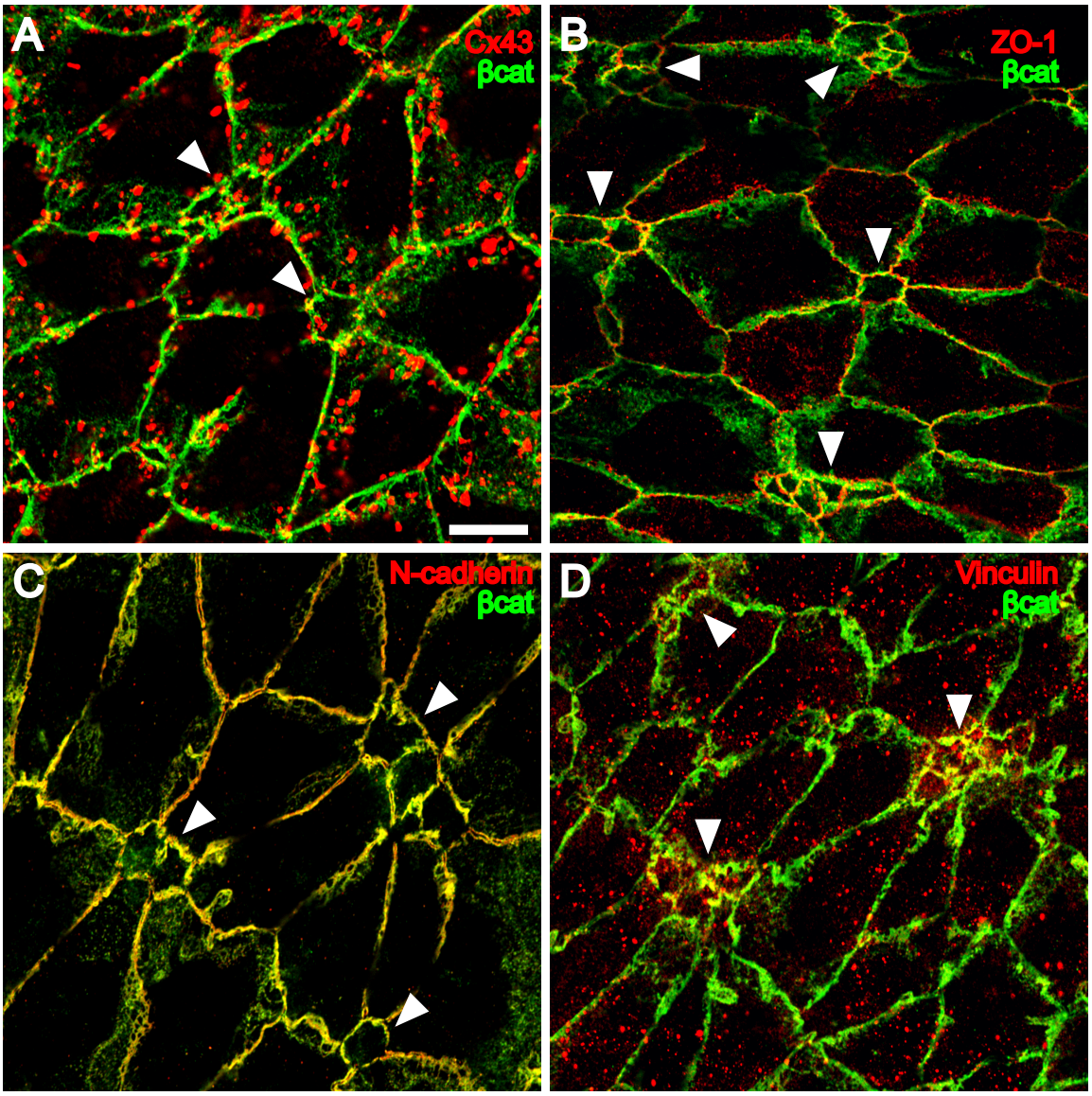

A
Cx43
βcat
B
ZO-1
βcat
C
N-cadherin
βcat
D
Vinculin
βcat

Figure 5. Apical intercellular membranes at B1-B1 and B1-ependymal junctions localize gap junction protein Cx43 and several adherens junction proteins.

All images shown are confocal optical sections at the ventricular surface of lateral wall wholemounts of the LV. Note the pinwheels consisting of large apical surfaces of ependymal cells surrounding 1 or a cluster of small apical surfaces belonging to B1 cells (arrowheads indicate B1 apical surfaces).

(A) Connexin 43 (Cx43, red), a component of gap junctions, localized to intercellular membranes at ependymal-ependymal, B1-ependymal, and B1-B1 junctions. Cx43 staining was either in small intercellular puncta or large globular masses. Scale bar = 10 um (A-D).

(B) ZO-1 can associate with both tight junctions and adherens junctions and it was sharply localized to intercellular membranes between all cell types.

(C) N-cadherin (red), a homotypic cell-cell adhesion molecule that bridges adherens junctions of adjacent cells was highly co-localized with β-catenin (green) and observed at intercellular junctions between all cell types.

(D) Vinculin (red), an intracellular component of adherens junctions, localized to intercellular membranes between all cell types but it appeared to be more intensely expressed at B1 junctions.

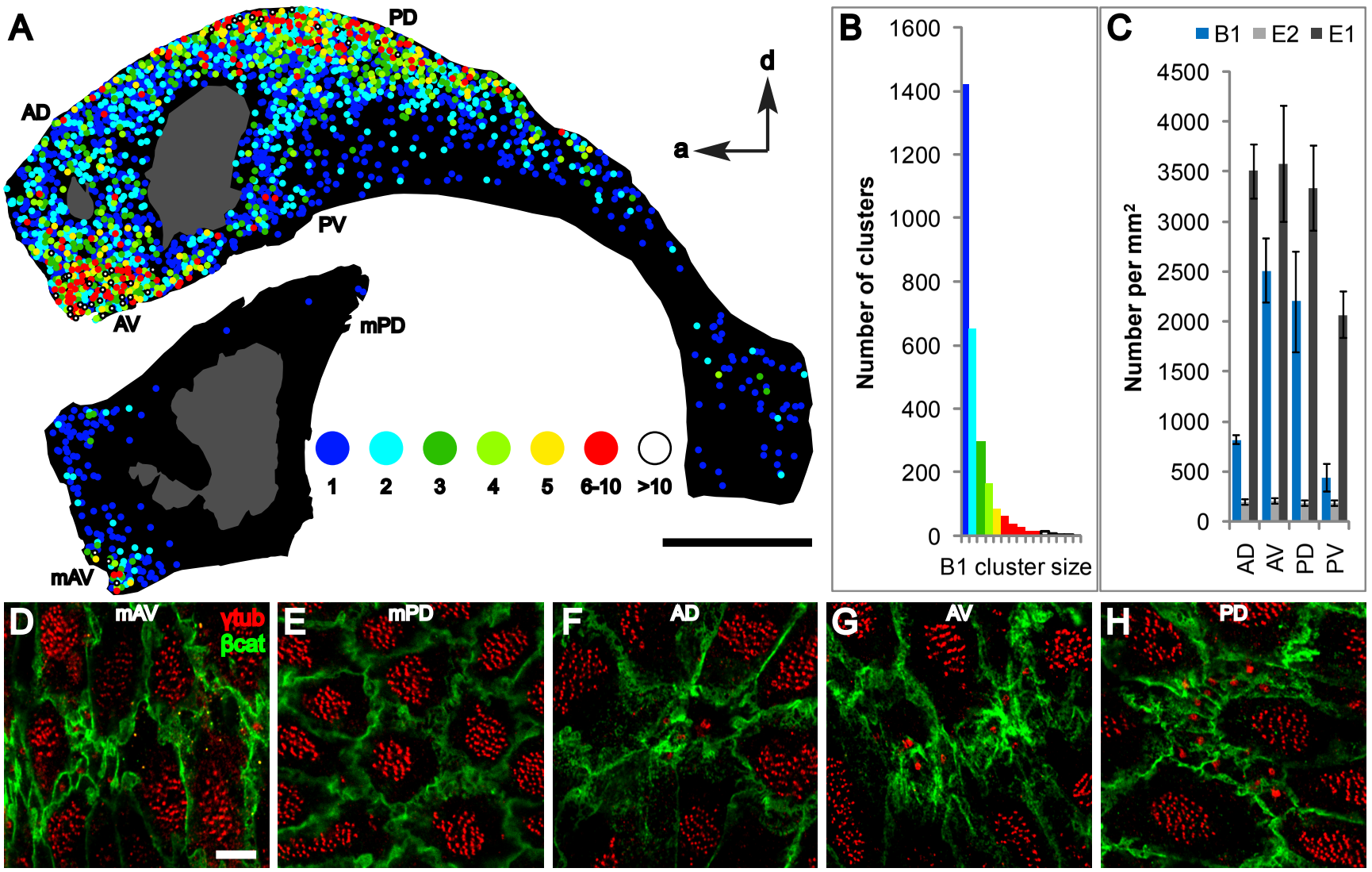

A
PD
AD
d
a
PV
AV
mPD
mAV
1
2
3
4
5
6-10
>10
B
1600
1400
1200
1000
800
600
400
200
0
Number of clusters
B1 cluster size
C
B1
E2
E1
4500
4000
3500
3000
2500
2000
1500
1000
500
0
Number per mm²
AD
AV
PD
PV
D
mAV
γtub
βcat
E
mPD
F
AD
G
AV
H
PD

Figure 6. Surface maps of the walls of the lateral ventricle revealed “hot spots” of B1 apical surfaces.
(A) The maps were reconstructed from high power (212 x 212 um2) tiled confocal images taken from only the surface of lateral and medial wall wholemounts stained for γ-tubulin and β-catenin. The position of B1 apical surfaces is indicated on the maps by color-coded circles depicting the number of B1 apical surfaces per cluster (1, 2, 3, 4, 5, 6-10, or >10 cells per cluster). Hot spots of B1 apical surfaces were found in the anterior-ventral (AV) and posterior-dorsal (PD) regions of the lateral wall and the anterior-ventral (mAV) region of the medial wall. The adhesion point is shown in gray. Scale bar = 1 mm.
(B) Distribution of cluster size of B1 apical surfaces.
(C) Density of B1, E1, and E2 apical surfaces in 4 regions of the lateral wall in 3 animals. The regions quantified are indicated in (A) and Figure S10. Error bars show standard error.
(D-H) Representative confocal images from different regions of the surface of the lateral and medial walls stained for γ-tubulin and β-catenin. Scale bar = 5 um.

A
GFAP
B
GFAP
C
GFAP
C'
90°
D
βcatYtub
GFAP
E
GFAP
F
βcatYtub
GFAP
G
GFP
H
GFP
GFP
GFAP
I
GFP
Ytub
J
K
L
GFP
GFAP
M
GFP
d
a
L
A,H
B,C,E,G
M

Figure 7. B1 cells with an apical surface contacting the ventricle have a long basal process.
The diagram of the lateral wall at the top right indicates where in the wholemount the images were taken (A-L); (M) is an image from a horizontal section.
(A, B) Z-projections of low power confocal stacks (50 um thick) taken from wholemounts stained for GFAP. The orientation of GFAP+ processes varies depending on the region in the lateral wall. Note that because the wholemounts are freshly dissected, secondary antibodies used against mouse anti-GFAP primary antibody also stain blood vessels that contain endogenous mouse IgGs. Scale bar = 50 um.
(C) Z-projection of a higher power confocal stack (50 um thick) taken from a wholemount stained for GFAP. Blue arrows indicate the apical endings of long GFAP+ processes. Scale bar = 50 um.
(C') 3-dimensional reconstruction of the stack in (C) rotated 90°. Many of the long GFAP+ processes appear to originate at the ventricular surface (blue arrows in C' indicate processes reaching the ventricular surface and correspond to blue arrows in C).
(D) Confocal optical section of the surface (co-stained for γ-tubulin and β-catenin in green) in the region between the blue arrows in (C) reveals that the apical endings indicated in (C) belong to a group of 11 B1 cells with GFAP+ apical surfaces on the ventricle (blue arrows in D correspond to blue arrows in C). Scale bar = 5 um.
(E, F) Often, the long basal process of a B1 cell with an apical surface (blue arrows) terminates on a blood vessel forming an endfoot (yellow arrow in E). Scale bar = 25 um (E), 5 um (F).
(G) B1 cells with an apical surface could be labeled by adeno-GFAPp:Cre virus injected into the lateral ventricle of Z/EG mice. This image is a z-projection of a confocal stack. Scale bar = 50 um.
(H) A higher power confocal z-stack projection reveals the complete morphology of a B1 cell. B1 cells are GFAP+ (boxed region), have an apical surface in contact with the ventricle (blue arrows in H, I), and a long basal process often terminating in an endfoot on a blood vessel (yellow arrow in H). Scale bar = 25 um.
(I-K) Confocal optical sections of the ventricle-contacting apical surface of B1 cells corresponding to the color-coded arrow in (H) and arrowheads in (L). Scale bar = 5 um.
(L) Labeling radial glia by injecting adeno-Cre virus into the ventro-lateral striatum of neonatal Z/EG mice reveals that B1 cells observed in the adult are derived from radial glia. Note the ventricle-contacting apical processes (white and magenta arrowheads in J, K, L) of two B1 cells derived from radial glial targeting. Both of these cells have long basal processes that wrap distally around blood vessels (yellow arrows in L). Scale bar = 25 um.
(M) B1 cells labeled by neonatal radial glial targeting observed in horizontal sections of the adult brain. The long basal processes of B1 cells, whose cell bodies are adjacent to the lateral ventricle (dashed line), reach deep into the underlying striatum. Note the difference in morphology between B1 cells and typical bushy astrocytes (arrow) in the striatum (also see Figure S8). Scale bar = 100 um.

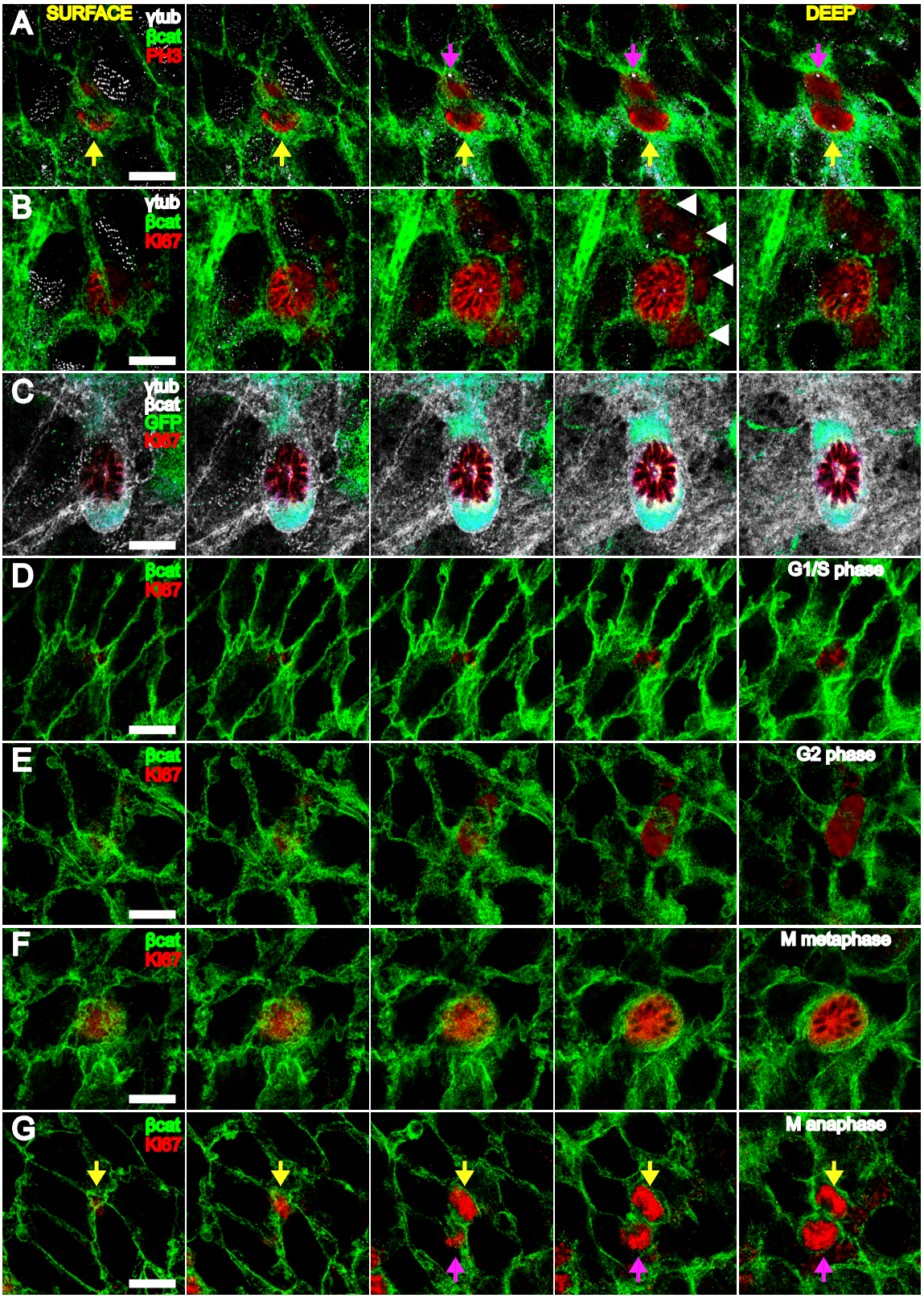

A
SURFACE
γtub
βcat
PH3
DEEP
B
γtub
βcat
KI67
C
γtub
βcat
GFP
KI67
D
βcat
KI67
G1/S phase
E
βcat
KI67
G2 phase
F
βcat
KI67
M metaphase
G
βcat
KI67
M anaphase

Figure 8. B1 cells in mitosis maintain contact with the ventricle.

(A-G) are confocal stacks imaged from wholemounts of the lateral wall of the lateral ventricle. The first optical section in each series was taken at the ventricular surface and the step size between sections is 0.5 um, except (G) where the steps are 1 um. Scale bar = 10 um.

(A) The first optical section shows a PH3+ B1 apical surface. This cell appears to be dividing asymmetrically with one sister chromatid (yellow arrow) visible beneath the apical surface and the other sister chromatid (magenta arrow) deeper beneath an ependymal cell.

(B) The first optical section shows a Ki67+ B1 apical surface. Deeper in the stack, this cell is flanked by a cluster of other Ki67+ cells (arrowheads), likely corresponding to transit-amplifying (type C) cells that were never observed in contact with the ventricle.

(C) A Ki67+/GFP+ apical surface corresponding to a B1 cell in mitosis. This cell was labeled 48 hours earlier by injection of adeno-GFAPp:Cre into the lateral ventricle of a Z/EG mouse, which confirmed that these mitotic cells have an apical surface and an active GFAP promoter.

(D-G) Confocal stacks demonstrating that B1 cells maintain contact with the ventricle throughout the cell cycle. Ki67+ B1 apical surfaces were found with staining patterns corresponding to late G1/S (D), G2 (E), metaphase (F), and anaphase (G). Another example of a B1 cell undergoing an apparently asymmetric division is shown in (G), where one sister chromatid (yellow arrow) retains an apical surface and the other (magenta arrow) is deeper in the SVZ.

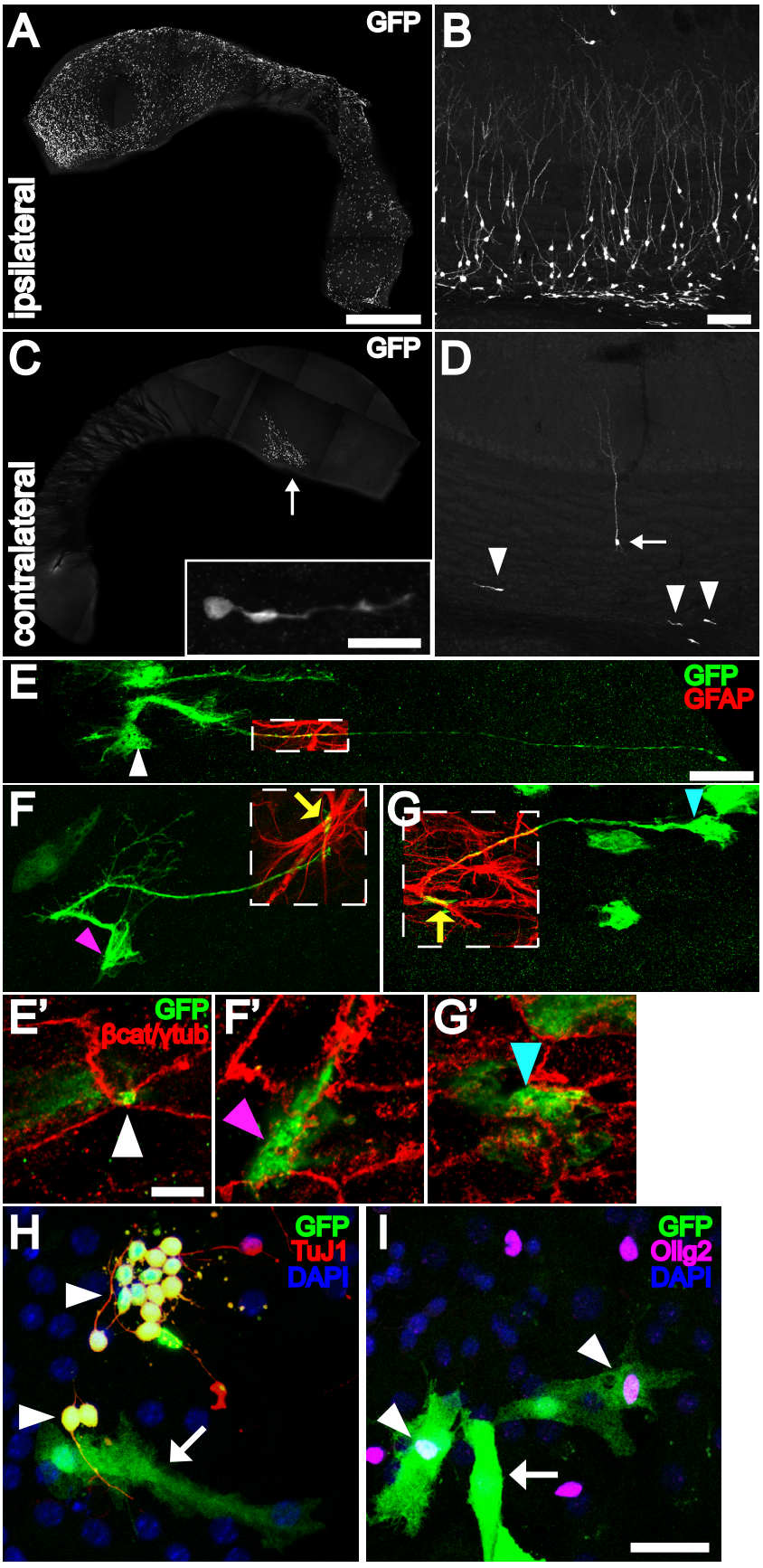

A
GFP
ipsilateral
B
C
GFP
contralateral
D
E
GFP
GFAP
F
G
E'
GFP
βcat/γtub
F'
G'
H
GFP
TuJ1
DAPI
I
GFP
Olig2
DAPI

Figure 9. B1 cells with a ventricle-contacting apical surface are neurogenic in vivo and exhibit multilineage differentiation in vitro.

(A) Injection of adeno-GFAPp:Cre into one lateral ventricle (LV) of Z/EG mice results in many labeled B1 cells with a ventricle-contacting apical surface on the ipsilateral lateral wall. The wholemount images (A, C) were reconstructed from low power (1.3 mm x 1.3 mm) tiled confocal images. Scale bar = 1 mm (A, C).

(B) 30 days after injection, many labeled neurons and neuroblasts can be found in the ipsilateral olfactory bulb. Scale bar = 100 um (B, D).

(C) A few ventricle-contacting B1 cells on the contralateral lateral wall are labeled by virus that backfills the contralateral LV from the ipsilateral LV through the third ventricle. Note that most labeled cells on the contralateral side were close to the foramen of Monro (arrow), which connects the third ventricle with the lateral ventricles. The few labeled B1 cells give rise to neuroblasts (inset) in the contralateral SVZ, examined 30 days after injection. Inset: Scale bar = 20 um.

(D) The few labeled ventricle-contacting B1 cells on the contralateral lateral wall gave rise 30 days later to neuroblasts (arrowheads) and neurons (arrow) in the contralateral olfactory bulb in 6/6 animals injected unilaterally.

(E-G) Examples of B1 cells found in the contralateral lateral wall with the characteristic features of an apical surface contacting the ventricle (color-coded arrowheads in E'-G'), GFAP expression (boxed regions), and a long basal process with endfeet on blood vessels (yellow arrows). Scale bar = 25 um.

(E'-G') Higher power confocal optical sections of the ventricle-contacting apical surface of B1 cells corresponding to the color-coded arrowheads in (E-G). Scale bar = 5 um.

(H, I) GFP-labeled B1 cells on the contralateral side could be dissected out two days after injection, plated as adherent neural stem cell cultures, passaged, and differentiated into neurons (arrowheads in H), astrocytes (arrow in H and I), and oligodendrocytes (arrowheads in I). Scale bar = 10 um.

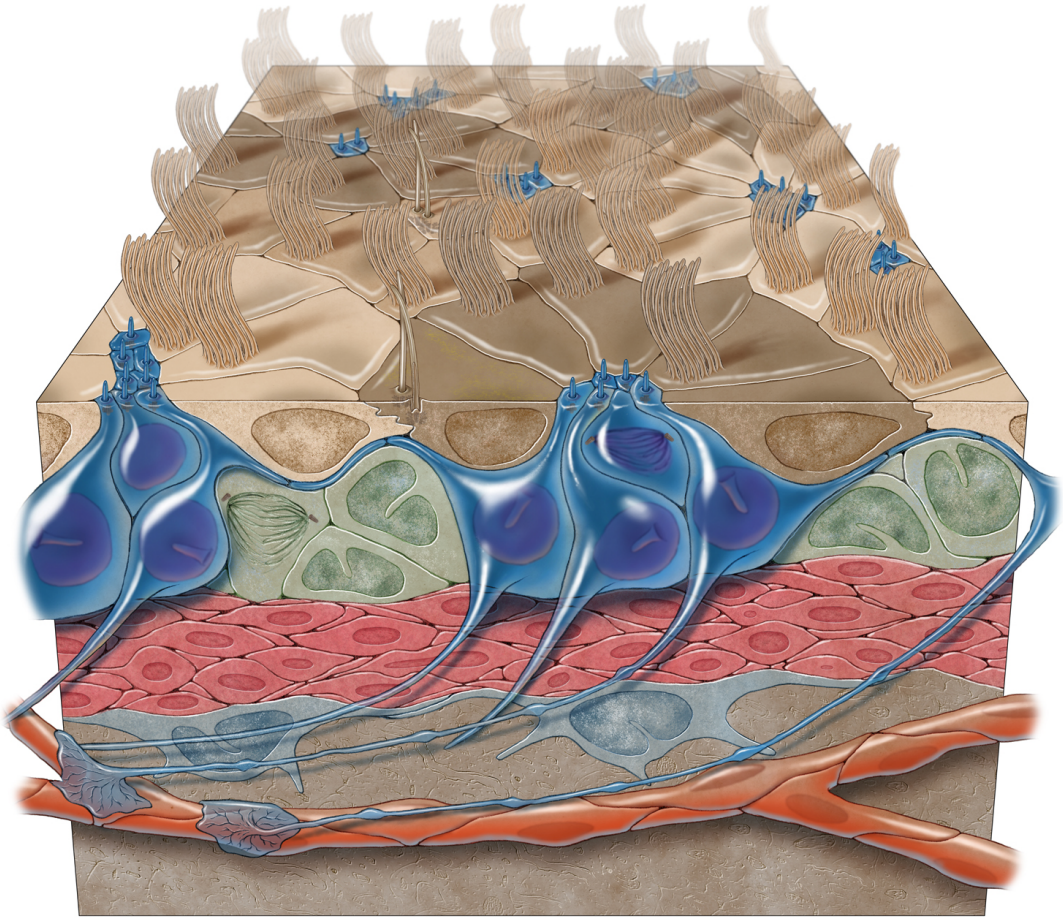


Figure 10. 3-dimensional model of the adult VZ neurogenic niche illustrating B1 cells (blue), C cells (green), and A cells (red). B1 cells have a long basal process that terminates on blood vessels(orange) and an apical ending at the ventricle surface. Note the pinwheel organization (light and dark brown) composed of ependymal cells encircling B1 apical surfaces.

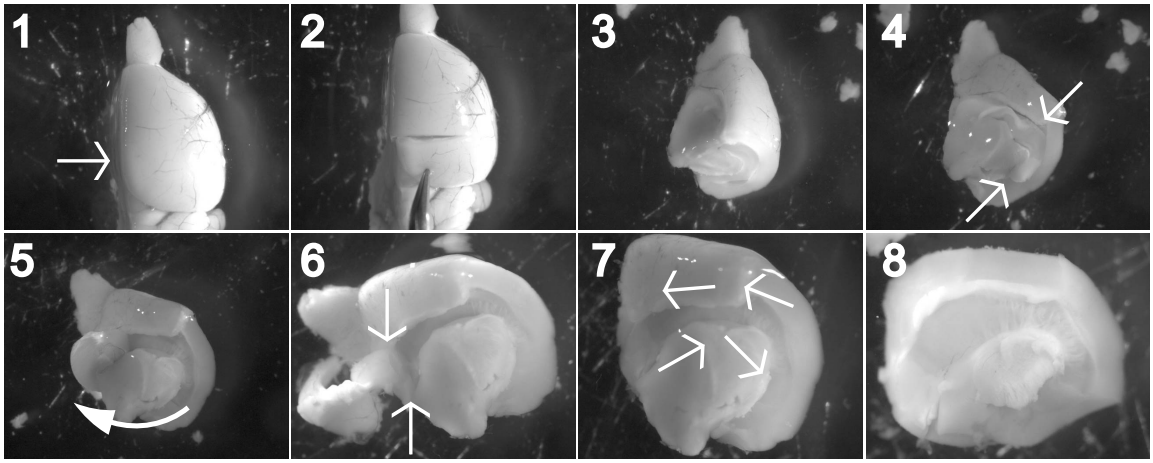


Figure S1. Sequence of stereomicroscopic images taken during dissection of a wholemount of the lateral wall of the lateral ventricle. Open arrows indicate positions where the brain was cut and the closed arrow indicates the direction of the pulling motion applied to the medial wall and underlying septum and hippocampus to expose the lateral wall. Detailed explanation of the dissection is in Experimental Procedures.

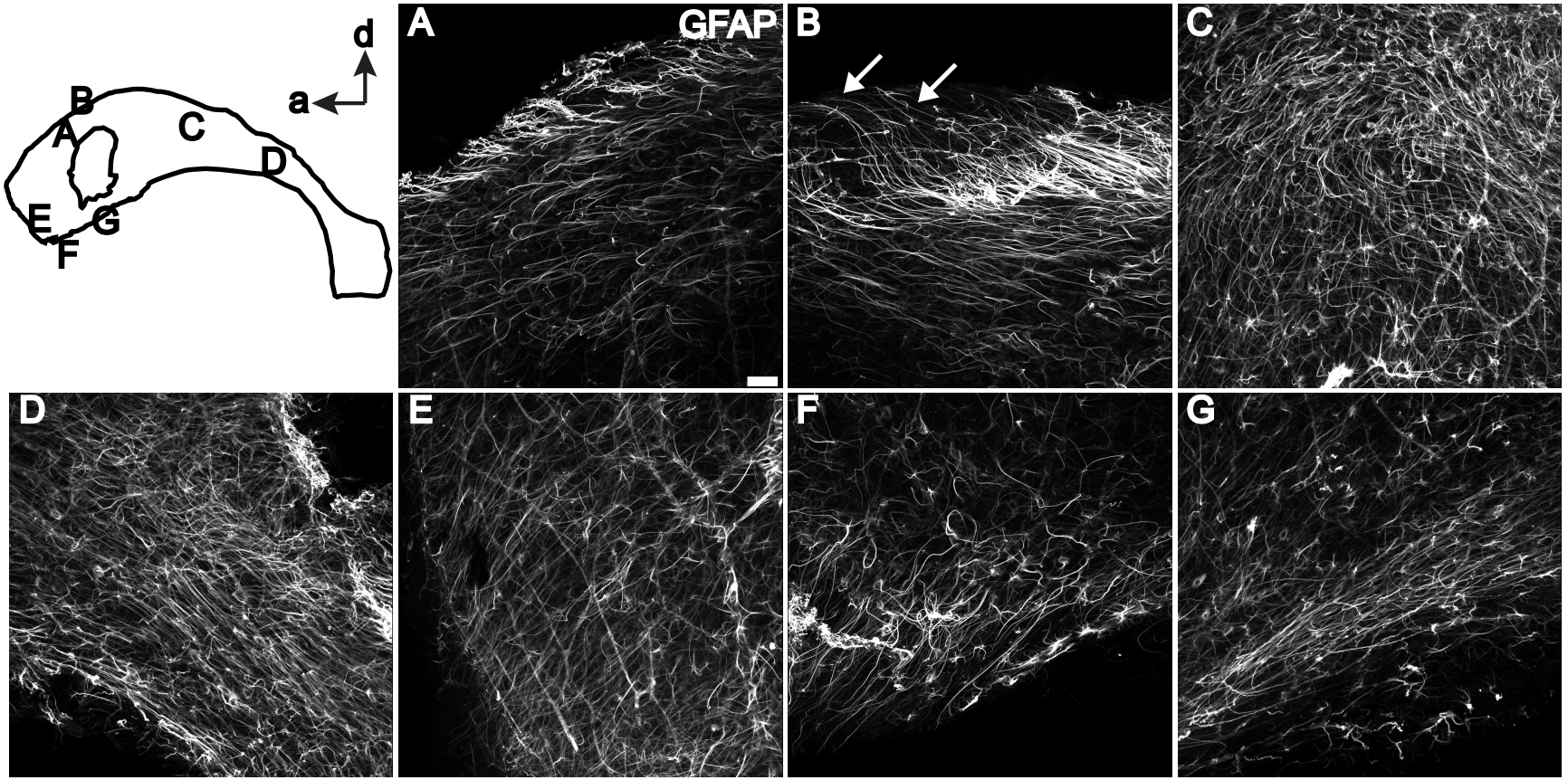

d
a
B
A
C
D
E
F
G
A
GFAP
B
C
D
E
F
G

Figure S2. The orientation of long GFAP+ fibers varies depending on the region in the lateral wall of the lateral ventricle.
(A-G) Z-projections of confocal stacks (50 um thick) taken from wholemounts of the lateral wall stained for GFAP. Diagram of the lateral wall indicates where the images are from. The compass shows anterior (a) and dorsal (d) directions. Note that because the wholemounts are freshly dissected, secondary antibodies used against mouse anti-GFAP primary antibody also stain blood vessels that contain endogenous mouse IgGs.
(A) Dorsal to the adhesion point, most fibers were oriented tangentially to the surface of the lateral wall and ran anteriorly. Scale bar = 50 um (A-G).
(B) At the dorsal-most extent of the wholemount, where the SVZ abuts the corpus callosum (dissected away in image), GFAP+ fibers were oriented obliquely with respect to the surface and ran deep into the underlying striatum (arrows).
(C) Posterior to the adhesion point, most fibers were oriented tangentially to the surface and ran antero-ventrally. Note that some fibers appear to have a different direction: in the right side of the image, corresponding to a more posterior position, the fibers ran postero-ventrally.
(D) More posteriorly in the lateral wall, most fibers ran posteriorly.
(E, F) Anterior to the adhesion point, most fibers ran anteriorly.
(G) Ventral to the adhesion point, although many fibers were oriented obliquely to the surface and ran ventrally deep into the parenchyma (Figure S5D), some fibers were oriented tangentially to the surface and ran anteriorly.

d
a
C
A
B
b
C'
GFAP
DAPI
C
LV
a
p
D
A
GFAP
LV
B
LV

Figure S3. Long GFAP+ fibers were observed in 100 um coronal and horizontal SVZ sections.
(A-D) Z-projections of confocal stacks of different regions of the SVZ in coronal (A, B, D) and horizontal (C) sections stained for GFAP. The diagram of the lateral wall indicates the coronal or horizontal level where images are from. The compass shows anterior (a) and dorsal (d) directions. LV is lateral ventricle.
(A) As seen in wholemounts, in coronal SVZ sections taken behind the adhesion point, many fibers are oriented tangentially to the surface and run ventrally (arrows, compare to Figure 6B). Scale bar = 50 um (A-D).
(B) More dorsally in the SVZ, many fibers (arrows) are oriented obliquely to the surface and run deeper into the underlying striatum beneath the corpus callosum.
(C) Horizontal sections at the level of the dorsal corridor of the SVZ, where many chains of neuroblasts are found (elongated DAPI nuclei in C'), revealed GFAP+ fibers oriented tangentially to the surface that ran anteriorly (arrows, compare to Figure S4A). Anterior (a) and posterior (p) directions are indicated.
(D) At the ventral tip of the lateral ventricle, many fibers were observed running deeper into the striatum oriented ventrally (arrows).

A
GFAP
DCX
GFAP
DCX
B
TOP
BOTTOM
C
MAX

Figure S4. Chains of migrating neuroblasts in the SVZ are oriented parallel to long GFAP+ fibers.
(A) Z-projection of a confocal stack from the region immediately posterior and dorsal to the adhesion point showed chains of DCX+ neuroblasts oriented in two general directions (arrows). Long GFAP+ fibers in this region were also oriented in these two general directions. Scale bar = 100 um.
(B) The top and bottom images of a higher power confocal stack from the region dorsal to the adhesion point. DCX+ neuroblasts appeared to be running largely along GFAP+ fibers, which wrapped around the chains closer to the ventricle surface (TOP) and were oriented tangential to the surface deeper in the SVZ (BOTTOM). Scale bar = 50 um.
(C) Maximum projection of the confocal stack shown in (B).

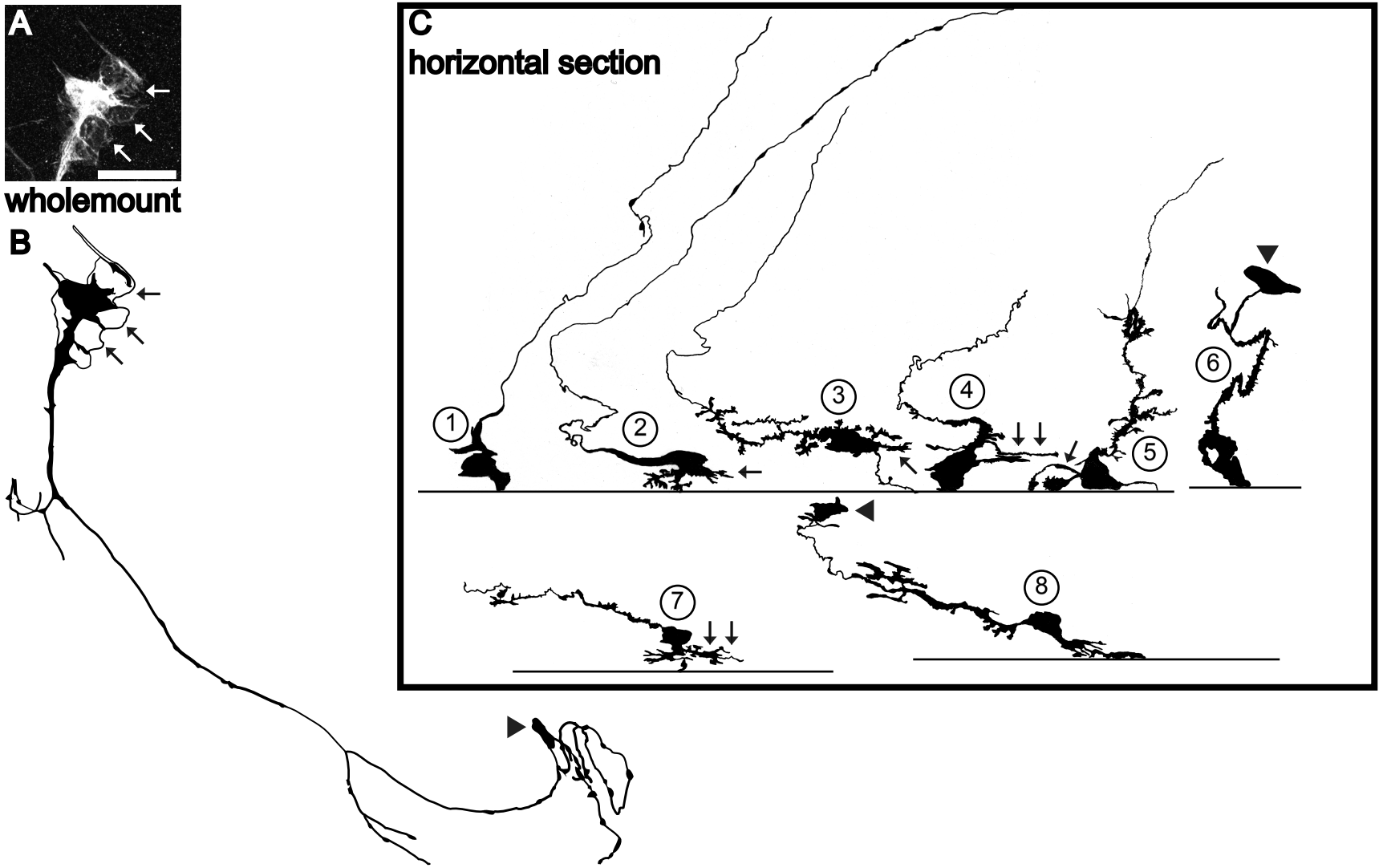

A
wholemount
B
C
horizontal section
1
2
3
4
5
6
7
8

Figure S5. Morphology of ventricle-contacting B1 cells in wholemounts and sections.
These GFP-filled B1 cells were observed in the lateral wall of the adult lateral ventricle. They were derived from radial glia targeted with adeno-Cre injections into the striatum of neonatal Z/EG mice.
(A) Z-projection of a confocal stack of a B1 cell body lying close to the ventricular surface in a wholemount of the lateral wall. This cell had an apical surface in contact with the ventricle. Note the web-like extensions of membrane spanning away from the cell body (arrows), which cover the basal side of adjacent ependymal cells.
(B) Tracing of the complete morphology of the cell shown in (A). This cell had a long basal process with small varicosities along its length and a specialized contact (arrowhead) with a blood vessel.
(C) Several tracings of B1 cells observed in horizontal sections. Here it is difficult to appreciate web-like lateral membranes spanning away from the cell body as most lateral extensions appear as individual processes (arrows). However, B1 cells observed in sections appeared to have apical contact with the ventricle and a long basal process often containing specialized contacts (arrowheads) with blood vessels.

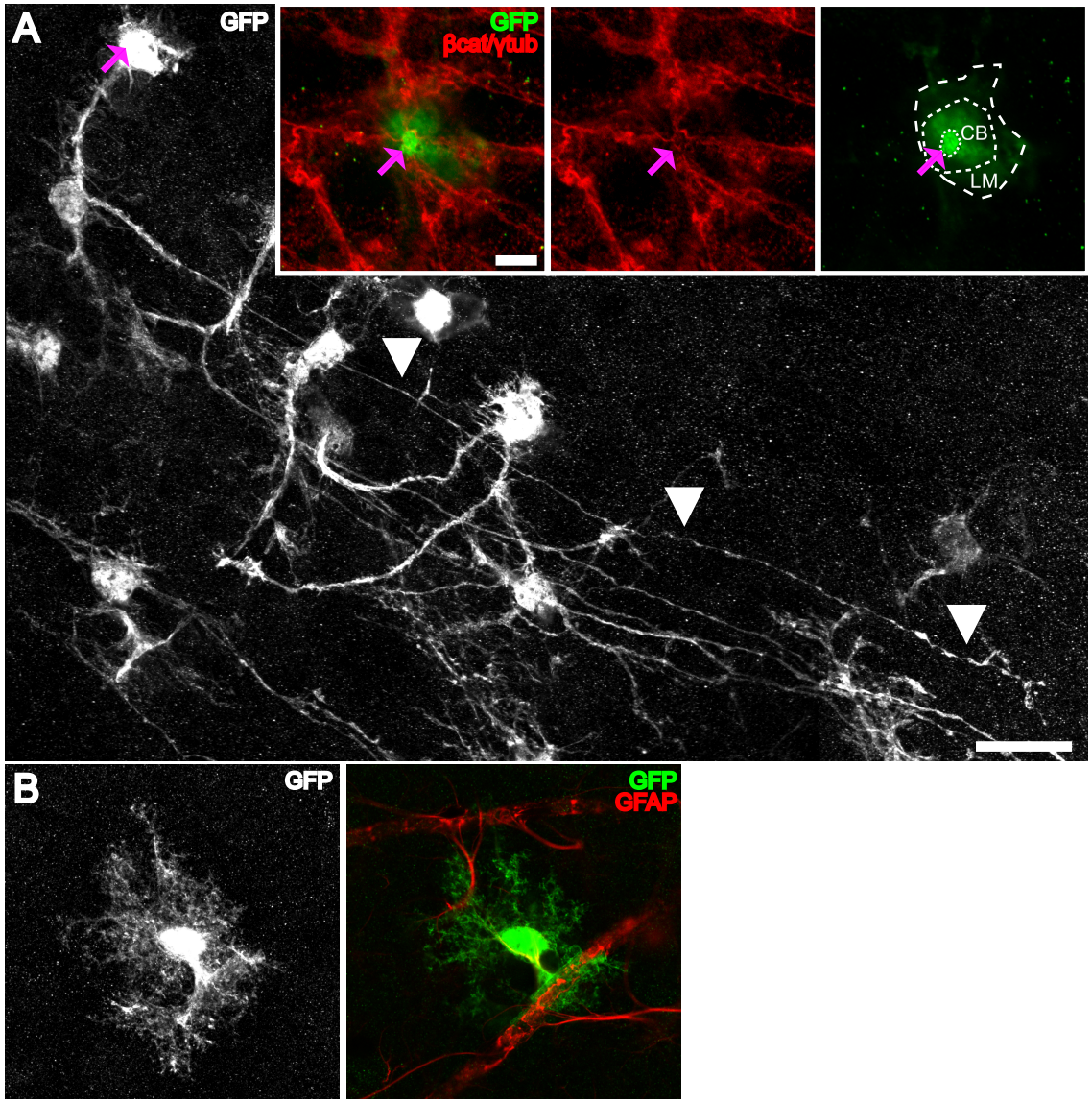


Figure S6. Morphological differences between ventricle-contacting B1 cells and typical parenchymal astrocytes.
(A and B) Z-projections of confocal stacks of GFP-labeled cells observed in the lateral wall of the adult lateral ventricle. These cells were derived from radial glia targeted with adeno-Cre injections into the striatum of neonatal Z/EG mice.
(A) Arrow indicates the position of the apical ending of a B1 cell with a very long basal process (arrowheads). Inset is a higher magnification confocal optical section taken at the surface, which showed the small B1 apical ending (arrow) surrounded by ependymal cells forming a pinwheel. The apical surface (arrow), cell body (CB), and thin lateral membrane (LM) are outlined.
(B) A typical parenchymal astrocyte observed 30-40 um beneath the ventricular surface, likely in the SVZ at the border with the striatum. Note the bushy, highly branched morphology.
(C) The parenchymal astrocyte shown in (B) also made a specialized contact with a blood vessel.

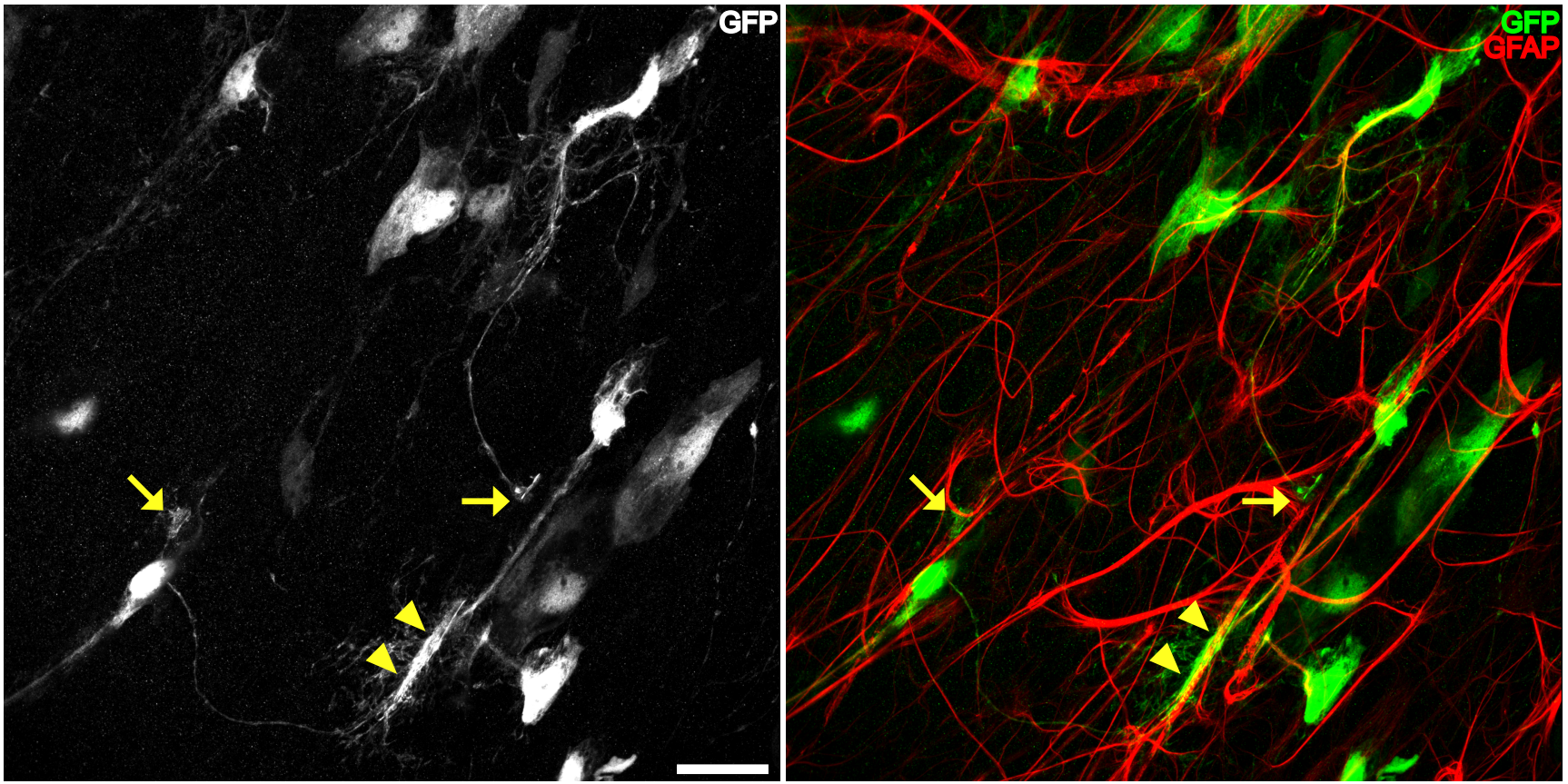


Figure S7. The basal process of B1 cells made specialized contacts with blood vessels, including en-passant contacts (arrowheads) and terminal endfeet (arrows).

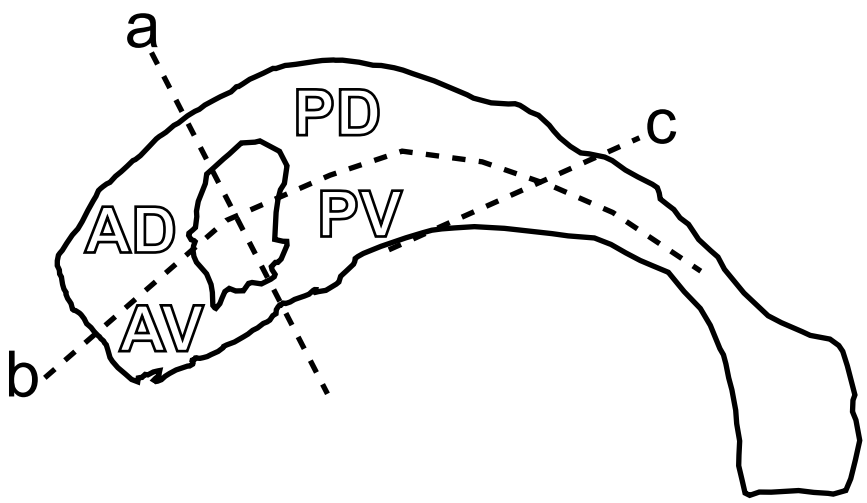


Figure S8. Diagram of the lateral wall illustrating how it was divided into four regions quantified for the density of B1, E1, and E2 cells.
Line (a) bisects the wholemount into a dorsal and ventral half along its anterior-posterior axis.
Line (b) bisects the adhesion point into an anterior and posterior half and runs orthogonal to line (a).
Line (c) is tangential to the ventral boundary of the anterior half of the wholemount and runs through the wholemount at the anterior-posterior level where the wholemount narrows considerably.
These 3 lines in combination with the boundaries of the wholemount divide the lateral wall into four regions, named with respect to the adhesion point: anterior-dorsal (AD), anterior-ventral (AV), posterior-dorsal (PD), and posterior-ventral (PV).

Chapter 4

A unique biciliated cell in the walls of the brain ventricles

Early light and electron microscopic studies of the adult brain identified multiple cell types in contact with the ventricles. In general, these were divided into two categories: cuboidal cells corresponding to multiciliated ependymal cells and elongated cells corresponding to tanycytes (Ramón y Cajal, 1911; Studnicka, 1900). In Chapter 3, we identified at least 3 cell types in contact with the adult brain ventricles: adult neural stem (Type B1) cells, multiciliated ependymal (type E1) cells and a unique biciliated cell type, which we called E2 cells. Here we provide a detailed description of the apical features, ultrastructure, and distribution of E2 cells in the epithelial lining of the brain ventricles. E2 cells were biciliated, had a previously undescribed basal body structure, and uniformly covered the floor of the 3rd and 4th ventricles.

Introduction

The observation that multiple cell types contact the ventricles in the adult brain dates back to studies by Studnicka (1900) and Ramón y Cajal (1911). In these studies, cells of the ependymal lining of the ventricles were classified into two general groups: cubical cells and cells with a basal process that penetrated deep into the underlying parenchyma. In 1954, Horstmann (Horstmann, 1954) first used the term “tanycyte” to refer to long thin cells in Selachians that

contacted the ventricle and had a basal process with terminations on perivascular spaces of fenestrated capillaries. Tanycytes are now considered to be a specialized type of ependymal cell that is morphologically and probably functionally distinct from multiciliated, cuboidal ependymal cells (Bruni, 1998). In addition, tanycytes are not uniformly distributed throughout the ventricular system like cuboidal ependymal cells; they are concentrated in particular regions, such as the floor of the 3rd and midline floor of the 4th ventricle (Collins, 1989; Cummings and Felten, 1979; Del Brio et al., 1991; Millhouse, 1975). The distinguishing morphological feature of tanycytes is their radially directed basal process that extends into the underlying neuropil, where it wraps around blood vessels or terminates on neurons, glia or the external glial limitans (Bruni, 1998). Unlike classical ependymal cells, these cells usually do not have cilia or occasionally have only a solitary cilium (Collins, 1989; Del Brio et al., 1991; Leonhardt, 1980). Although the function of tanycytes has not been well studied, based on the relationship of their basal process with capillaries of the hypophysial portal system at the base of the 3rd ventricle, it has been suggested that these cells serve a neuroendocrine or transport function (Bruni et al., 1985; Flament-Durand and Brion, 1985).

Tanycytes have been studied using a variety of methods, including light microscopy after histological staining, and scanning and transmission electron microscopy, in many different animals. This includes studies in mammals (rat, cat, rabbit, and human) (Gonzalez-Santander, 1979; Knowles, 1972; Leonhardt, 1980; Millhouse, 1971; Mitro and Palkovits, 1981), birds (Sharp, 1972), and

sharks (Horstmann, 1954; Saland et al., 1974). In addition, tanycytes can be differentiated and studied in primary tissue culture from rat embryonic cerebral cortex (Jordan et al., 1987). These studies provide useful anatomical descriptions of tanycytes. However, based on differences in the classification methods used and the animal examined, these studies identify between two and seven different cell types (including tanycytes) in contact with the brain ventricles (Del Brio et al., 1991). In addition, it has been suggested that tanycytes themselves are not a homogeneous population of cells, but can differ in structure, location, and enzyme content (Bruni, 1998; Bruni et al., 1983; Millhouse, 1971, 1975). It appears that classifying into just two groups the multiple different cell types in the ependymal lining of the adult ventricles is an oversimplification.

Our results from Chapter 3 demonstrate that there are at least three cell types in contact with the adult brain ventricles: Type B1 cells, or the adult neural stem cells, Type E1 cells, which are the multiciliated cuboidal ependymal cells, and Type E2 cells, which have a previously undescribed basal body structure and represent a novel ependymal cell type not previously described in the lateral ventricles. In this chapter, we provide a more detailed analysis of the ultrastructure of type E2 cells and their basal bodies. We also analyze the structure of their basal bodies by confocal microscopy and their distribution in different regions of the adult ventricular system. Interestingly, although we initially identified these cells as a rare cell type in contact with the lateral ventricles (Chapter 3), we subsequently found them in much higher numbers in

the 3rd and 4th ventricles. Specifically, these cells uniformly covered the floor of the 3rd ventricle and the midline floor of the 4th ventricle. Although the ultrastructure of E2 cells in the walls of the lateral ventricles was not characteristic of tanycytes, their overlapping distributions in the 3rd and 4th ventricles suggested that at least a subpopulation of tanycytes must correspond to E2 cells.

Results

Apical structures of E2 cells by confocal microscopy

As shown in Chapter 3, E2 cells were identified by the unique structure of their basal bodies, which can be labeled by antibodies to γ-tubulin in wholemounts of the lateral wall of the lateral ventricle (LV). E2 cells had 2 large, complex basal bodies, with intense γ-tubulin expression distributed in small, individual points as in E1 cells, but arranged in large donut or horseshoe formations (diameter: 1.35 um) (see Chapter 3:Figure 1). Immunostaining lateral wall wholemounts for γ-tubulin in combination with β-catenin, which labels adherens junctions and delineates the apical surface of cells lining the ventricle, revealed that E2 cells have an intermediate-sized apical surface (mean=137 um^2, 25-75 percentile= 91-175 um^2), smaller than E1 cells (mean=265 um^2, 25-75 percentile=177-323 um^2) but larger than B1 cells (mean=24 um^2, 25-75 percentile=11-31 um^2) (also see Chapter 3:Figure 1). An extensive analysis of the apical surface of many E2 cells revealed diverse configurations of their basal bodies (**Figure 1**). Most E2 cells had two large basal body complexes (**Figure**

1A), but in some cells only one large, intensely stained basal body was visible (arrow in **Figure 1C**) while in others there were three basal bodies (**Figure 1D**). Usually, γ-tubulin staining of one of the basal bodies revealed a complete donut-shaped structure, while staining of the other basal body revealed a horseshoe-shaped structure (arrows in **Figure 1A** indicate horseshoe-shaped structures; the other structure appears donut-shaped). This γ-tubulin staining pattern is consistent with the localization of γ-tubulin to the pericentriolar material (PCM) tube (Ou et al., 2004), which envelopes the basal body proximally but does not wrap around the distal end, and suggests that the two basal bodies in E2 cells are oriented orthogonal to one another (**Figure 1B**). In addition, there were configurations of γ-tubulin staining that were observed much more rarely, in which no identifiable, donut-shaped basal body structure was observed (**Figure 1E, F**). These cells were classified as E2 cells based on: (1) their intermediate-sized apical surface, (2) the absence of multiple basal bodies, which identify E1 cells and (3) the presence of apical structures intensely stained by γ-tubulin antibodies. Interestingly, **Figure 1F** shows a cell that has two small structures intensely stained with γ-tubulin overlying a granular pattern of weak γ-tubulin staining. One of the two intensely stained structures appears to be similar to the horseshoe-shaped structures in **Figure 1A**. The significance of these different basal body configurations in E2 cells remains unknown.

There was also some variability in the number of cilia extended by E2 cells. To examine E2 cilia, we stained lateral wall wholemounts for γ-tubulin, to identify E2 cells, and acetylated tubulin, to label cilia. >90% E2 cells were

biciliated (**Figure 2A**), with long cilia comparable to those of ependymal (E1) cells (see Chapter 3:Figure 1). One cilium was associated to the basal body with donut-shaped γ-tubulin staining (arrows in **Figure 2A**) and the other to the basal body with horseshoe-shaped γ-tubulin staining (arrowheads in **Figure 2A**). As indicated in **Figure 1B**, the γ-tubulin staining pattern of basal bodies in E2 cells suggests that they are oriented orthogonal to one another, similar to mother and daughter centrioles at the apical surface of cells with primary cilia (Ou et al., 2004). The mother centriole in cells with primary cilia has its long axis orthogonal to the apical surface and nucleates the primary cilium. In E2 cells, the horseshoe-shaped staining pattern of one basal body suggested that this structure was oriented parallel to the apical surface. Yet this basal body also had an associated cilium (arrowheads in **Figure 2A**). In addition to biciliated E2 cells, some E2 cells had a single long cilium (arrows in **Figure 2B**) and a few had no cilia (arrow in **Figure 2C**, also note arrowhead indicates a typical biciliated E2 cell). In one case, we found a cell that appeared to have the characteristic basal body structure of E2 cells, but also had a few basal bodies typical of E1 cells, and it had 7 cilia (arrow in **Figure 2E**). Determining the exact proportion of E2 cells that were biciliated vs. mono-ciliated or non-ciliated was difficult and unreliable because in many instances, it appeared that the cilia were broken. Broken cilia, indicated by arrows in **Figure 2D**, were identified by their lack of the distal segment of the cilium and the specialized ciliary tip, which in intact cilia had more intense acetylated tubulin expression. Another possibility is that these incomplete cilia are in the process of forming or resorbing. However, analyses of

cilia formation in E1 cells during the neonatal period (data not shown) suggest that this is less likely. Newly forming cilia on the surface of differentiating E1 cells, even though they are very short, still have a distinct ciliary tip with more intense acetylated tubulin expression.

Ultrastructure of E2 cells

To characterize the ultrastructure of E2 cells, we reconstructed several of them by TEM (transverse sections in **Figure 3**, en-face sections in **Figure 4**). E2 cells had two basal bodies with two associated (9+2) cilia, deep interdigitations of the cell membrane with long lateral extensions, light cytoplasm, and spherical nuclei with no invaginations and dispersed chromatin. The base of the cilia of E2 cells was engulfed in an invagination of the apical membrane (arrow in **Figure 3D**), similar to the invagination that has been described at the base of primary cilia (Menco and Farbman, 1985; Sorokin, 1968; Whiteley and Young, 1985) (compare Chapter 3:Figure 1E and 1G). Mitochondria were also abundant, but unlike E1 cells where mitochondria localize near the basal bodies, in E2 cells they were concentrated around the nucleus (arrowheads in **Figure 3C**). Small dictyosomes similar to those observed in E1 cells were also present. The main distinguishing characteristics, however, were their unique electron dense basal bodies with laterally associated particulate matter (**Figure 3B** and **Figure 4B**). In some planes of section, this particulate matter appeared to be organized into a reticulum around the barrel of the basal body (**Figure 4B**). This reticulum was composed of electron dense, small polygonal forms arranged such that each polygon shared sides with adjacent polygons, and the entire network appeared to

be connected to the basal body barrel through thin links. Additionally, although the reticulum appeared to be distributed around the basal body with radial symmetry, often an asymmetric, laterally projecting elaboration of this reticulum was observed (arrowhead in **Figure 4B**). Possible functions for these unique basal bodies are discussed below.

Distribution of E2 cells throughout the adult ventricular system

E2 cells were initially identified as rare cells in the lateral wall of the LV (see Chapter 3, Figure 1). To determine the distribution of these cells throughout the adult ventricular system, we analyzed the medial wall of the LV and the walls of the 3rd and 4th ventricles. Wholemounts from these walls were immunostained with γ-tubulin and β-catenin antibodies to identify the apical surfaces of E1 and E2 cells. Throughout the anterior medial wall of the LV (overlying the septum), E2 cells were rare and had a sparse distribution similar to that in the lateral wall of the LV (**Figure 5A**). However, in the posterior medial wall (overlying the hippocampus), E2 cells were densely clustered in small pockets (**Figure 5B**). The relative proportion of E2 cells within these regions was considerably higher than the remainder of the medial or lateral walls of the LV. Interestingly, these pockets were identified not only by the unique basal body of E2 cells, but also by the highly interdigitating apical intercellular membranes revealed by β-catenin staining. An even more striking distribution of E2 cells was observed in the walls of the 3rd and 4th ventricles. Although these walls displayed a sparse distribution of E2 cells interspersed in an epithelium largely composed of E1 cells, similar to that in the LV walls, there was one important exception. Both the floor of the 3rd

ventricle (**Figure 6**) and the midline floor of the 4th ventricle (**Figure 8**) were uniformly covered by E2 cells, with little or no intermingling of E1 cells. In fact, in both ventricles, there was a sharp boundary (indicated by arrows in **Figure 6B and 8B**) that demarcated the region covered by E1 cells (more laterally) from the region covered by E2 cells (at the ventral midline). This boundary gave the appearance of two juxtaposed epithelia. In addition to differences in basal body structure between cells of these two epithelia, E1 and E2 cells also demonstrated differences in membrane architecture, as observed in the pockets of E2 cells in the posterior medial wall described above. The apical intercellular membranes of E2 cells exhibited more interdigitations and had more intense expression of β-catenin than observed in E1 cells (**Figure 6B**). The highly interdigitating membranes, consistent with our EM observations (**Figure 4D**), were more discernable in regions where E2 cells form intercellular junctions with one another (medial wall clusters in LV, 3rd and 4th ventricle floor) than in regions where they are isolated among E1 cells (lateral wall of LV, **Figure 5A**). Furthermore, E2 cells in the floor of the 3rd ventricle appeared to be heterogeneous. Cells that were located more laterally, closer to the boundary with the E1 epithelium, tended to have a larger apical surface and almost always had two large, intensely stained basal bodies that were easily discerned from one another (**Figure 6B**). Cells that were located closer to the midline had a smaller apical surface and had either one large, intensely stained basal body or two basal bodies that were positioned very close together (**Figure 6E**). Interestingly, apical surface size of E2 cells appeared to be inversely correlated with the level

of interdigitation of their apical membranes: the smaller the apical surface, the more interdigitations observed in the apical intercellular membranes. This is shown in **Figure 6B** to **E**, which were images taken from lateral to progressively more medial regions of the 3rd ventricle floor.

The distribution of E2 cells in the 3rd and 4th ventricles suggested that at least some of these cells must correspond to tanycytes (Collins, 1989; Cummings and Felten, 1979; Del Brio et al., 1991; Millhouse, 1971, 1975). But the apical structures of tanycytes have not been explored previously using the techniques used here. Ultrastructural studies of tanycytes have not reported the unusual basal body structure found in E2 cells and scanning EM studies on tanycytes typically report either no cilia or a single cilium on the apical surface (Collins, 1989; Del Brio et al., 1991; Leonhardt, 1980). We found that most E2 cells in the walls of the LV were bi-ciliated (**Figure 2**). To examine the cilia of E2 cells in the floor of the 3rd and 4th ventricles, where tanycytes are usually studied, we immunostained wholemounts of these regions with antibodies to acetylated tubulin and γ-tubulin. We found that almost all E2 basal bodies in these regions were associated with a cilium (**Figure 7 and 9**). In the floor of the 3rd ventricle, E2 cells located more laterally (closer to the E1 epithelium) usually had two long cilia (**Figure 7A**). In contrast, E2 cells located closer to the midline had a single, short cilium (**Figure 7B**). These single, short cilia were observed on E2 cells that had either a single, large-type basal body or two closely positioned basal bodies. In the midline floor of the 4th ventricle, E2 cells were all biciliated with long cilia (**Figure 9**). The differences observed in cilia number and length, like the

differences in basal body number and apical surface size, further suggested that E2 cells may be a heterogeneous population.

Discussion

This work provides a detailed analysis of the apical features, ultrastructure, and distribution of E2 cells in the walls of the adult ventricular system. These unique biciliated cells have a previously undescribed basal body structure and a distribution suggesting that at least a subpopulation of previously identified tanycytes correspond to E2 cells.

E2 cells vs. tanycytes

Although the ultrastructural features observed in E2 cells (light cytoplasm, spherical nuclei with no invaginations and dispersed chromatin) are different than classical descriptions of tanycytes (dark cytoplasm, irregular nuclei with invaginations and dark chromatin aggregates) (Doetsch et al., 1997; Flament-Durand and Brion, 1985), the distribution of E2 cells in the ventricular system indicates that a subpopulation of previously identified tanycytes must correspond to E2 cells. In fact, E2 cells and tanycytes have some ultrastructural characteristics in common, such as extensive interdigitations of the lateral membranes. Previous studies of tanycytes have explored the apical structures of these cells, such as cilia, microvilli, and apical cytoplasmic protrusions, using mostly scanning and transmission EM (Collins, 1989; Del Brio et al., 1991; Leonhardt, 1980). These studies have lead to the general conclusion that tanycytes are either non-ciliated or occasionally have a single cilium at the apical

surface. In our study, we examined the apical structures of E2 cells by immunostaining wholemounts of the ventricular walls with antibodies to reveal the apical cell membrane (β-catenin), basal bodies (γ-tubulin), and cilia (acetylated tubulin). We found that the basal bodies of E2 cells were almost always associated with a cilium, with most E2 cells having two long cilia. The difference between our results and previous findings based on scanning EM may be due to the method of detection. The cilia of tanycytes in scanning EM may be difficult to see if the contrast is low, especially amidst apical cytoplasmic protrusions and abundant microvilli. Immunostaining for ciliary proteins circumvents this problem and provides excellent contrast based on antibody specificity. In addition, long slender E2 cilia may become brittle and break during tissue processing and metal coating for scanning EM. Consistent with this possibility, we observed some broken E2 cilia in our preparations. In the present study, we found that E2 cells usually had two long cilia, but some of these cells in the 3rd ventricle appeared to have a single shorter cilium. One possibility is that E2 cells with the single short cilium are the subpopulation of E2 cells that correspond to tanycytes. Interestingly, E2 cells with different ciliary profiles were distributed from lateral (biciliated) to medial (singly ciliated) in the floor of the 3rd ventricle. This distribution corresponded to differences in basal body number and position (two basal bodies per cell laterally, one basal body or two closely positioned basal bodies per cell medially) and a gradient in apical surface size (larger laterally and smaller medially). These differences suggested that E2 cells, identified by their apical structures, are a heterogeneous population of

cells. Heterogeneity has also been observed in Golgi studies of tanycytes, along the lateral-medial axis of the 3rd ventricle, in the dimensions of the cell body and the complexity of the basal process (Bruni et al., 1983; Card and Rafols, 1978; Millhouse, 1971). Moreover, the smaller apical surface of E2 cells at the ventral midline of the 3rd ventricle is consistent with increased density of tanycytes observed in this region (Millhouse, 1971). Altogether, our analysis of the apical specializations of E2 cells indicates that the heterogeneity of cell types contacting the adult ventricular system necessitates more than a simple categorization into tanycytes v. ependymal cells.

Possible functions of E2 cells

Our ultrastructural analysis revealed that E2 cells, like E1 cells, had long (9+2) cilia that were presumably motile (Salathe, 2007). The most distinctive feature of E2 cells was their extraordinarily large basal body complex in the shape of grape racemes extending laterally from the basal body axes (**Figures 3B, 3D and 4B, 4E**). There have been multiple studies describing the ultrastructure of ependymal cells (Bruni, 1998; Del Brio et al., 1991; Flament-Durand and Brion, 1985; Peters et al., 1991) and the ultrastructure of cilia and basal bodies in other multiciliated epithelial cells (Dirksen, 1971; Sanderson et al., 1990), but to our knowledge, this basal body organization has not been observed before. What could be the function of these biciliated epithelial cells with their unique basal bodies? Although E2 cells were initially identified in the lateral wall of the LV, they were subsequently found in higher numbers in the walls of the 3rd and 4th ventricle, as well as the posterior medial walls of the LVs, suggesting that they

have a more general function within the ventricular system and are not uniquely associated to neurogenesis. It is unlikely that E2 cells in the LV, which comprised less than 5% of cells on the ventricular surface and had only two cilia, contribute importantly to the circulation of CSF. Interestingly, unlike E1 cells, the base of the cilia of E2 cells was engulfed in an invagination of the apical membrane (**Figure 3D**). A similar invagination has also been described at the base of primary cilia (Menco and Farbman, 1985; Sorokin, 1968; Whiteley and Young, 1985) (see Chapter 3:Figure 1). Recent studies indicate that primary cilia function as transducers for cell signaling pathways including Shh (Corbit et al., 2005; Huangfu et al., 2003; Rohatgi et al., 2007), Wnts (Gerdes et al., 2007; Simons et al., 2005), and growth factors (Schneider et al., 2005). The basal body and pericentriolar region appears to play an important role in the interpretation of signals transmitted from the primary cilium (Gerdes et al., 2007) and may regulate the localization of signaling molecules to the primary cilium (Rohatgi et al., 2007). E2 cilia found within these deep invaginations may have some of the properties of primary cilia and may function as important signaling centers. E2 cells and their cilia could have some sensory function. The elaborate basal body of E2 cells may be involved in transmitting information between the ciliary axoneme and other intracellular compartments or the nucleus. Interestingly, it has been suggested that tanycytes in the floor of the third ventricle have a neuroendocrine or transport function, sensing hormones or other molecules in the CSF at their apical surface and relaying information to the hypophysial portal vasculature via their basal process (Bruni et al., 1985;

Flament-Durand and Brion, 1985). Apical specializations of E2 cells in this region may shed light on how a subpopulation of tanycytes senses its apical environment. E2 cells could also be involved in monitoring the function of E1 cells, helping to regulate CSF flow or composition (Bruni et al., 1985). In particular, E2 cells may directly regulate CSF flow in the midline floor of the 3rd and 4th ventricles, where they are the only cells in the epithelial lining. One hypothesis explaining the reduction in cilia number on the E2 epithelium is that it may be important for hydrodynamic control of CSF flow in these regions. Clearly, more work is needed to elucidate the potentially important functions of E2 cells in the ventricular system. This work provides a detailed description of the apical structures of this unique brain cell type, which in addition to its potentially important roles in the ventricular system, may yield insights into the biology of cilia and basal bodies as signaling centers.

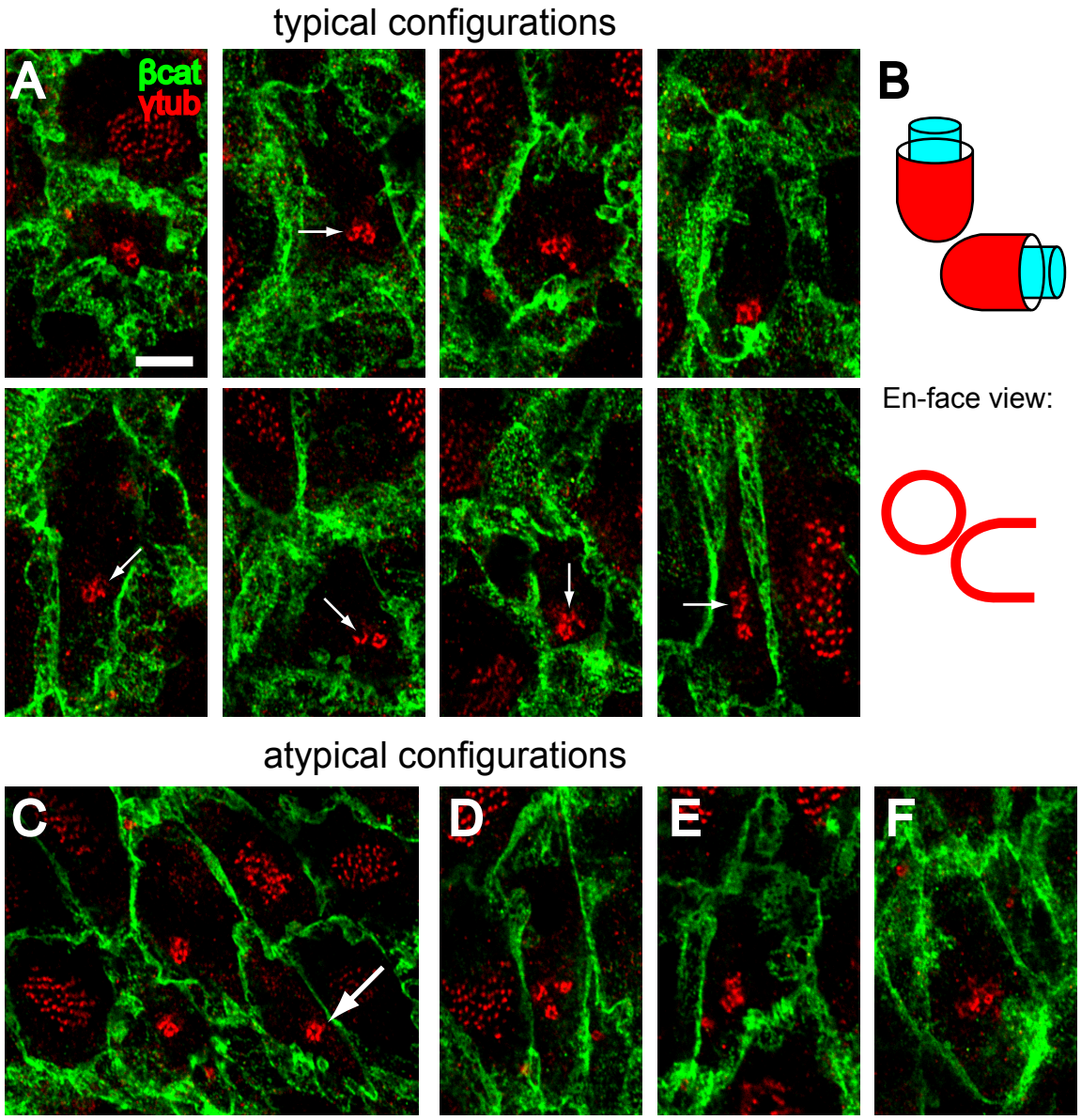

typical configurations
A
βcat
γtub
B
En-face view:
atypical configurations
C
D
E
F

Figure 1. Basal body structure of E2 cells by confocal microscopy.

The images are confocal optical sections taken at the ventricular surface of lateral wall wholemounts from the LV stained for β-catenin (green) and γ-tubulin (red).

(A) Typical configurations of E2 basal bodies. Note that E2 cells have two basal bodies: usually, γ-tubulin staining of one of the basal bodies revealed a horseshoe-shaped structure (arrows), while staining of the other basal body revealed a donut-shaped structure. Scale bar = 5 um (A-F).

(B) Model of the pericentriolar material tube (PCM tube, red) enveloping the proximal portion of the basal body and centriole (cyan) (see reference in text). When viewed en-face, γ-tubulin staining of the PCM tube reveals a donut-shaped and a horseshoe-shaped structure, as seen in (A).

(C-F) Atypical configurations of E2 basal bodies. Although most E2 cells had two basal bodies, some were observed with a single basal body (arrow in C) or with three basal bodies (D). More rarely, no discernable donut or horseshoe-shaped structure of the basal bodies could be observed (E, F). Note the presence of γ-tubulin stained granular material beneath the basal bodies in (F).

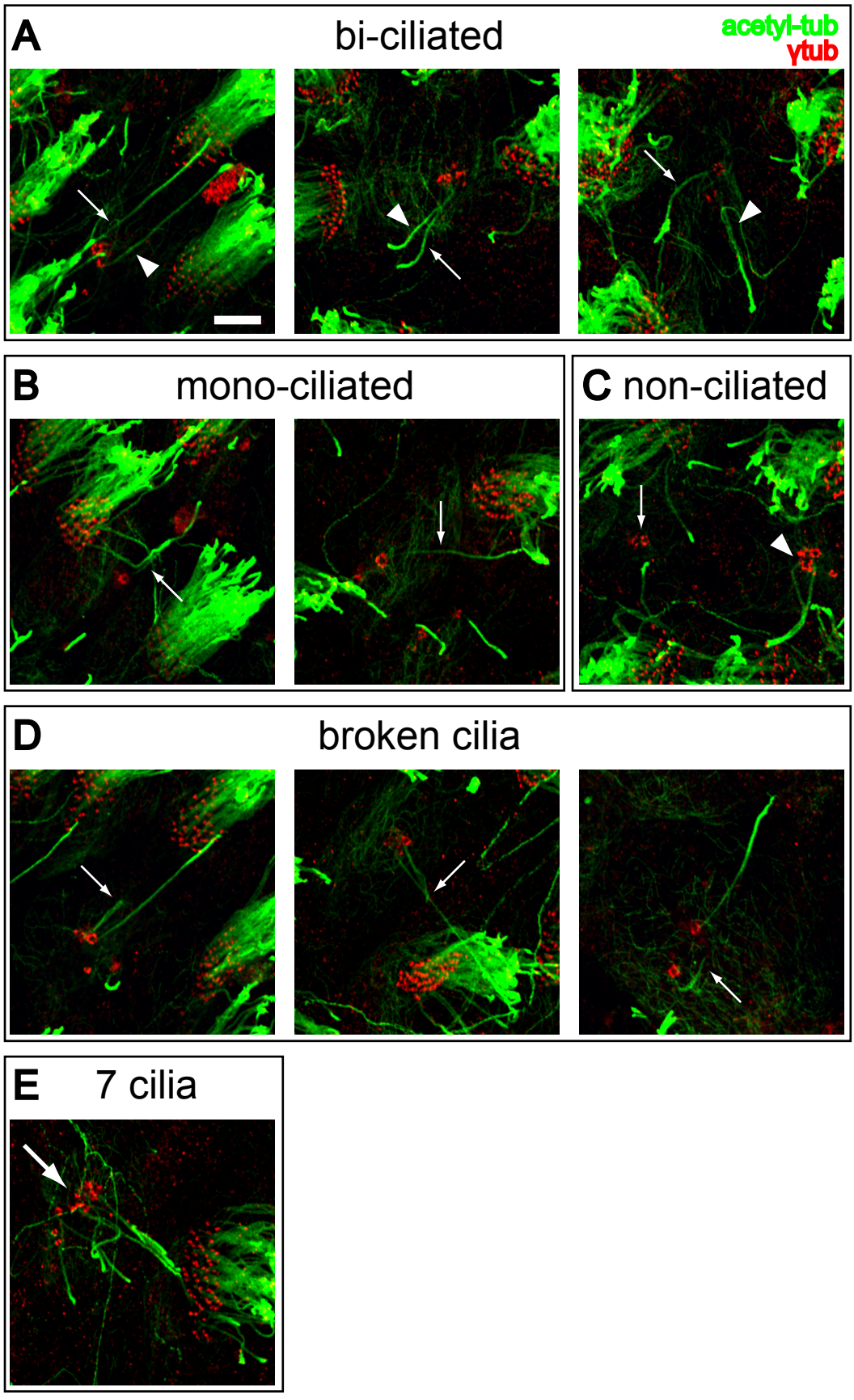

A
bi-ciliated
acetyl-tub
ytub
B
mono-ciliated
C non-ciliated
D
broken cilia
E
7 cilia

Figure 2. Cilia of E2 cells by confocal microscopy.

The images are confocal optical sections taken at the ventricular surface of lateral wall wholemounts from the LV stained for acetylated tubulin (green) and γ-tubulin (red).

(A) E2 cells were usually bi-ciliated with long cilia comparable in length to multiciliated ependymal (E1) cell cilia. One cilium was associated to the basal body with donut-shaped γ-tubulin staining (arrows) and the other to the basal body with horseshoe-shaped γ-tubulin staining (arrowheads).

(B) Occasionally E2 cells had a single long cilium (arrow). These were observed in E2 cells that had either a single basal body (left panel) or two basal bodies (right panel).

(C) E2 cells were also observed that lacked cilia (arrow). Arrowhead indicates a biciliated E2 cell.

(D) Often E2 cells were observed with apparently broken cilia (arrow indicates breakpoint). Broken cilia were identified by their lack of the distal segment of the cilium and the specialized ciliary tip, which in intact cilia had more intense acetylated tubulin expression. This is damage that likely occurred during wholemount preparation and staining.

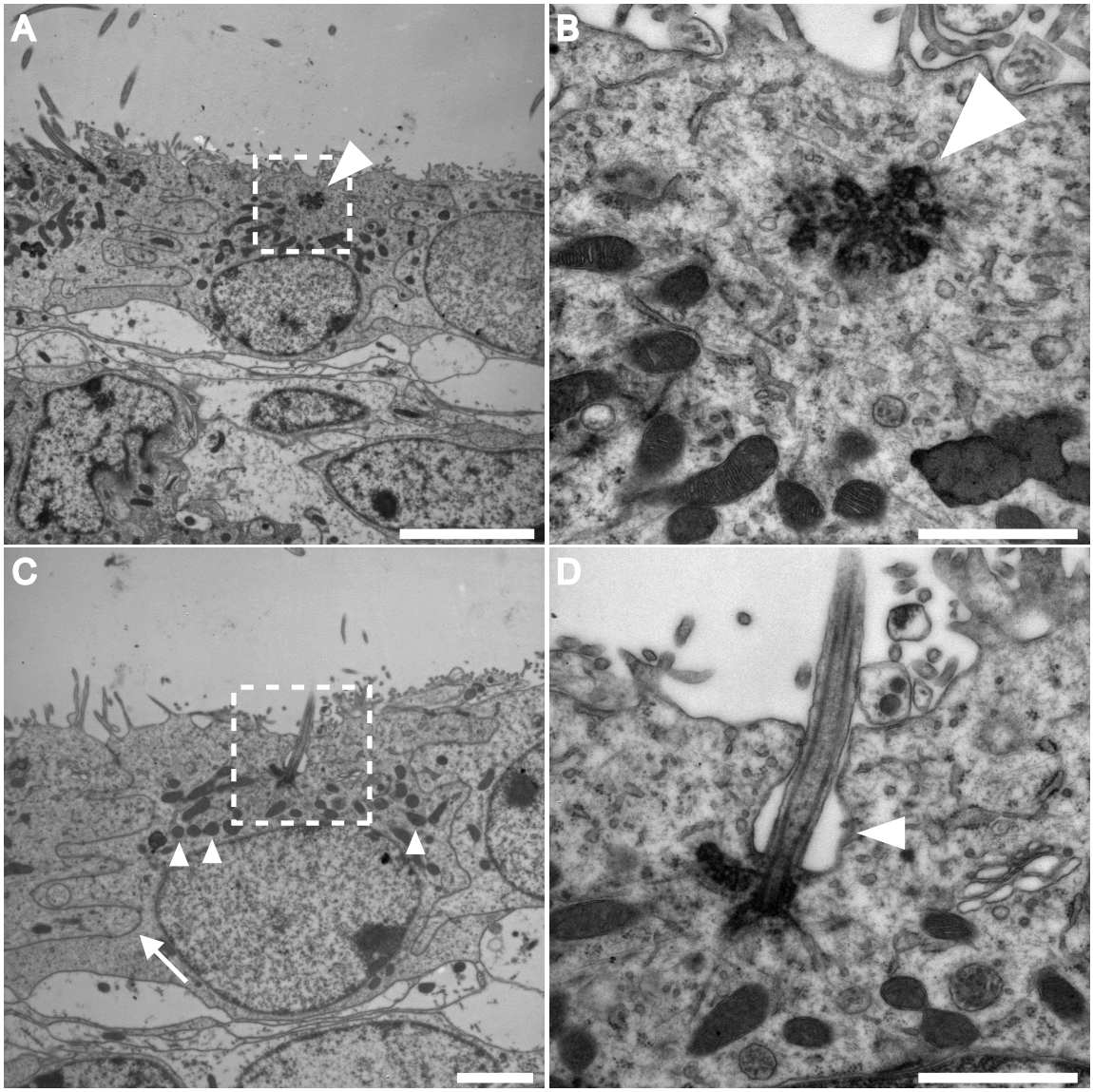


Figure 3. Ultrastructure of E2 cells in transverse sections.

(A-D) are images from a single serially reconstructed E2 cell.

(A,B) Boxed region in A is enlarged in B. The most distinctive feature of E2 cells was their heavily electron dense basal bodies (arrowheads in A and B). Scale bar = 5 um (A), 1 um (B).

(C, D) Boxed region in C is enlarged in D. The cilia of E2 cells were engulfed in an invagination of the apical membrane (arrowhead in D), similar to that observed in cells with primary cilia. E2 nuclei were spherical with no invaginations and contained dispersed chromatin (C). Many mitochondria (arrowheads in C) were observed in a supranuclear position. Note the deep interdigitations of the lateral membranes (arrow in C). Scale bar = 2 um (C), 1 um (D).

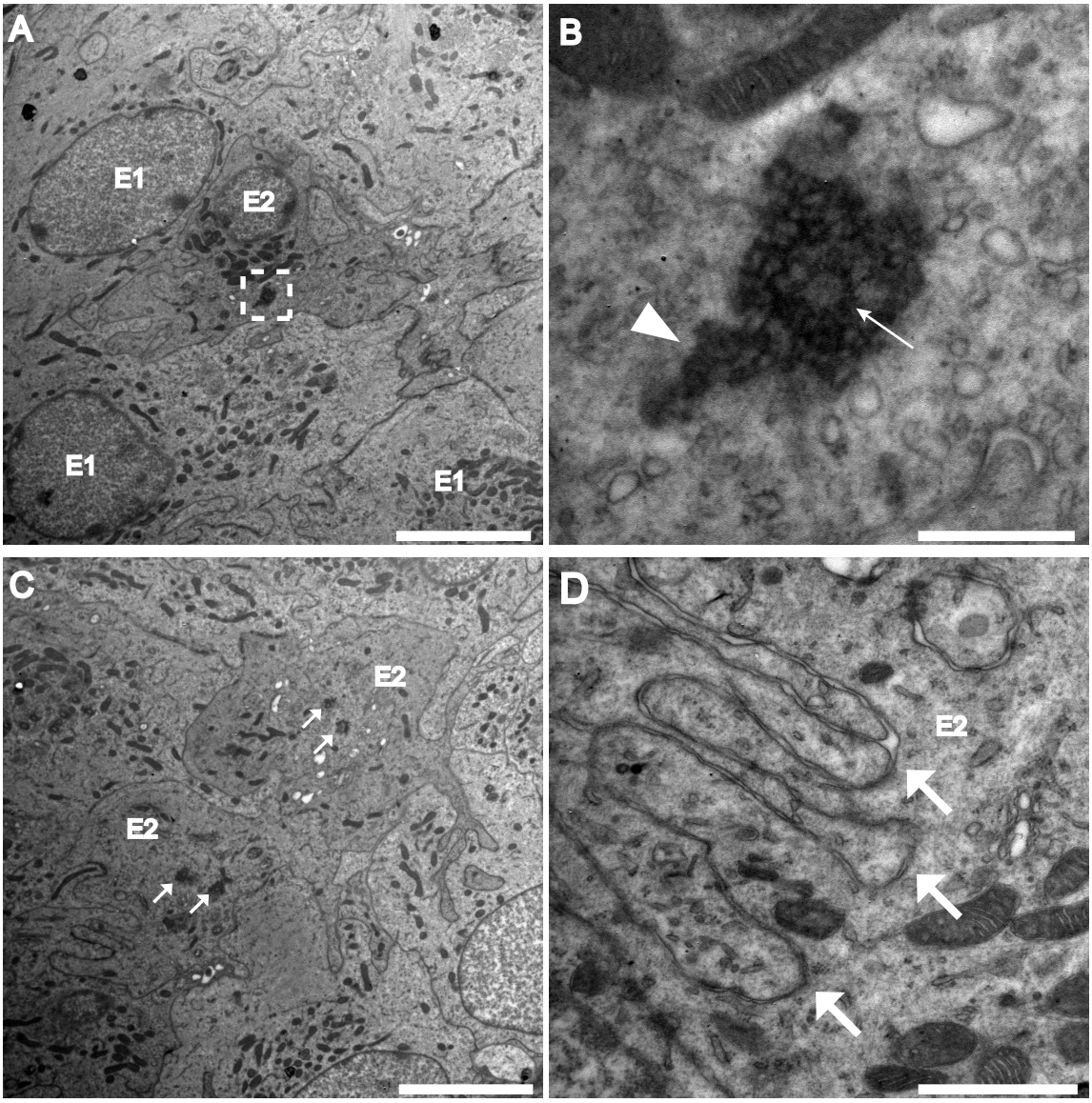


Figure 4. Ultrastructure of E2 cells in en-face sections.

(A) E2 cells had light cytoplasm, comparable to but slightly darker than E1 cells. Boxed region in (A) is enlarged in (B). Scale bar = 5 um.

(B) The most unique feature of E2 cells was their heavily electron-dense basal bodies. Note the circumferentially distributed reticular structure around the barrel (arrow) of the basal body, which is cut in cross-section. Also note the asymmetric, laterally projecting elaboration of this reticulum (arrowhead). Scale bar = 0.5 um.

(C) A lower magnification image of two E2 cells observed en-face, each with two characteristic heavily electron dense and complex basal bodies (arrows). Scale bar = 5 um.

(D) A higher magnification image that shows the deeply interdigitating lateral membranes (arrows) of E2 cells. Scale bar = 1 um.

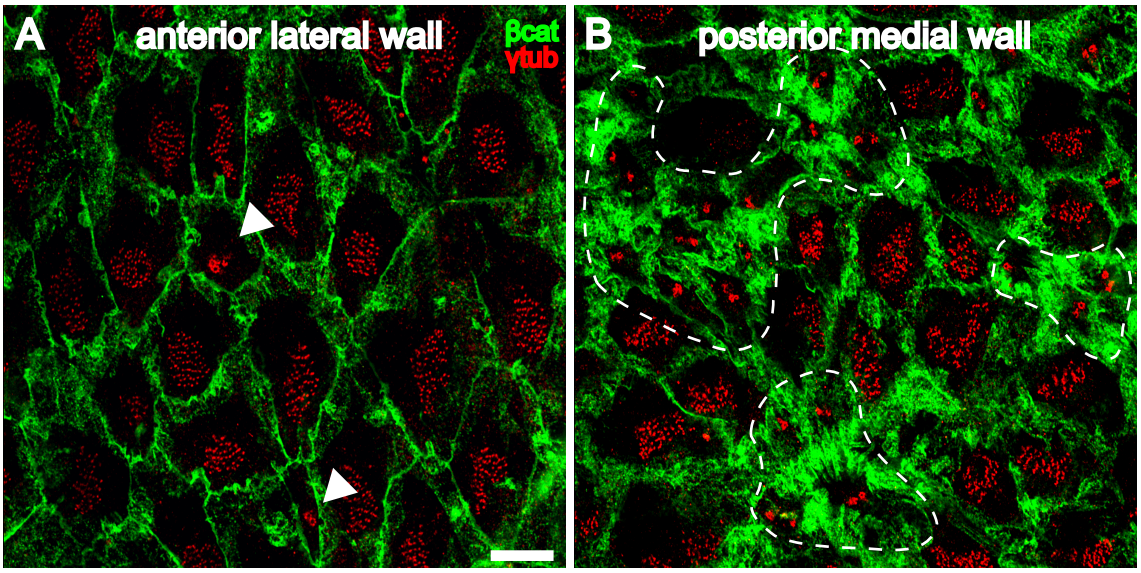

A
anterior lateral wall
βcat
γtub
B
posterior medial wall

Figure 5. Distribution of E2 cells in the lateral and medial walls of the lateral ventricle.

The images are confocal optical sections taken at the ventricular surface of lateral (A) and medial (B) wall wholemounts of the LV stained for β-catenin (green) and γ-tubulin (red).

(A) Throughout the lateral wall, E2 cells (arrowheads) were rare (<5% cells contacting the LV) and were sparsely distributed. Scale bar = 10 um (A, B).

(B) Although the distribution of E2 cells in the anterior medial wall (overlying the septum) was similar to that observed throughout the lateral wall, in the posterior medial wall (overlying the hippocampus), E2 cells were found in dense clusters. Dashed lines outline 3 clusters of E2 cells within a single high power field (89.1 x 89.1 um^2).

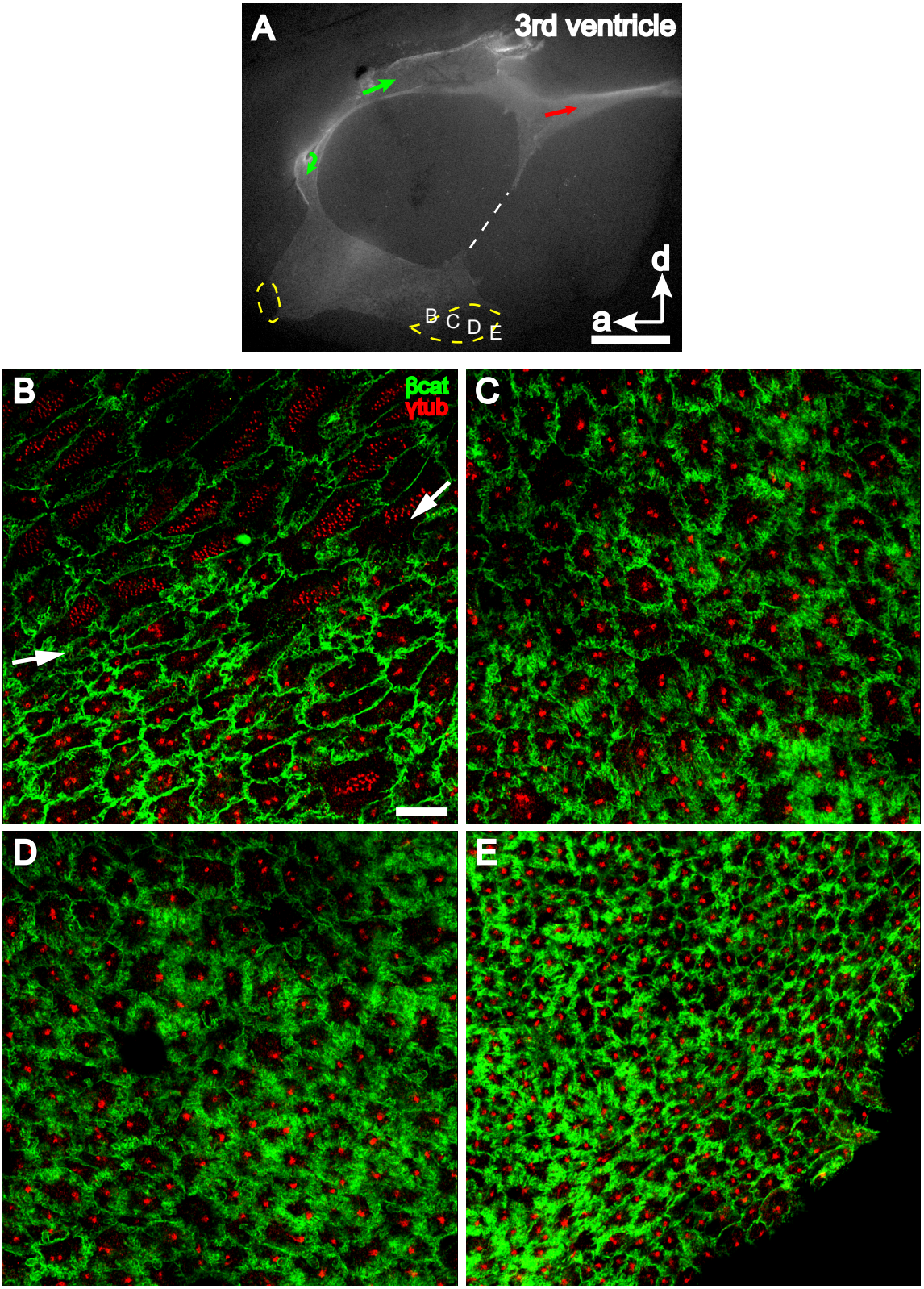

A
3rd ventricle
d
a
B C D E
B
βcat
γtub
C
D
E

Figure 6. Distribution of E2 cells in the walls of the 3rd ventricle.

(B-E) are confocal optical sections taken at the ventricular surface of wholemounts from the ventral 3rd ventricle walls stained for β-catenin (green) and γ-tubulin (red).

(A) Fluorescent stereomicroscopic image of a 3rd ventricle wall wholemount taken to demonstrate the anatomy of the 3rd ventricle and the location of E2 cells (dashed yellow lines) shown in (B-E). This wholemount was dissected from a *FoxJ1::Cre/ZEG* mouse, derived from a cross between transgenic mice expressing Cre under the FoxJ1 promoter (expressed in multiciliated epithelial cells including ependymal cells) and ZEG mice (a Cre reporter line expressing GFP upon Cre mediated recombination). Native GFP fluorescence was observed in the ependymal lining of the 3rd ventricle. Dashed white line indicates a region where the 3rd ventricle was bypassed by the dissection. Dashed yellow lines circumscribe the ventral midline regions where E2 cells were found uniformly covering the ventricle wall. High power images of regions marked B-E within this circumscribed area are shown in (B)-(E) respectively. Note that the distribution of E2 cells in the remainder of the 3rd ventricle wall was sparse, similar to that in the lateral wall of the LV. Green arrows indicate incoming CSF flow from the lateral ventricle and red arrow indicates outgoing flow into the cerebral aqueduct. Arrows in the lower right indicate anterior (a) and dorsal (d) directions. Scale bar = 1 mm.

(B) Arrows indicate the sharp boundary between E1 cells, which covered the lateral walls of the 3rd ventricle, and E2 cells, which uniformly covered the floor of the 3rd ventricle. Note that E2 cells located close to the E1 epithelium have a large apical surface and two basal bodies that are readily discerned from one another. Scale bar = 10 um (B-E).

(C-E) In images taken progressively closer to the ventral midline, the apical surface size of E2 cells diminished with a corresponding increase in cell density and their apical intercellular membranes were more highly interdigitated. In addition, closer to the ventral midline (D, E), E2 cells had either a single basal body or two closely positioned basal bodies.

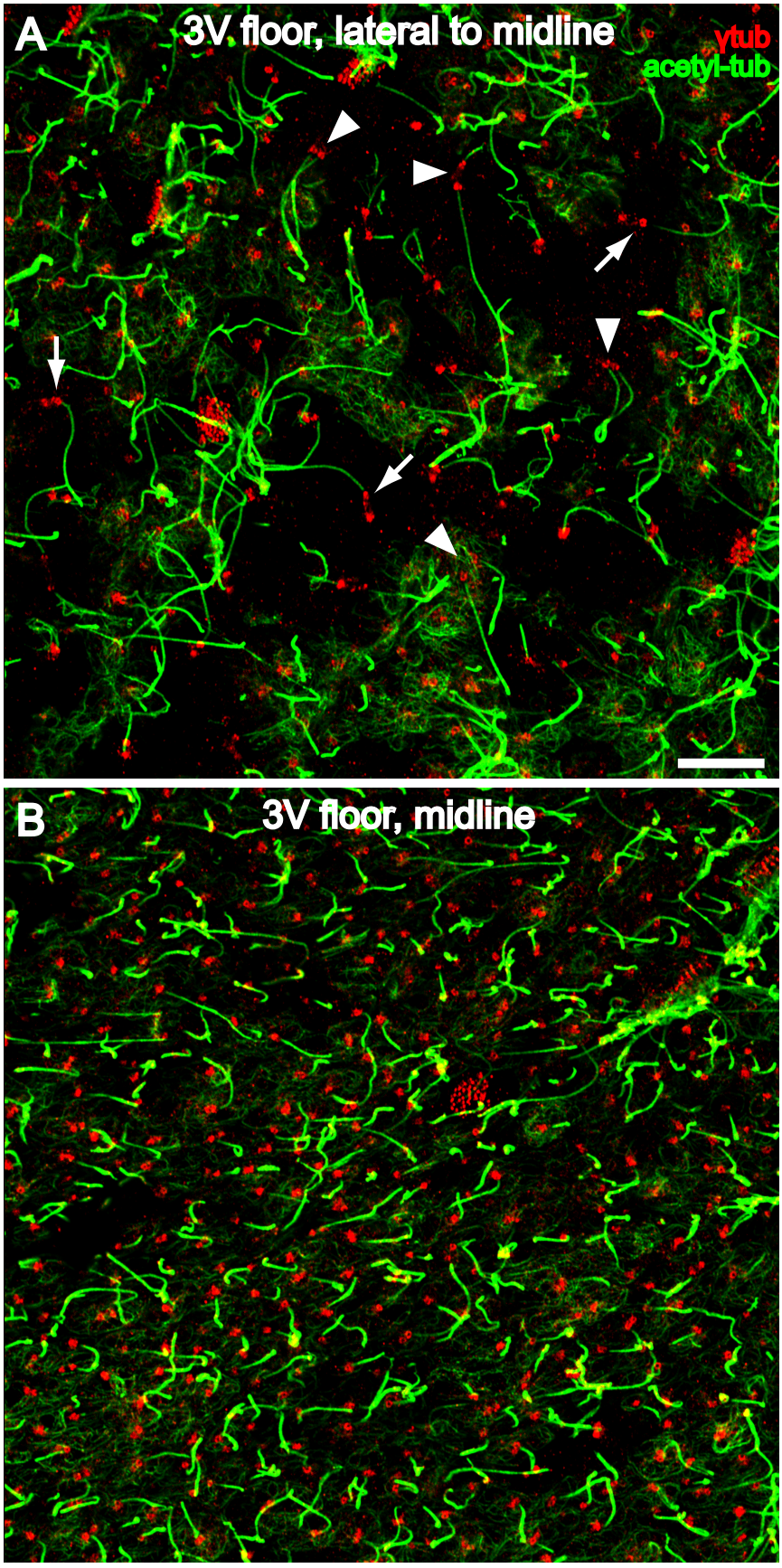
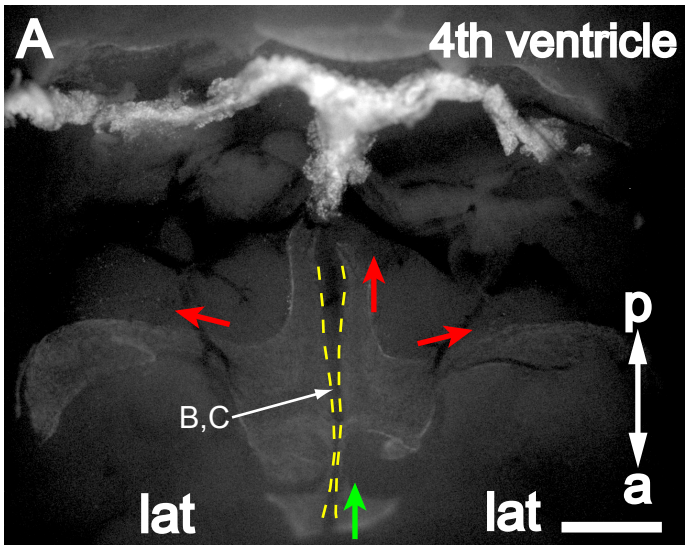

A
3V floor, lateral to midline
γtub
acetyl-tub
B
3V floor, midline

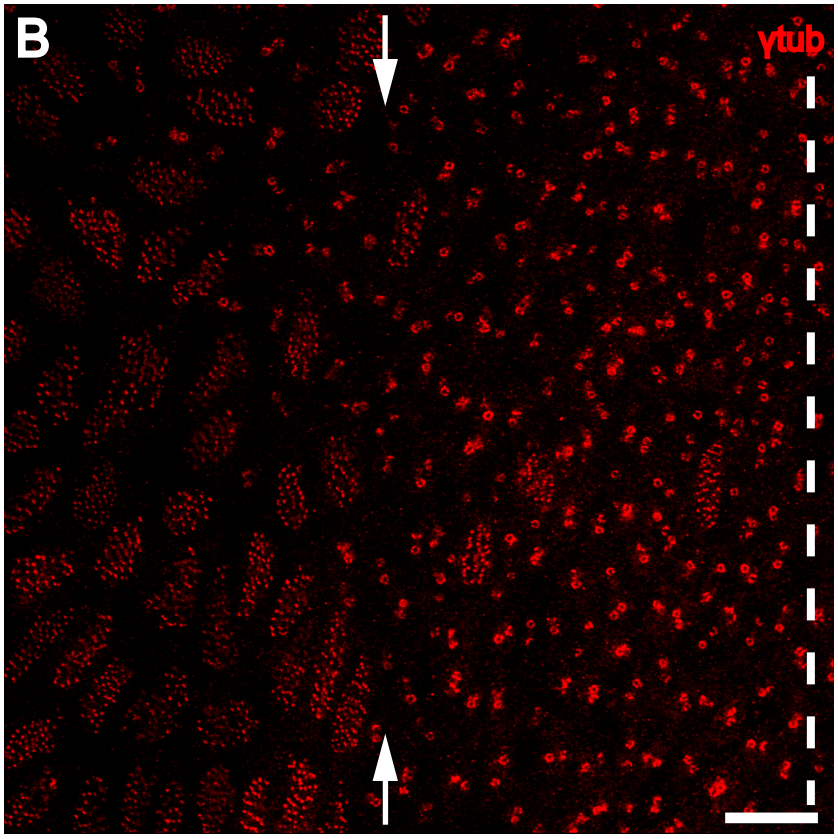
Figure 7. E2 cilia on the floor of the 3rd ventricle.

These images are confocal optical sections taken at the ventricular surface of the 3rd ventricle floor in wholemounts stained for acetylated tubulin (green) and γ-tubulin (red).

(A) In the lateral 3rd ventricle floor, closer to the E1 epithelium, E2 cells had long cilia. Usually, these cells were biciliated (arrowheads), although E2 cells with a single long cilium were also observed (arrows). Scale bar = 10 um (A, B).

(B) Closer to the ventral midline, the density of E2 cells increased and these cells usually had a single, shorter cilium than those observed in the lateral floor. Note that within this high power field, cells at the top of the image (lateral) have longer cilia than those at the bottom (midline).


A
4th ventricle
B,C
p
a
lat
lat


B
γtub

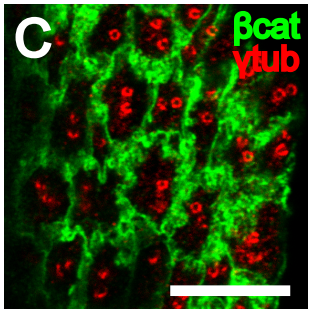

C
βcat
γtub

Figure 8. Distribution of E2 cells in the floor of the 4th ventricle.

(A) Fluorescent stereomicroscopic image of the 4th ventricle floor taken to demonstrate the anatomy of the 4th ventricle and the location of E2 cells (within dashed yellow lines) shown in (B, C). This wholemount was dissected from a *FoxJ1::Cre/ZEG* mouse (see Fig. 6A). At the top of the image, note the choroid plexus, also covered by multiciliated epithelial cells, is highly GFP+ in *FoxJ1::Cre/ZEG* mice. Dashed yellow lines around the ventral midline bound the region where E2 cells uniformly covered the 4th ventricle floor. High power images of this ventral midline region are shown in (B) an (C). Note that the distribution of E2 cells in the remainder of the 4th ventricle floor was sparse, similar to that in the lateral wall of the LV. Green arrow indicates incoming CSF flow from the cerebral aqueduct and red arrows indicate outgoing flow to the central canal and subarachnoid space. Bidirectional arrow in the lower right indicates anterior (a) and posterior (p) directions. Scale bar = 1 mm.

(B) Confocal optical section of the ventricular surface of a 4th ventricle floor wholemount stained with γ-tubulin (red). Arrows indicate the sharp boundary that demarcated the region covered by E1 cells (laterally) and E2 cells (at the midline). Dashed white line indicates the midline of the 4th ventricle floor. Scale bar = 10 um.

(C) Confocal optical section of the midline floor of the 4th ventricle stained with β-catenin (green) and γ-tubulin (red). Note the interdigitating membrane architecture is similar to that in the ventral midline of the 3rd ventricle. Scale bar = 10 um.

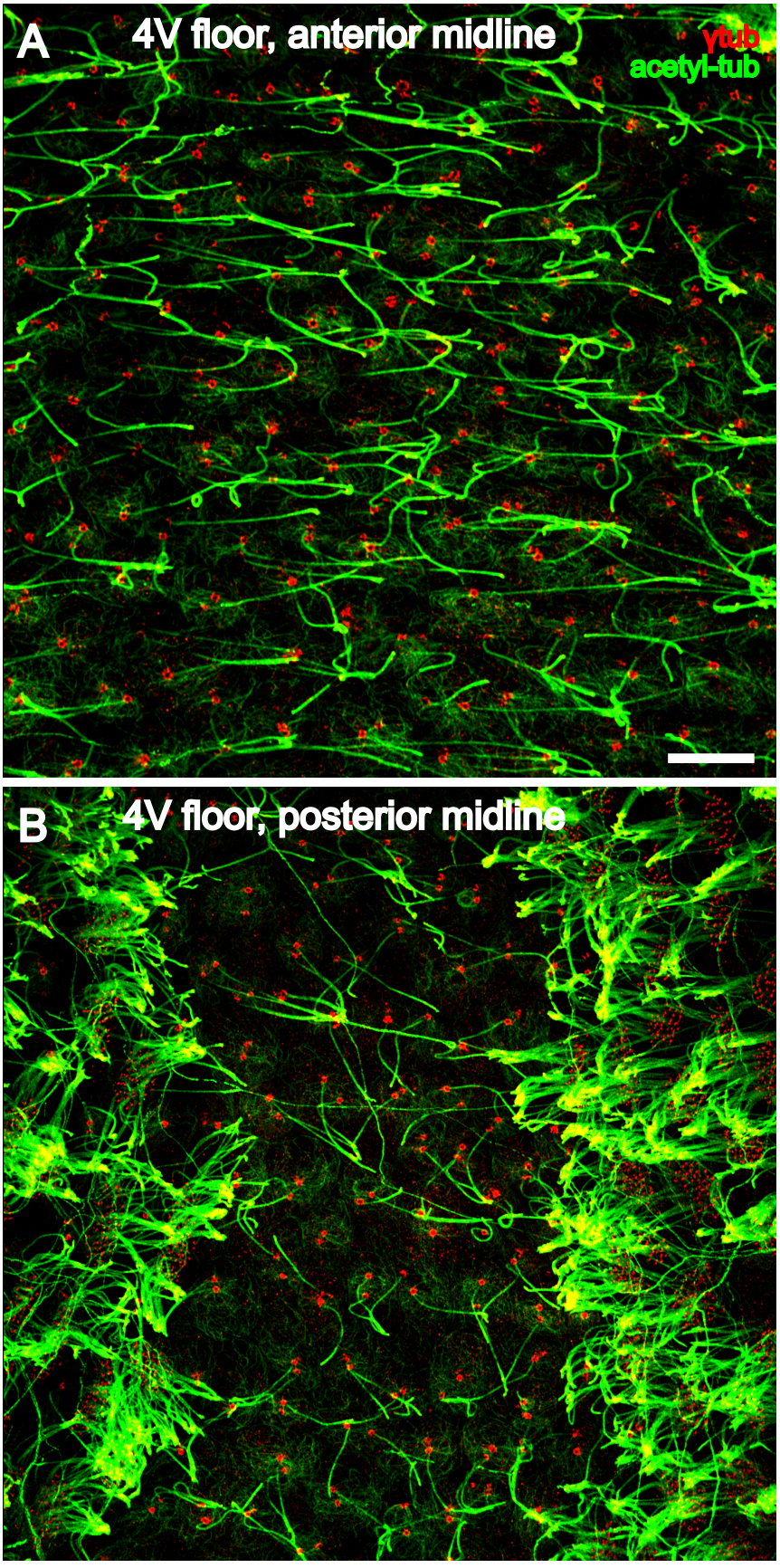

A
4V floor, anterior midline
γtub
acetyl-tub
B
4V floor, posterior midline

Figure 9. E2 cilia on the midline floor of the 4th ventricle.

(A, B) Confocal optical sections of 4th ventricle floor wholemounts stained for acetylated tubulin (green) and γ-tubulin (red). Note that both anteriorly (A) and posteriorly (B), E2 cells at the midline of the 4th ventricle floor were biciliated with long cilia comparable in length to E1 cilia (located laterally in B). The sharp boundary between E1 cells (laterally) and E2 cells (at the midline) was also observed in these preparations (B).

Chapter 5

Ependymal planar polarity does not require motile cilia

Normal brain function depends on the orderly circulation of cerebrospinal fluid (CSF) through the ventricular system. CSF is propelled through the ventricles by planar polarized ependymal cells that contain beating cilia. Disrupted ependymal ciliary beating results in aberrant CSF circulation and is one mechanism of hydrocephalus, one of the most common anomalies of the central nervous system. However, very little is known about the planar polarity of ependymal cells. Although functional assays have been used to study the oriented beating of ependymal cilia, no anatomical correlates to this planar polarity are known. Here we show that like other multiciliated epithelial cells, planar polarity of ependymal cells is evident in the rotational orientation of their basal bodies. However, unlike other multiciliated epithelia, basal bodies at the apical surface of ependymal cells also have a planar polarized position. We show that basal body position is an indicator of ependymal planar polarity and remarkably, this polarity is established and maintained in the absence of ependymal cilia. This indicates that ependymal planar polarity does not require cilia-generated CSF flow and suggests that ependymal cells have intrinsic polarity determined by their position in the epithelial plane lining the brain ventricles.

Introduction

Ependymal cells are multiciliated postmitotic cells, derived from radial glia (Spassky et al., 2005), that form a single cell layer epithelium lining the ventricular system in the adult mammalian brain. The ependyma plays an important role as a protective barrier at the brain-cerebrospinal fluid (CSF) interface (Del Bigio, 1995). Ependymal cells have been conceived as a filtration system, transporting ions, small molecules, and fluid between the brain and CSF (Bruni, 1998; Kuchler et al., 1994). In addition, they have enzymatic and structural characteristics used for scavenging and detoxifying various substances in the CSF (Del Bigio, 1995). Monoamine oxidase enzymes, which metabolize biogenic amines, are expressed in ependymal cells and suggest that the ependyma functions as an amine-barrier system (Saura et al., 1994; Williams et al., 1979). Structurally, ependymal cells are specialized for the propulsion of CSF, which helps redistribute and dilute local concentrations of toxins and metabolites (Del Bigio, 1995). Ependymal cells extend multiple motile (9+2) cilia from their apical surface into the ventricles (Bruni, 1998). Through coordinated, planar-polarized beating of these cilia across the epithelium, ependymal cells generate directed cerebrospinal fluid (CSF) flow in the ventricles (Ibanez-Tallon et al., 2004; Sawamoto et al., 2006; Worthington and Cathcart, 1963) and help maintain CSF homeostasis (Cathcart and Worthington, 1964). In addition, recent evidence suggests that ependymal generated CSF flow establishes gradients of chemorepellants that guide the migration of young neurons in the adult mammalian subventricular zone (Sawamoto et al., 2006).

CSF circulates in the ventricular system from the lateral ventricles to the third ventricle, through the cerebral aqueduct into the fourth ventricle, and then into the central canal of the spinal cord and the subarachnoid space, where it is reabsorbed into the blood and lymphatic system (Koh et al., 2005; Yamadori and Nara, 1979). Disrupting ependymal ciliary beating results in an accumulation of CSF in the brain ventricles and is a pathogenic mechanism of hydrocephalus (Ibanez-Tallon et al., 2004; Nakamura and Sato, 1993), one of the most common anomalies of the central nervous system (Bruni et al., 1985). In addition to hydrocephalic mouse models where the genetic defect disrupts ciliary motility (Ibanez-Tallon et al., 2004; Torikata et al., 1991) or ciliogenesis (Banizs et al., 2005; Chen et al., 1998; Davy and Robinson, 2003; Sapiro et al., 2002), human patients with primary ciliary dyskinesia also develop hydrocephalus (Afzelius, 2004; al-Shroof et al., 2001; Ibanez-Tallon et al., 2002; Jabourian et al., 1986; Wessels et al., 2003). The planar polarized beating of ependymal cilia is therefore essential for normal brain function. However, very little is known about ependymal planar polarity.

Although there are functional assays for the planar polarity of ependymal cells, which measure the orientation of fluid flow above the surface of the epithelium (Ibanez-Tallon et al., 2004; Sawamoto et al., 2006), to date there are no anatomical correlates within these cells indicative of their planar polarity. Previous studies have inferred the direction of CSF flow from ciliary bending forms in fixed tissue. However, this is not a reliable anatomical indicator of ependymal planar polarity since polarized ciliary bending forms are not

maintained invariantly during fixation. In other multiciliated epithelia, such as the lining of the quail oviduct (Boisvieux-Ulrich et al., 1985), the mammalian respiratory tract (Satir and Dirksen, 1985), or the *Xenopus* larval skin (Mitchell et al., 2007), the basal foot, an accessory structure of the basal body, points in the direction of the ciliary beat. The basal foot bestows rotational asymmetry to the basal body and is a useful indicator of the basal body's rotational orientation, which dictates the direction of fluid flow (Marshall and Kintner, 2008; Tamm et al., 1975). It remains to be determined whether this basal body accessory is also an indicator of planar polarity in ependymal cells. In addition to rotational orientation, other parameters describe basal body position and orientation: Cartesian coordinates (XYZ) describe its translational position within the cell and two angles describe its tilt (Marshall and Kintner, 2008). Basal bodies are therefore useful anatomical indicators of planar polarity in multiciliated epithelia.

We examined the basal bodies of ependymal cells by electron microscopy and immunofluorescence confocal microscopy. We found that in addition to rotational orientation, indicated by the basal foot, the translational position of basal bodies on the apical surface of ependymal cells correlated with the direction of fluid flow. This has not been described in other multiciliated epithelia. Furthermore, by analyzing basal body position in mutants that lack motile (9+2) cilia in ependymal cells, we show that this planar polarity is not secondary to mechanical forces exerted by beating cilia. We therefore identify basal body rotational orientation and translational position as structural indicators of

ependymal planar polarity. The ependymal cilia and consequently, cilia-generated CSF flow, were not required for the establishment of this polarity.

Results

Functional assays for ependymal planar polarity

Ependymal planar polarity was assayed functionally in two ways: (1) directly, by examining the beating motion of cilia under high power bright field video-microscopy (**supplemental Movie 1**) or (2) indirectly, by observing the flow of fluorescent microbeads deposited on the surface of the ependymal epithelium (**Fig. 1A and supplemental Movie 2**). To directly visualize ciliary beating, we freshly dissected a coronal slab of the adult mouse brain and exposed the lateral wall of the lateral ventricle. The dissected tissue was placed in a glass slide well in 37°C Leibovitz media under a 60x water immersion lens that dipped directly into the medium. Using bright field microscopy, we could focus on the ciliated surface of the lateral wall and observe the beating motion of ependymal cilia. Analysis of the ciliary beating cycle revealed two distinct bending forms corresponding to the effective and recovery strokes. During the effective stroke, the cilia had an approximately vertical (unbending) form with respect to the ependymal lining. In this vertical position, the cilium had a large profile that moved the media above the ependymal lining in a uniform direction, indicated by debris flowing within the media in **supplemental Movie 1**. In contrast, during the recovery stroke, the cilium had a horizontal (bent) form that appeared to sweep beneath the fluid flowing above without disturbing its laminar quality. These

distinct bending forms have been described for other multiciliated epithelia (Sanderson et al., 1990). Ependymal cilia across the ventricular lining had similarly oriented bending forms, which were coordinated into metachronous cycles that propagated from one side to the other across the epithelium. Although visualizing ciliary beating was a direct test of ependymal planar polarity, it did not provide a comprehensive view of planar organization across the entire epithelium.

For a comprehensive view, we assayed ependymal planar polarity indirectly by examining the orientation of fluid flow across the epithelium. First, we freshly dissected wholemounts of the lateral wall of the lateral ventricle and placed them in 37°C Leibovitz media under a fluorescent stereomicroscope. Then, a glass micropipette filled with fluorescent microbeads (2.0 um diameter) and attached to a micromanipulator was lowered onto the lateral wall wholemount, where microbeads were ejected onto the surface. Movement of microbeads indicated the orientation of fluid flow across the epithelium. We recorded the flow of microbeads, which ranged from 0.5-2 mm/s, in real time. The orientation of fluid flow varied in different regions of the ventricle. In general, microbeads flowed from posterior to anterior and dorsal to ventral, directed towards the foramen of Munro leading to the 3rd ventricle. In particular, we examined flow in the anterior half of the lateral wall, in regions around the lateral ventricle adhesion point, where the medial and lateral ventricular walls are fused within the ventricular cavity. The orientation of flow changed significantly at different positions around the periphery of the adhesion point (**Fig. 1A and**

supplemental Movie 2). In the region anterior and dorsal to the adhesion (Region AD), flow was directed anteroventrally whereas in the region ventral to this (Region AV), flow was directed posteroventrally. Posterior to the adhesion at the dorsal-ventral midline of the lateral wall (Region PM), flow was directed anteroventrally. The direction of flow in these three regions was highly stereotyped in 10 mice analyzed and these regions could be readily located with respect to the adhesion point (**supplemental Fig. S1**). These regions were therefore tested in subsequent analyses of ependymal planar polarity.

Anatomical correlates to ependymal planar polarity

To date, no anatomical correlates to the functional planar polarization of ependymal cells have been described. However, evidence from other multiciliated epithelia suggests that the orientation of the basal foot is polarized in the direction of fluid flow (Boisvieux-Ulrich et al., 1985; Mitchell et al., 2007; Satir and Dirksen, 1985). We therefore examined, by electron microscopy (EM), basal foot orientation on the basal bodies of ependymal cells lining the lateral wall of the lateral ventricle. For this analysis, ultrathin sections were cut in the plane parallel to the ventricular surface, resulting in en-face views of the ependyma. **Fig. 1B** is an en-face electron micrograph showing two adjacent ependymal cells in Region AD, where flow was directed in the anteroventral direction. The orientation of the image in **Fig. 1B** and all subsequent images in this study correspond to the orientation of the lateral wall wholemount shown in **Fig. 1A**. **Fig. 1C and D** are higher power images of the boxed regions in **Fig. 1B**, showing that basal feet (green arrowheads) of basal bodies in adjacent cells were well

aligned (magenta arrows indicate direction of basal foot). Like other multiciliated epithelia, this direction was aligned with the direction of fluid flow (compare anteroventral flow in Region AD in **Fig. 1A** with magenta arrows in **Fig. 1C and D**). Because of slight variations in the apical position of basal bodies, single ultrathin sections transected neighboring basal bodies at different levels along their long axis. The basal foot, which projects from the basal body at a specific level along this axis, is therefore not observed in every transected basal body. To track basal foot orientation for all basal bodies in a single cell, we reconstructed individual ependymal cells by serial ultrathin sectioning. **Fig. 1E** shows the reconstructed basal bodies of an ependymal cell from Region AD. Basal foot orientation was highly consistent among the basal bodies within a given cell and corresponded to the direction of fluid flow throughout the lateral wall of the lateral ventricle (data not shown). Therefore, similar to other multiciliated epithelia, the basal foot of the basal body is an anatomical indicator of planar polarity in ependymal cells.

Surprisingly, in the course of our EM analysis, we noticed that the position of the basal bodies themselves appeared to be polarized to one side of the apical surface of ependymal cells. This corresponded to the side towards which the basal feet were directed (**Fig. 1B-D**). Planar polarity of basal body position on the apical surface has not been reported in other multiciliated epithelia. To investigate this possible planar organization of the ependymal layer, we recently developed new ways to image the apical structures of cells lining the ventricles in the adult brain. Briefly, wholemounts are dissected from the walls of the

ventricular system, immersion fixed and immunofluorescently stained, and then the ventricular surface of the wholemount is imaged by confocal microscopy. We used this en-face imaging to examine the position of the ciliary bundle on the apical surface of ependymal cells lining the lateral wall of the lateral ventricle. Immunostaining for acetylated-tubulin, a component of stabilized microtubules of the ciliary axoneme, in combination with β-catenin, a component of apical adherens junctions that delineates the apical surface of ependymal cells, revealed that the ciliary bundle emanated from one side of the cell's surface (**Fig. 1F, G**). Neighboring cells had ciliary bundles displaced to the same side of their apical surfaces. Interestingly, this appeared to correspond to the "downstream" side of the cell, with respect to fluid flow and the ciliary beat (compare position of ciliary bundle on apical surface in **Fig. 1F,G** with fluid flow in regions AD and AV in **Fig. 1A**). This was consistent with our initial observations of basal foot orientation and basal body position at the EM. Additionally, note that it would be impossible to determine planar orientation in fixed tissue based on ciliary form alone (acetylated tubulin staining without β-catenin in **Fig. 1F, G**). Although during active beating, the cilia have polarized bending forms, these oriented forms are not maintained invariantly during tissue fixation.

Because cilia grow from basal bodies, co-staining for γ-tubulin, which labels basal bodies, and β-catenin provided an unobstructed view of this planar organization of ependymal cells (**Fig. 2A, B**). The basal bodies were clustered into a well-circumscribed patch (32-73 basal bodies per patch, mean: 49) that accounted for 16±5% (range: 4-35%) of the total apical surface of ependymal

cells on the lateral wall of the lateral ventricle. This enabled us to quantify the planar polarized position of the basal body patch relative to the apical surface. For this analysis, we wrote a program in Metamorph (Molecular Devices) that drew a vector from the center of the cell's apical surface to the center of the basal body patch (**Fig. 2C, D**). The vector's angle was taken as a measure of the polarized position of the basal body patch on the apical surface. We will refer to this vector angle as the basal body (BB) patch angle. Only ependymal cells that had their entire apical surface contained within the high power field (127 x 127 um^2) were analyzed. For each high power field, we calculated the deviation of each cell's BB patch angle from the median BB patch angle in the field. This data was plotted on a histogram (**Fig. 2E, F**). A vertical line at 0° on this histogram would indicate that all the cells had the exact same BB patch angle (no deviation between cells), while a horizontal line would indicate that the basal body patches were randomly positioned. Our data from high power fields in Regions AD and AV (175 cells analyzed in AD, 155 cells analyzed in AV from n=4 mice) indicated that BB patch angles were highly oriented in the ependymal layer. Specifically, 87% cells in Region AD and 88% cells in region AV had BB patch angles within 45° of the median. Furthermore, because immunostained wholemounts were imaged in approximately the same orientation as wholemounts used to make flow movies, we were able to correlate the BB patch angles with the orientation of fluid flow in Regions AD and AV. The BB patch angles computed in Metamorph are relative to the XY axis where the positive X axis is 0°, the negative X axis is 180°, and the positive and negative Y axes are

90° and -90°, respectively. The median BB patch angle (averaged from n=4 mice) in Region AD was -141°±8° (correlated with anteroventral fluid flow in this region), while in Region AV, it was -85°±7° (correlated with posteroventral fluid flow). These median values correspond to 0° on the histograms showing the distribution around the median in **Fig. 2E, F** (the medians are graphically represented by red arrows in insets). These results confirmed that basal body patches were positioned on the "downstream" side of the ependymal cells' apical surfaces.

In addition, it appeared that the apical surface itself was oriented in the plane of the ependymal layer. Using the same Metamorph program, we calculated this apical surface orientation (the long axis of the apical surface) for each cell within the field, and the deviation of each cell's apical surface orientation from the median within the field. This data was plotted on a histogram (**Fig. 2G, H**)**,** similar to that for the BB patch angle, and revealed that apical surface orientation was also highly consistent from cell to cell in Regions AD and AV. In region AD, 87% of cells had their elongated apical surface oriented within 22.5° of the median, while in region AV, 72% were within 22.5°. Like the BB patch angles, this orientation was correlated with the direction of fluid flow. However, unlike the BB patch angle, apical surface orientation is not derived from a vector (with directionality) but rather the single long axis of the cell's surface (with no directionality). Values can only vary from -90° to 90°. In region AD, the median apical surface orientation (averaged from n=4 mice) was 36°±2° (or 36-180= -144° since directionality is irrelevant), while in region AV, the

median orientation was -85°±6°. These median values correspond to 0° on the histograms in **Fig. 2G, H** (graphically represented by red lines in insets). Apical surface orientation in these regions was therefore approximately parallel to the orientation of fluid flow and the BB patch angle. Specifically, the difference between apical surface orientation and the BB patch angle was 3° in Region AD and 0.7° in Region AV. These findings indicate that the position of the BB patch on the apical surface of ependymal cells and the orientation of the long axis of the apical surface are good correlates of ependymal planar polarity.

Basal body patch angle, but not apical surface orientation, correlates with ependymal planar polarity throughout the adult ventricular system

Next we examined the planar organization of basal bodies and the apical surface in other regions of the lateral wall of the lateral ventricle, including Region PM (**Fig. 3A, D, G, H)**, and also in the medial wall of the lateral ventricle and the 3rd ventricle walls (**Fig. 3B, C, E, F)**. In Region PM of the lateral wall, the BB patch angle was highly oriented in the direction of fluid flow (**Fig. 3D, G**). 83% of cells in this region had BB patch angles within 45° of the median, with a median BB patch angle of -124°±10° (197 cells from n=4 mice). Region AV of the medial wall of the lateral ventricle also appeared to have highly oriented BB patch angles that were correlated to the orientation of fluid flow in the region (**Fig. 3B, E**). **Supplemental Fig. S2** and **Supplemental movie 3** show the orientation of fluid flow across the medial wall and the location of Region AV with respect to this flow. *In vivo*, Region AV of the medial wall is directly across the ventricular cavity from Region AV of the lateral wall. Note the similarity in BB patch angles

in Region AV of the medial and lateral walls (compare **Fig. 3B, E** with **Fig. 2B, D**).

Interestingly, although the BB patch angles in Region PM of the lateral wall were highly oriented (**Fig. 3G**), the apical surface was not (**Fig. 3H**). Many ependymal cells in this region had a diamond-shaped apical surface that was roughly symmetric. In addition to the broad distribution of apical surface orientations, the median orientation in this region was -77°±6° (n=4 mice), not aligned with the anteroventral direction of fluid flow or the BB patch angle (compare insets in upper right of **Fig. 3G** and **H**). This suggested that apical surface orientation was not correlated with ependymal planar polarity throughout the lateral wall of the lateral ventricle. The misalignment between apical surface orientation and the BB patch angle, which was very small for Regions AD (3°) and AV (0.7°) of the lateral wall, was 47° for Region PM. There were also other regions in the adult ventricular system where ependymal cells exhibited this misalignment. For example, in the dorsal 3rd ventricle wall (**Fig. 3C, F**), the apical surface orientation was almost perpendicular to the BB patch angle, which was correlated to the orientation of fluid flow in this region (data not shown). For this reason, in subsequent experiments we used only the BB patch angle as a reliable measure of ependymal planar polarity by confocal microscopy.

Planar polarity of basal body patches does not require motile (9+2) cilia

The “downstream” position of basal body patches on the apical surface of ependymal cells suggested that this anatomical planar polarity may be secondary

to the mechanical force exerted by beating cilia on their basal body apparatus. In this scenario, the position of the basal body patches is not an independent indicator of structural polarity within the cell, but rather a consequence of functionally polarized beating of cilia. To test this possibility, we conditionally ablated ependymal cilia by crossing mice expressing Cre under the human glial fibrillary acidic protein promoter (*hGFAP::Cre*) with mice carrying conditional *Kif3a* alleles (*Kif3a*$^{fl/fl}$). *Kif3a* encodes a subunit of the kinesin-2 motor that is essential for ciliogenesis (Kozminski et al., 1995). Cre expression in *hGFAP::Cre* mice begins in forebrain radial glia at E13.5 (Malatesta et al., 2003), and because ependymal cells are derived from radial glia (Spassky et al., 2005), this results in widespread recombination in the adult ependyma (Zhuo et al., 2001). Ependymal cells in adult *hGFAP::Cre;Kif3a*$^{fl/fl}$ mutants therefore lack cilia (**Fig. 4A-D**). As a consequence, these mutants have hydrocephalus (**supplemental Fig. S3**).

Remarkably, the organization of basal body patches on the apical surface of ependymal cells lacking cilia was largely preserved (**Fig. 4E-H**). To quantify this organization, we analyzed 6 non-overlapping high power fields (127 x 127 um^2) from each of 5 mutants (790 cells analyzed) and 5 control littermates (624 cells analyzed). Three high power fields were taken posterior to the adhesion point, along the dorsal-ventral midline of the lateral wall (corresponding to Region PM), and three high power fields were taken anterior to the adhesion point along the dorsal-ventral midline. However, since *Kif3a* mutants lack an adhesion point, likely due to hydrocephalus and expanded ventricles, we could not use this

landmark as a reference in mutants. Instead, the anterior-posterior position of high power fields taken in controls was recorded relative to the anterior boundary of the wholemount (0.2-0.7 mm for the anterior region and 1.7 to 2.5 mm for the posterior region) and corresponding fields were imaged in mutant wholemounts.

Basal bodies in mutant ependymal cells were maintained in tightly clustered patches, accounting for 19%±6% of the total apical surface area, similar to controls at 22%±7% (**Fig. 4E, F**). Moreover, the BB patch angles in the mutant ependyma were highly oriented, with just a slight increase in deviation from the median compared to controls (**Fig. 4G-I**). **Fig. 4I** is a histogram, similar to histograms of BB patch angles in **Fig. 2 and 3**, showing the distribution of BB patch angles around the median in mutant and control ependyma. Although mutant BB patch angles were more widely distributed around the median than in controls (curve fit test, p=0.0003), they were still highly clustered around the median. In the mutant, 75% cells had BB patch angles within 45° of the median, while in controls it was 90% cells. Conversely, the mutant ependyma had a slightly greater proportion of cells distributed greater than 45° from the median. This data suggested that motile (9+2) cilia are not required for the planar polarization of basal body patches on the apical surface of ependymal cells, but they may have a role in optimizing this polarization. Therefore, the BB patch angle was an independent indicator of structural planar polarity within ependymal cells, not reliant on functional planar polarity of beating cilia.

Timing of cilia loss in *hGFAP::Cre;Kif3a$^{fl/fl}$* mutants

The finding that *hGFAP::Cre;Kif3a*$^{fl/fl}$ mutants had planar polarized basal body patches in ependymal cells was surprising in light of recent evidence that primary cilia regulate planar polarity (Jones et al., 2008; Park et al., 2006; Ross et al., 2005). Although ependymal cells do not have primary cilia, their radial glial progenitors do. Because Cre expression in *hGFAP::Cre* mice is reported to begin in radial glial cells at E13.5 (Malatesta et al., 2003), we expected that radial glia in *hGFAP::Cre;Kif3a*$^{fl/fl}$ mutants would lose their primary cilium prior to transformation into ependymal cells. Did this mean that the primary cilium of radial glial progenitors is not required for basal body planar polarity in ependymal cells?

To answer this question, we investigated the timing of cilia loss in *hGFAP::Cre;Kif3a*$^{fl/fl}$ mutants. First, we determined Cre activity in *hGFAP::Cre* mice by examining lacZ expression in the lateral ventricle walls of *hGFAPCre;R26R* mice at P0. *R26R* mice carry a transgene expressing lacZ upon Cre recombination. At P0, radial glial transformation into ependymal cells is underway in the medial wall of the lateral ventricle in a posterior to anterior gradient. Ependymal transformation has also just begun in the most posterior and ventral regions of the lateral wall at this age (Spassky et al., 2005) (**supplemental Fig. S4**). Interestingly, lacZ expression in serial coronal sections from *hGFAPCre;R26R* brains revealed a medial to lateral wall, and posterior to anterior, gradient of recombination in the lateral ventricle (**Fig. 5A-D**), similar to the gradients of ependymal cell differentiation. In both anterior and posterior sections, the medial wall appeared mostly recombined at P0. Cells in the

posterior medial wall were intensely stained and had a cuboidal shape (arrowheads in **Fig. 5D**), consistent with ependymal morphology. In contrast, cells on the lateral wall appeared mostly recombined only in posterior regions, whereas anterior regions showed mosaic recombination. Cells in the anterior and posterior lateral wall had columnar shape, consistent with radial glial morphology (arrows in **Fig. 5B, D**). This suggested that while all ependymal cells were recombined, radial glia had mosaic recombination. To further examine this mosaicism, we analyzed wholemounts from the medial and lateral walls of P0 *hGFAP::Cre;Z/EG* mice. *Z/EG* mice carry a transgene that switches from lacZ to GFP expression upon Cre recombination. En-face imaging of wholemounts from P0 *hGFAP::Cre;Z/EG* mice confirmed that while all ependymal cells in the medial and lateral walls were recombined, radial glia exhibited mosaic recombination (**Fig. 5E, F**). We next tested whether these differences in recombination translated into differences in the presence or absence of cilia on radial glial and ependymal cells.

We examined wholemount co-staining of acetylated-tubulin and γ-tubulin in *hGFAP::Cre;Kif3a*$^{fl/fl}$ mutants at P3. At this age, the lateral wall has a mixture of ependymal cells and radial glia, distributed in a posterior (more ependymal cells) to anterior (more radial glia) gradient. The medial wall is mostly covered by ependymal cells, except in the most anterior region where some radial glia have not yet differentiated (**supplemental Fig. S4**). Surprisingly, on both the medial and lateral walls, all radial glial cells had a primary cilium associated with a single basal body at their apical surface (**Fig. 5G, I**). In sharp contrast, ependymal cells

had no cilia associated with their multiple basal bodies (**Fig. 5H, J**). The maintenance of the primary cilium in radial glial cells, even though many of these cells exhibited Cre recombination in reporter mice (**Fig. 5E**), suggested that the *Kif3a* protein may have a long half-life. This has been previously suggested in other tissues (Lin et al., 2003). In fact, some radial glia with a primary cilium expressed Cre (**Fig. 5K**). Altogether, our data indicated that the loss of cilia in *hGFAP::Cre;Kif3a*$^{fl/fl}$ mutants occurs during the transformation from radial glial to ependymal cell, when *de novo* synthesis of *Kif3a* protein is likely needed to extend multiple motile cilia. Alternatively, there is a mechanism in radial glia by which Cre recombination of the *Kif3a* locus is delayed. The finding that ependymal planar polarity was largely preserved in *hGFAP::Cre;Kif3a*$^{fl/fl}$ mutants therefore did not address the role of the radial glial primary cilium in this process, but it showed that motile ependymal cilia are not required for this polarization.

Discussion

We have shown that, in addition to basal body rotational orientation indicated by the basal foot, the position of the basal body patch on the apical surface of ependymal cells is an anatomical correlate to their functional planar polarity, the oriented beating of their multiple cilia. The position of the basal body patch was measured with respect to the center of the cell's apical surface by a vector. The angle of this vector, which we call the basal body (BB) patch angle, was highly consistent among neighboring cells in the epithelium and was correlated to the direction of fluid flow and ciliary beating throughout the adult ventricular system. Moreover, the orientation of BB patch angles was largely

preserved in the absence of motile (9+2) cilia, indicating that this was an independent indicator of structural polarity within the cell, not secondary to ciliary beating.

Apical surface orientation vs. the position of the basal body patch

Initially we identified two potential anatomical correlates of ependymal planar polarity by immunofluorescent confocal microscopy: apical surface orientation, measured by the long axis of the apical surface, and the planar position of the basal body patch, measured by the BB patch angle. However, while the BB patch angle was correlated with the direction of fluid flow in all regions tested, apical surface orientation was not. As a result, there was misalignment between apical surface orientation and the BB patch angle, which varied in different regions of the epithelium. In some regions of the lateral wall of the LV (AD and AV), this misalignment was very small, while in others (PM) it was substantial (up to 47°). Furthermore, we recently described a local apical surface architecture, called pinwheels, in which this misalignment varies among neighboring cells within a region (see Chapter 3:Figure 3). Using techniques similar to those described here, we showed that the ependymal epithelium lining the adult lateral ventricles is in fact a mixed neuroepithelium that also contains adult neural stem cells (Type B cells). Small apical surfaces of Type B cells make contact with the LV and are surrounded by ependymal cells forming the pinwheels. Within these structures, ependymal cell apical surfaces are radially oriented towards the B cell apical surface in the center of the pinwheel, while their basal body patch is oriented in the direction of fluid flow. Therefore, about

half of the ependymal cells within a pinwheel have apical surface orientation that is aligned with the BB patch angle and the other half are misaligned by up to 90°. Altogether, this suggests that the mechanisms governing apical surface orientation and positioning of the basal body patch are distinct, but related. The degree of similarity between the long axis of the apical surface and the BB patch angle may reflect the interplay between these two mechanisms.

Insights into these mechanisms might be gained from another biological problem, orientation of the mitotic spindle for cell division. Orienting the spindle involves positioning of the spindle poles, which are composed of centrioles and pericentriolar material. Centrioles are nearly identical in structure to basal bodies and in most cells, except multiciliated epithelia, they are the precursors to basal bodies (Dawe et al., 2007). Therefore, centriole/spindle pole positioning in mitotic cells and basal body planar positioning in ependymal cells may have shared mechanisms. Interestingly, recent evidence supports an essential role for cell adhesion, both intercellular and cell-substrate, in orienting the mitotic spindle (Thery and Bornens, 2006). In both *Drosophila* neuroepithelium (Lu et al., 2001) and mammalian skin (Lechler and Fuchs, 2005), intercellular adherens junctions appear to control the spatial distribution of spindle pole positioning cues in the cell's cortex. Disrupting adherens junctions in the skin results in mislocalization of these cues and misoriented spindles (Lechler and Fuchs, 2005). We have shown previously the ultrastructure of adherens junctions bordering the apical surfaces of adjacent ependymal cells (see Chapter 3:Figure 4). Interestingly, recent evidence shows that numb, a molecule well-studied for its roles in

asymmetric cell division, is localized to these ependymal adherens junctions (Kuo et al., 2006). Investigating whether these adherens junctions (labeled by β-catenin in **Figs. 2-4**) regulate the planar polarization of basal body patches might reveal interesting parallels in spindle pole and basal body positioning. Importantly, cell adhesion and the tensional patterns it creates within the cell determine cell shape (Thery and Bornens, 2006). Similarly, adherens junctions between the apical surfaces of ependymal cells may regulate apical surface shape. Apical junctional complexes therefore represent a possible point of interaction between the mechanisms governing apical surface orientation and basal body planar positioning in ependymal cells.

Motile (9+2) vs. Primary (9+0) cilia in basal body planar polarity

We found that in the absence of motile (9+2) cilia in *hGFAP::Cre;Kif3a*$^{fl/fl}$ mutants, the position of the basal body patch on the apical surface of ependymal cells remained highly oriented, although less well oriented than in controls. This indicated that the polarized position of the basal body patch, “downstream” of the ciliary effective stroke, was not secondary to mechanical forces imposed by ciliary beating. However, the discrepancy in orientation between mutants and controls suggested that motile (9+2) cilia might play a role in optimization of planar polarity. This is consistent with recent findings in the multiciliated epithelium of the *Xenopus* larval skin, where the basal foot points in the direction of the ciliary effective stroke and is used as a measure of anatomical planar polarity (Mitchell et al., 2007). Interestingly, this planar polarity is acquired through a two-step process. During early differentiation of multiciliated cells,

before the generation of significant flow, basal feet are roughly planar polarized in the posterior direction based on anterior-posterior tissue patterning. Subsequently, flow generated by ciliary beating in mature cells operates in a positive feedback loop to refine the polarity of basal feet. Disrupting ciliary motility in these cells results in greater variability in the orientation of basal feet, although they remain roughly oriented in the posterior direction. This two-step positive feedback mechanism could explain why the position of basal body patches on the apical surface of cilia-deficient ependyma, while oriented, was less optimized than in control ependyma. In this scenario, the absence of cilia and flow in the *hGFAP::Cre;Kif3a*$^{fl/fl}$ mutant epithelium precluded the refinement phase and resulted in a failure to complete the polarization process. The absence of motile cilia might contribute to the slight decrease in ependymal planar polarity through other non cell-autonomous mechanisms as well. For example, *hGFAP::Cre;Kif3a*$^{fl/fl}$ mutants had hydrocephalus, which may distort the epithelium lining the ventricles and influence the polarity of ependymal cells.

Our analysis of *hGFAP::Cre;Kif3a*$^{fl/fl}$ mutants did not address a possible role for the primary cilia of radial glial progenitors in the development of planar polarity in their ependymal progeny. As a result of both delayed Cre recombination and possibly stability of the *Kif3a* protein, radial glia in the walls of the lateral ventricle in *hGFAP::Cre;Kif3a*$^{fl/fl}$ mice maintained their primary cilia throughout development until their transformation into ependymal cells. Ependymal cells, in contrast, never extended any cilia. Exploring the possible role of radial glial primary cilia in the development of ependymal planar polarity is

intriguing in light of recent evidence that primary cilia regulate planar polarity in other tissues. In both the mammalian cochlea and early neural tube, ciliary proteins regulate planar polarity (Ross et al., 2005). Disrupting these ciliary proteins (BBS1, 4, and 6) results in misoriented stereociliary bundles on cochlear hair cells and defects in neural tube closure due to failed convergent extension, a planar polarized cell movement. In addition, these ciliary proteins genetically interact with Vangl2, a component of the conserved planar cell polarity (PCP) pathway, which regulates planar polarity in tissues from flies to mammals (Zallen, 2007). Interestingly, in *Xenopus*, components of the PCP pathway appear to regulate ciliogenesis (Park et al., 2006). Recently, a study in the mammalian cochlea directly addressed the role of primary cilia in planar polarity. Conditional mutants unable to extend a primary cilium from the apical surface of cochlear hair cells fail to correctly orient the actin cytoskeleton or to extend planar polarized stereocilia (Jones et al., 2008). However, cilia-deficient cells do exhibit planar polarized membrane distribution of PCP pathway molecules. This study suggests that the primary cilium relays PCP signals from the cell membrane to the cytoskeleton. Does the primary cilium of radial glia have similar roles in planar organization of the cytoskeleton? Future work using transgenic mice that express Cre at earlier developmental stages should allow ablation of *Kif3a* and the primary cilium from radial glia in order to examine these questions.

Our study focused on the anatomical planar polarity of ependymal cells. This polarity underlies the coordinated beating of ependymal cilia, which propels CSF through the ventricular system and is essential for normal brain function.

Our findings showed that ependymal planar polarity did not require motile ependymal cilia. That is, cilia-generated CSF flow was not a precursor to anatomical planar polarity. Instead, our results suggest that ependymal cells have intrinsic polarity based on their position in the epithelial plane lining the brain ventricles. It has been hypothesized that radial glia lining the embryonic brain ventricles contain positional information that is projected onto the developing cortex as a spatial code through the radial fiber (Rakic, 1988). The planar polarity of ependymal cells may be a read out of this spatial code; a translation of the ependymal cell's (or its radial glial progenitor's) position in the epithelial plane into a polarized orientation. Indeed, ependymal planar polarity may be indicative of more widespread planar polarity throughout the developing and mature brain. Evidence from other multiciliated epithelia, such as the Xenopus larval skin (Tung and Y-F., 1940; Twitty, 1928) or the quail oviduct (Boisvieux-Ulrich and Sandoz, 1991), suggests that the establishment of planar polarity precedes multiciliated cell differentiation. In fact, at the earliest stages of neural development, neuroepithelial cells display a planar polarized behavior called convergent extension, which is essential for neural tube formation (Copp et al., 2003). Later in development, many of the epithelial properties of neuroepithelial cells, including apical-basal polarity, are inherited by radial glial cells (Gotz and Huttner, 2005). However, to date planar polarity has not been demonstrated in radial glia. Determining whether radial glia are planar polarized, and if and how they transmit planar polarity information, perhaps via the primary cilium, to their ependymal progeny are provocative and unresolved questions. If

radial glia do have planar organization, this could have tremendous ramification for their diverse roles in neural development. Overall, this work has important implications for human patients with hydrocephalus, one of the most common anomalies of the central nervous system, which can be caused by defective ependymal ciliary beating. The anatomical understanding provided here paves the way for future studies examining the relationship between ependymal planar polarity and the pathogenic mechanisms of hydrocephalus.

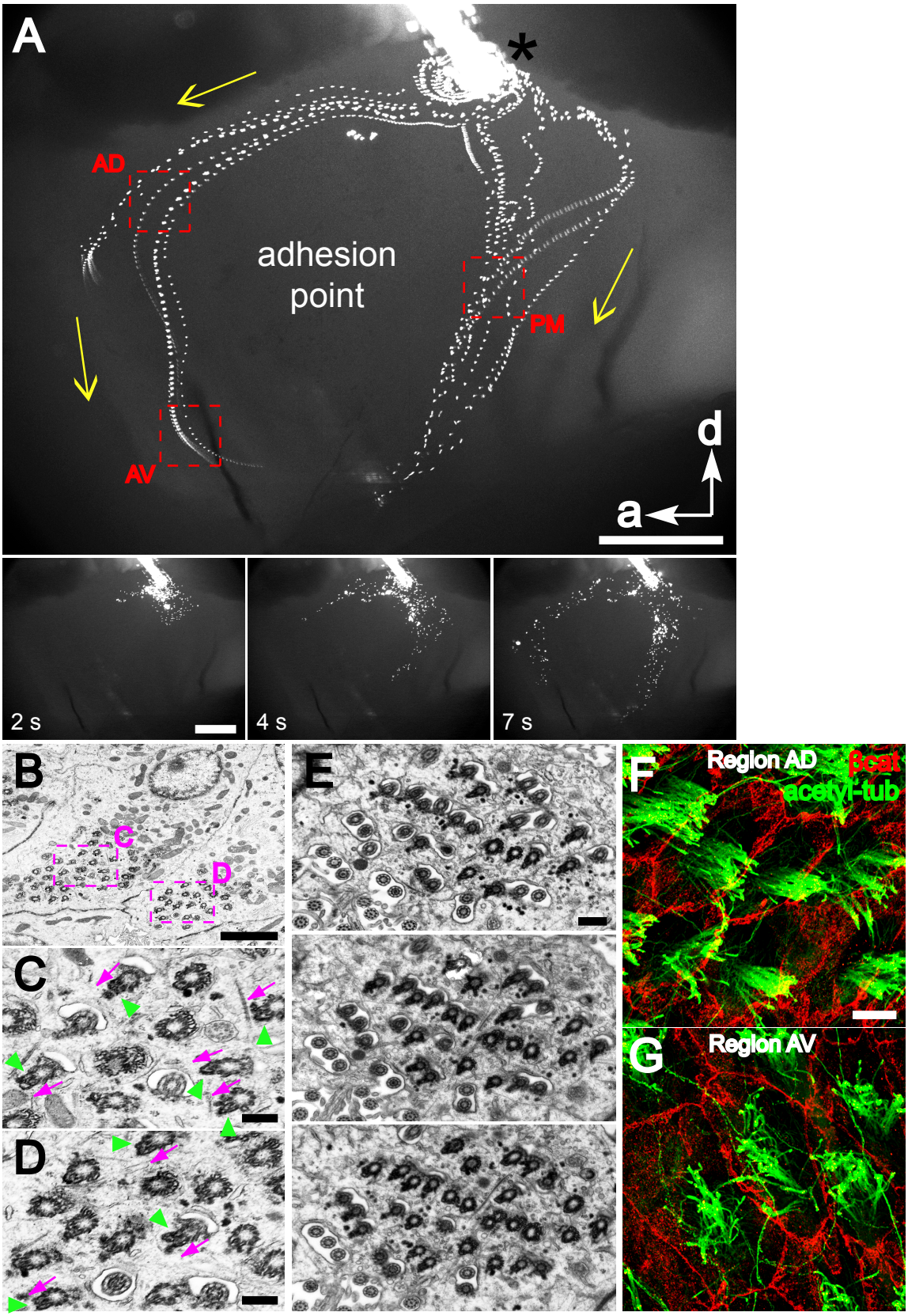

A
*
AD
adhesion
point
PM
AV
d
a
2 s
4 s
7 s
B
C
D
E
F
Region AD
β-cat
acetyl-tub
G
Region AV

Figure 1. Functional and anatomical planar polarity of the ependymal epithelium.

(**A**) Upper panel is from 89 frames of a movie that was merged into a single picture. To make this movie, beads were deposited (*) on the surface of a wholemount of the lateral wall of the lateral ventricle. Planar polarized beating of ependymal cilia on the wholemount surface is indirectly visualized by oriented flow lines of fluorescent (2 um) microbeads. Within a line, the position of an individual bead is seen in consecutive frames. Yellow arrows indicate direction of flow. Note that the ventral region where the two groups of flow lines come together corresponds to the foramen of Munro, leading to the 3rd ventricle. Red boxes indicate regions AD, AV, and PM on the lateral wall where subsequent anatomical analyses were performed. The adhesion point is where the medial and lateral walls are fused within the ventricular cavity; it is not covered by ependyma. Anterior (a) and dorsal (d) directions are indicated by arrows in the lower right corner. Lower three panels show individual frames of this movie at 3 different time points. Scale bar = 0.5 mm.

(**B**) En-face electron micrograph near the apical surface of two adjacent ependymal cells in region AD. The orientation of this image and all subsequent images in this study correspond to the orientation of the wholemount in (A). Note the clustering of basal bodies to one side of the apical surface of both cells. Higher power images of the basal bodies are shown in (C) and (D) (boxed regions). Scale bar = 2 um.

(**C, D**) Some of the basal bodies in the ultrathin section shown in (B) were transected at the level of the basal foot (green arrowheads), which is observed projecting from the basal body. The orientation of the basal foot is consistent within each cell and between the two cells (magenta arrows). The basal foot in these cells points in the direction of fluid flow (compare to region AD in (A)). Scale bar = 0.25 um.

(**E**) 3 sequential electron micrographs from a serially reconstructed ependymal cell in region AD. Note the consistency of basal foot orientation with the direction of fluid flow in all of the basal bodies. Scale bar = 0.5 um.

(**F, G**) En-face confocal images of lateral wall wholemounts stained for acetylated tubulin (green) and β-catenin (red) confirmed that ciliary bundles in ependymal cells emanate from one side of the cell's apical surface, consistent with the localization of basal bodies in (B). Note that in both region AD and AV, the ciliary bundles are displaced to the "downstream" side of the apical surface with respect to fluid flow. Scale bar = 10 um.

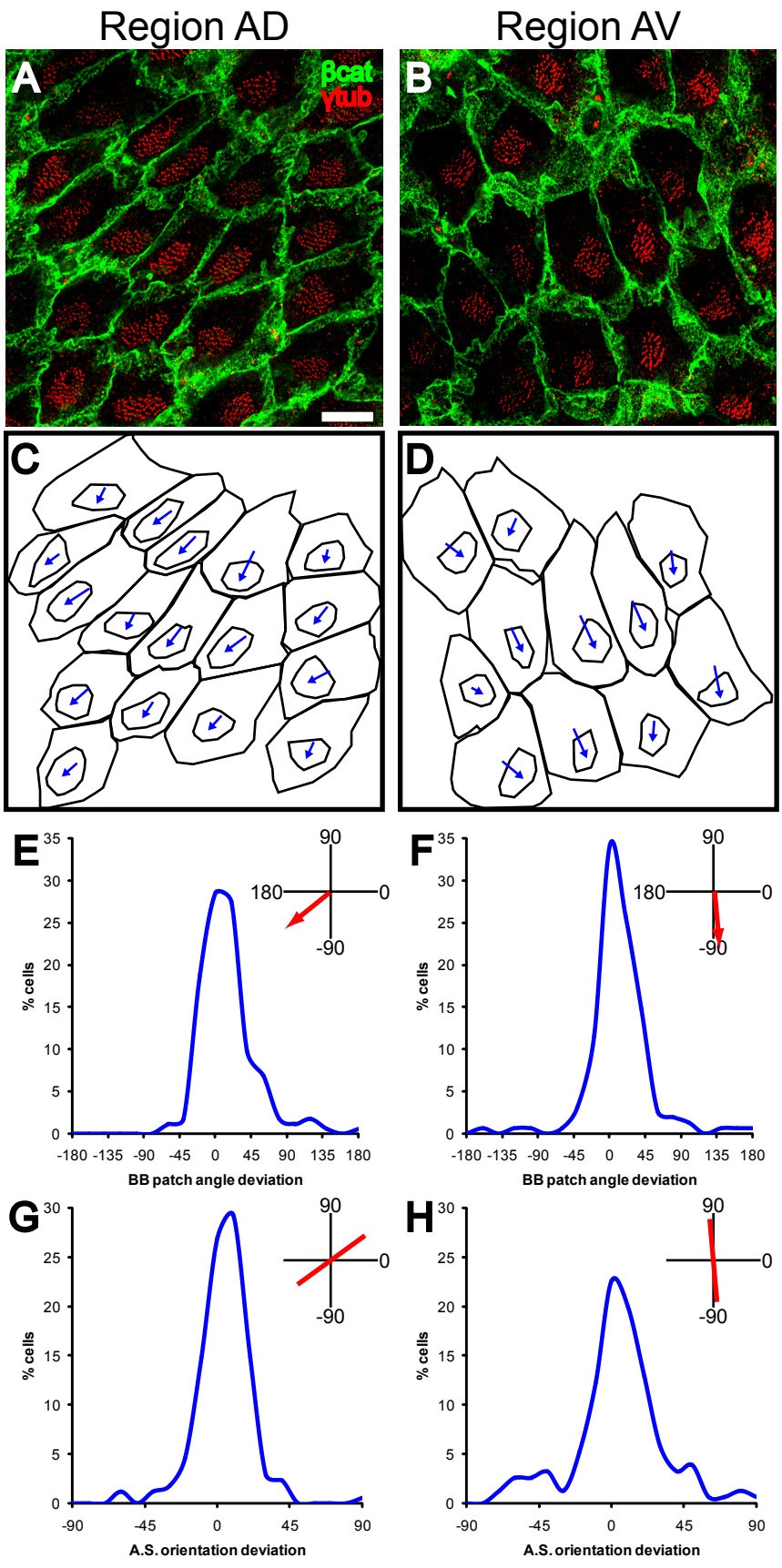

Region AD
Region AV
A
βcat
γtub
B
C
D
E
F
G
H
% cells
BB patch angle deviation
A.S. orientation deviation
90
180
0
-90
-180 -135 -90 -45 0 45 90 135 180
-90 -45 0 45 90

Figure 2. Basal body patch position and apical surface orientation are anatomical correlates to ependymal planar polarity in regions AD and AV of the lateral wall.

(**A, B**) Confocal images from regions AD and AV (see Fig. 1A) of lateral wall wholemounts stained for β-catenin (green) and γ-tubulin (red). This provided an unobstructed view of the planar organization of basal bodies on the apical surface of ependymal cells. In both regions, the patch of basal bodies is located on the "downstream" side of the apical surface with respect to fluid flow (compare to flow in boxed regions in Fig. 1A). Also note that the long axis of the apical surface (or the apical surface orientation) of cells in both regions is parallel to fluid flow. Scale bar = 10 um.

(**C, D**) Traces of the apical surfaces and basal body patches in (A, B). To quantify basal body patch position relative to the apical surface, Metamorph image analysis software was used to determine the vector connecting the centers of these two traced regions for each cell. The angle of this vector was called the basal body (BB) patch angle.

(**E, F**) For each high power field (127 x 127 um^2) analyzed, the difference between each cell's BB patch angle and the median BB patch angle in the field was calculated. This data was collected from high power fields in regions AD and AV from 4 mice (175 cells in AD, 155 cells in AV) and displayed as a histogram. The narrow distribution around 0° revealed that BB patch angles in each region were highly oriented. The red arrows in the inset axes show the orientation of the median angle (n=4 mice) for regions AD and AV. Note that this correlated with the direction of fluid flow in corresponding boxed regions in Fig. 1A.

(**G, H**) Apical surface orientation, measured by the long axis of the cell surface, was analyzed and plotted on a histogram similar to the BB patch angle and also revealed a narrow distribution around the median. The red lines in the inset axes indicate the median apical surface orientation (n=4 mice) for regions AD and AV, which correlated with fluid flow and the BB patch angles (compare with red arrows in E, F). Note that because apical surface orientation lacks directionality (unlike BB patch angle), it can only vary from -90° to 90° and is depicted by a line.

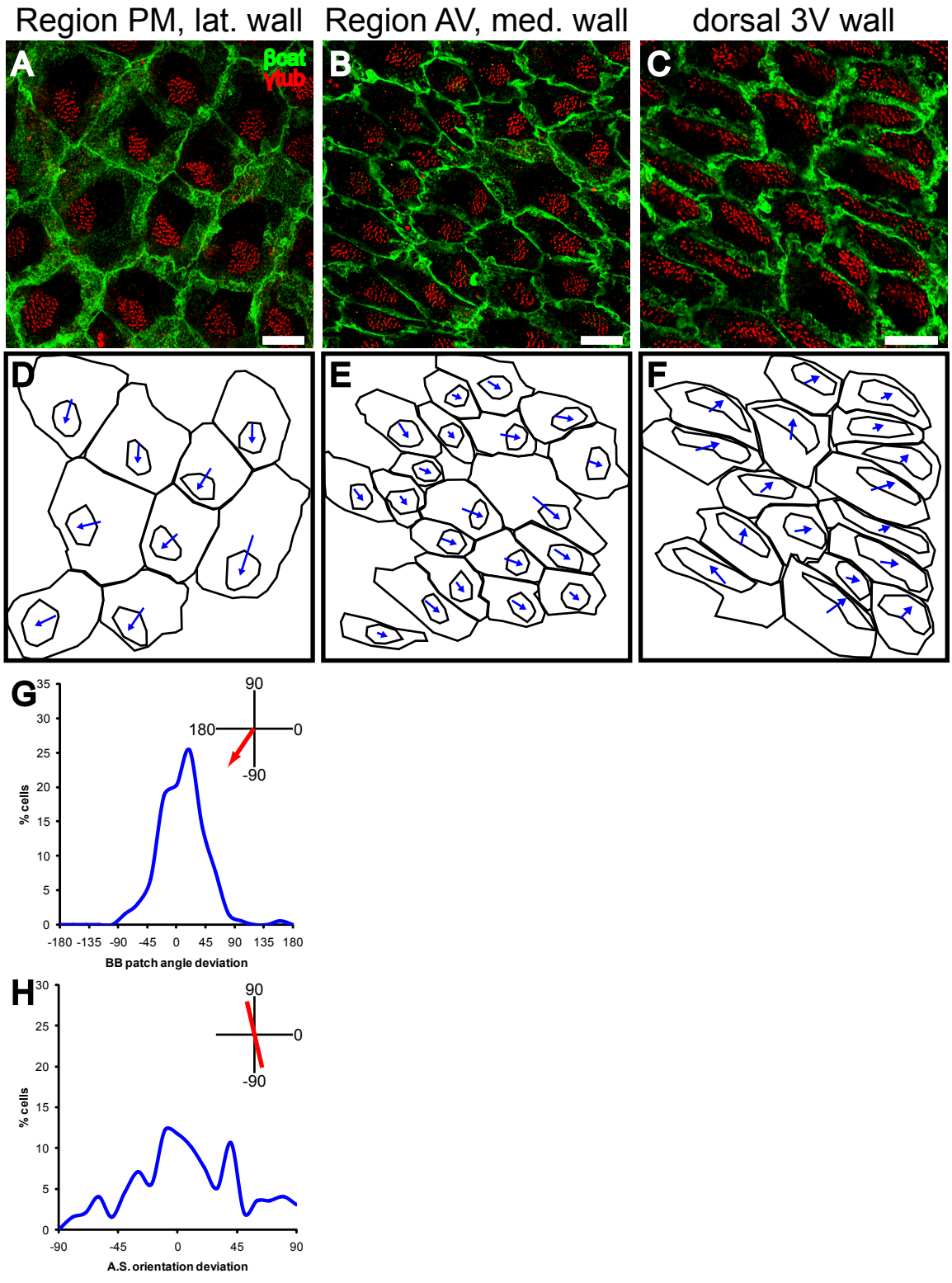

Region PM, lat. wall
Region AV, med. wall
dorsal 3V wall
A
βcat
Ytub
B
C
D
E
F
G
90
180
0
-90
% cells
35
30
25
20
15
10
5
0
-180 -135 -90 -45 0 45 90 135 180
BB patch angle deviation
H
90
0
-90
% cells
30
25
20
15
10
5
0
-90 -45 0 45 90
A.S. orientation deviation

Figure 3. Basal body patch angle, but not apical surface orientation, correlates with ependymal planar polarity throughout the adult ventricular system.

(**A**) Confocal image from region PM of the lateral wall of the LV (see Fig. 1A) stained for β-catenin (green) and γ-tubulin (red). The position of basal body patches appeared to correlate with fluid flow but apical surface orientation was less clear. Many cells in this region had symmetric, diamond-shaped apical surfaces without a clear long axis. Cells that had a clear long axis were not always aligned. Scale bar = 10 um.

(**B**) Confocal image from region AV of the medial wall of the LV stained for β-catenin (green) and γ-tubulin (red). Both the position of the basal body patch and the apical surface orientation in this region appeared to correlate with the direction of fluid flow (see flow in supplemental Fig. S2). Scale bar = 10 um.

(**C**) Confocal image from the dorsal 3rd ventricle wall stained for β-catenin (green) and γ-tubulin (red). Unlike in (B) or Fig. 2, where basal body patches appear to be displaced from center along the long axis of the apical surface, in the dorsal 3rd ventricle they appeared to be displaced along the cell's short axis. Scale bar = 10 um.

(**D-F**) Traces of the apical surfaces and basal body patches in (A-C), respectively, with vectors indicating the BB patch angle. Note the inconsistent apical surface orientation of cells in (A). Consequently, there is misalignment between apical surface orientation and BB patch angle, which is highly oriented in these cells. This misalignment is more clearly observed in (F), where the BB patch angle in many cells is almost perpendicular to the long axis.

(**G**) Histogram showing the narrow distribution of BB patch angles around the median in region PM of the lateral wall of LV. The median angle (197 cells from n=4 mice) in this region correlated with the direction of fluid flow (compare red arrow in inset axis to flow in region PM of Fig. 1A).

(**H**) Histogram showing that apical surface orientation is widely distributed around the median in region PM of the lateral wall. Note also that the median orientation (n=4 mice) in this region (red line in inset axis) was not correlated with the direction of fluid flow or with the BB patch angle (compare with red arrow in (G)).

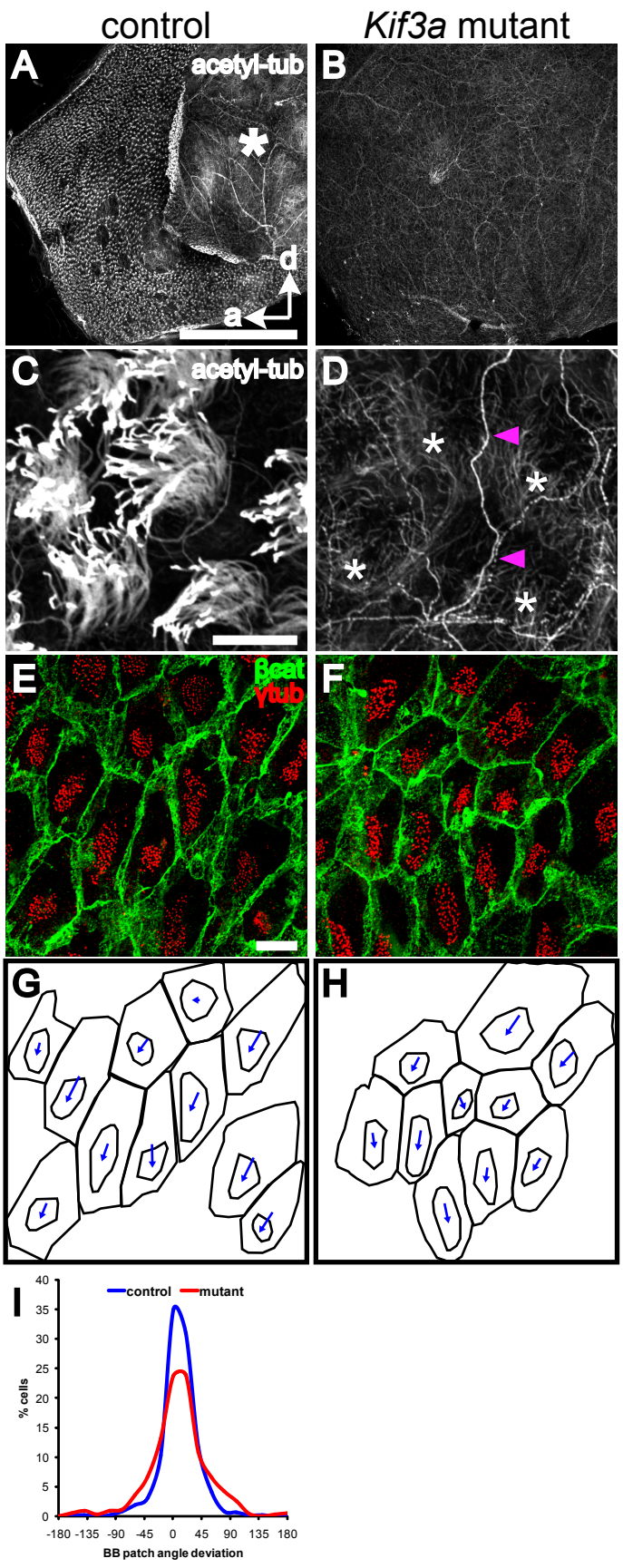

control
Kif3a mutant
A
acetyl-tub
d
a
B
C
acetyl-tub
D
E
βcat
γtub
F
G
H
I
control
mutant
% cells
40
35
30
25
20
15
10
5
0
-180 -135 -90 -45 0 45 90 135 180
BB patch angle deviation

Figure 4. Planar polarity of basal body patches does not require motile (9+2) cilia.

(**A, B**) Low power confocal images of lateral wall wholemounts from the LV of *hGFAP::Cre;Kif3a*$^{fl/fl}$ mutants and control littermates stained for acetylated-tubulin. Tufts of cilia, seen as small white puncta on the ependymal surface of controls at this magnification, are missing in mutants. Asterisk on the control wholemount indicates the adhesion point, which is not present in the mutant, likely due to hydrocephalus. Anterior (a) and dorsal (d) directions are indicated by arrows in the lower right corner of (A). Scale bar = 0.5 mm.

(**C, D**) High power confocal images from the wholemounts in (A, B) show that while microtubule-based cilia were absent on the apical surface of mutant ependymal cells, the microtubule network (*) within these cells was preserved. Note also that intraventricular axons (magenta arrowheads), stained by acetylated-tubulin, were seen on the ventricular surface of both wholemounts, although more clearly on the cilia-deficient mutant ependyma. Scale bar = 10 um.

(**E, F**) Confocal images of control and *hGFAP::Cre;Kif3a*$^{fl/fl}$ mutant lateral wall wholemounts stained for β-catenin (green) and γ-tubulin (red). Basal bodies in mutant ependymal cells were maintained in tightly clustered patches. The planar polarized position of these patches was also largely preserved in the absence of motile (9+2) cilia in mutants. Scale bar = 10 um.

(**G, H**) Traces of the apical surfaces and basal body patches in (E, F), with vectors indicating the BB patch angle.

(**I**) Histogram showing the distribution of BB patch angles around the median in control (blue) and mutant (red) ependyma. As indicated by the narrow distribution, the mutant ependyma had highly oriented BB patch angles (n=5 mutants (790 cells), 5 control littermates (624 cells); curve fit test, p=0.0003).

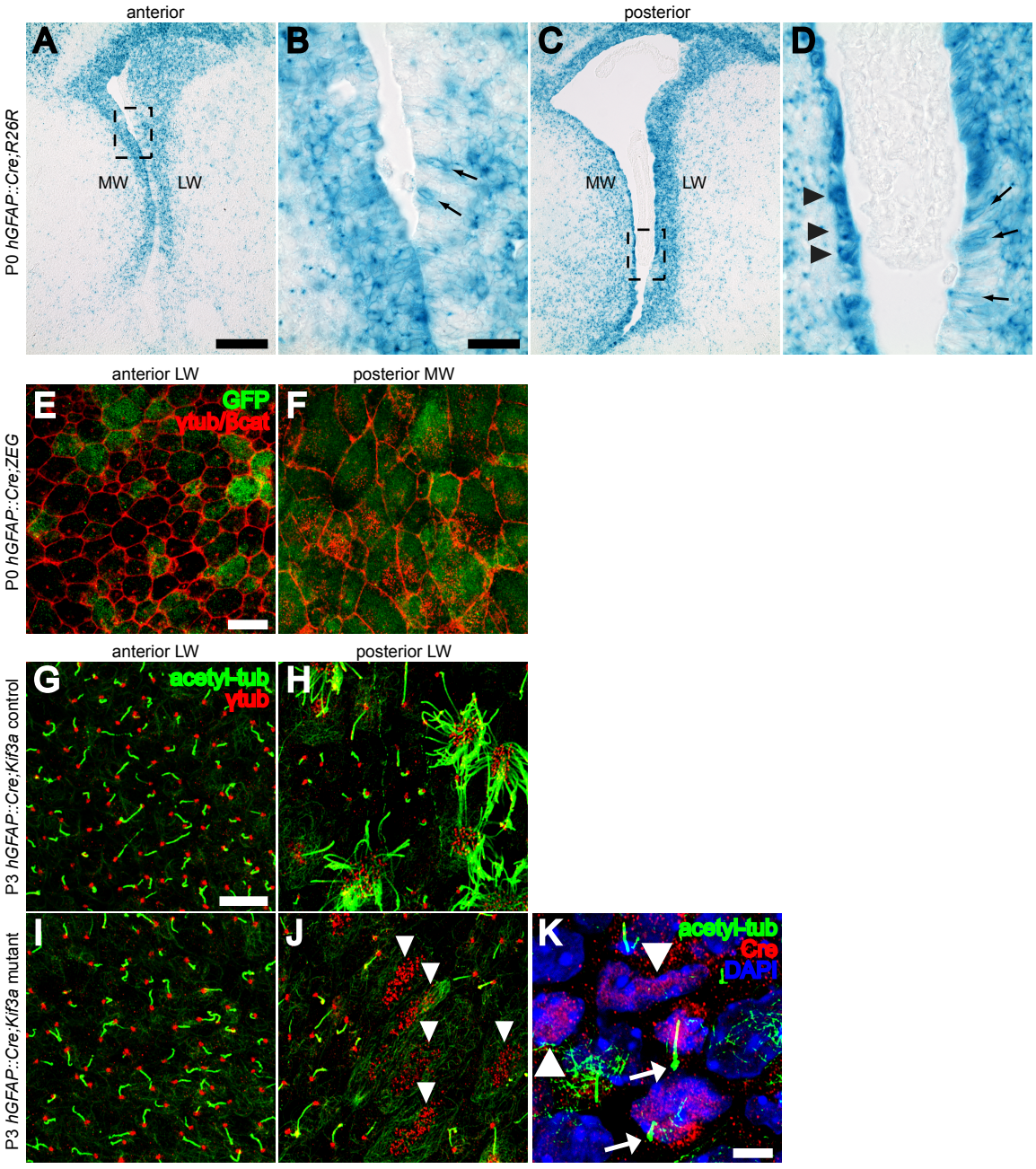

anterior
posterior
A
B
C
D
MW
LW
MW
LW
P0 hGFAP::Cre;R26R
anterior LW
posterior MW
E
GFP
ytub/βcat
F
P0 hGFAP::Cre;ZEG
anterior LW
posterior LW
G
acetyl-tub
ytub
H
P3 hGFAP::Cre;Kif3a control
I
J
K
acetyl-tub
Cre
DAPI
P3 hGFAP::Cre;Kif3a mutant

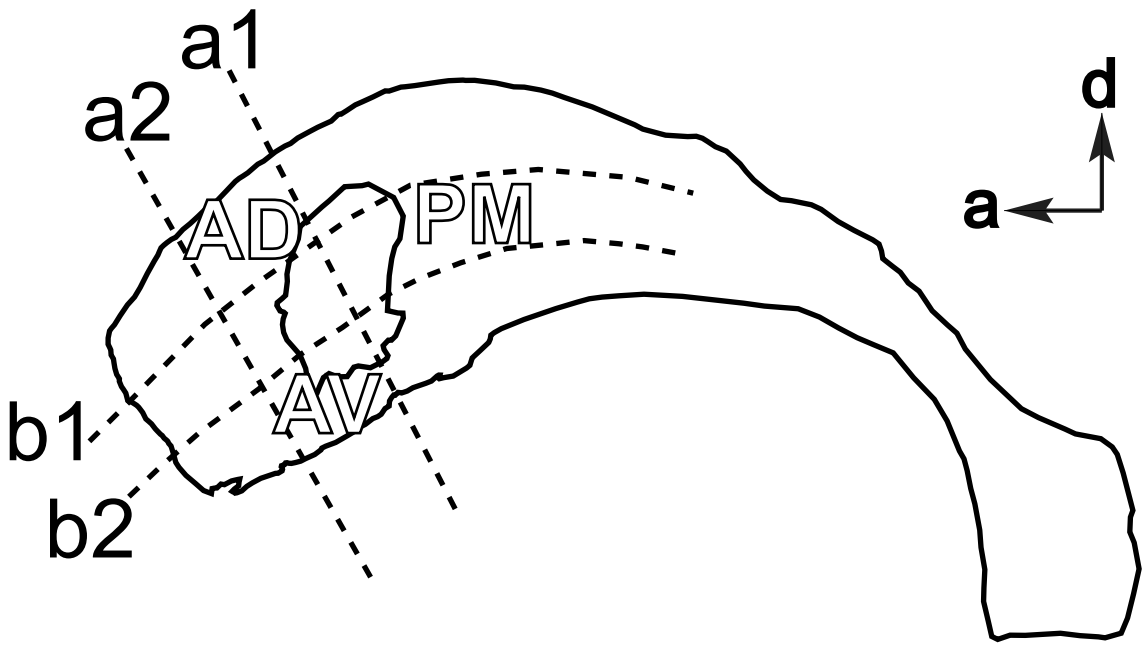
Figure 5. Timing of cilia loss in *hGFAP::Cre;Kif3a*$^{fl/fl}$ mutants.

(**A-D**) (A) and (C) are low power images of coronal sections stained for lacZ expression from the anterior (A) and posterior (C) LV of P0 *hGFAP::Cre;R26R* mice. While lacZ expression in the medial wall (MW) was nearly uniform in both the anterior and posterior LV, in the lateral wall (LW) high expression was observed only posteriorly. In the anterior LW, lacZ expression was mosaic. Higher power images of boxed regions in (A, C) are shown in (B, D) respectively. Note that lacZ expression in the anterior and posterior LW corresponded to columnar shaped cells (black arrows in B, D), while in the posterior MW it corresponded to cuboidal cells (black arrowheads in D). Scale bar = 200 um (A, C) and 30 um (B, D).

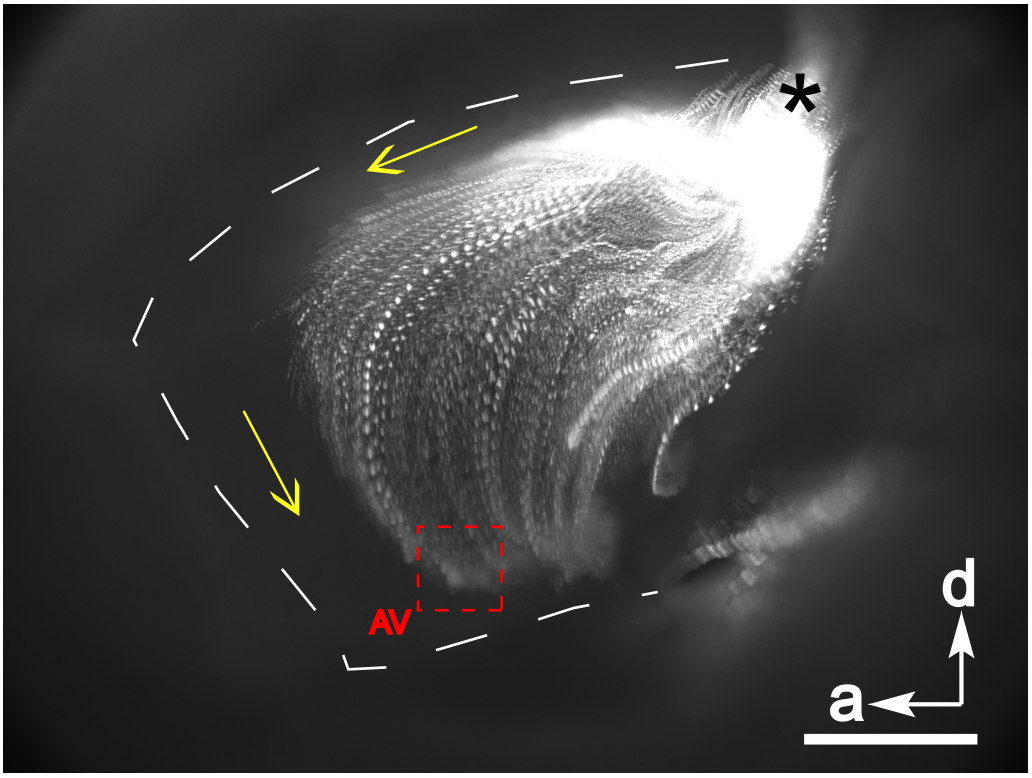
(**E, F**) Confocal images of lateral (E) and medial (F) wall wholemounts from the LV of P0 *hGFAP::Cre;Z/EG* mice stained for GFP (green), and β-catenin and γ-tubulin (red). This confirmed that while ependymal cells, identified by their multiple basal bodies, were uniformly recombined by Cre expression under the hGFAP promoter (F), radial glia, identified by their single basal body and smaller apical surface, exhibited mosaic recombination (E). Scale bar = 10 um.

(**G-J**) Confocal images of anterior (G, I) and posterior (H, J) regions in lateral wall wholemounts from P3 controls (G, H) and *hGFAP::Cre;Kif3a*$^{fl/fl}$ mutants (I, J) stained for acetylated tubulin (green) and γ-tubulin (red). Note that basal body patches at the apical surface of mutant ependymal cells (arrowheads in J) did not have associated cilia, while in control ependymal cells (H) many long cilia were observed emanating from basal body patches. In contrast, nearly all radial glia in both controls and mutants had a primary cilium (G, I). The maintenance of the radial glial primary cilium in mutants, even though many radial glia were recombined (E), suggested that the *Kif3a* protein has a long half-life. Scale bar = 10 um.

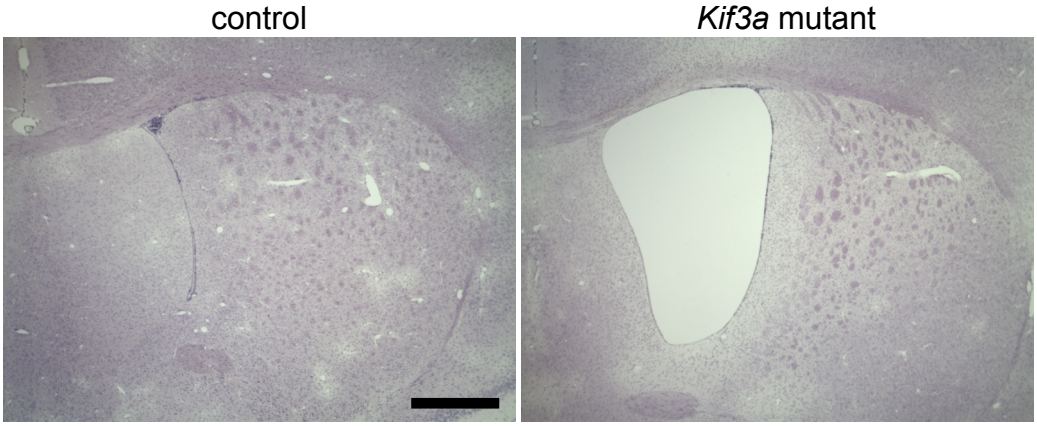
(**K**) Confocal image from the posterior lateral wall of a P3 *hGFAP::Cre;Kif3a*$^{fl/fl}$ mutant wholemount stained for acetylated tubulin (green), Cre (red), and DAPI (blue). Although some cells that expressed Cre had no associated cilia (white arrowheads), likely corresponding to ependymal cells, other cells that expressed Cre had a primary cilium (white arrows), corresponding to radial glia. This suggested that the *Kif3a* protein may have a long half-life and that while these cells may no longer be expressing the protein, *Kif3a* made before the cell expressed Cre is sufficient to maintain ciliary function for several days. Scale bar = 5 um.



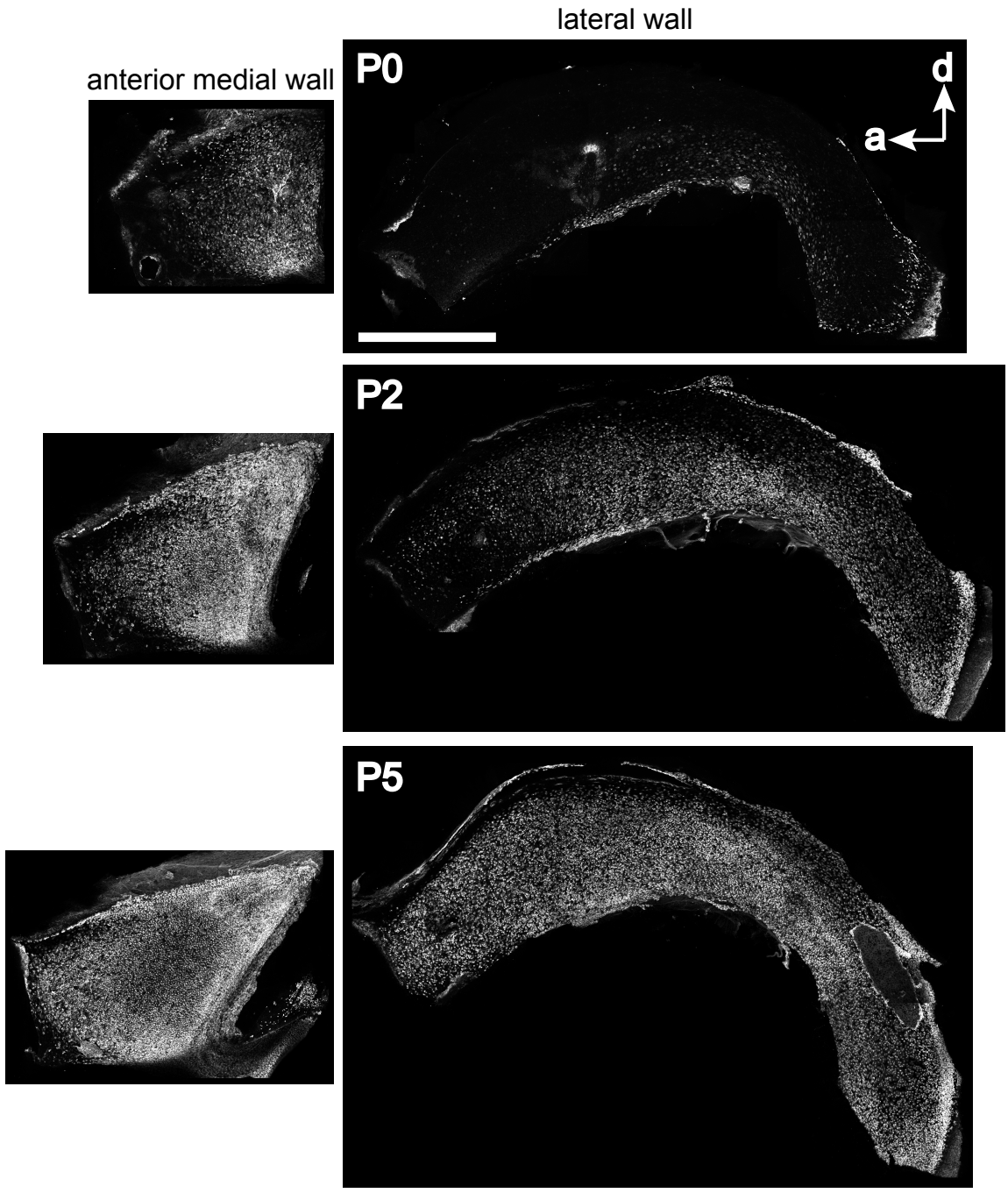
Supplemental Figure S1. Regions AD, AV, and PM of the lateral wall of the lateral ventricle were defined by 4 lines. Line (a1) bisects the adhesion point into an anterior and posterior half and runs orthogonal to the dorsal boundary of the wholemount. Line (a2) runs parallel to line (a1) and bisects the region between line (a1) and the anterior boundary of the wholemount. Line (b1) and (b2) run parallel to each other along the anterior-posterior axis of the wholemount and divide the dorsal-ventral axis into 3 equally wide regions. These 4 lines in combination with the boundaries of the wholemount and the adhesion point divide the lateral wall into three regions, named with respect to the adhesion point: anterior-dorsal (AD), anterior-ventral (AV), and posterior-middle (PM). Note that PM is located directly behind the adhesion point. Anterior (a) and dorsal (d) directions are indicated by arrows in the upper right corner.



Supplemental Figure S2. Orientation of fluid flow on the anterior medial wall of the LV. This represents 30 frames of a movie were merged into a single picture. To make this movie, beads were deposited (*) on the surface of a wholemount of the anterior medial wall of the lateral ventricle. Planar polarized beating of ependymal cilia on the wholemount surface is indirectly visualized by oriented flow lines of fluorescent (2 um) microbeads. Within a line, the position of an individual bead is seen in consecutive frames. Yellow arrows indicate direction of flow. Red box indicates region AV of the medial wall, which is shown in Fig. 3B. Note that the orientation of flow shown here corresponds to that on the anterior lateral wall (Fig. 1A). Anterior (a) and dorsal (d) directions are indicated by arrows in the lower right corner. Scale bar = 0.5 mm.



Supplemental Figure S3. Hematoxylin-stained coronal sections from control and *hGFAP::Cre;Kif3a*$^{fl/fl}$ mutant mice demonstrate hydrocephalus in cilia-deficient mutants. Scale bar = 0.5 mm.



Supplemental Figure S4. CD24 immunostaining on wholemounts reveals gradients of ependymal cell differentiation on the lateral and anterior medial wall of the LV in the early postnatal period. Ependymal differentiation proceeds from medial to lateral, posterior to anterior, and ventral to dorsal. Anterior (a) and dorsal (d) directions are indicated by arrows in the upper right corner. Scale bar = 1 mm.

Chapter 6
Concluding Remarks and Future Directions

This dissertation explored the epithelial properties of cells lining the adult brain ventricles. It revealed that type B cells, neural stem cells residing along the walls of the lateral ventricles, are part of a mixed neuroepithelium in the adult brain that also contains multiciliated ependymal (type E1) cells and biciliated (type E2) cells with a previously undescribed basal body structure. Type B cells exhibited apical-basal polarity; they made apical contact with the ventricle and basal contact with blood vessels. Type E1 cells exhibited structural planar polarity evident in the position of basal bodies on their apical surface, which did not require ependymal cilia or cilia-generated CSF flow. Type E2 cells had a unique basal body structure with a complex meshwork that extended laterally from the basal body, they usually had two (9+2) cilia, and their distribution in the ventricular system suggested that they correspond to tanycytes. Below I discuss the broader implications of these findings and future directions in the study of the epithelial properties of these cell types, with special attention to Type B cells and Multiciliated Ependymal (Type E1) cells.

Type B cells

The detailed morphological description given for Type B cells and their topological relationship with the ventricle (apically) and blood vessels (basally)

provides an anatomical model where molecules can be placed. Several intercellular signaling pathways are known to regulate the germinal activities of type B cells, including FGF (Kuhn et al., 1997), PDGF (Jackson et al., 2006), Shh (Machold et al., 2003; Palma et al., 2005), Wnt (Adachi et al., 2007; Yu et al., 2006), Noggin/BMP (Lim et al., 2000), and Ephrin signaling (Conover et al., 2000). In addition, type B cells are regulated by signaling pathways dependent on cell-cell contact, such as Notch signaling (Givogri et al., 2006; Nyfeler et al., 2005), and may be regulated by intercellular junctional complexes, such as gap junctions described in Chapter 3. These diverse regulatory mechanisms may impinge upon type B cells with spatially specific organization. Conversely, the elaborate morphology of type B cells may allow these cells to bridge between different regulatory microenvironments, such as the ventricular surface and the vasculature. In addition, the ability of type B cells to respond to specific signaling pathways may depend on localization of receptors to specific microdomains within the cell. For example, the ability of these cells to respond to Shh may depend on the localization of Smoothened, the Shh co-receptor, to the primary cilium (Corbit et al., 2005; Huangfu et al., 2003). Noggin, which is highly expressed by ependymal cells and creates a neurogenic niche for type B cells (Lim et al., 2000), may act at the level of the apical process. Other signaling pathways may operate at the level of the basal process: a recent study showed that blood vessel basal lamina in the SVZ concentrates FGF2 (Kerever et al., 2007), which promotes the neurogenic activity of type B cells. Altogether, this indicates that the morphological specializations of type B cells may allow them to

establish topological relationships with essential regulatory microenvironments. A hypothetical model is provided in **Figure 1**.

The pinwheel structures described in Chapter 3, composed of the apical surfaces of type B cells surrounded by ependymal cells, are another potential mechanism of spatially segregating the regulation of type B cells. For example, gap junctions may couple clusters of B cells within a single pinwheel, and isolate them from adjacent clusters in other pinwheels. During developmental neurogenesis, gap junction coupling of radial glial clusters in the embryonic ventricular zone regulates their re-entry into the cell cycle after every M phase (Bittman et al., 1997). Gap junction coupling in type B cells may therefore coordinate the proliferative activity within pinwheels and segregate it from adjacent pinwheels. Alternatively, gap junctions between type B cells and ependymal cells may allow information to pass between neighboring pinwheels. Future work is necessary to determine the extent of gap junction coupling between B cells in the center of a pinwheel, between B cells and ependymal cells in a pinwheel, and between neighboring pinwheels. Analogous to studies of gap junction coupling in radial glia (Bittman et al., 1997; Weissman et al., 2004), Ca^{2+} imaging and intracellular biocytin labeling experiments can be performed on acutely dissected, cultured wholemounts labeled with vital membrane dyes (e.g. Bodipy-FL-C_5-Ceramide) to locate the position of type B cells and ependymal cells within pinwheels. The timing and extent of Ca^{2+} wave propagation and biocytin transfer between different cell types in a pinwheel may reveal some of the functional significance of this architecture.

The developmental origin of pinwheel structures, specifically the spatial organization of differentiating ependymal and type B cells that comprise them, presents another interesting and unresolved problem. Recent evidence has demonstrated that both ependymal cells and type B cells are derived from radial glia. But, are these distinct populations of radial glia? If so, when do these two populations diverge from a common ancestor? If not, what mechanisms in radial glia determine the choice of type B vs. ependymal cell fate in their progeny? Lateral wall wholemounts from the neonatal LV stained with γ-tubulin and β-catenin antibodies reveal that radial glia ubiquitously cover the ventricular surface at P0 (**Figure 2**). However, heterogeneity in the size of the apical surface of these cells suggests that there are already distinct populations of radial glia at this age; those cells with larger apical surfaces are likely beginning the transformation into ependymal cells. Better characterizing the spatial organization of radial glia with enlarged apical surfaces at early postnatal ages may help elucidate the development of pinwheel architecture. These experiments, although technically difficult, would best be performed on cultured neonatal wholemounts labeled with vital membrane dyes, such that apical surface size could be followed in time-lapse over a few days. The caveat to this approach is that the wholemounts may deteriorate over time, making it difficult to interpret changes in the apical surface size of the cells. An alternative approach would be to analyze the change in radial glial apical surface area in fixed and immunostained lateral wall wholemounts from several early postnatal ages (i.e. P0, P1, P2, P3). In addition to examining the spatial organization of pinwheel

development, it will be important to determine the relative contribution of single radial glia to either the center (B cells), surround (ependymal cells) or both center and surround of the pinwheel. Sparsely labeling radial glia at different developmental stages (E11-E18), by *in utero* injection of retrovirus expressing GFP, and then analyzing pinwheel structures in wholemounts postnatally (P21), may indicate whether and when the radial glial progenitors of Type B cells and those of ependymal cells diverge from a common ancestor. Injections that result in labeling of both type B cells and ependymal cells within a single pinwheel would suggest that these cells were derived from a common ancestor at the age injected. Injections that result in labeling of either exclusively ependymal cells or exclusively type B cells within single pinwheels would suggest that the progenitors at that age were already specified. A potential caveat to this approach is the possibility of directly labeling neighboring radial glia, such that neighboring cells observed postnatally were not necessarily derived from a common ancestor. However, preliminary studies indicate that sparse labeling of radial glia can be achieved using retroviruses (data not shown). These experiments are a first step towards understanding the neuroepithelial transformation between the embryonic and postnatal brain.

Recent evidence shows that the neurogenic niche in the walls of the lateral ventricle extends far beyond the anterior lateral wall, which was initially described as the extent of germinal region (Luskin, 1993). In fact, type B cells are present throughout the lateral wall (Merkle et al., 2007), and also the anterior medial wall (Doetsch et al., 1999; Merkle et al., 2007; Morshead et al., 1994) and

the dorsal or pallial wall of the LV (Kohwi et al., 2007; Merkle et al., 2007; Ventura and Goldman, 2007), the rostral migratory stream (Bonfanti et al., 1997; Gritti et al., 2002; Hack et al., 2005; Liu and Martin, 2003; Merkle et al., 2007; Pencea et al., 2001), and the subcallosal zone (Seri et al., 2006). But some of these regions, such as the RMS, do not appear to be close to the ventricular lining. How do we reconcile this with the notion presented here that apical ventricular contact is important for the identity of Type B cells? Similarly, how do we explain the persistence of type B cells in the subgranular zone of the dentate gyrus in the adult hippocampus? The answer to these questions relies not so much on absence of ventricular contact, but rather maintenance of neuroepithelial properties including apical-basal polarity. In fact, the morphology of the type B cells (radial astrocytes) in the adult hippocampus suggests that these cells also have apical-basal polarity. In the absence of the ventricular lumen, the apical membrane in these cells may be defined by other molecular determinants of apical-basal polarity such as the Par3/Par6/aPKC complex (Martin-Belmonte and Mostov, 2008), or specialized structures like the primary cilium. Determining the localization of the primary cilium in radial astrocytes would be insightful in this regard. In fact, a recent study showed that primary cilia are required to establish radial astrocytes in the dentate gyrus of the postnatal hippocampus (Han et al., 2008). Radial astrocytes in the dentate gyrus are derived from precursors that originate in the dentate neuroepithelium lining the ventricles and migrate to the dentate gyrus. In mutants that lack primary cilia in the migratory precursors, radial astrocytes fail to form. Based on genetic

epistasis experiments, one mechanism suggested in this study for loss of radial astrocytes was abrogated Shh signaling in the absence of primary cilia. However, in addition to loss of Shh signaling, another possibility is that loss of primary cilia prevented migratory precursors from re-establishing apical-basal polarity and other neuroepithelial properties upon arriving in the dentate gyrus. To explore this possibility, a first step would be to analyze the expression patterns in radial astrocytes of proteins known to regulate apical-basal polarity, such as Par3, PTEN, and Cdc42 (Martin-Belmonte and Mostov, 2008). Subsequent experiments could analyze the function of these proteins in radial astrocytes by crossing conditional (Cre/loxP) mutants with the Cre line used in (Han et al., 2008). These experiments would directly test whether radial astrocytes and their germinal activity are dependent on molecular determinants of apical-basal polarity. A potential caveat of these experiments is that some of these proteins may have dual functions in the cell, which could also affect radial astrocyte form and function. However, these experiments, and similar studies of the Type B cells in the lateral ventricle walls, should help elucidate the significance of maintained neuroepithelial properties in adult neural stem cells.

Multiciliated Ependymal (Type E1) cells

The work presented in Chapter 4 demonstrated that both rotational orientation of the basal body and its translational position on the apical surface of multiciliated ependymal (type E1) cells are structural indicators of their planar polarity. This represents the first description of reliable anatomical indicators of

this polarity, which was previously assayed functionally by examining the direction of CSF flow (Ibanez-Tallon et al., 2004; Sawamoto et al., 2006; Yamadori and Nara, 1979). However, many questions remain. Most importantly, when is basal body polarity established and how? The results presented in Chapter 4 indicate that ependymal cilia are not required. However, the role of the primary cilium of their radial glial progenitors was not addressed. In light of recent evidence from other tissues that primary cilia have important roles in planar polarity (Jones et al., 2008; Park et al., 2006; Ross et al., 2005), determining whether the primary cilium of radial glia is required for ependymal planar polarity is a logical next step. Using methods similar to those described in Chapter 4, these questions may be addressed by ablating *Kif3a* and primary cilia from radial glia earlier in development. One strategy would be to cross *Kif3a*$^{fl/fl}$ mice with transgenic mouse lines expressing Cre at earlier developmental stages in radial glia (e.g. Nestin::Cre). Interestingly, preliminary observations of basal body position on the apical surface of neonatal radial glia suggests that a subset of these cells already have polarity that is predictive of subsequent ependymal planar polarity (**Figure 3**). But this polarized basal body position is only seen in subsets of radial glia and it appears to be more evident in regions that are located just anterior to the wave of ependymal cell differentiation (see Chapter 4:Figure S4 for gradients of ependymal cell differentiation). Future work is necessary to quantify this apparent radial glial planar polarity and to examine how the acquisition of this polarity correlates with ependymal cell differentiation. For example, are radial glia with larger apical surfaces (undergoing ependymal

transformation) more likely to have planar polarized basal body position? Or is planar polarity a stable feature of other radial glia as well, and only becomes evident in these radial glia because their apical surface is expanded? Answering these questions by quantitatively measuring basal body position on the radial glial apical surface in different regions of the walls of the neonatal LV, as done for ependymal cells in Chapter 4, should help elucidate when and how ependymal planar polarity is established.

Evidence from other multiciliated epithelia suggests that planar polarity is established before multiciliated cell differentiation (Boisvieux-Ulrich and Sandoz, 1991; Tung and Y-F., 1940; Twitty, 1928). For example, in the quail oviduct, if a middle segment of the duct is transected from proximal and distal segments and its orientation reversed before multiciliated cells appear, the cells that differentiate within the middle segment exhibit reversed planar polarity. This indicates that polarity was established before experimental reversal of the segment. Similar experiments may be possible on cultured lateral wall wholemounts from the LV of neonatal mice. The results from Chapter 4, indicating that CSF flow is not required to establish ependymal planar polarity, suggest that neonatal wholemounts in culture would establish normal polarity. However, this would need to be proven first. If cultured wholemounts do acquire normal planar polarity, subsequent experiments reversing the orientation of small segments within the wholemount might provide an experimental paradigm analogous to that used in the quail oviduct. But answering the question of when ependymal planar polarity is established might be better done using techniques

amenable to this particular system. Wholemounts may not be viable for several days in culture. One alternative is to graft dissociated cells acquired from the ventricular zone of *βactin::GFP* mice into the lateral ventricle of recipient wild-type mice. When this is done using E16.5 *βactin::GFP* embryos, a subset of grafted GFP+ cells incorporates into the walls of the lateral ventricle and some differentiate into ependymal cells (data not shown). By performing these grafts into neonatal mice using donor tissue from *βactin::GFP* mice of different embryonic and early postnatal ages, it should be possible to determine when ependymal planar polarity is established. Similar to the analysis of basal body position in Chapter 4, the basal body angles of GFP+ cells could be used as an indicator of their planar polarity, and this can be compared to the basal body angle distribution of the host region where they engraft. One possible result is that donor cells from earlier embryonic ages may be able to orient to match the host epithelium's polarity, while cells from later stages may have already specified orientation, resulting in misalignment of polarity between GFP+ cells and host cells. Alternatively, donor cells with already specified polarity may not be able to engraft into the epithelium. A caveat of this experiment is that dissociating cells disrupts their epithelial nature and may irreversibly alter their behavior. For example, dissociating cells may erase polarity information that requires an intact epithelium. However, if this paradigm does work, it could also be used to test whether different host environments can re-polarize an already polarized cell. For these experiments, polarized donor cells (from an age determined in the first phase of experiments) could be grafted into wild-type LV of

hosts at different embryonic and postnatal ages. The ability to mix donor cells and host epithelium of different ages offers an advantage over the cultured wholemount paradigm. These experiments present an exciting opportunity to unravel the mechanisms of ependymal planar polarity.

In addition to analyzing mechanisms at the cellular and tissue level, an understanding of the molecular determinants of ependymal planar polarity requires further attention. One candidate molecular pathway, which governs epithelial planar polarity in diverse tissues from mammalian cochlea to the Drosophila wing, is the planar cell polarity (PCP) pathway (Wang and Nathans, 2007; Zallen, 2007). This pathway is composed of the "core" components *Flamingo/Celsr*, *Strabismus/Van-gogh like 2 (vangl2)*, *Frizzled*, *Disheveled*, and *Prickle*. Mutations in these "core" PCP pathway genes result in disrupted planar polarity, such as misalignment of stereociliary bundles in cochlear hair cells and misoriented hairs on Drosophila wing cells. Interestingly, preliminary evidence indicates that several "core" PCP pathway genes are expressed in the walls of the lateral ventricle at P0, the time of ependymal differentiation (**Figure 4**). In particular, expression of frizzled-3, which is observed on the medial wall at P0 and on both the medial and lateral wall at P5, is spatiotemporally correlated with ependymal differentiation. At present, it is difficult to test the role of these genes in ependymal planar polarity using knockout mice because they are also required for an earlier process in the neuroepithelium, called convergent extension. Knocking out components of the "core" PCP pathway results in failed convergent extension leading to open neural tube defects (Curtin et al., 2003; Hamblet et al.,

2002; Kibar et al., 2001; Murdoch et al., 2001; Wallingford, 2006; Wang et al., 2006a; Wang et al., 2006b). This precludes analysis of ependymal planar polarity because the mutants die at birth. In addition, there are no published reports of conditional mutants (based on the Cre/loxP system) for these genes. However, there may be an alternative method to testing the function of these genes in ependymal planar polarity: based on the grafting experiments proposed above, it may be possible to use knockout mice for PCP pathway components as embryonic donors of cells for grafting. For these experiments, heterozygous mice (e.g. *Vangl2-/+*) would first be bred onto a *βactin::GFP* background, and then crossed to produce GFP+ KO embryos that could be used in grafting experiments as above. The ability of these GFP+ KO cells to polarize in a host environment could then be compared with grafted GFP+ control cells. A caveat to this approach is that grafted KO cells isolated in an epithelium of wild-type cells may polarize normally if the gene acts non-cell autonomously, or if its function can be otherwise compensated by neighboring wild-type cells. However, short of generating conditional (Cre/loxP) mutants for PCP pathway components, developing the grafting paradigm provides an alternative method to address the mechanisms of ependymal planar polarity.

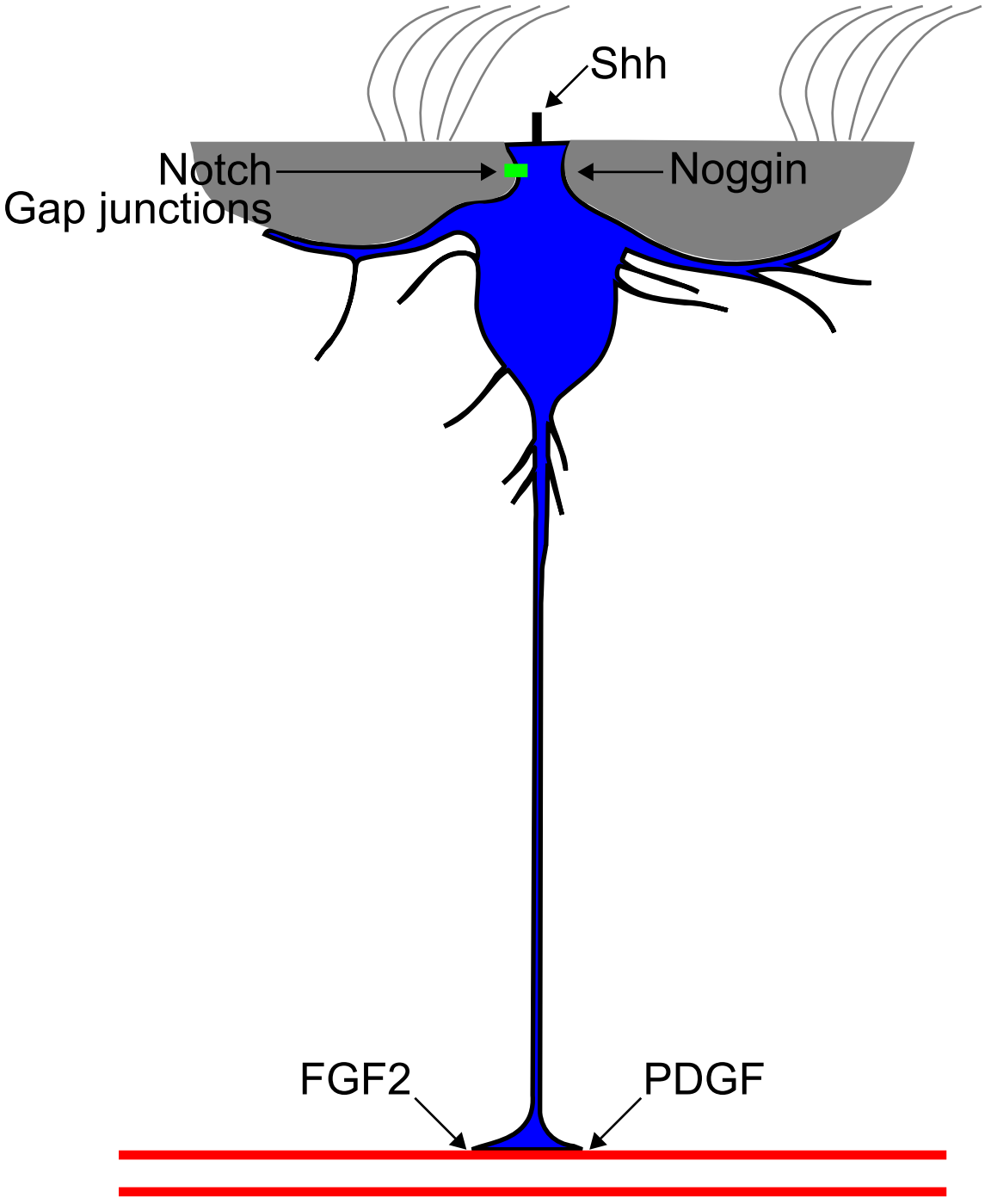


Figure 1. Hypothetical model demonstrating how the elaborate morphology and topological relationships of type B cells (blue) may allow them to integrate spatially segregated regulatory signals. These include basal signals from the vasculature (red) such as FGF2, which was recently shown to be concentrated in blood vessel basal lamina in the SVZ, and PDGF; as well as apical signals including Shh, which may act through the B cell primary cilium, Noggin, known to be secreted by ependymal cells (gray) to promote neurogenesis from B cells, contact-dependent Notch signaling (green), and intercellular gap junction mediated signaling (green).

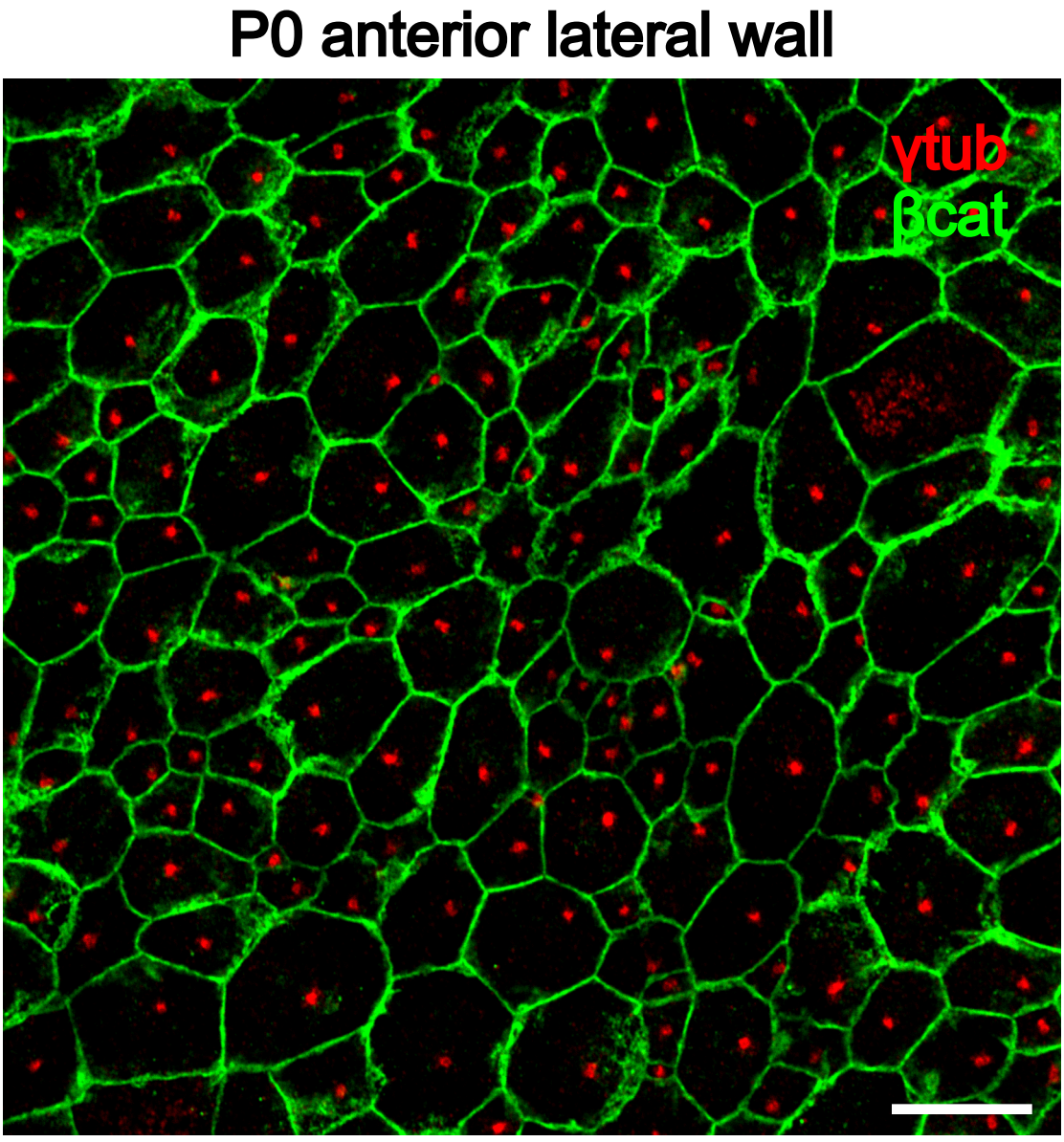


Figure 2. Heterogeneity of radial glial apical surface size on the lateral wall of the LV at P0.

With the exception of a few ependymal cells that have already differentiated (arrowhead), the lateral wall of the neonatal LV is almost exclusively covered by radial glia. However, heterogeneity in apical surface sizesuggests that these radial glia are already transforming into distinct cell types.

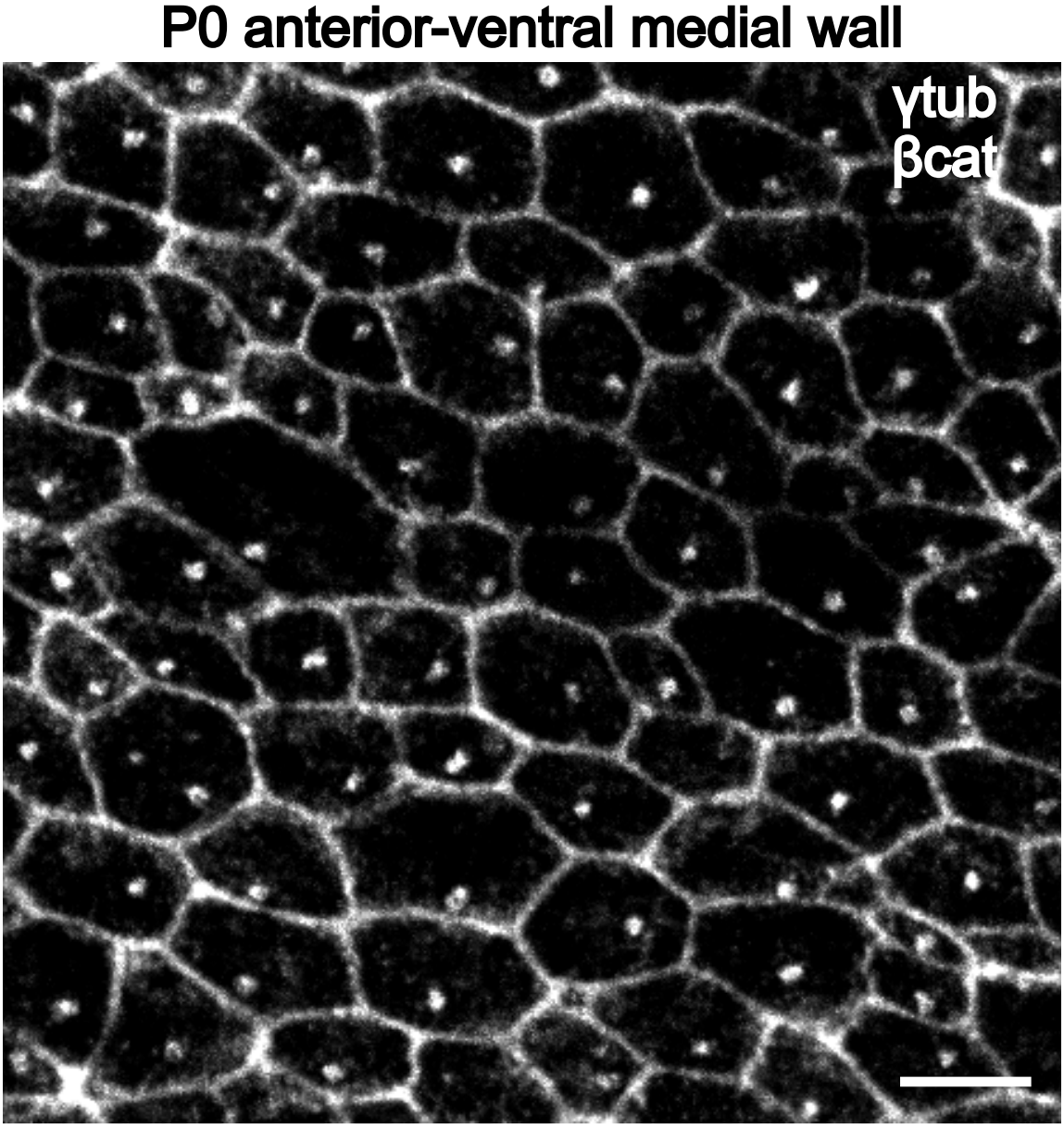


Figure 3. Preliminary evidence that basal bodies of radial glia undergoing ependymal transformationhave a polarized position on the cell's apical surface. This image is a confocal optical section from Region AV of a P0 medial wall wholemount stained for γ-tubulin and β-catenin. Yellow arrow indicates the directionof CSF flow in this region in the adult (see Chapter 4:Figure S2). For comparison, see Chapter 4:Figure 3B, which shows similar staining of this region in the adult. Note that basal body position in many radial glia shown here is predictive of the basal body position of ependymal cells observed in the adult.

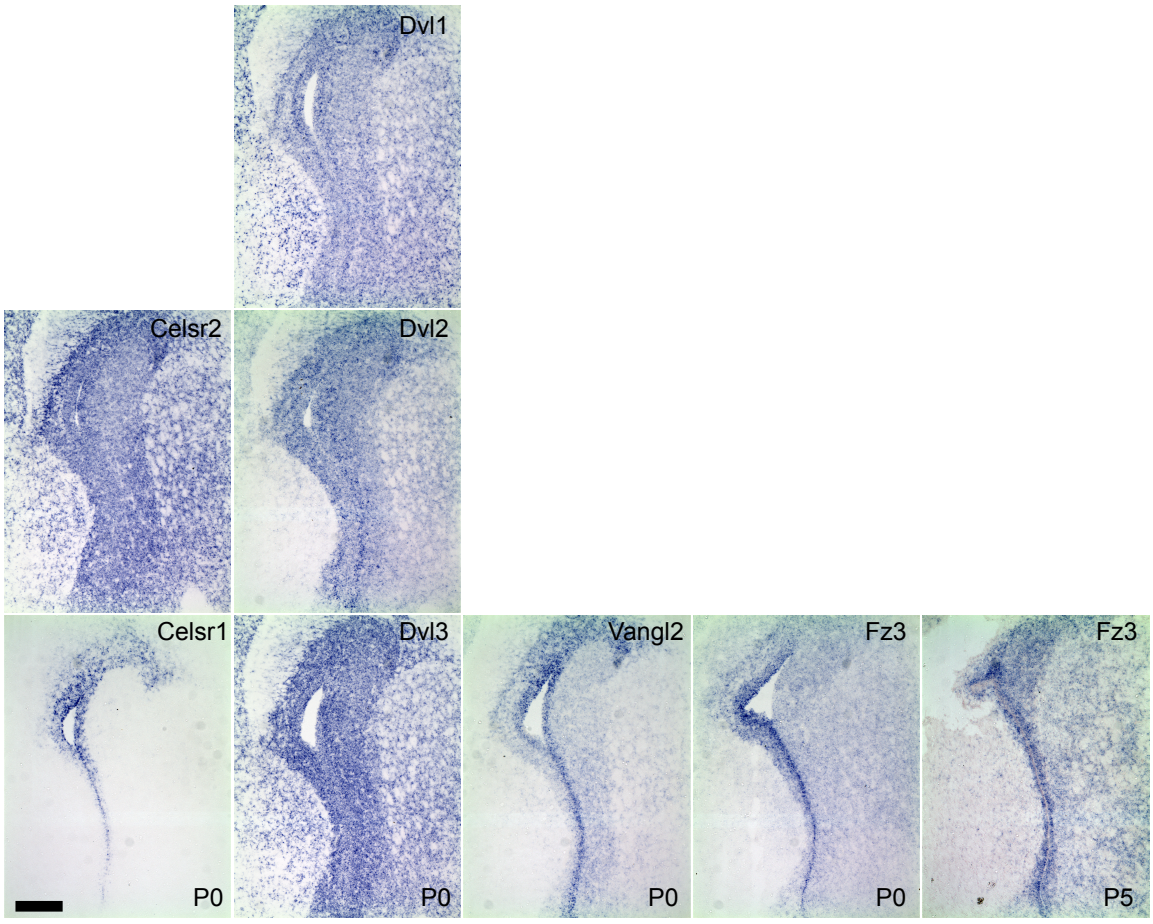


Figure 4. Core PCP genes are expressed in the lateral ventricle walls of neonatal mice.

Several components of the PCP pathway, including Celsr1/2 (Flamingo), Dvl1/2/3, and Vangl2 (Strabismus) are expressed on both the lateral and medial walls of the lateral ventricle at P0. Fz3 expression, which was observed only on the medial wall at P0, but on both walls at P5, is particularly intriguing since it is spatially and temporally correlated with ependymal cell differentiation.

Chapter 7

References

Aaku-Saraste, E., Hellwig, A., and Huttner, W.B. (1996). Loss of occludin and functional tight junctions, but not ZO-1, during neural tube closure--remodeling of the neuroepithelium prior to neurogenesis. Developmental biology *180*, 664-679.

Adachi, K., Mirzadeh, Z., Sakaguchi, M., Yamashita, T., Nikolcheva, T., Gotoh, Y., Peltz, G., Gong, L., Kawase, T., Alvarez-Buylla, A.*, et al.* (2007). Beta-catenin signaling promotes proliferation of progenitor cells in the adult mouse subventricular zone. Stem Cells *25*, 2827-2836.

Afzelius, B.A. (2004). Cilia-related diseases. The Journal of pathology *204*, 470-477.

al-Shroof, M., Karnik, A.M., Karnik, A.A., Longshore, J., Sliman, N.A., and Khan, F.A. (2001). Ciliary dyskinesia associated with hydrocephalus and mental retardation in a Jordanian family. Mayo Clinic proceedings *76*, 1219-1224.

Alberts, B., Bray, D., Lewis, J., Raff, M., Roberts, K., and Watson, J.D. (1994). Molecular Biology of the Cell, 3rd Edition edn (New York: Garland Publishing, Inc.).

Altman, J. (1962). Are new neurons formed in the brains of adult mammals? Science *135*, 1127-1128.

Altman, J. (1963). Autoradiographic investigation of cell proliferation in the brains of rats and cats. Anat.Rec. *145*, 573-591.

Altman, J. (1967). Postnatal growth and differentiation of the mammalian brain, with implications for a morphological theory of memory. In The Neurosciences: first study program, N.R. Program, ed. (New York: Rockefeller University Press), pp. 763-743.

Altman, J. (1969). Autoradiographic and Histological Studies of Postnatal Neurogenesis. IV. Cell Proliferation and Migration in The Anterior Forebrain, With Special Reference to Persisting Neurogenesis in The Olfactory Bulb. J.Comp.Neurol. *137*, 433-458.

Altman, J., and Bayer, S.A. (1990). Mosaic organization of the hippocampal neuroepithelium and the multiple germinal sources of dentate granule cells. J.Comp.Neurol. *301*, 325-342.

Altman, J., and Das, G.D. (1965). Autoradiographic and histological evidence of postnatal hippocampal neurogenesis in rats. J.Comp.Neurol. *124*, 319-336.

Alvarez-Buylla, A., Buskirk, D.R., and Nottebohm, F. (1987). Monoclonal antibody reveals radial glia in adult avian brain. J.Comp.Neurol. *264*, 159-170.

Alvarez-Buylla, A., and Garcia-Verdugo, J.M. (2002). Neurogenesis in adult subventricular zone. J Neurosci *22*, 629-634.

Alvarez-Buylla, A., García-Verdugo, J.M., Mateo, A., and Merchant-Larios, H. (1998). Primary neural precursors and intermitotic nuclear migration in the ventricular zone of adult canaries. J.Neurosci. *18*, 1020-1037.

Alvarez-Buylla, A., and Lim, D.A. (2004). For the long run: maintaining germinal niches in the adult brain. Neuron *41*, 683-686.

Alvarez-Buylla, A., and Nottebohm, F. (1988). Migration of young neurons in adult avian brain. Nature *335*, 353-354.

Alvarez-Buylla, A., Seri, B., and Doetsch, F. (2002). Identification of neural stem cells in the adult vertebrate brain. Brain Res Bull *57*, 751-758.

Alvarez-Buylla, A., Theelen, M., and Nottebohm, F. (1990). Proliferation "hot spots" in adult avian ventricular zone reveal radial cell division. Neuron *5*, 101-109.

Anderson, R.G. (1972). The three-dimensional structure of the basal body from the rhesus monkey oviduct. J Cell Biol *54*, 246-265.

Anthony, T.E., Klein, C., Fishell, G., and Heintz, N. (2004). Radial glia serve as neuronal progenitors in all regions of the central nervous system. Neuron *41*, 881-890.

Axelrod, J.D., Miller, J.R., Shulman, J.M., Moon, R.T., and Perrimon, N. (1998). Differential recruitment of Dishevelled provides signaling specificity in the planar cell polarity and Wingless signaling pathways. Genes & development *12*, 2610-2622.

Banizs, B., Pike, M.M., Millican, C.L., Ferguson, W.B., Komlosi, P., Sheetz, J., Bell, P.D., Schwiebert, E.M., and Yoder, B.K. (2005). Dysfunctional cilia lead to altered ependyma and choroid plexus function, and result in the formation of hydrocephalus. Development *132*, 5329-5339.

Bettencourt-Dias, M., and Glover, D.M. (2007). Centrosome biogenesis and function: centrosomics brings new understanding. Nature reviews *8*, 451-463.

Bisgrove, B.W., and Yost, H.J. (2006). The roles of cilia in developmental disorders and disease. Development *133*, 4131-4143.

Bittman, K., Owens, D.F., Kriegstein, A.R., and LoTurco, J.J. (1997). Cell coupling and uncoupling in the ventricular zone of developing neocortex. J Neurosci *17*, 7037-7044.

Boisvieux-Ulrich, E., Laine, M.C., and Sandoz, D. (1985). The orientation of ciliary basal bodies in quail oviduct is related to the ciliary beating cycle commencement. Biology of the cell / under the auspices of the European Cell Biology Organization *55*, 147-150.

Boisvieux-Ulrich, E., and Sandoz, D. (1991). Determination of ciliary polarity precedes differentiation in the epithelial cells of quail oviduct. Biology of the cell / under the auspices of the European Cell Biology Organization *72*, 3-14.

Bonfanti, L., Peretto, P., Merighi, A., and Fasolo, A. (1997). Newly-generated cells from the rostral migratory stream in the accessory olfactory bulb of the adult rat. Neuroscience *81*, 489-502.

Bornens, M. (2002). Centrosome composition and microtubule anchoring mechanisms. Current opinion in cell biology *14*, 25-34.

Breunig, J.J., Silbereis, J., Vaccarino, F.M., Sestan, N., and Rakic, P. (2007). Notch regulates cell fate and dendrite morphology of newborn neurons in the postnatal dentate gyrus. Proc Natl Acad Sci U S A *104*, 20558-20563.

Bruni, J.E. (1998). Ependymal Development, Proliferation, and Functions: A Review. Microsc.Res.Tech. *41*, 2-13.

Bruni, J.E., Clattenburg, R.E., and Millar, E. (1983). Tanycyte ependymal cells in the third ventricle of young and adult rats: a Golgi study. Anatomischer Anzeiger *153*, 53-68.

Bruni, J.E., Del Bigio, M.R., and Clattenburg, R.E. (1985). Ependyma: Normal and pathological. A review of the literature. Brain Res.Rev. *9*, 1-19.

Calaora, V., Chazal, G., Nielsen, P.J., Rougon, G., and Moreau, H. (1996). mCD24 expression in the developing mouse brain and in zones of secondary neurogenesis in the adult. Neuroscience *73*, 581-594.

Cano, D.A., Murcia, N.S., Pazour, G.J., and Hebrok, M. (2004). Orpk mouse model of polycystic kidney disease reveals essential role of primary cilia in pancreatic tissue organization. Development *131*, 3457-3467.

Capela, A., and Temple, S. (2002). LeX/ssea-1 is expressed by adult mouse CNS stem cells, identifying them as nonependymal. Neuron *35*, 865-875.

Card, J.P., and Rafols, J.A. (1978). Tanycytes of the third ventricle of the neonatal rat: a Golgi study. The American journal of anatomy *151*, 173-189.

Carleton, A., Petreanu, L.T., Lansford, R., Alvarez-Buylla, A., and Lledo, P.M. (2003). Becoming a new neuron in the adult olfactory bulb. Nat Neurosci *6*, 507-518.

Cathcart, R.S., 3rd, and Worthington, W.C., Jr. (1964). Ciliary Movement in the Rat Cerebral Ventricles: Clearing Action and Directions of Currents. J Neuropathol Exp Neurol *23*, 609-618.

Caviness, V.S., Jr., Takahashi, T., and Nowakowski, R.S. (1995). Numbers, time and neocortical neuronogenesis: A general developmental and evolutionary model. Trends Neurosci. *18*, 379-383.

Chen, J., Knowles, H.J., Hebert, J.L., and Hackett, B.P. (1998). Mutation of the mouse hepatocyte nuclear factor/forkhead homologue 4 gene results in an absence of cilia and random left-right asymmetry. The Journal of clinical investigation *102*, 1077-1082.

Chenn, A., Zhang, Y.A., Chang, B.T., and McConnell, S.K. (1998). Intrinsic polarity of mammalian neuroepithelial cells. Molecular and cellular neurosciences *11*, 183-193.

Chiasson, B.J., Tropepe, V., Morshead, C.M., and Van der Kooy, D. (1999). Adult Mammalian Forebrain Ependymal and Subependymal Cells Demonstrate Proliferative Potential, but only Subependymal Cells Have Neural Stem Cell Characteristics. J.Neurosci. *19*, 4462-4471.

Cohen, E., Binet, S., and Meininger, V. (1988). Ciliogenesis and centriole formation in the mouse embryonic nervous system. An ultrastructural analysis. Biology of the cell / under the auspices of the European Cell Biology Organization *62. 62*, 165-169-165-169.

Colas, J.F., and Schoenwolf, G.C. (2001). Towards a cellular and molecular understanding of neurulation. Dev Dyn *221*, 117-145.

Collins, P. (1989). The sulcus medianus organ in the fourth cerebral ventricle of the rabbit: a previously undescribed circumventricular organ. Journal of anatomy *162*, 185-193.

Committee, T.B. (1970). Embryonic Vertebrate Central Nervous System: Revised Terminology. Anat.Rec. *166*, 257-262.

Conover, J.C., Doetsch, F., Garcia-Verdugo, J.M., Gale, N.W., Yancopoulos, G.D., and Alvarez-Buylla, A. (2000). Disruption of Eph/ephrin signaling affects migration and proliferation in the adult subventricular zone. Nat Neurosci *3*, 1091-1097.

Copp, A.J., Greene, N.D., and Murdoch, J.N. (2003). Dishevelled: linking convergent extension with neural tube closure. Trends in neurosciences *26*, 453-455.

Corbit, K.C., Aanstad, P., Singla, V., Norman, A.R., Stainier, D.Y., and Reiter, J.F. (2005). Vertebrate Smoothened functions at the primary cilium. Nature *437*, 1018-1021.

Corbit, K.C., Shyer, A.E., Dowdle, W.E., Gaulden, J., Singla, V., and Reiter, J.F. (2008). Kif3a constrains beta-catenin-dependent Wnt signalling through dual ciliary and non-ciliary mechanisms. Nature cell biology *10*, 70-76.

Cummings, J.P., and Felten, D.L. (1979). A raphe dendrite bundle in the rabbit medulla. J.Comp.Neurol. *183*, 1-24.

Curtin, J.A., Quint, E., Tsipouri, V., Arkell, R.M., Cattanach, B., Copp, A.J., Henderson, D.J., Spurr, N., Stanier, P., Fisher, E.M.*, et al.* (2003). Mutation of Celsr1 disrupts planar polarity of inner ear hair cells and causes severe neural tube defects in the mouse. Curr Biol *13*, 1129-1133.

Davy, B.E., and Robinson, M.L. (2003). Congenital hydrocephalus in hy3 mice is caused by a frameshift mutation in Hydin, a large novel gene. Human molecular genetics *12*, 1163-1170.

Dawe, H.R., Farr, H., and Gull, K. (2007). Centriole/basal body morphogenesis and migration during ciliogenesis in animal cells. J Cell Sci *120*, 7-15.

Del Bigio, M.R. (1995). The ependyma: A protective barrier between brain and cerebrospinal fluid. Glia *14*, 1-13.

Del Brio, M.A., Riera, P., García, J.M., and Alvarez-Uría, M. (1991). Cell types of the third ventricle wall of the rabbit (*Oryctolagus cuniculus*). J.Submicrosc.Cytol.Pathol. *23*, 147-157.

Dirksen, E.R. (1971). Centriole morphogenesis in developing ciliated epithelium of the mouse oviduct. J Cell Biol *51*, 286-302.

Doetsch, F., and Alvarez-Buylla, A. (1996). Network of tangential pathways for neuronal migration in adult mammalian brain. Proc.Natl.Acad.Sci.USA *93*, 14895-14900.

Doetsch, F., Caille, I., Lim, D.A., García-Verdugo, J.M., and Alvarez-Buylla, A. (1999a). Subventricular Zone Astrocytes Are Neural Stem Cells in the Adult mammalian Brain. Cell *97*, 1-20.

Doetsch, F., Garcia-Verdugo, J.M., and Alvarez-Buylla, A. (1997). Cellular composition and three-dimensional organization of the subventricular germinal zone in the adult mammalian brain. J.Neurosci. *17*, 5046-5061.

Doetsch, F., Garcia-Verdugo, J.M., and Alvarez-Buylla, A. (1999b). Regeneration of a germinal layer in the adult mammalian brain. Proc.Natl.Acad.Sci.USA *96*, 11619-11624.

Doetsch, F., Petreanu, L., Caille, I., Garcia-Verdugo, J.M., and Alvarez-Buylla, A. (2002). EGF converts transit-amplifying neurogenic precursors in the adult brain into multipotent stem cells. Neuron *36*, 1021-1034.

du Manoir, S., Guillaud, P., Camus, E., Seigneurin, D., and Brugal, G. (1991). Ki-67 labeling in postmitotic cells defines different Ki-67 pathways within the 2c compartment. Cytometry *12*, 455-463.

Dubreuil, V., Marzesco, A.M., Corbeil, D., Huttner, W.B., and Wilsch-Brauninger, M. (2007). Midbody and primary cilium of neural progenitors release extracellular membrane particles enriched in the stem cell marker prominin-1. J Cell Biol *176*, 483-495.

Eggenschwiler, J.T., and Anderson, K.V. (2007). Cilia and developmental signaling. Annual review of cell and developmental biology *23*, 345-373.

Eves, E.M., Tucker, M.S., Roback, J.D., Downen, M., Rosner, M.R., and Wainer, B.H. (1992). Immortal rat hippocampal cell lines exhibit neuronal and glial lineages and neurotrophin gene expression. Proc.Natl.Acad.Sci.USA *89*, 4373-4377.

Feng, L., and Heintz, N. (1995). Differentiating neurons activate transcription of the brain lipid-binding protein gene in radial glia through a novel regulatory element. Development *121*, 1719-1730.

Flament-Durand, J., and Brion, J.P. (1985). Tanycytes:Morphology and Functions: A review. International Review of Cytology *96*, 121-155.

Frederiksen, K., and McKay, R.D.G. (1988). Proliferation and differentiation of rat neuroepithelial precursor cells in vivo. J.Neurosci. *8*, 1144-1151.

Gabay, L., Lowell, S., Rubin, L.L., and Anderson, D.J. (2003). Deregulation of dorsoventral patterning by FGF confers trilineage differentiation capacity on CNS stem cells in vitro. Neuron *40*, 485-499.

Gadisseux, J.F., and Evrard, P. (1985). Glial neuronal relationship in the developing central nervous system. Dev.Neurosci. *7*, 12-32.

Gage, F.H. (2000). Mammalian neural stem cells. Science *287*, 1433-1438.

Garcia-Verdugo, J.M., Ferron, S., Flames, N., Collado, L., Desfilis, E., and Font, E. (2002). The proliferative ventricular zone in adult vertebrates: a comparative study using reptiles, birds, and mammals. Brain Res Bull *57*, 765-775.

Garcia, A.D., Doan, N.B., Imura, T., Bush, T.G., and Sofroniew, M.V. (2004). GFAP-expressing progenitors are the principal source of constitutive neurogenesis in adult mouse forebrain. Nat Neurosci *7*, 1233-1241.

Gerdes, J.M., Liu, Y., Zaghloul, N.A., Leitch, C.C., Lawson, S.S., Kato, M., Beachy, P.A., Beales, P.L., Demartino, G.N., Fisher, S.*, et al.* (2007). Disruption of the basal body compromises proteasomal function and perturbs intracellular Wnt response. Nat Genet *39*, 1350-1360.

Geschwind, D.H., Ou, J., Easterday, M.C., Dougherty, J.D., Jackson, R.L., Chen, Z., Antoine, H., Terskikh, A., Weissman, I.L., Nelson, S.F., and Kornblum, H.I. (2001). A genetic analysis of neural progenitor differentiation. Neuron *29*, 325-339.

Ghashghaei, H.T., Weimer, J.M., Schmid, R.S., Yokota, Y., McCarthy, K.D., Popko, B., and Anton, E.S. (2007). Reinduction of ErbB2 in astrocytes promotes radial glial progenitor identity in adult cerebral cortex. Genes & development *21*, 3258-3271.

Gibbons, I.R., and Rowe, A.J. (1965). Dynein: a protein with adenosine triphosphatase activity from cilia. Science *149*, 424-426.

Givogri, M.I., de Planell, M., Galbiati, F., Superchi, D., Gritti, A., Vescovi, A., de Vellis, J., and Bongarzone, E.R. (2006). Notch signaling in astrocytes and neuroblasts of the adult subventricular zone in health and after cortical injury. Dev Neurosci *28*, 81-91.

Gonzalez-Santander, R. (1979). Electron-microscopic study of the secretion of the ependymal cells in the domestic cat (ependymin-beta cells). Acta anatomica *103*, 266-277.

Gotz, M., and Huttner, W.B. (2005). The cell biology of neurogenesis. Nature reviews *6*, 777-788.

Gray, G.E., and Sanes, J.R. (1992). Lineage of radial glia in the chicken optic tectum. Development *114*, 271-283.

Greene, N.D., Gerrelli, D., Van Straaten, H.W., and Copp, A.J. (1998). Abnormalities of floor plate, notochord and somite differentiation in the loop-tail (Lp) mouse: a model of severe neural tube defects. Mechanisms of development *73*, 59-72.

Gritti, A., Bonfanti, L., Doetsch, F., Caille, I., Alvarez-Buylla, A., Lim, D.A., Galli, R., Verdugo, J.M., Herrera, D.G., and Vescovi, A.L. (2002). Multipotent neural stem cells reside into the rostral extension and olfactory bulb of adult rodents. J Neurosci *22*, 437-445.

Hack, M.A., Saghatelyan, A., de Chevigny, A., Pfeifer, A., Ashery-Padan, R., Lledo, P.M., and Gotz, M. (2005). Neuronal fate determinants of adult olfactory bulb neurogenesis. Nat Neurosci.

Halfter, W., Dong, S., Yip, Y.P., Willem, M., and Mayer, U. (2002). A critical function of the pial basement membrane in cortical histogenesis. J Neurosci *22*, 6029-6040.

Hamblet, N.S., Lijam, N., Ruiz-Lozano, P., Wang, J., Yang, Y., Luo, Z., Mei, L., Chien, K.R., Sussman, D.J., and Wynshaw-Boris, A. (2002). Dishevelled 2 is essential for cardiac outflow tract development, somite segmentation and neural tube closure. Development *129*, 5827-5838.

Han, Y.G., Spassky, N., Romaguera-Ros, M., Garcia-Verdugo, J.M., Aguilar, A., Schneider-Maunoury, S., and Alvarez-Buylla, A. (2008). Hedgehog signaling and primary cilia are required for the formation of adult neural stem cells. Nat Neurosci *11*, 277-284.

Hatta, K., Takagi, S., Fujisawa, H., and Takeichi, M. (1987). Spatial and temporal expression pattern of N-cadherin cell adhesion molecules correlated with morphogenetic processes of chicken embryos. Developmental biology *120*, 215-227.

Hatten, M.E. (1999). Central nervous system neuronal migration. [Review] [124 refs]. Annual Review of Neuroscience *22*, 511-539.

Haubensak, W., Attardo, A., Denk, W., and Huttner, W.B. (2004). Neurons arise in the basal neuroepithelium of the early mammalian telencephalon: a major site of neurogenesis. Proc Natl Acad Sci U S A *101*, 3196-3201.

Haubst, N., Georges-Labouesse, E., De Arcangelis, A., Mayer, U., and Gotz, M. (2006). Basement membrane attachment is dispensable for radial glial cell fate and for proliferation, but affects positioning of neuronal subtypes. Development *133*, 3245-3254.

Haycraft, C.J., Banizs, B., Aydin-Son, Y., Zhang, Q., Michaud, E.J., and Yoder, B.K. (2005). Gli2 and Gli3 localize to cilia and require the intraflagellar transport protein polaris for processing and function. PLoS Genet *1*, e53.

Hockfield, S., and McKay, R.D.G. (1985). Identification of major cell classes in the developing mammalian nervous system. J.Neurosci. *5, no. l2*, 3310-3328.

Horstmann, E. (1954). Die Faserglia des Selachiergehirns. Z.Zellforsch. *39*, 588-617.

Huangfu, D., and Anderson, K.V. (2005). Cilia and Hedgehog responsiveness in the mouse. Proc Natl Acad Sci U S A *102*, 11325-11330.

Huangfu, D., Liu, A., Rakeman, A.S., Murcia, N.S., Niswander, L., and Anderson, K.V. (2003). Hedgehog signalling in the mouse requires intraflagellar transport proteins. Nature *426*, 83-87.

Huttner, W.B., and Brand, M. (1997). Asymmetric division and polarity of neuroepithelial cells. Curr.Opin.Neurobiol. *7*, 29-39.

Huttner, W.B., and Kosodo, Y. (2005). Symmetric versus asymmetric cell division during neurogenesis in the developing vertebrate central nervous system. Current opinion in cell biology *17*, 648-657.

Ibanez-Tallon, I., Gorokhova, S., and Heintz, N. (2002). Loss of function of axonemal dynein Mdnah5 causes primary ciliary dyskinesia and hydrocephalus. Human molecular genetics *11*, 715-721.

Ibanez-Tallon, I., Pagenstecher, A., Fliegauf, M., Olbrich, H., Kispert, A., Ketelsen, U.P., North, A., Heintz, N., and Omran, H. (2004). Dysfunction of axonemal dynein heavy chain Mdnah5 inhibits ependymal flow and reveals a novel mechanism for hydrocephalus formation. Human molecular genetics *13*, 2133-2141.

Ikeda, W., Nakanishi, H., Miyoshi, J., Mandai, K., Ishizaki, H., Tanaka, M., Togawa, A., Takahashi, K., Nishioka, H., Yoshida, H.*, et al.* (1999). Afadin: A key molecule essential for structural organization of cell-cell junctions of polarized epithelia during embryogenesis. J Cell Biol *146*, 1117-1132.

Imura, T., Kornblum, H.I., and Sofroniew, M.V. (2003). The Predominant Neural Stem Cell Isolated from Postnatal and Adult Forebrain But Not Early Embryonic Forebrain Expresses GFAP. J Neurosci *23*, 2824-2832.

Jabourian, Z., Lublin, F.D., Adler, A., Gonzales, C., Northrup, B., and Zwillenberg, D. (1986). Hydrocephalus in Kartagener's syndrome. Ear, nose, & throat journal *65*, 468-472.

Jackson, E.L., Garcia-Verdugo, J.M., Gil-Perotin, S., Roy, M., Quinones-Hinojosa, A., Vandenberg, S., and Alvarez-Buylla, A. (2006). PDGFRalpha-Positive B Cells Are Neural Stem Cells in the Adult SVZ that Form Glioma-like Growths in Response to Increased PDGF Signaling. Neuron *51*, 187-199.

Jankovski, A., and Sotelo, C. (1996). Subventricular zone-olfactory bulb migratory pathway in the adult mouse: Cellular composition and specificity as determined by heterochronic and heterotopic transplantation. J.Comp.Neurol. *371*, 376-396.

Jiang, J., McMurtry, J., Niedzwiecki, D., and Goldman, S.A. (1998). Insulin-like growth factor-1 is a radial cell-associated neurotrophin that promotes neuronal recruitment from the adult songbird ependyma/subependyma. Journal of Neurobiology *36*, 1-15.

Johansson, C.B., Momma, S., Clarke, D.L., Risling, M., Lendahl, U., and Frisén, J. (1999). Identification of a Neural Stem Cell in the Adult Mammalian Central Nervous System. Cell *96*, 25-34.

Jones, C., Roper, V.C., Foucher, I., Qian, D., Banizs, B., Petit, C., Yoder, B.K., and Chen, P. (2008). Ciliary proteins link basal body polarization to planar cell polarity regulation. Nat Genet *40*, 69-77.

Jordan, F., Rieke, G., and Thomas, W. (1987). Presence and development of ependymal cells in primary tissue cultures derived from embryonic rat cerebral cortex. Brain Research *432*, 97-110.

Kaplan, M.S., and Bell, D.H. (1983). Neuronal proliferation in the 9-month-old rodent-radioautographic study of granule cells in the hippocampus. Exp. Brain Res. *52*, 1.

Kaplan, M.S., and Hinds, J.W. (1977). Neurogenesis in the adult rat: Electron microscopic analysis of light radioautographs. Science *197*, 1092-1094.

Kelsch, W., Mosley, C.P., Lin, C.W., and Lois, C. (2007). Distinct mammalian precursors are committed to generate neurons with defined dendritic projection patterns. PLoS biology *5*, e300.

Kerever, A., Schnack, J., Vellinga, D., Ichikawa, N., Moon, C., Arikawa-Hirasawa, E., Efird, J.T., and Mercier, F. (2007). Novel extracellular matrix structures in the neural stem cell niche capture the neurogenic factor fibroblast growth factor 2 from the extracellular milieu. Stem Cells *25*, 2146-2157.

Kibar, Z., Vogan, K.J., Groulx, N., Justice, M.J., Underhill, D.A., and Gros, P. (2001). Ltap, a mammalian homolog of Drosophila Strabismus/Van Gogh, is altered in the mouse neural tube mutant Loop-tail. Nat Genet *28*, 251-255.

Knowles, F. (1972). Ependyma of the third ventricle in relation to pituitary function. Progress in brain research *38*, 255-270.

Koh, L., Zakharov, A., and Johnston, M. (2005). Integration of the subarachnoid space and lymphatics: is it time to embrace a new concept of cerebrospinal fluid absorption? Cerebrospinal fluid research *2*, 6.

Kohwi, M., Osumi, N., Rubenstein, J.L., and Alvarez-Buylla, A. (2005). Pax6 is required for making specific subpopulations of granule and periglomerular neurons in the olfactory bulb. J Neurosci *25*, 6997-7003.

Kohwi, M., Petryniak, M.A., Long, J.E., Ekker, M., Obata, K., Yanagawa, Y., Rubenstein, J.L., and Alvarez-Buylla, A. (2007). A subpopulation of olfactory bulb GABAergic interneurons is derived from Emx1- and Dlx5/6-expressing progenitors. J Neurosci *27*, 6878-6891.

Kosodo, Y., Roper, K., Haubensak, W., Marzesco, A.M., Corbeil, D., and Huttner, W.B. (2004). Asymmetric distribution of the apical plasma membrane during neurogenic divisions of mammalian neuroepithelial cells. Embo J *23*, 2314-2324.

Kozminski, K.G., Beech, P.L., and Rosenbaum, J.L. (1995). The Chlamydomonas kinesin-like protein FLA10 is involved in motility associated with the flagellar membrane. J Cell Biol *131*, 1517-1527.

Kuchler, S., Graff, M.N., Gobaille, S., Vincendon, G., Roche, A.C., Delaunoy, J.P., Monsigny, M., and Zanetta, J.P. (1994). Mannose dependent tightening of the rat ependymal cell barrier. In vivo and in vitro study using neoglycoproteins. Neurochemistry international *24*, 43-55.

Kuhn, H.G., Winkler, J., Kempermann, G., Thal, L.J., and Gage, F.H. (1997). Epidermal growth factor and fibroblast growth factor-2 have different effects on neural progenitors in the adult rat brain. J.Neurosci. *17*, 5820-5829.

Kuo, C.T., Mirzadeh, Z., Soriano-Navarro, M., Rasin, M., Wang, D., Shen, J., Sestan, N., Garcia-Verdugo, J., Alvarez-Buylla, A., Jan, L.Y., and Jan, Y.N. (2006). Postnatal deletion of Numb/Numblike reveals repair and remodeling capacity in the subventricular neurogenic niche. Cell *127*, 1253-1264.

Laywell, E.D., Rakic, P., Kukekov, V.G., Holland, E.C., and Steindler, D.A. (2000). Identification of a multipotent astrocytic stem cell in the immature and adult mouse brain. Proc Natl Acad Sci U S A *97*, 13883-13888.

Lechler, T., and Fuchs, E. (2005). Asymmetric cell divisions promote stratification and differentiation of mammalian skin. Nature *437*, 275-280.

Leonhardt, H. (1980). Neuroglia. I. Handbuch der mikroskopischen Anatomie des Menschen. (Berlin, Heidelberg: Springer Verlag).

Levitt, P., and Rakic, P. (1980). Immunoperoxidase localization of glial fibrillary acidic protein in radial glial cells and astrocytes of the developing rhesus monkey brain. J.Comp.Neurol. *193*, 815-840.

Lewandoski, M., Meyers, E.N., and Martin, G.R. (1997). Analysis of Fgf8 gene function in vertebrate development. Cold Spring Harb Symp Quant Biol *62*, 159-168.

Lim, D.A., and Alvarez-Buylla, A. (1999). Interaction between astrocytes and adult subventricular zone precursors stimulates neurogenesis. Proc Natl Acad Sci U S A *96. 96*, 7526-7531.

Lim, D.A., Tramontin, A.D., Trevejo, J.M., Herrera, D.G., Garcia-Verdugo, J.M., and Alvarez-Buylla, A. (2000). Noggin antagonizes BMP signaling to create a niche for adult neurogenesis. Neuron *28*, 713-726.

Lin, F., Hiesberger, T., Cordes, K., Sinclair, A.M., Goldstein, L.S., Somlo, S., and Igarashi, P. (2003). Kidney-specific inactivation of the KIF3A subunit of kinesin-II inhibits renal ciliogenesis and produces polycystic kidney disease. Proc Natl Acad Sci U S A *100*, 5286-5291.

Lindemann, C.B. (2004). Testing the geometric clutch hypothesis. Biology of the cell / under the auspices of the European Cell Biology Organization *96*, 681-690.

Liu, A., Wang, B., and Niswander, L.A. (2005). Mouse intraflagellar transport proteins regulate both the activator and repressor functions of Gli transcription factors. Development *132*, 3103-3111.

Liu, Z., and Martin, L.J. (2003). Olfactory bulb core is a rich source of neural progenitor and stem cells in adult rodent and human. The Journal of comparative neurology *459*, 368-391.

Logan, C.Y., and Nusse, R. (2004). The Wnt signaling pathway in development and disease. Annual review of cell and developmental biology *20*, 781-810.

Lois, C., and Alvarez-Buylla, A. (1993). Proliferating subventricular zone cells in the adult mammalian forebrain can differentiate into neurons and glia. Proc.Natl.Acad.Sci.USA *90*, 2074-2077.

Lois, C., and Alvarez-Buylla, A. (1994). Long-distance neuronal migration in the adult mammalian brain. Science *264*, 1145-1148.

Lois, C., Garcia-Verdugo, J.M., and Alvarez-Buylla, A. (1996). Chain migration of neuronal precursors. Science *271*, 978-981.

Lu, B., Roegiers, F., Jan, L.Y., and Jan, Y.N. (2001). Adherens junctions inhibit asymmetric division in the Drosophila epithelium. Nature *409*, 522-525.

Luskin, M.B. (1993). Restricted proliferation and migration of postnatally generated neurons derived from the forebrain subventricular zone. Neuron *11*, 173-189.

Machold, R., Hayashi, S., Rutlin, M., Muzumdar, M.D., Nery, S., Corbin, J.G., Gritli-Linde, A., Dellovade, T., Porter, J.A., Rubin, L.L.*, et al.* (2003). Sonic hedgehog is required for progenitor cell maintenance in telencephalic stem cell niches. Neuron *39*, 937-950.

Malatesta, P., Hack, M.A., Hartfuss, E., Kettenmann, H., Klinkert, W., Kirchhoff, F., and Gotz, M. (2003). Neuronal or glial progeny: regional differences in radial glia fate. Neuron *37*, 751-764.

Malatesta, P., Hartfuss, E., and Gotz, M. (2000). Isolation of radial glial cells by fluorescent-activated cell sorting reveals a neuronal lineage. Development *127. 127*, 5253-5263-5253-5263.

Manabe, N., Hirai, S., Imai, F., Nakanishi, H., Takai, Y., and Ohno, S. (2002). Association of ASIP/mPAR-3 with adherens junctions of mouse neuroepithelial cells. Dev Dyn *225*, 61-69.

Marshall, W.F. (2008). The cell biological basis of ciliary disease. J Cell Biol *180*, 17-21.

Marshall, W.F., and Kintner, C. (2008). Cilia orientation and the fluid mechanics of development. Current opinion in cell biology *20*, 48-52.

Marshall, W.F., and Rosenbaum, J.L. (2001). Intraflagellar transport balances continuous turnover of outer doublet microtubules: implications for flagellar length control. J Cell Biol *155*, 405-414.

Marszalek, J.R., Liu, X., Roberts, E.A., Chui, D., Marth, J.D., Williams, D.S., and Goldstein, L.S. (2000). Genetic evidence for selective transport of opsin and arrestin by kinesin-II in mammalian photoreceptors. Cell *102*, 175-187.

Marszalek, J.R., Ruiz-Lozano, P., Roberts, E., Chien, K.R., and Goldstein, L.S. (1999). Situs inversus and embryonic ciliary morphogenesis defects in mouse mutants lacking the KIF3A subunit of kinesin-II. Proc Natl Acad Sci U S A *96*, 5043-5048.

Martin-Belmonte, F., and Mostov, K. (2008). Regulation of cell polarity during epithelial morphogenesis. Current opinion in cell biology.

May, S.R., Ashique, A.M., Karlen, M., Wang, B., Shen, Y., Zarbalis, K., Reiter, J., Ericson, J., and Peterson, A.S. (2005). Loss of the retrograde motor for IFT disrupts localization of Smo to cilia and prevents the expression of both activator and repressor functions of Gli. Developmental biology *287*, 378-389.

Menco, B.P., and Farbman, A.I. (1985). Genesis of cilia and microvilli of rat nasal epithelia during pre-natal development. I. Olfactory epithelium, qualitative studies. J Cell Sci *78*, 283-310.

Menn, B., Garcia-Verdugo, J.M., Yaschine, C., Gonzalez-Perez, O., Rowitch, D., and Alvarez-Buylla, A. (2006). Origin of oligodendrocytes in the subventricular zone of the adult brain. J Neurosci *26*, 7907-7918.

Mercier, F., Kitasako, J.T., and Hatton, G.I. (2002). Anatomy of the brain neurogenic zones revisited: fractones and the fibroblast/macrophage network. The Journal of comparative neurology *451*, 170-188.

Merkle, F.T., Mirzadeh, Z., and Alvarez-Buylla, A. (2007). Mosaic organization of neural stem cells in the adult brain. Science *317*, 381-384.

Merkle, F.T., Tramontin, A.D., Garcia-Verdugo, J.M., and Alvarez-Buylla, A. (2004). Radial glia give rise to adult neural stem cells in the subventricular zone. Proc Natl Acad Sci U S A *101*, 17528-17532.

Millhouse, O.E. (1971). A Golgi study of third ventricle tanycytes in the adult rodent brain. Z.Zellforsch. *121*, 1-13.

Millhouse, O.E. (1975). Lining of the third ventricle in the rat. In Brain Endocrine Interaction. II. The ventricular system (Basel, Karger), pp. 3-18.

Misson, J.P., Edwards, M.A., Yamamoto, M., and Caviness Jr., V.S. (1988). Mitotic cycling of radial glial cells of the fetal murine cerebral wall: a combined autoradiographic and immunohistochemical study. Dev.Brain Res. *38*, 183-190.

Mitchell, B., Jacobs, R., Li, J., Chien, S., and Kintner, C. (2007). A positive feedback mechanism governs the polarity and motion of motile cilia. Nature *447*, 97-101.

Mitro, A., and Palkovits, M. (1981). Morphology of the rat brain ventricles, ependyma, and periventricular structures (Basel: Bibliotheca Anatomica, No.21. S.Karger.).

Miyata, T., Kawaguchi, A., Okano, H., and Ogawa, M. (2001). Asymmetric inheritance of radial glial fibers by cortical neurons. Neuron *31*, 727-741.

Morshead, C.M., Reynolds, B.A., Craig, C.G., McBurney, M.W., Staines, W.A., Morassutti, D., Weiss, S., and van der Kooy, D. (1994). Neural stem cells in the adult mammalian forebrain: a relatively quiescent subpopulation of subependymal cells. Neuron *13*, 1071-1082.

Morshead, C.M., and van der Kooy, D. (2004). Disguising adult neural stem cells. Current opinion in neurobiology *14*, 125-131.

Munro, E.M. (2006). PAR proteins and the cytoskeleton: a marriage of equals. Current opinion in cell biology *18*, 86-94.

Murdoch, J.N., Doudney, K., Paternotte, C., Copp, A.J., and Stanier, P. (2001). Severe neural tube defects in the loop-tail mouse result from mutation of Lpp1, a novel gene involved in floor plate specification. Human molecular genetics *10*, 2593-2601.

Murdoch, J.N., Henderson, D.J., Doudney, K., Gaston-Massuet, C., Phillips, H.M., Paternotte, C., Arkell, R., Stanier, P., and Copp, A.J. (2003). Disruption of scribble (Scrb1) causes severe neural tube defects in the circletail mouse. Human molecular genetics *12*, 87-98.

Nadarajah, B., Jones, A.M., Evans, W.H., and Parnavelas, J.G. (1997). Differential expression of connexins during neocortical development and neuronal circuit formation. J Neurosci *17*, 3096-3111.

Nakamura, Y., and Sato, K. (1993). Role of disturbance of ependymal ciliary movement in development of hydrocephalus in rats. Childs Nerv Syst *9*, 65-71.

Noctor, S.C., Flint, A.C., Weissman, T.A., Dammerman, R.S., and Kriegstein, A.R. (2001). Neurons derived from radial glial cells establish radial units in neocortex. Nature *409*, 714-720.

Noctor, S.C., Martinez-Cerdeno, V., Ivic, L., and Kriegstein, A.R. (2004). Cortical neurons arise in symmetric and asymmetric division zones and migrate through specific phases. Nat Neurosci *7*, 136-144.

Noctor, S.C., Martinez-Cerdeno, V., and Kriegstein, A.R. (2007). Contribution of intermediate progenitor cells to cortical histogenesis. Arch Neurol *64*, 639-642.

Noctor, S.C., Martinez-Cerdeno, V., and Kriegstein, A.R. (2008). Distinct behaviors of neural stem and progenitor cells underlie cortical neurogenesis. The Journal of comparative neurology *508*, 28-44.

Nonaka, S., Tanaka, Y., Okada, Y., Takeda, S., Harada, A., Kanai, Y., Kido, M., and Hirokawa, N. (1998). Randomization of Left-Right Asymmetry due to Loss of Nodal Cilia Generating Leftward Flow of Extraembryonic Fluid in Mice Lacking KIF3B Motor Protein. Cell *95*, 829-837.

Nottebohm, F. (2004). The road we travelled: discovery, choreography, and significance of brain replaceable neurons. Ann. N.Y. Acad. Sci. *1016*, 628.

Novak, A., Guo, C., Yang, W., Nagy, A., and Lobe, C.G. (2000). Z/EG, a double reporter mouse line that expresses enhanced green fluorescent protein upon Cre-mediated excision. Genesis *28*, 147-155.

Nyfeler, Y., Kirch, R.D., Mantei, N., Leone, D.P., Radtke, F., Suter, U., and Taylor, V. (2005). Jagged1 signals in the postnatal subventricular zone are required for neural stem cell self-renewal. Embo J *24*, 3504-3515.

Ooshio, T., Fujita, N., Yamada, A., Sato, T., Kitagawa, Y., Okamoto, R., Nakata, S., Miki, A., Irie, K., and Takai, Y. (2007). Cooperative roles of Par-3 and afadin in the formation of adherens and tight junctions. J Cell Sci *120*, 2352-2365.

Ou, Y., Zhang, M., and Rattner, J.B. (2004). The centrosome: The centriole-PCM coalition. Cell Motil Cytoskeleton *57*, 1-7.

Palma, V., Lim, D.A., Dahmane, N., Sanchez, P., Brionne, T.C., Herzberg, C.D., Gitton, Y., Carleton, A., Alvarez-Buylla, A., and Ruiz i Altaba, A. (2005). Sonic

hedgehog controls stem cell behavior in the postnatal and adult brain. Development *132*, 335-344.

Palmer, T.D., Willhoite, A.R., and Gage, F.H. (2000). Vascular Niche for Adult Hippocampal Neurogenesis. Journal of Comparative Neurology *425*, 479-494.

Park, T.J., Haigo, S.L., and Wallingford, J.B. (2006). Ciliogenesis defects in embryos lacking inturned or fuzzy function are associated with failure of planar cell polarity and Hedgehog signaling. Nat Genet *38*, 303-311.

Parras, C.M., Galli, R., Britz, O., Soares, S., Galichet, C., Battiste, J., Johnson, J.E., Nakafuku, M., Vescovi, A., and Guillemot, F. (2004). Mash1 specifies neurons and oligodendrocytes in the postnatal brain. Embo J *23*, 4495-4505.

Paton, J.A., and Nottebohm, F. (1984). Neurons generated in the adult brain are recruited into functional circuits. Science *225*, 1046-1048.

Pazour, G.J., Wilkerson, C.G., and Witman, G.B. (1998). A dynein light chain is essential for the retrograde particle movement of intraflagellar transport (IFT). J Cell Biol *141*, 979-992.

Pencea, V., Bingaman, K.D., Freedman, L.J., and Luskin, M.B. (2001). Neurogenesis in the subventricular zone and rostral migratory stream of the neonatal and adult primate forebrain. Exp Neurol *172*, 1-16.

Peretto, P., Giachino, C., Aimar, P., Fasolo, A., and Bonfanti, L. (2005). Chain formation and glial tube assembly in the shift from neonatal to adult subventricular zone of the rodent forebrain. The Journal of comparative neurology *487*, 407-427.

Peretto, P., Merighi, A., Fasolo, A., and Bonfanti, L. (1997). Glial tubes in the rostral migratory stream of the adult rat. Brain Res.Bull. *42*, 9-21.

Peters, E., Palay, S.L., and Webster de F., H. (1991). The Fine Structure of the Nervous System: Neurons and their Supporting Cells, 3 edn (New York: Oxford University Press).

Petreanu, L., and Alvarez-Buylla, A. (2002). Maturation and death of adult-born olfactory bulb granule neurons: role of olfaction. J Neurosci.

Pixley, S.K.R., and De Vellis, J. (1984). Transition between immature radial glia and mature astrocytes studied with a monoclonal antibody to vimentin. Dev.Brain Res. *15*, 201-209.

Pleasure, S.J., Collins, A.E., and Lowenstein, D.H. (2000). Unique expression patterns of cell fate molecules delineate sequential stages of dentate gyrus development. J Neurosci *20*, 6095-6105.

Qin, H., Diener, D.R., Geimer, S., Cole, D.G., and Rosenbaum, J.L. (2004). Intraflagellar transport (IFT) cargo: IFT transports flagellar precursors to the tip and turnover products to the cell body. J Cell Biol *164*, 255-266.

Rakic, P. (1972). Mode of cell migration to the superficial layers of fetal monkey neocortex. J.Comp.Neurol. *145*, 61-84.

Rakic, P. (1985). Limits of neurogenesis in primates. Science *227*, 1054-1056.

Rakic, P. (1988). Specification of cerebral cortical areas. Science *241*, 170-176.

Ramón y Cajal, S. (1911). Histologie du Système Nerveux de l'Homme et des Vertébrés. (Paris: Maloine).

Rasin, M.R., Gazula, V.R., Breunig, J.J., Kwan, K.Y., Johnson, M.B., Liu-Chen, S., Li, H.S., Jan, L.Y., Jan, Y.N., Rakic, P., and Sestan, N. (2007). Numb and Numbl are required for maintenance of cadherin-based adhesion and polarity of neural progenitors. Nat Neurosci *10*, 819-827.

Reynolds, B., and Weiss, S. (1992). Generation of neurons and astrocytes from isolated cells of the adult mammalian central nervous system. Science *255*, 1707-1710.

Rickmann, M., Amaral, D.G., and Cowan, W.M. (1987). Organization of radial glial cells during the development of the rat dentate gyrus. The Journal of comparative neurology *264*, 449-479.

Rieder, C.L., Faruki, S., and Khodjakov, A. (2001). The centrosome in vertebrates: more than a microtubule-organizing center. Trends in cell biology *11*, 413-419.

Rohatgi, R., Milenkovic, L., and Scott, M.P. (2007). Patched1 regulates hedgehog signaling at the primary cilium. Science *317*, 372-376.

Rosenbaum, J.L., and Witman, G.B. (2002). Intraflagellar transport. Nature reviews *3*, 813-825.

Ross, A.J., May-Simera, H., Eichers, E.R., Kai, M., Hill, J., Jagger, D.J., Leitch, C.C., Chapple, J.P., Munro, P.M., Fisher, S.*, et al.* (2005). Disruption of Bardet-Biedl syndrome ciliary proteins perturbs planar cell polarity in vertebrates. Nat Genet *37*, 1135-1140.

Russo, R.E., Fernandez, A., Reali, C., Radmilovich, M., and Trujillo-Cenoz, O. (2004). Functional and molecular clues reveal precursor-like cells and immature neurones in the turtle spinal cord. J Physiol *560*, 831-838.

Saland, L.C., Evan, A.P., and Demski, L.S. (1974). Ultrastructure of ependymal cells of the shark median eminence. The Anatomical record *178*, 657-665.

Salathe, M. (2007). Regulation of mammalian ciliary beating. Annu Rev Physiol *69*, 401-422.

Sanderson, M.J., Dirksen, E.R., and Satir, P. (1990). Electron microscopy of respiratory tract cilia. In Electron Microscopy of the Lung, D.E. Schaufnagel, ed. (New York: Marcel Dekker), pp. 47-69.

Sapiro, R., Kostetskii, I., Olds-Clarke, P., Gerton, G.L., Radice, G.L., and Strauss, I.J. (2002). Male infertility, impaired sperm motility, and hydrocephalus in mice deficient in sperm-associated antigen 6. Molecular and cellular biology *22*, 6298-6305.

Satir, P. (1965). Studies on cilia. II. Examination of the distal region of the ciliary shaft and the role of the filaments in motility. J Cell Biol *26*, 805-834.

Satir, P., and Christensen, S.T. (2007). Overview of structure and function of mammalian cilia. Annu Rev Physiol *69*, 377-400.

Satir, P., and Dirksen, E.R. (1985). Function-structure correlations in cilia from mammalian respiratory tract. In Handbook of Physiology-The Respiratory System, A.P. Fishman, N.S. Cherniak, J.G. Widdicombe, and S.R. Gieger, eds. (Bethesda: American Physiological Society), pp. 473-494.

Sauer, F.C. (1935). Mitosis in the neural tube. J.Comp.Neurol. *62*, 377-405.

Saura, J., Richards, J.G., and Mahy, N. (1994). Differential age-related changes of MAO-A and MAO-B in mouse brain and peripheral organs. Neurobiology of aging *15*, 399-408.

Sawamoto, K., Wichterle, H., Gonzalez-Perez, O., Cholfin, J.A., Yamada, M., Spassky, N., Murcia, N.S., Garcia-Verdugo, J.M., Marin, O., Rubenstein, J.L.*, et al.* (2006). New neurons follow the flow of cerebrospinal fluid in the adult brain. Science *311*, 629-632.

Scheffler, B., Walton, N.M., Lin, D.D., Goetz, A.K., Enikolopov, G., Roper, S.N., and Steindler, D.A. (2005). Phenotypic and functional characterization of adult brain neuropoiesis. Proc Natl Acad Sci U S A *102*, 9353-9358.

Schmechel, D.E., and Rakic, P. (1979). A Golgi study of radial glia cells in developing monkey telencephalon: Morphogenesis and transformation into astrocytes. Anat.Embryol. *156*, 115-152.

Schneider, L., Clement, C.A., Teilmann, S.C., Pazour, G.J., Hoffmann, E.K., Satir, P., and Christensen, S.T. (2005). PDGFRalphaalpha signaling is regulated through the primary cilium in fibroblasts. Curr Biol *15*, 1861-1866.

Schoenwolf, G.C., and Alvarez, I.S. (1989). Roles of neuroepithelial cell rearrangement and division in shaping of the avian neural plate. Development *106*, 427-439.

Schoenwolf, G.C., and Smith, J.L. (2000). Mechanisms of neurulation. Methods in molecular biology (Clifton, N.J *136*, 125-134.

Scholzen, T., and Gerdes, J. (2000). The Ki-67 protein: from the known and the unknown. J Cell Physiol *182*, 311-322.

Seaberg, R.M., and van der Kooy, D. (2002). Adult rodent neurogenic regions: the ventricular subependyma contains neural stem cells, but the dentate gyrus contains restricted progenitors. J Neurosci *22*, 1784-1793.

Seri, B., and Alvarez-Buylla, A. (2002). Neural stem cells and the regulation of neurogenesis in the adult hippocampus. Clin. Neurosci. Res. *2*, 11-16.

Seri, B., Garcia-Verdugo, J.M., Collado-Morente, L., McEwen, B.S., and Alvarez-Buylla, A. (2004). Cell types, lineage, and architecture of the germinal zone in the adult dentate gyrus. The Journal of comparative neurology *478*, 359-378.

Seri, B., Garcia-Verdugo, J.M., McEwen, B.S., and Alvarez-Buylla, A. (2001). Astrocytes give rise to new neurons in the adult mammalian hippocampus. J Neurosci *21*, 7153-7160.

Seri, B., Herrera, D.G., Gritti, A., Ferron, S., Collado, L., Vescovi, A., Garcia-Verdugo, J.M., and Alvarez-Buylla, A. (2006). Composition and organization of the SCZ: a large germinal layer containing neural stem cells in the adult mammalian brain. Cereb Cortex *16 Suppl 1*, i103-111.

Sharp, P.J. (1972). Tanycyte and vascular patterns in the basal hypothalamus of Coturnix quail with reference to their possible neuroendocrine significance. Z Zellforsch Mikrosk Anat *127*, 552-569.

Shen, Q., Goderie, S.K., Jin, L., Karanth, N., Sun, Y., Abramova, N., Vincent, P., Pumiglia, K., and Temple, S. (2004). Endothelial cells stimulate self-renewal and expand neurogenesis of neural stem cells. Science *304*, 1338-1340.

Shibata, T., Yamada, K., Watanabe, M., Ikenaka, K., Wada, K., Tanaka, K., and Inoue, Y. (1997). Glutamate transporter GLAST is expressed in the radial glia-astrocyte lineage of developing mouse spinal cord. J Neurosci *17*, 9212-9219.

Shingo, T., Gregg, C., Enwere, E., Fujikawa, H., Hassam, R., Geary, C., Cross, J.C., and Weiss, S. (2003). Pregnancy-stimulated neurogenesis in the adult female forebrain mediated by prolactin. Science *299*, 117-120.

Simons, M., Gloy, J., Ganner, A., Bullerkotte, A., Bashkurov, M., Kronig, C., Schermer, B., Benzing, T., Cabello, O.A., Jenny, A.*, et al.* (2005). Inversin, the

gene product mutated in nephronophthisis type II, functions as a molecular switch between Wnt signaling pathways. Nat Genet *37*, 537-543.

Singla, V., and Reiter, J.F. (2006). The primary cilium as the cell's antenna: signaling at a sensory organelle. Science *313*, 629-633.

Soriano, P. (1999). Generalized lacZ expression with the ROSA26 Cre reporter strain. Nat Genet *21*, 70-71.

Sorokin, S.P. (1968). Reconstructions of centriole formation and ciliogenesis in mammalian lungs. J Cell Sci *3*, 207-230.

Spassky, N., Merkle, F.T., Flames, N., Tramontin, A.D., Garcia-Verdugo, J.M., and Alvarez-Buylla, A. (2005). Adult ependymal cells are postmitotic and are derived from radial glial cells during embryogenesis. J Neurosci *25*, 10-18.

Studnicka, F.K. (1900). Untersuchungen uber den Bau des Ependyms der nervosen Centralorgane. Anat.H. *15*, 301-431.

Summers, K.E., and Gibbons, I.R. (1971). Adenosine triphosphate-induced sliding of tubules in trypsin-treated flagella of sea urchin sperm. Proc Natl Acad Sci U S A *68*, 3092-3096.

Sun, Y., Goderie, S.K., and Temple, S. (2005). Asymmetric distribution of EGFR receptor during mitosis generates diverse CNS progenitor cells. Neuron *45*, 873-886.

Sundholm-Peters, N.L., Yang, H.K., Goings, G.E., Walker, A.S., and Szele, F.G. (2004). Radial glia-like cells at the base of the lateral ventricles in adult mice. J Neurocytol *33*, 153-164.

Takeda, S., Yonekawa, Y., Tanaka, Y., Okada, Y., Nonaka, S., and Hirokawa, N. (1999). Left-right asymmetry and kinesin superfamily protein KIF3A: new insights in determination of laterality and mesoderm induction by kif3A-/- mice analysis. J Cell Biol *145*, 825-836.

Takeichi, M. (1995). Morphogenetic roles of classic cadherins. Current opinion in cell biology *7*, 619-627.

Tamamaki, N., Nakamura, K., Okamoto, K., and Kaneko, T. (2001). Radial glia is a progenitor of neocortical neurons in the developing cerebral cortex. Neurosci Res *41*, 51-60.

Tamm, S.L., Sonneborn, T.M., and Dippell, R.V. (1975). The role of cortical orientation in the control of the direction of ciliary beat in Paramecium. J Cell Biol *64*, 98-112.

Thery, M., and Bornens, M. (2006). Cell shape and cell division. Current opinion in cell biology *18*, 648-657.

Torikata, C., Kijimoto, C., and Koto, M. (1991). Ultrastructure of respiratory cilia of WIC-Hyd male rats. An animal model for human immotile cilia syndrome. The American journal of pathology *138*, 341-347.

Tramontin, A.D., Garcia-Verdugo, J.M., Lim, D.A., and Alvarez-Buylla, A. (2003). Postnatal development of radial glia and the ventricular zone (VZ): a continuum of the neural stem cell compartment. Cereb Cortex *13*, 580-587.

Tropepe, V., Sibilia, M., Ciruna, B.G., Rossant, J., Wagner, E.F., and van der Kooy, D. (1999). Distinct neural stem cells proliferate in response to EGF and FGF in the developing mouse telencephalon. Developmental biology *208*, 166-188.

Tung, T.-C., and Y-F., T. (1940). Experimental studies on the determination of polarity of ciliary action of anuran embryos. Arch Biol (Liege) *51*, 203-218.

Twitty, V.C. (1928). Experimental studies on the ciliary action of amphibian embryos. J Exp Zool *50*, 310-344.

van Praag, H., Schinder, A.F., Christie, B.R., Toni, N., Palmer, T.D., and Gage, F.H. (2002). Functional neurogenesis in the adult hippocampus. Nature *415*, 1030-1034.

Veeman, M.T., Axelrod, J.D., and Moon, R.T. (2003). A second canon. Functions and mechanisms of beta-catenin-independent Wnt signaling. Developmental cell *5*, 367-377.

Ventura, R.E., and Goldman, J.E. (2007). Dorsal radial glia generate olfactory bulb interneurons in the postnatal murine brain. J Neurosci *27*, 4297-4302.

Voigt, T. (1989). Development of glial cells in the cerebral wall of ferrets: Direct tracing of their transformation from radial glia into astrocytes. J.Comp.Neurol. *289*, 74-88.

Wallingford, J.B. (2006). Planar cell polarity, ciliogenesis and neural tube defects. Human molecular genetics *15 Spec No 2*, R227-234.

Wallingford, J.B., and Harland, R.M. (2002). Neural tube closure requires Dishevelled-dependent convergent extension of the midline. Development *129*, 5815-5825.

Wallingford, J.B., Rowning, B.A., Vogeli, K.M., Rothbacher, U., Fraser, S.E., and Harland, R.M. (2000). Dishevelled controls cell polarity during Xenopus gastrulation. Nature *405*, 81-85.

Wang, J., Hamblet, N.S., Mark, S., Dickinson, M.E., Brinkman, B.C., Segil, N., Fraser, S.E., Chen, P., Wallingford, J.B., and Wynshaw-Boris, A. (2006a). Dishevelled genes mediate a conserved mammalian PCP pathway to regulate convergent extension during neurulation. Development *133*, 1767-1778.

Wang, Y., Guo, N., and Nathans, J. (2006b). The role of Frizzled3 and Frizzled6 in neural tube closure and in the planar polarity of inner-ear sensory hair cells. J Neurosci *26*, 2147-2156.

Wang, Y., and Nathans, J. (2007). Tissue/planar cell polarity in vertebrates: new insights and new questions. Development *134*, 647-658.

Weigmann, A., Corbeil, D., Hellwig, A., and Huttner, W.B. (1997). Prominin, a novel microvilli-specific polytopic membrane protein of the apical surface of epithelial cells, is targeted to plasmalemmal protrusions of non-epithelial cells. Proc Natl Acad Sci U S A *94*, 12425-12430.

Weissman, T.A., Riquelme, P.A., Ivic, L., Flint, A.C., and Kriegstein, A.R. (2004). Calcium waves propagate through radial glial cells and modulate proliferation in the developing neocortex. Neuron *43*, 647-661.

Wessels, M.W., den Hollander, N.S., and Willems, P.J. (2003). Mild fetal cerebral ventriculomegaly as a prenatal sonographic marker for Kartagener syndrome. Prenatal diagnosis *23*, 239-242.

Whiteley, H.E., and Young, S. (1985). Cilia in the fetal and neonatal canine retina. Tissue Cell *17*, 335-340.

Williams, D., Gascoigne, J.E., Street, M., and Williams, E.D. (1979). Histochemical characterization of monoamine oxidase in ependyma of rat hypothalamus. The Histochemical journal *11*, 83-95.

Wodarz, A., and Huttner, W.B. (2003). Asymmetric cell division during neurogenesis in Drosophila and vertebrates. Mechanisms of development *120*, 1297-1309.

Worthington, W.C., Jr., and Cathcart, R.S., 3rd (1963). Ependymal cilia: distribution and activity in the adult human brain. Science *139*, 221-222.

Yamadori, T., and Nara, K. (1979). The directions of ciliary beat on the wall of the lateral ventricle and the currents of the cerebrospinal fluid in the brain ventricles. In Scanning electron microscopy, A.M.F. O'Hare, ed. (Chicago: III SEM Inc.), pp. 335-340.

Yu, J.M., Kim, J.H., Song, G.S., and Jung, J.S. (2006). Increase in proliferation and differentiation of neural progenitor cells isolated from postnatal and adult mice brain by Wnt-3a and Wnt-5a. Mol Cell Biochem *288*, 17-28.

Zallen, J.A. (2007). Planar polarity and tissue morphogenesis. Cell *129*, 1051-1063.

Zhadanov, A.B., Provance, D.W., Jr., Speer, C.A., Coffin, J.D., Goss, D., Blixt, J.A., Reichert, C.M., and Mercer, J.A. (1999). Absence of the tight junctional protein AF-6 disrupts epithelial cell-cell junctions and cell polarity during mouse development. Curr Biol *9*, 880-888.

Zhao, C., Deng, W., and Gage, F.H. (2008). Mechanisms and functional implications of adult neurogenesis. Cell *132*, 645-660.

Zhuo, L., Theis, M., Alvarez-Maya, I., Brenner, M., Willecke, K., and Messing, A. (2001). hGFAP-cre transgenic mice for manipulation of glial and neuronal function in vivo. Genesis *31*, 85-94.

Zupanc, G.K. (2006). Neurogenesis and neuronal regeneration in the adult fish brain. J Comp Physiol A Neuroethol Sens Neural Behav Physiol *192*, 649-670.

UCSF Library Release

Publishing Agreement

It is the policy of the University to encourage the distribution of all theses and dissertations. Copies of all UCSF theses and dissertations will be routed to the library via the Graduate Division. The library will make all theses and dissertations accessible to the public and will preserve these to the best of their abilities, in perpetuity.

I hereby grant permission to the Graduate Division of the University of California, San Francisco to release copies of my thesis or dissertation to the Campus Library to provide access and preservation, in whole or in part, in perpetuity.



4/28/08

Author Signature Date